THE UNIVERSITY
of EDINBURGH

COMPUTED TOMOGRAPHY AND POSITRON EMISSION TOMOGRAPHY IN THE ASSESSMENT OF AORTIC VALVE DISEASE

Timothy Robert Graham Cartlidge

BSc(hons), MB ChB, MRCP

A thesis presented for the degree of Doctor of Philosophy at the

University of Edinburgh, February 2021

To Manjit, Olivia, Victoria, Mum & Dad

TABLE OF CONTENTS

Declaration **9**

Acknowledgements **10**

Abbreviations **12**

Abstract **13**

Lay summary **16**

Chapter 1. Introduction **19**

1.1 Overview 20

1.2 Native Aortic Valve Stenosis 22

1.3 Bioprosthetic Valve Disease 41

1.4 Summary 65

1.5 Aims and Hypotheses 66

Chapter 2. Material and Methods **68**

2.1 Overview 69

2.2 Study Populations 70

2.3 Study Assessments 72

2.4 Echocardiography 77

2.5 Computed Tomography 82

2.6 ^{18}F-Fluoride PET/CT 88

2.7 Micro-^{18}F-Fluoride PET/CT 96

2.8 Histological Validation 98

2.9 Statistical Analysis 102

Chapter 3. Contrast-Enhanced Computed Tomography in the Assessment of Aortic Stenosis **103**

3.1 Abstract 104

3.2 Introduction 106

3.3 Methods 108

3.4 Results 116

3.5 Discussion 134

Chapter 4. Optimisation and Reproducibility of Aortic Valve ^{18}F-Fluoride Positron Emission Tomography in Aortic Stenosis **140**

4.1 Abstract 141

4.2 Introduction 143

4.3 Methods 145

4.4 Results 151

4.5 Discussion 165

Chapter 5. ^{18}F-Fluoride-Positron Emission Tomography/Computed Tomography and Histopathology of Explanted Bioprosthetic Valves **171**

5.1 Abstract 172

5.2 Introduction 174

5.3 Methods 181

5.4 Results 188

5.5 Discussion 229

Chapter 6. Detection and Prediction of Bioprosthetic Aortic Valve Degeneration **234**

6.1 Abstract 235

6.2 Introduction 237

6.3 Methods 239

6.4 Results 249

6.5 Discussion 278

Chapter 7. Conclusions and Future Directions 284

7.1 Summary of findings 285

7.2 CT angiography detects calcification and fibrosis of the aortic valve, and provides insights into the contribution of fibrosis and calcification in aortic stenosis. 287

7.3 ^{18}F-Fluoride PET/CT can be established as an accurate and reproducible technique to assess disease activity in aortic stenosis. 290

7.4 Assessment of degenerated bioprosthetic valves with micro-^{18}F-fluoride PET/CT and correlating histology will provide novel insights about the mechanisms of bioprosthetic valve degeneration. 292

7.5 ^{18}F-Fluoride PET/CT can be applied to the assessment of bioprosthetic aortic valves to detect and predict structural valve degeneration. 294

7.6 Future directions 296

7.7 Perspective 299

Bibliography 300

Appendix 324

INDEX OF TABLES

Item	Description	Page
Chapter 3		
Table 3.1	Patient baseline characteristics	117
Table 3.2	Association between CT and echocardiographic assessments in aortic stenosis	122
Table 3.3	Patient Characteristics of Validation Cohort from Universite Laval, Canada	133
Chapter 4		
Table 4.1	Patient Characteristics	152
Table 4.2	Scan-rescan and intra-observer reproducibility for presence or absence of ^{18}F-fluoride uptake.	159
Table 4.3	Kappa Statistics for Interobserver and Scan-rescan agreement for ^{18}F-Fluoride PET signal distribution.	160
Table 4.4	Bland-Altman values and percentage errors for each stepwise change to the image acquisition and analysis technique.	163
Chapter 5		
Table 5.1	Classification of features of bioprosthetic valve degeneration	182
Table 5.2	Characteristics of explanted bioprosthetic valves, measures of ^{18}F-fluoride PET activity and CT calcium volume.	189
Table 5.3	Summary of macroscopic, histopathology, micro-CT and micro-PET findings from explanted bioprosthetic valves	190
Chapter 6		
Table 6.1	Baseline characteristics of the clinical study population undergoing *in vivo* positron emission tomography and computed tomography imaging.	255
Table 6.2	The different types of bioprosthetic valve models in the clinical *in-vivo* cohorts.	258
Table 6.3	Bioprosthetic valve model size in the clinical *in-vivo* cohorts	259
Table 6.4	Factors associated with deterioration in bioprosthetic valve function (annualised change in peak velocity after 2 years): univariable analysis	265
Table 6.5	A. Factors associated with deterioration in bioprosthetic valve function: multivariable analysis	273
Table 6.6	Factors associated with the development of bioprosthetic valve dysfunction: binary logistic regression using.	275
Table 6.7	Summary statistics of effective radiation dose for baseline PET-CT using up-to-date PET effective dose conversion factor 0.028 $mSv \cdot mGy^{-1}cm^{-1}$ (9)	277

INDEX OF FIGURES

Item	Description	Page
Chapter 1		
Figure 1.1	Proposed mechanisms in the pathogenesis of aortic stenosis	31
Figure 1.2	Contrast-enhanced computed tomography in the assessment of aortic stenosis	37
Figure 1.3	^{18}F-Fluoride PET-CT predicts new aortic valve calcification in aortic stenosis	40
Figure 1.4	Classification of bioprosthetic heart valves	42
Figure 1.5	Expert consensus statement: Definition of structural valve degeneration and clinical approach to patients with bioprosthetic valves	47
Figure 1.6	Macroscopic photography of explanted bioprosthetic valves illustrating mechanisms of structural degeneration	59
Figure 1.7	Schematic of the mechanisms of bioprosthetic structural valve degeneration	60
Chapter 2		
Figure 2.1	Transthoracic echocardiography in the assessment of aortic stenosis	81
Figure 2.2	CT to detect leaflet pathology in bioprosthetic valves	87
Figure 2.3	Principles of positron emission tomography	90
Figure 2.4	Methodology for co-registration of positron emission tomography and contrast computed tomography in bioprosthetic aortic valves.	95
Chapter 3		
Figure 3.1	Contrast-enhanced computed tomography in aortic stenosis: detection of valve calcification and fibrosis.	120
Figure 3.2	Calcific and Non-Calcific Aortic Valve Volumes	121
Figure 3.3	The Fibro-Calcific Ratio	124
Figure 3.4	Fibro-Calcific Burden and its association with aortic stenosis severity compared with non-contrast CT calcium scoring	126
Figure 3.5	Case illustration of utility of the fibrocalcific burden in assessment of aortic stenosis	128
Figure 3.6	Comparison between contrast CT analysis and histologic examination.	131
Chapter 4		
Figure 4.1	Creation of Co-registered En Face Short-Axis PET/CT Images of the Aortic Valve	153
Figure 4.2	Improved Localisation of PET Signal Within the Aortic Valve and its Leaflets	155
Figure 4.3	Measuring Blood Pool Activity in the Brachiocephalic vein and the Right Atrium	161

Figure 4.4	Scan-rescan Reproducibility for ^{18}F-Fluoride PET quantification in the aortic valve with consequent sample size estimates	164
Chapter 5		
Figure 5.1	Autoradiography and histology of an explanted bioprosthetic aortic valve	193
Figure 5.2	Association of ^{18}F-fluoride and total calcium volume ex vivo	196
Figures 5.3-5.17	*Ex vivo* findings of explanted bioprosthetic valves	214-228
Chapter 6		
Figure 6.1	Methodology for co-registration of positron emission tomography and contrast computed tomography in bioprosthetic aortic valves.	245
Figure 6.2	*Ex-vivo* degenerated bioprosthetic aortic valves: macroscopic appearances, micro-computed tomography, micro-positron emission tomography and histology.	251
Figure 6.3	CONSORT flow diagram of study recruitment, allocation, follow-up and analysis.	253
Figure 6.4	*In-vivo* ^{18}F-fluoride positron emission tomography and computed tomography imaging of patients with bioprosthetic aortic valves.	261
Figure 6.5	Tertile analysis according to ^{18}F-fluoride PET uptake demonstrating tissue-to-background (TBR) values across the tertiles and relationship with change in valve function during follow-up.	266
Figure 6.6	Baseline ^{18}F-fluoride positron emission tomography uptake predicts subsequent deterioration in bioprosthetic valve function after 2 years.	269
Figure 6.7	Case illustrations: baseline ^{18}F-fluoride positron emission tomography and computed tomography predict imminent failure of bioprosthetic function.	271

DECLARATION

This thesis describes work undertaken in the British Heart Foundation Centre for Cardiovascular Research, University of Edinburgh. The work described in this thesis was funded by the British Heart Foundation (FS/13/77/30488). I was responsible for the planning, conduct and data analysis of the studies herein. Consistent with the continuous and collaborative nature of research, the patient recruitment and baseline assessments of the 'SATLIRE2' randomised controlled trial (which provided the study populations in chapters 3 and 4) were led by my colleague, Dr Tania Pawade. The histopathology of bioprosthetic valves (referred to in chapters 5 and 6) was undertaken in conjunction with international collaborators, Dr Renu Virmani and Dr Stephanie Sellers, as the required expertise was not locally available. The material forming the basis of Chapters 3, 4, 5 and 6 has been published in peer-reviewed journals. The thesis has not been submitted in any previous applications for a degree or professional qualification, and all sources of information have been acknowledged. All studies were conducted in accordance with the Declaration of Helsinki of the World Medical Association, and with the regulations of the regional Ethics Board within NHS Scotland.

Timothy Robert Graham Cartlidge **12th February 2021**

ACKNOWLEDGEMENTS

I am hugely indebted to my supervisors, Professor Marc Dweck and Professor David Newby, for their inspiration, support and guidance. At the University of Edinburgh Centre for Cardiovascular Science, they have established an environment in which novice researchers benefit from access to world-leading expertise, facilities, collaborative networks, and the opportunity to participate in high-impact research.

I thank the British Heart Foundation for providing the funding and infrastructure to support my clinical research training fellowship, and by extension I thank those who sustain the Foundation with their generosity. Furthermore, I am very grateful to all of the patients who kindly donated their time and effort to participate in the clinical research upon which this thesis is based.

I would like to express my appreciation to the staff of the University of Edinburgh Imaging Centre, where the team of radiographers made a major contribution in acquiring all PET/CT scans, Dr Christophe Lucatelli led the radiochemistry support, Dr Alison Fletcher provided expertise in PET physics, Professor Edwin van Beek provided clinical oversight of scans, and Dr Callum Gray provided guidance in image analysis. The staff of the Clinical Research Facility at the Royal Infirmary of Edinburgh freely offered their assistance and camaraderie during the daily business of running a clinical research study. Pre-clinical PET/CT was performed with the expertise and support of Dr Adriana Tavares and Carlos Alcaide at the University of Edinburgh.

I owe a significant vote of thanks to Dr Stephanie Sellers and Dr Jonathan Leipsic of the University of British Columbia, Vancouver, and Dr Marie Annick Clavel and her team from the Université Laval, Quebec, for their significant contribution and ongoing collaboration. Along with Dr Renu Virmani of the CVPath Institute, Maryland, these collaborators provided the histopathology expertise required to validate our imaging insights.

It has been a great pleasure to work amongst a group of such enthusiastic, talented and supportive colleagues in the cardiovascular research group at the University of Edinburgh. In particular, this research would not have been possible without Dr Tania Pawade and Ms Audrey White, who were essential contributors but also provided much valued personal support.

Finally, I would like to thank my family and close friends for their encouragement, support and guidance. Above all my wife, Manjit, has supported me and shouldered added burden with good humour throughout to allow me to complete this thesis. Along with our two daughters, Olivia and Victoria, they are my daily inspiration.

ABBREVIATIONS

AS	Aortic stenosis
AU	Agatston Units
AV	Aortic valve
AVR	Aortic valve replacement
CT	Computed tomography
CT-AVC	Computed tomography aortic valve calcium score
ECG	Electrocardiogram
HU	Hounsfield units
ICC	Interclass correlation coefficient
LVOT	Left ventricular outflow tract
MBq	MegaBequerel
MDS	Most diseased segment
MSv	MilliSievert
PET	Positron Emission Tomography
RA	Right atrium
ROI	Region of interest
SUV	Standardised uptake value
TAVI	Transcatheter aortic valve implantation
TBR	Tissue to background ratio

ABSTRACT

Introduction

Native and bioprosthetic aortic valve diseases are an increasingly common clinical challenge as a consequence of the ageing demographic and the expansion of new valve technology. In both conditions, there remains substantial scope to broaden our understanding of the pathophysiology, improve diagnostic sensitivity and accuracy, and develop new markers of disease activity with which to measure therapeutic effect. Computed tomography (CT) and positron emission tomography (PET) are non-invasive imaging assessments that combine high resolution anatomical detail with real-time functional information about disease activity, and as such are ideally suited to complement echocardiography in the investigation of native and bioprosthetic aortic valve diseases.

Methods

Aortic Stenosis

Volunteers with aortic stenosis (n=143) across a range of severity underwent echocardiography, CT aortic valve calcium scoring and contrast-enhanced CT angiography. Aortic valve fibrosis and calcification were quantified to produce two novel measures: the fibro-calcific ratio and fibro-calcific burden. From the same study population, a subset of 15 volunteers underwent hybrid ^{18}F-fluoride PET/CT on two separate occasions and we investigated different methods of image analysis to optimise accuracy and reproducibility.

Bioprosthetic Valves

Explanted degenerated bioprosthetic valves (n=16) were examined *ex vivo* using histopathology and preclinical ^{18}F-fluoride PET/CT. Patients with bioprosthetic aortic valves (n=78) were then recruited into two cohorts, with and without prosthetic valve dysfunction, and underwent *in-vivo* contrast-enhanced CT angiography, ^{18}F-fluoride PET, and serial echocardiography over 2 years of follow-up.

Results

Aortic Stenosis

Contrast-enhanced CT calcium volume correlated closely with conventional CT calcium score in the aortic valve (r=0.86, p=<0.001). Fibrosis dominated in mild aortic stenosis while calcification dominated in severe stenosis (fibro-calcific ratio: 1.33 [0.91-2.4]) *versus* 0.53 [0.35-1.05] respectively; p=0.001). Males exhibited more calcium than fibrosis, with the reverse true for females (fibro-calcific ratio: 0.89 [0.45-1.54] *versus* 1.49 [0.82-5.74] respectively; p=0.001). The fibro-calcific burden demonstrated the strongest correlation with peak aortic-jet velocity (r=0.71, p<0.001), especially in women (r=0.77, p=0.001) where it outperformed CT calcium score (p=0.027). In our investigation of ^{18}F-fluoride-PET/CT, contrast-enhanced, ECG-gated PET/CT provided superior spatial localisation of ^{18}F-fluoride uptake. Scan-rescan reproducibility was markedly improved using enhanced analysis techniques leading to a reduction in variability from 25% to <10%.

Bioprosthetic Valves

In degenerated bioprosthetic valves *ex vivo*, calcification was the most prevalent pathological feature (87%), whilst thrombus (40%) and pannus overgrowth (47%) were other common findings. All valves exhibited ^{18}F-fluoride uptake on PET, with a strong positive correlation between ^{18}F-fluoride uptake and calcium volume (r=0.73, p=0.0031). ^{18}F-Fluoride uptake was highest in regions of leaflet calcification but also localised to regions of organised thrombus, fibrosis and features of matrix degradation on histopathology.

In the cohort study of patients with bioprosthetic aortic valves, all those with recognised valve dysfunction exhibited abnormalities on CT and high ^{18}F-fluoride uptake. In the 71 patients without valve dysfunction, 20% had leaflet pathology on CT and 34% had increased ^{18}F-fluoride uptake (target-to-background ratio 1.55 [1.44-1.88]). Patients with increased ^{18}F-fluoride uptake exhibited more rapid deterioration in valve function than those without (annualised change in peak transvalvular velocity: 0.30 [0.13-0.61] *versus* 0.01 [-0.05-0.16] ms^{-1}/year, p<0.001). ^{18}F-Fluoride uptake correlated with deterioration in all echocardiographic measures of valve function (e.g. change in peak velocity, r=0.72; p<0.001) and, on multivariable analysis, was the only independent predictor of future bioprosthetic dysfunction.

Conclusions

In both native aortic valve disease and bioprosthetic valve disease, CT and ^{18}F-fluoride PET afford valuable insights into disease mechanisms, inform patient risk stratification and prognosis, and provide biomarkers of disease activity that may be used for the development of future therapeutic interventions.

LAY SUMMARY

Heart valve disease and the disease of artificial heart valves are health challenges that share key features and have become increasingly common as a result of the increased life expectancy in developed countries and the availability of new approaches to valve replacement for people who may not previously have been eligible. Computed tomography (CT) uses X-rays to build a detailed 3-dimensional image of all or part of the human body. Positron emission tomography (PET) involves injection of a substance called ^{18}F-fluoride which binds to chalk-like material (calcium) often found in the heart valves and blood vessels. PET/CT then allows the areas in the body where ^{18}F-fluoride has attached to calcium to be identified and the strength of signal can be measured. In this thesis, we investigate the use of CT and PET to build a greater understanding of the factors that cause heart valve disease, to improve our ability to identify these problems, and to establish measurements that can be used to test if new treatments are working.

Volunteers (143 people) with a narrowing of the main outlet valve of the heart (aortic valve), called aortic stenosis, underwent testing with an ultrasound scan and two different types of CT scan, one of which involved injection of an iodine-based ‘dye’ to light up the circulating blood. The CT scan was used to measure the amount of scar tissue (fibrosis) and chalk-like material (calcium) in the aortic valve. These new measurements were compared to standard measurements of the severity of valve narrowing. From the same group of volunteers, 15 people underwent PET scans using an identical method on two separate occasions within 3 months. We then used the

information from these scans to work out the best technique to make our measurements as accurate and repeatable as possible.

In our study of artificial heart valves, we first examined 16 artificial heart valves, which were no longer working satisfactorily and had been removed from patients at the time of an operation, under a microscope and with a miniaturised form of PET/CT. In addition, a total of 78 volunteers with artificial heart valves participated in a study during which they received a PET/CT scan and annual ultrasound scans over 2 years.

The results of our work in people with a narrowed heart valve (aortic stenosis) demonstrated that scarring (fibrosis) is particularly important in the early stages of the condition, and also appears to be a more significant factor in women than men. Our unique combined measurement of scar tissue (fibrosis) and chalk-like material (calcium) in the valve seemed to offer a better test of the severity of valve narrowing than the current widely used test to measure calcium alone.

In the same condition (aortic stenosis), we experimented with different methods to improve measurements obtained from PET/CT. We successfully showed that using iodine ‘dye’ during the CT scan and taking steps to account for movement of the beating heart resulted in major improvements in the quality of our images and measurements. Also, using average rather than maximum measurements of PET signal in the valve resulted in much improved repeatability.

In our study of failing artificial heart valves that had been removed from patients, we found heavy build of chalk-like material (calcium) in a large majority, and evidence of clotted blood and scar tissue less commonly. PET/CT identified abnormalities in all of the failed valves and findings suggested that blood clot and scar tissue may be early events which eventually lead to the formation of calcium. In patients with artificial heart valves, we discovered that PET/CT can be used to detect valves with early stages of disease, long before any symptoms might develop, and to predict worsening performance of the artificial valve over time.

In summary, CT and PET scans can be used to increase our understanding of how heart valves and artificial heart valves fail, to monitor progression of these conditions over time, and to assist the development of new treatments for heart valve disease in future.

CHAPTER 1

INTRODUCTION

1.1 OVERVIEW

Aortic valve disease presents a growing clinical problem, with the incidence of severe aortic stenosis in developed countries predicted to double over the next 30 years (Osnabrugge RL *et al*, 2013). Advances in our understanding of aortic stenosis pathogenesis increasingly point towards a closely regulated process that is ultimately dominated by calcification (Pawade TA *et al*, 2015). However, there are gaps in our knowledge of disease pathways and we have not adequately accounted for the subgroup of patients who develop aortic stenosis with severe fibrotic cusp thickening rather than calcification (Shen M *et al*, 2016). With no medical therapies currently proven to alleviate the progression of aortic stenosis, the only treatments options for patients with symptomatic severe aortic stenosis are aortic valve replacement or palliation of symptoms.

Modern techniques in computed tomography (CT) allow detailed tissue characterisation whilst ^{18}F-fluoride positron emission tomography-computed tomography (PET-CT) is a functional imaging modality with the ability to quantify and localise calcification activity (Irkle A *et al*, 2015). CT and PET-CT therefore hold promise in both elucidating the mechanisms of aortic stenosis and monitoring disease activity, providing an early measure of the efficacy of novel medical therapies to attenuate calcification.

Aortic valve replacement may be performed via a surgical or transcatheter procedure, and the significant majority of valves implanted are now bioprosthetic. Bioprosthetic

aortic valves themselves are associated with long term complications including the risk of endocarditis, systemic embolism and finite durability due to structural valve degeneration (Rodriguez-Gabella T *et al*, 2017). Though the pathophysiology of bioprosthetic valve degeneration is not well understood, calcification again appears to be a central feature (Siddiqui RF *et al*, 2009). However, non-invasive methods for detecting this process have been lacking and current care relies on serial echocardiography to identify the valve dysfunction that occurs towards the end stages of the degeneration process.

Here, we firstly explore the use of micro-^{18}F-fluoride PET-CT and histological examination of degenerated explanted valves to illuminate the mechanisms of structural valve degeneration. We then assess the application of ^{18}F-fluoride PET-CT in patients with bioprosthetic valves to identify structural valve degeneration and predict deterioration in valve function.

1.2 NATIVE AORTIC VALVE STENOSIS

Epidemiology of Native Valve Aortic Stenosis

Valvular heart disease is a common pathology, with a recent U.K. study identifying clinically significant (moderate or severe) undiagnosed valvular disease in 6.4% of individuals aged 65 years and over, in combination with 4.9% of the study population who had pre-existing valve disease giving a total prevalence of 11.3% (d'Arcy *et al*, 2016). Aortic stenosis is the most common clinically significant heart valve pathology in the developed world, characterised by progressive fibro-calcific remodelling and thickening of the aortic valve cusps which ultimately restricts cardiac output (Lindman *et al*, 2016). In a North American population with mean age 60 years, the annual incidence of new cases of aortic stenosis was ~5 per 1,000 and the prevalence of aortic stenosis at age 65 years was 5%. In a meta-analysis of studies conducted in Europe, the U.S.A. and Taiwan, the prevalence of aortic stenosis in people aged 75 years and over was 12.4%. Consistent with these observations, there is a significant increase in the prevalence of aortic stenosis with advancing age. It can therefore be anticipated that, with the changing population demographics of developed nations, aortic stenosis is set to become an increasingly common clinical challenge and place a growing burden on healthcare resources. Indeed, the incidence of aortic stenosis in Scotland increased from 246 cases per million population in 1997 to 365 per million in 2005 (Berry C *et al*, 2013) and the number of people with severe aortic stenosis in Europe and North America is projected to double by 2050 (Osnabrugge RL *et al*, 2013). Whilst advanced age is the central feature, important sex differences are also apparent in the clinical presentation of aortic stenosis. The overall incidence of aortic stenosis is

similar in men and women, although women are more likely to present later in the disease trajectory, at older age and with greater frailty, renal dysfunction and evidence of heart failure (Kong *et al*, 2017).

Anatomy of the Native Aortic Valve

Under normal circumstances, the aortic valve is composed of three cusps that are named according to their anatomic relationship to the coronary arteries, termed the right coronary, left coronary and non-coronary cusps. Each cusp has a trilaminar structure comprising the fibrosa, spongiosa and ventricularis. The central spongiosa layer contains a loose matrix of glycosaminoglycans, the fibrosa with its dense connective tissue forms the aortic layer and the pliable ventricularis forms the ventricular layer. The fibrosa is primarily composed of circumferentially orientated type 1 and III fibrillar collagen whilst the ventricularis is composed of radially orientated elastin fibres, permitting greater compliance and allowing apposition of the free edges of the cusps to prevent regurgitation of blood flow (Schoen FJ, 2008). The cellular composition includes endothelial cells covering the aortic and ventricular surfaces of the valve, smooth muscle cells residing at the base of the ventricularis, and valve interstitial cells which constitute the majority of the cell population (Taylor PM *et al*, 2000).

Pathophysiology of Native Aortic Valve Stenosis

Each aortic valve cusp is a thin (<1 mm), smooth, flexible and mobile structure. In aortic stenosis, these cusps become thickened with fibrosis and calcification resulting in increasingly restricted cusp movement and valvular obstruction. Aortic stenosis has

conventionally been considered a degenerative “wear and tear” condition driven by mechanical stress and progressive valve disruption leading to tissue injury and calcification. However, emerging evidence supports a more complex and closely regulated pathophysiology. There is postulated to be an early *initiation* phase of lipid deposition and inflammation with similarities to atherosclerosis, followed by a later *propagation* phase mediated by pro-calcific and pro-osteogenic factors (Pawade *et al*, 2015).

Initiation Phase

Similar to atherosclerosis, endothelial injury is triggered by high mechanical stress and reduced sheer stress. This at least partly accounts for the more rapid development of aortic stenosis in patients with congenital abnormalities of the aortic valve. A bicuspid aortic valve, for example, is the commonest form of congenital heart disease with a population prevalence of 0.5-0.8%. The two cusp structure results in less effective dissipation of mechanical stress, accelerated endothelial damage and disease progression, with a mean age under 50 years at the time of aortic valve replacement surgery (Pachulski *et al*, 1993; Coffey *et al*, 2016). Aortic stenosis and atherosclerosis also share important risk factors with large studies demonstrating an association between the incidence of aortic stenosis and age, cigarette smoking, diabetes mellitus and hypertension (Thanassoulis *et al*, 2010; Stewart *et al*, 1997; Stritzke *et al*, 2009). These conditions are likely to contribute to altered mechanical stress and endothelial dysfunction.

Endothelial injury is accompanied by early histological changes including deposition of low-density lipid predominantly within the fibrosa (Otto *et al*, 1994). A variety of lipids have been associated with aortic stenosis including total cholesterol, low-density-lipoprotein (LDL) cholesterol, oxidised LDL cholesterol, lipoprotein(a), apolipoprotein B, triglycerides and proprotein convertase subtilisin/kexin type 9 (PCSK9). Lipoprotein(a) is an LDL-like particle that carries apolipoprotein B-100 and is the main transporter of oxidised phospholipids. Oxidised phospholipids are a key driver of vascular inflammation and atherosclerosis, with substantial evidence of an adverse role in ischaemic heart disease, cerebrovascular disease, peripheral arterial disease and risk of cardiovascular death (Capoulade *et al*, 2015). Circulating plasma levels of both lipoprotein (a) and oxidised phospholipids are associated with incident aortic stenosis, haemodynamic progression of aortic stenosis, need for aortic valve replacement and cardiovascular death (Zheng *et al*, 2019; Tsimikas S *et al*, 2012). Levels of lipoprotein (a) are almost entirely genetically determined, and a single nucleotide polymorphism of lipoprotein (a) has been identified as the only single nucleotide polymorphism to reach genome-wide significance for the presence of aortic valve calcification (Thanassoulis *et al*, 2013).

During the early phase of aortic stenosis, endothelial disruption, infiltration and oxidisation of lipid particles drives translocation of immune cells into the valve and production of pro-inflammatory cytokines. The early inflammatory response is histologically characterised by increased presence of non-foam cell macrophages and foam cell macrophages (macrophages that have engulfed lipid), T lymphocytes and small numbers of alpha-actin-positive cells. These features become more marked as

aortic stenosis progresses (Otto *et al*, 1994). Endothelial damage results in upregulation of cell adhesion molecules such as ICAM-1 and VCAM-1 which triggers an influx of leucocytes, principally monocytes (Sucosky P et al, 2009). Monocytes differentiate into macrophages and these cells release cytokines such as TNF-alpha, TNF-beta and IL-1 beta which stimulate the inflammatory response (Steiner I *et al*, 2012). Gene expression profiling in aortic stenosis confirms the upregulation of various chemokines and chemokine receptors (Bosse *et al*, 2009).

The adaptive immune system is also implicated in the pathogenesis of aortic stenosis. Elevated numbers of T lymphocytes are found in the peripheral blood and aortic valves of people with aortic stenosis, in particular multiple oligoclonal CD4+ and CD8+ T cells (Wu HD *et al*, 2007; Winchester R *et al*, 2011). T lymphocyte proliferation may occur not only in lymphoid tissue but also in the valve itself where these cells secrete further pro-inflammatory cytokines. B lymphocytes are not normally found in cardiac valves, however, CD20+ B cells and CD138+ plasma cells infiltrate the subendothelial layer on the aortic surface of diseased aortic valves. B lymphocytes can be activated by macrophage-secreting cytokines, such as B cell-activating factor belonging to the TNF family (BAFF). There is a positive correlation between the number of BAFF receptor-positive B cells and disease severity in aortic stenosis (Natorska *et al*, 2016).

Furthermore, mast cells exhibit an increase in number in valve tissue in aortic stenosis, again mainly localising to the subendothelial space of the aortic surface of the valve and associating with macrophages. When activated, mast cells release cathepsin G which causes elastin degradation in the disease valve (Helske S *et al*, 2006). The other

significant mast cell effect is to promote angiogenesis in valve tissue via production of vascular endothelial growth factor (VEGF). And tryptase, which inhibits levels of the angiogenesis inhibitor endostatin (Syvaranta S *et al*, 2010).

Propagation Phase

Microcalcification is observed histologically even in the early lesion of aortic stenosis, colocalising with regions of lipid infiltration (Otto *et al*, 1994). It is likely that early calcification in the form of hydroxyapatite is mediated by cell death and release of apoptotic bodies containing calcium and inorganic phosphate. Thereafter calcification is thought to become the fundamental and self-perpetuating mechanism by which aortic valve stenosis progresses in severity.

In the context of inflammation, valve interstitial cells (VIC) can differentiate into myofibroblasts and osteoblast-like cells. A number of cytokines have been shown to facilitate this, including interleukin (IL)-1beta, IL-6, IL-8, insulin-like growth factor (IGF)-1, tumour necrosis factor (TNF)-alpha and tissue growth factor (TGF)-beta (Jian B *et al*, 2003; New SE, *et al*, 2011). Myofibroblasts are capable of absorbing lipid and producing pro-inflammatory cytokines and chemokines. Myofibroblasts also produce extracellular collagen and tenascin-C resulting in changes to the composition of the extracellular matrix and tissue fibrosis. This collagen matrix provides a structural template upon which calcification may develop (Heinz B, 2007). Osteoblast-like cells secrete bone morphogenic protein 2 (BMP-2) and osteopontin which stimulate mineralisation, and express runt-related transcription factor 2 and osterix which encourage further osteoblastic differentiation (Yang X *et al*, 2009 a). The

inflammatory and pro-calcific functions of valve interstitial cells are closely associated, with in vitro activation of inflammatory processes correlating strongly with valvular calcification (Yang X *et al*, 2009 b).

As mineralisation advances, it develops a more organised crystalline structure with features of lamellar bone (Pawade *et al*, 2015). Interestingly, valve ossification is contingent upon angiogenesis and the role of mast cells in this regard is described above. In established aortic valve disease, osteoblastic differentiation is maintained by mechanisms including Notch, Wnt and receptor activator of nuclear factor kappa B (RANK), receptor activator of nuclear factor kappa B ligand (RANKL) and osteoprotegerin (OPG) pathways. Notch cell surface receptors are widely expressed in the aortic valve and a Notch-1 loss-of-function mutation predisposes to potent osteoblastic differentiation via the action of BMP-2 (Nigam V *et al*, 2009). This mutation has been identified in families with premature vascular and aortic valve calcification (Garg *et al*, 2005). Wnt binds to LDL receptor-related proteins to activate the Wnt/beta-catenin pathway that again drives osteoblastic differentiation. TGF-beta1 is stimulated by mechanical stress and further promotes Wnt signalling, thus establishing a perpetual cycle of increasing morphological disruption and haemodynamic turbulence (Chen *et al*, 2011). In bone marrow stromal cells, RANKL binds to RANK and induces osteoclastic differentiation and activity, resulting in demineralisation of bone. This is regulated by OPG which is a competitive inhibitor of RANK. By contrast in the aortic valve and vasculature, RANKL promotes osteoblastic differentiation and upregulation of BMP-2. VICs adopt an osteoblastic phenotype resulting in greater expression of alkaline phosphatase and osteocalcin,

increase in matrix mineralisation and formation of calcific nodules. The contradictory effects of RANK/RANKL in bone marrow and valve tissue may in part be due to the presence of a pre-osteoclast population of cells in bone which favours pro-osteoclastic activities, whereas no such pool exists in the vasculature and pro-osteoblastic effects prevail. The paradox is exemplified in OPG-deficient mice that suffer from osteoporosis but also exhibit accelerated vascular calcification (Bucay N *et al*, 1998). In stenotic aortic valves, there appears to be reduced OPG expression and increased levels of RANKL (Kaden JJ *et al*, 2004)

Ectonucleotide pyrophosphate 1 (ENPP1) is manufactured by VICs in order to regulate extracellular production of inorganic phosphate. ENPP1 is highly upregulated in calcific aortic valve disease and a polymorphism to this effect is found in diseased valves. ENPP1 results in the hydrolysis of adenosine triphosphate (ATP) and production of inorganic phosphate. Depletion of ATP induces cell apoptosis and further stimulates ENPP1 production in a positive feedback loop. This may be another important mechanism by which the cycle perpetuates such that 'calcium begets calcium' (Cote N *et al*, 2012)

Fibrosis

Fibrotic remodelling is a consistent finding in histological studies of aortic stenosis and leads to increased stiffening of the valve cusps, escalation of adverse mechanical stress and contributes to calcification of the valve (Lindman BR *et al*, 2016; Otto *et al*, 1994). Under the influence of cytokines, integrin expression and TGF-beta 1, activated myofibroblasts in the diseased aortic valve increase production of collagen, alpha-

smooth muscle actin and extracellular matrix proteins such as tenascin-C and proteoglycans. Angiotensin converting enzyme is also believed to play an important role. It is delivered to the valve tissue by LDL, where chymases and cathepsin G (produced by mast cells) promote conversion of angiotensin I to angiotensin II. The latter is a potent driver of vascular inflammation and fibrosis. Recent studies have further implicated altered expression of regulating proteins including Klotho and plasminogen activator inhibitor in directing this process (Chen J *et al*, 2018; (Chen J *et al*, 2016).

The relationship between aortic valve calcification and haemodynamic stenosis is imperfect, and there are patients in whom significant aortic stenosis develops in the absence of notable calcification. This has been observed, in particular, in younger female patients and those with bicuspid aortic valves. Fibrosis may therefore be an important but under-appreciated mechanism in the pathogenesis of aortic stenosis that merits closer attention.

FIGURE 1.1.

Proposed mechanisms in the pathogenesis of aortic stenosis

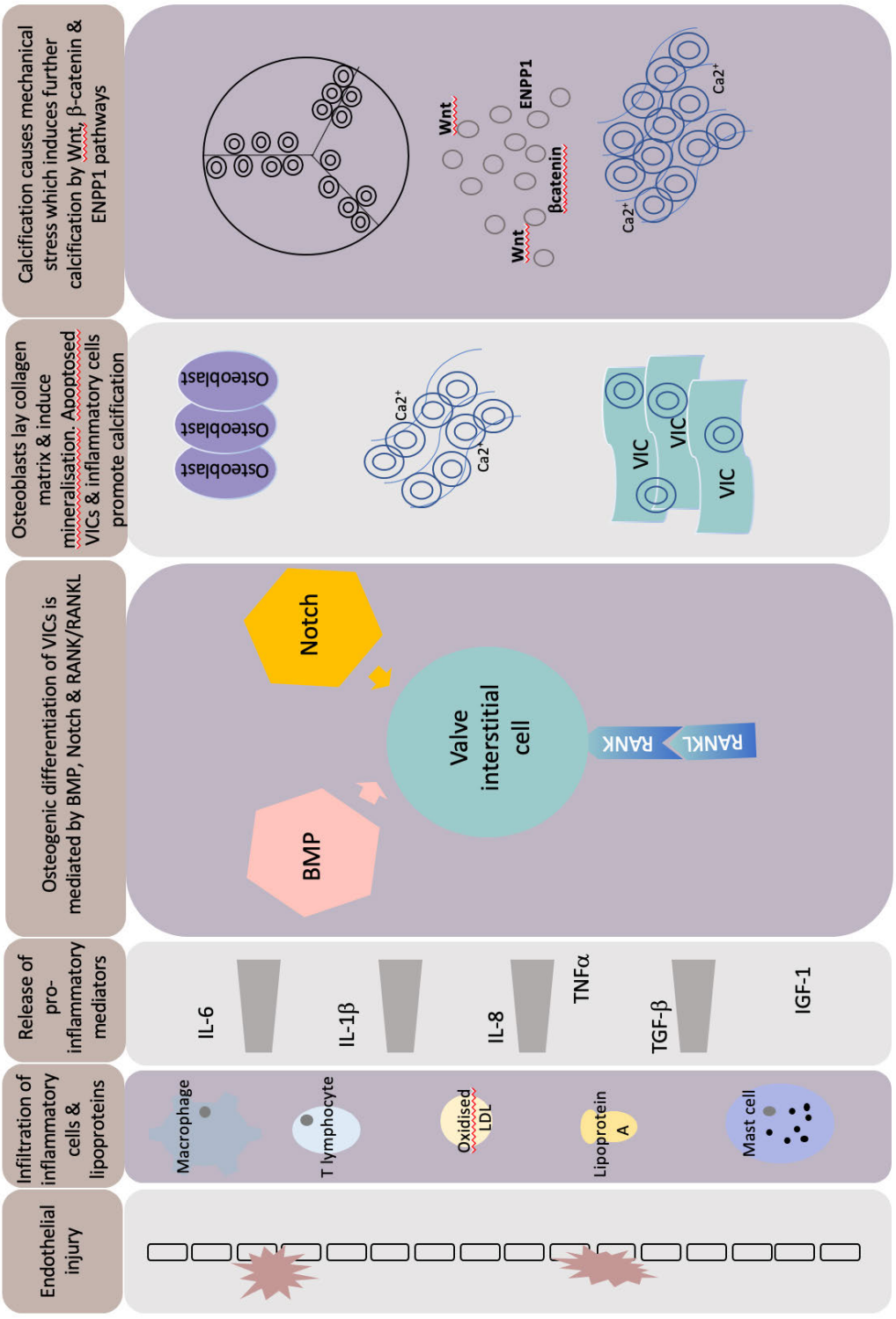

BMP = bone morphogenetic protein; ENPP1 = ectonucleotide pyrophosphate 1; LDL = low-density lipoprotein; RANK = receptor activator of nuclear kappa B; RANKL = receptor activator of nuclear kappa B ligand; VIC = valvular interstitial cell. (Adapted from Pawade *et al*, JACC 2015)

Clinical Imaging in Native Aortic Valve Stenosis

Doppler echocardiography, computed tomography (CT) and more recently positron emission tomography (PET) have all been employed to help characterise native aortic valve stenosis. Together these imaging modalities have informed our understanding of disease aetiology, underpin the assessment of disease severity, and help us to predict both haemodynamic progression and clinical outcomes.

Echocardiography

Echocardiography is well established as a mainstay of routine clinical assessment in aortic stenosis. Doppler ultrasound can be used to examine the jets of stenotic valves and to measure the peak and mean aortic valve gradient with good reproducibility. These values demonstrate good agreement with invasive haemodynamic measurements (Holen *et al*, 1976) and offer strong prediction of the need for intervention and adverse cardiovascular outcomes (Otto *et al*, 1997; Bohbot *et al*, 2017). Additionally, echocardiography can provide helpful anatomic detail about aortic valve morphology, severity of fibro-calcification, the structure of the aorta and the left ventricular response to aortic stenosis. Furthermore, it is widely available, inexpensive, non-invasive and does not utilise radiation.

Current guidelines recommend the assessment of aortic valve stenosis based upon peak velocity, mean gradient, and aortic valve area. Whilst peak aortic jet velocity may offer superior reproducibility, both peak jet velocity and mean gradient are intrinsically dependent on flow status. Derived aortic valve area (calculated by the continuity

equation) is independent of flow status, however, is subject to inconsistencies in measurement of the left ventricular outflow tract with even minor differences resulting in significant discrepancy.

In light of the above, there is often disagreement between echocardiographic measurement of disease severity, in around one third of patients (Clavel *et al*, 2013). This is seen in patients with impaired left ventricular ejection fraction, termed 'low-flow, low gradient' aortic stenosis, in whom the peak velocity and mean gradient may be below the threshold for severe stenosis (<4 et al and <40 mmHg respectively), but the calculation of aortic valve area suggests severe stenosis (<1 cm^2). In this setting, augmenting left ventricular function with an intravenous infusion of dobutamine and repeating the echocardiographic assessment can be helpful. Nonetheless, a significant proportion of patients with discordant echocardiographic parameters have normal flow status and this makes interpretation of disease severity problematic.

Computed Tomography Aortic Valve Calcium Scoring

Aortic valve calcification is the dominant macroscopic feature of aortic stenosis resulting in valvular obstruction. Echocardiography may be used to provide a subjective quantification of aortic valve calcification, although this is limited by suboptimal reproducibility. Computed tomography (CT) aortic valve calcium scoring has therefore emerged as a complementary tool in the assessment of aortic stenosis that is accurate, highly reproducible and independent of flow status (Messika-Zeitoun D, *et al*, 2004).

Employing a similar protocol as that developed for CT coronary artery calcium scoring, a non-contrast and ECG-gated acquisition can be used to quantify calcium using the Agatston technique. This provides information with respect to the volume, mass and weighted density of calcium. With the recognition of the need for sex-specific thresholds to determine severe stenosis (Aggarwal *et al*, 2013), CT aortic valve calcium scoring correctly classifies severe aortic stenosis with a sensitivity >86% and specificity >79% (Clavel *et al*, 2013). These thresholds have been validated in a multicentre cohort of over 900 patients (Pawade *et al*, 2018). Furthermore, CT aortic valve calcium score independently predicts clinical events including aortic valve replacement and cardiovascular death (Tastet L *et al*, 2017). Although CT aortic valve calcium scoring is not currently recommended for disease surveillance in the clinical setting, recent European Society of Cardiology guidelines advocate its use to adjudicate disease severity in patients with discordant echocardiographic findings and normal flow (Baumgartner H *et al*, 2017).

CT aortic valve calcium scoring does have several important limitations. First, non-contrast CT imaging offers little detail about valve morphology and is unable to localise the anatomical distribution of calcium in the valve and surrounding structures. Second, it is unable to detect or quantify fibrosis, an important contributor to valve stenosis, and may therefore misclassify disease severity, particularly in young women and those with bicuspid valves (Shen *et al*, 2016; Simard *et al*, 2016). Third, it demonstrates only a moderate correlation with haemodynamic severity on echocardiography and different severity thresholds are required in the two sexes, with women consistently demonstrating lower calcium burden for a given degree of

valvular stenosis even after correction for body size (Clavel *et al*, 2013; Clavel *et al*, 2014; Pawade *et al* 2018).

Contrast CT angiography is widely used to assess and to quantify both calcific and non-calcific plaques in the coronary vasculature (Dweck *et al*, 2016). It may therefore be possible to apply a similar approach to the aortic valve, allowing evaluation of aortic valve calcium burden and also fibrotic leaflet thickening. The development of such a technique would have potential to provide novel insights into the pathogenesis of aortic stenosis and improve the quantification of disease severity.

FIGURE 1.2.

Contrast-enhanced computed tomography in the assessment of aortic stenosis:

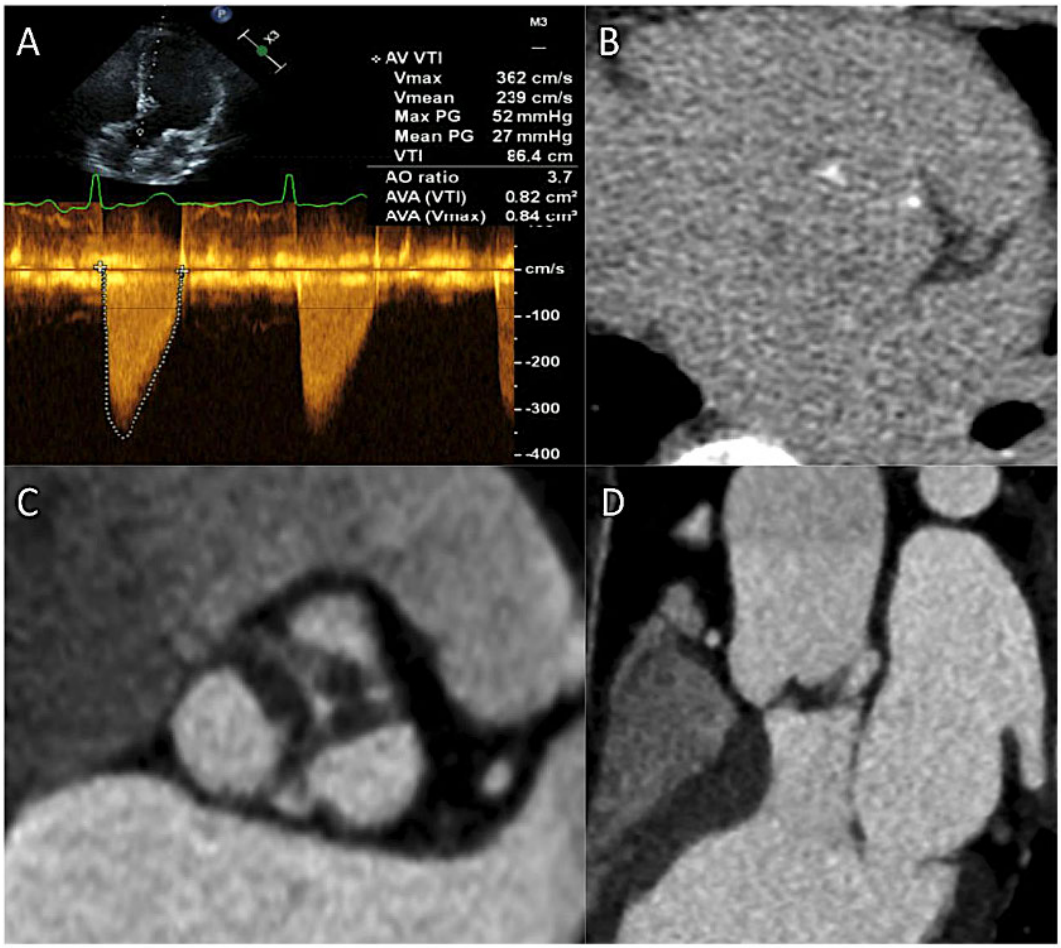

Figure 1.2. Doppler echocardiography assessment of the aortic valve demonstrating moderate aortic stenosis (A), non-contrast CT axial image of the aortic valve showing only minor calcification (B), contrast-enhanced CT en-face image (C) and long axis image of the aortic valve illustrating significant non-calcific thickening of the valve cusps (D).

Positron Emission Tomography

Positron emission tomography (PET) is a novel imaging technique in the assessment of aortic stenosis. PET is a functional imaging modality which utilises administration of a radioactive ligand to detect and quantify metabolic processes in the body. In combination with computed tomography (CT), PET-CT provides information about disease activity allied with detailed anatomical localisation.

Radiolabeled sodium fluoride has long been used as a radioactive tracer in the skeleton but has more recently been employed successfully to assess vascular calcification (Dweck MR *et al*, 2012 b; Forsythe RO *et al*, 2018; Joshi NV *et al*, 2014). ^{18}F-Fluoride exchanges hydroxyl groups in hydroxyapatite to produce fluoroapatite, and thus detects calcification. Availability of hydroxyl binding sites is greatest in immature nanocrystalline forms of calcium phosphate and as such ^{18}F-fluoride has higher affinity for regions of newly developing microcalcification (Irkle A *et al*, 2015). In clinical studies, ^{18}F-fluoride binding is increased in the aortic valves of patients with aortic stenosis when compared to a healthy population, and measures of ^{18}F-fluoride uptake correlate positively with echocardiographic measures of disease severity (Dweck *et al*, 2012). Interestingly, ^{18}F-fluoride binding in the aortic valve was often spatially distinct from calcium deposits apparent on CT, and new macroscopic calcification later became apparent in these regions on 1 and 2-year follow-up CT. This suggests that ^{18}F-fluoride PET offers information about calcification activity beyond the resolution of CT and that it has the potential to predict disease progression. Accordingly, ^{18}F-fluoride uptake has been found to correlate closely with change in aortic valve calcium score over time and moderately with the haemodynamic progression of aortic stenosis.

After almost 5 years of follow-up, ^{18}F-fluoride emerged as an independent predictor of aortic valve replacement and cardiovascular mortality (Jenkins *et al*, 2015).

Whilst ^{18}F-fluoride PET holds promise as a sensitive marker of disease activity, it is not likely to find a major role in routine clinical practice due to the limited provision of PET imaging facilities, the relative expense when compared to echocardiography and CT aortic valve calcium scoring, and the accompanying radiation exposure. The most advantageous application of PET-CT in aortic stenosis is therefore likely to be within a research setting to provide an early measure of the efficacy of novel treatments. Indeed, in bone imaging, significant changes in ^{18}F-fluoride uptake can be detected after ~1 month of bisphosphonate treatment (Installé J *et al*, 2005). However, before ^{18}F-fluoride PET-CT can be employed as an outcome measure of therapeutic efficacy in randomised controlled trials, the methodology for image acquisition and analysis must be optimised and the accuracy and reproducibility assessed.

FIGURE 1.3.

^{18}F-Fluoride PET-CT predicts new aortic valve calcification in aortic stenosis

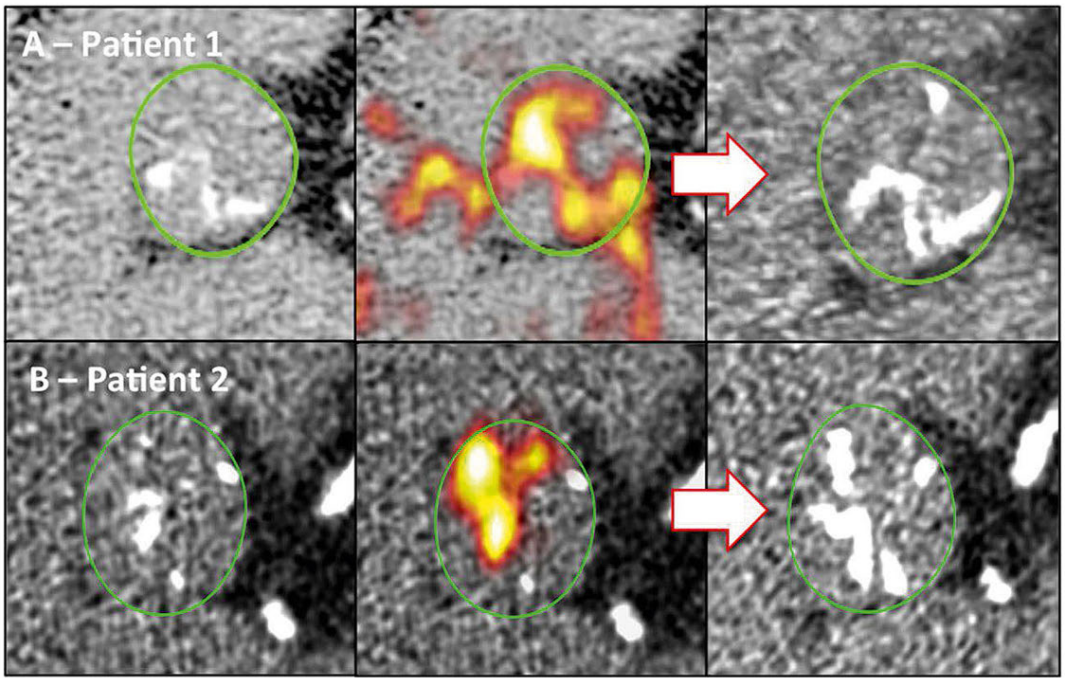

Figure 1.3. Baseline CT calcium scores (left) for patients 1 and 2 (top and bottom). Fused coaxial ^{18}F-fluoride PET-CT scans (middle) show fluoride uptake in red and yellow. The 1-year follow-up (right) suggests that the baseline PET signal predicts the spatial distribution of subsequent macrocalcification. (Dweck *et al*, 2014)

1.3 BIOPROSTHETIC VALVE DISEASE

Epidemiology of Bioprosthetic Valves

Patients with valvular heart diseases are living longer and with a better quality of life than at any time in the past as a result of advances in the design of prosthetic heart valves and related clinical care. Prosthetic valves may be categorised as either mechanical or bioprosthetic, and these differ from one another in terms of longevity, thrombogenicity and haemodynamic performance (Bloomfield PB *et al*, 1991). In the present era, it is estimated that between 300,000 and 400,000 heart valve replacements are performed each year worldwide (Fiedler AG *et al*, 2018). There has been a significant transformation in practice over recent decades such that the majority of implanted valves are now bioprosthetic rather than mechanical. For example, bioprosthetic valves accounted for 43.6% of surgically implanted aortic valves in North America in 1997, rising to 78.4% in 2006 (Brown *et al*, 2009). The use of bioprostheses has perhaps increased due to a combination of patient preference (opting for improved durability allied to the lower risk of bleeding complications), the increasing prevalence of valve disease in the ageing population, and the emergence of transcatheter aortic valve replacement (Iung B *et al*, 2011; Nkomo VT *et al*, 2006). Consequently, more patients with bioprosthetic valves are under surveillance and complications related to bioprosthetic valves are an increasing clinical problem.

FIGURE 1.4.

Classification of bioprosthetic heart valves

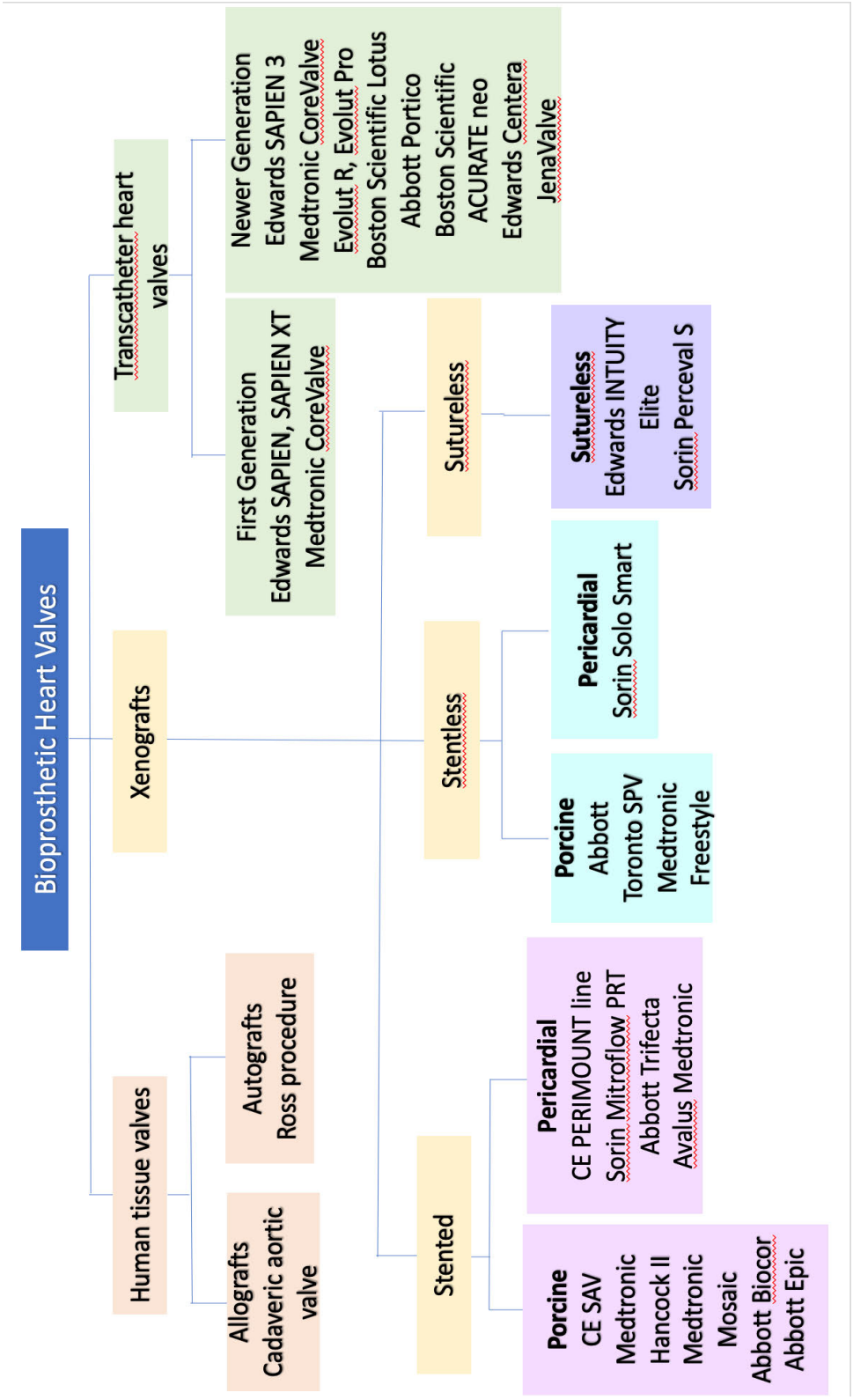

History of Bioprosthetic Valves

Bioprosthetic valves can be composed of either human tissue (allografts and autografts) or animal tissue (xenografts). Xenograft bioprosthetic valves are manufactured from either bovine pericardial or porcine tissue and can be stentless or mounted on a stent. The first xenograft replacement aortic valve was successfully implanted in 1965 in Paris by Carpentier and his team. However, the early porcine valves suffered from a high rate of failure with ~45% functioning well at 1 year (Carpentier A *et al*, 1969). Whilst there were some technical surgical reasons for valve failure, there was also histological evidence of an immune response. Subsequent work identified glutaraldehyde to be effective in reducing, although not eliminating, the antigenicity of xenograft valves. This led to improvements in valve durability, from ~45% to ~82% functioning well at 1 year (Carpentier A *et al*, 1969). The success of glutaraldehyde-fixed bioprosthetic heart valves resulted in commercialisation and increasingly widespread use.

Modern xenograft surgical valves are predominantly of the stented type, comprising 3 porcine or bovine pericardial tissue leaflets mounted on a stent frame made from alloy or polymer, and a circular fabric-covered external sewing ring that provides an anchor to the aortic annulus. Stentless valves constitute a preserved porcine aortic valve and aortic root removed *en block* that can be individually tailored to each patient for sub-coronary implantation, a mini-root or full root replacement. In theory, the absence of an external sewing ring in stentless valves offers a greater effective orifice area and superior haemodynamic performance. The most commonly used transcatheter valves to date have been the Edward's Sapien and Medtronic Corevalve series. The Edwards

Lifesciences Sapien consists of bovine pericardial leaflets sutured within a balloon-expandable cobalt chromium stent frame, whereas the Medtronic Corevalve consists of porcine pericardial leaflets sutured in a supra-annular position to a self-expanding nitinol stent frame.

Diagnosis and Definition of Bioprosthetic Valve Degeneration

Structural valve degeneration is a gradual process leading to valve dysfunction secondary to prosthetic valve stenosis (40%), regurgitation (30%), or a combination of both (30%) (Cote N *et al*, 2017). Historically, most surgical studies have associated valve degeneration with the need for reoperation, but without specific criteria to define structural valve degeneration. Given that reoperation does not necessary imply structural valve degeneration, and that patients with structural valve degeneration are often not suitable for redo-surgery, one would expect an underestimation of the true incidence if defined only on the basis of reoperation. A systematic assessment of prosthetic valve morphology and function may more accurately describe the true prevalence of structural valve degeneration.

Despite the considerable experience reported with different types of surgical bioprostheses, there are widely ranging definitions of structural valve degeneration and varying criteria have been suggested based upon evaluation of haemodynamic performance by Doppler echocardiography. One proposed definition for bioprosthetic structural valve degeneration according to echocardiographic criteria included increase in the transvalvular aortic gradient with mean gradient ≥30 mm Hg associated with an effective orifice area ≤1 cm^2, or prosthetic aortic regurgitation grade ≥3

(Senage T *et al*, 2014). Another contemporaneous study defined structural valve degeneration of aortic surgical bioprostheses as severe aortic stenosis with mean gradient >40 mm Hg, or severe prosthetic regurgitation (Bourgignon T *et al*, 2014). Alternatively, one group recommended structural valve degeneration be recognised by an increase in mean gradient ≥20 mm Hg with a concomitant decrease in effective orifice area and/or a progression of intraprosthetic regurgitation by at least 1 grade (Mahjoub H *et al*, 2013). The more recent European Association of Cardiovascular Imaging guidelines suggest defining structural valve degeneration using the following criteria: (i) an increase in mean gradient ≥10 mm Hg (possible valve degeneration) or ≥20 mm Hg (significant valve degeneration) during follow-up, with a concomitant decrease in effective orifice area and abnormal valve leaflet morphology and mobility; and/or (ii) new onset or worsening transprosthetic regurgitation (Lancellotti P *et al*, 2016). Structural valve deterioration was defined upon quite similar criteria by the European Association of Percutaneous Cardiovascular Interventions, with severe structural valve deterioration identified by any of mean transprosthetic gradient ≥40 mm Hg, an increase in mean transprosthetic gradient ≥20 mm Hg from baseline, and new or worsening severe intraprosthetic regurgitation (Capodanno D *et al*, 2017).

An alternative definition of bioprosthetic valve degeneration and dysfunction has been proposed in a recent expert consensus statement, and for the first time, references the complementary role of computed tomography in the detection of early degenerative changes. Stage 1 is characterised by morphological abnormality (detected on echocardiography or computed tomography) in the absence of haemodynamic changes; stage 2 is characterised by the presence of either moderate valve obstruction,

moderate regurgitation or both; and stage 3 is characterised by the presence of either severe valve obstruction or regurgitation. Central to this definition is a dynamic change, for example, new valve obstruction should be accompanied by a change in mean gradient >10 mmHg associated with a decrease in Doppler velocity index and effective orifice area (Dvir D *et al*, 2018).

In light of the above definitions of bioprosthetic valve degeneration, a robust assessment of valve morphology and function at baseline is therefore fundamental along with ongoing interval surveillance. This is reflected in international guidelines which strongly recommend an initial transthoracic echocardiogram for evaluation of valve haemodynamics following prosthetic valve implantation (Otto C *et al*, 2021; Baumgartner H *et al*, 2017). At follow-up, guidelines suggest echocardiography in response to any change in clinical symptoms or signs suggesting valve dysfunction, with routine annual echocardiography recommended by the European Society of Cardiology (Baumgartner H *et al*, 2017), and echocardiography at 5 years then annually from 10 years post-implantation by the American College of Cardiology / American Heart Association (Otto C *et al*, 2021). Depending on approach, it is possible that subclinical changes in prosthetic valve hemodynamic performance go undetected for some time.

FIGURE 1.5.

Expert consensus statement: Definition of structural valve degeneration and clinical approach to patients with bioprosthetic valves

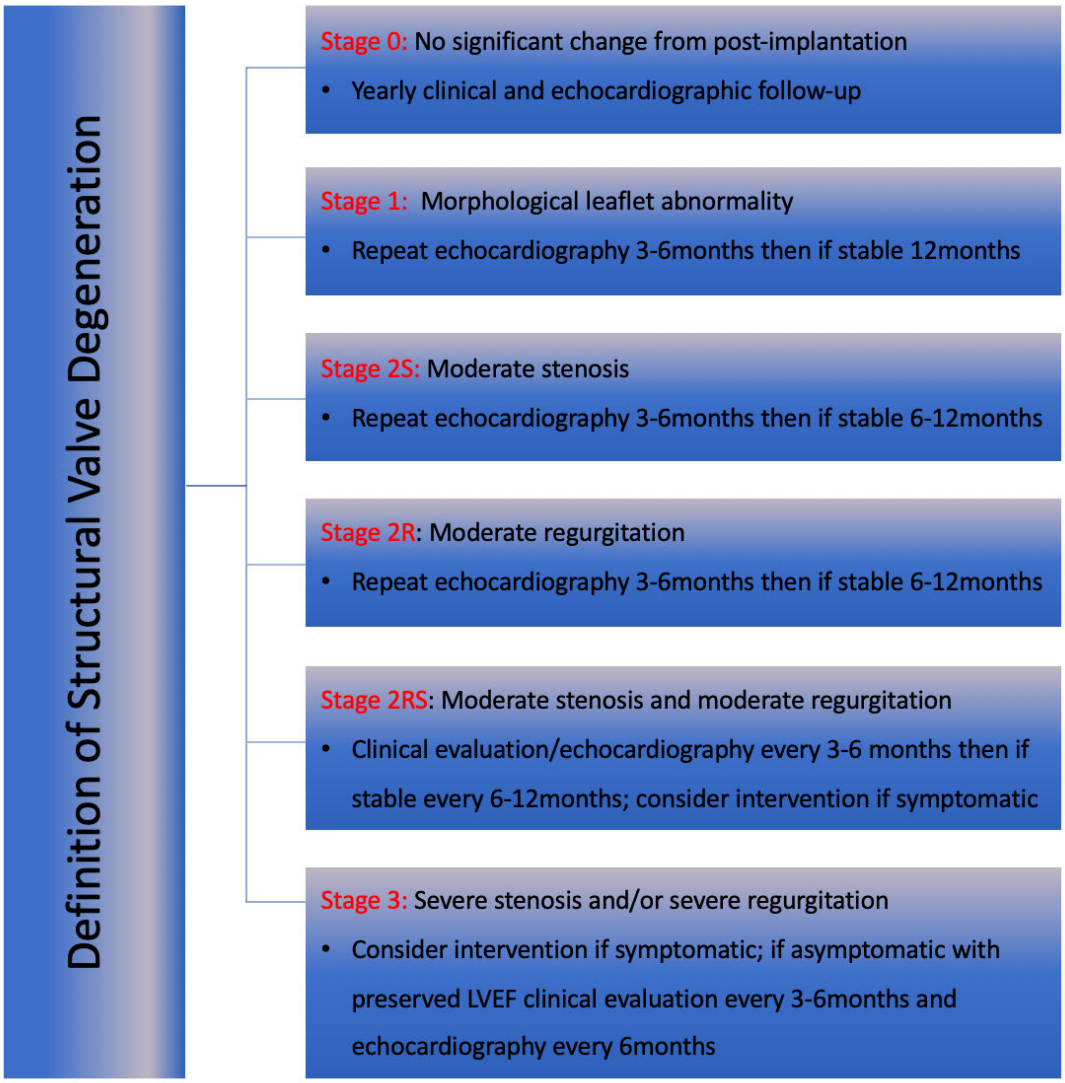

*Structural valve degeneration excludes endocarditis, valve thrombosis and isolated patient-prosthesis mismatch. (Adapted from Dvir *et al*, Circulation 2018)

Durability of Bioprosthetic Valves

Finite durability is the chief limitation of bioprosthetic valves when compared to mechanical prostheses. There are several inherent challenges when assessing the long term performance of contemporary valves. First, reporting of valve durability often relates to specific models of prosthesis, and the progress of valve technology is such that data about outcomes 15-20 years after implantation are published when newer models have already superseded them in clinical practice. Moreover, the duration of follow-up and criteria for defining valve dysfunction vary widely and so make direct comparisons very difficult.

Surgically Implanted Bioprosthetic Valves

Bioprosthetic valve degeneration is generally slow, gradual and time dependent (Bloomfield P *et al*, 2001). After implantation of 1,315 first generation Carpentier-Edwards porcine bioprosthetic valves in the aortic and mitral positions, <1% demonstrated dysfunction within 5 years, 20-30% within 10 years, and >50% failed as a consequence of structural valve degeneration with 12-15 years (Jamieson W *et al*, 1995). In a rare prospective study of 1,134 patients who underwent aortic valve replacement with the Medtronic Hancock II second generation porcine stented bioprosthesis, ~98% were free from structural valve deterioration (defined by echocardiography or need for reoperation) at 10 years, ~87% at 15 years and ~63% at 20 years (David TE *et al*, 2010).

In a more contemporary study of 12,569 patients undergoing aortic valve replacement with a Carpentier-Edwards Perimount stented bovine pericardial valve, the rate of

explant for structural valve deterioration was 1.9% at 10 years and 15% at 20 years. The rate of explant does not, however, take account of patients with earlier stages of valve dysfunction or who were unsuitable for reoperation, and in this study ~3.3% of patients had structural valve deterioration without reoperation (Johnston DR *et al*, 2015). In slight contrast, another study of the same valve type implanted in 2,405 patients of similar age reported freedom from valve reoperation at 10 years of ~96% and at 20 years of ~67%. Despite discrepancies, these data on the long term performance of modern bioprostheses are generally encouraging.

Within surgically implanted bioprostheses, stented models most commonly fail as a result of late calcification and stenosis. Stentless valves display similar rates of structural degeneration to stented valves but with a predilection to develop valvular regurgitation over stenosis (Dvir D *et al*, 2012). Complications of degenerating stentless grafts can also include aortic wall calcification and stenosis, aortic dilatation or a nidus for systemic embolism (Siddiqui RF *et al*, 2009). Allografts tend to be used in select clinical scenarios, such as the setting of endocarditis or complex aortic anatomy, and often in younger patients. In one study of 353 patients undergoing aortic valve replacement with an allograft, with mean age 45 years, the rate of reoperation for structural valve deterioration over 12 years follow-up was ~28% (Arabkhani B *et al*, 2016).

Transcatheter Bioprosthetic Valves

Potential differences in the long term durability of transcatheter valves in comparison to surgical bioprostheses have been a source of extensive speculation. It has been

hypothesised that crimping of the valve cusps during transcatheter delivery may result in disruption of collagen structure and so accelerate valve degeneration (Alavi SH *et al*, 2014). The commissural cusp attachment to a rigid stent frame in transcatheter valves rather than the flexible stent post in stented surgical valves might also negatively impact on dissipation of mechanical stress. Furthermore, severe calcification of the native aortic valve cusps and annulus may lead to suboptimal deployment and paravalvular leaks after transcatheter valve implantation, with a negative impact on long term durability (Arsalan M *et al*, 2016). Alternatively, there has been early evidence that transcatheter valves produce superior haemodynamic results to surgical valves and thus lower rates of patient-prosthesis mismatch, which is known to affect longevity (Pibarot P *et al*, 2014).

The long term durability of transcatheter valves is particularly difficult to assess for a number of reasons. Transcatheter valve delivery was until recently a novel technology in the hands of inexperienced operators, with both valve technology and operator expertise having progressed rapidly since FDA approval in 2011. Moreover, the patient population is generally elderly with multiple-morbidities and so there is a scarcity of patients available for long term follow-up. Nonetheless, data up to 5 years from the PARTNER trials with the Edwards SAPIEN valve demonstrate comparable haemodynamic performance to surgical bioprostheses, other than a higher rate of paravalvular regurgitation, and the absence of structural valve degeneration (Mack MJ *et al*, 2015; Kapadia SR *et al*, 2015; Daubert MA *et al*, 2017). In the NOTION trial, randomising low risk patients to either surgical aortic valve replacement or transcatheter valve implantation with the Medtronic Corevalve self-expanding valve,

there was no difference in the composite primary endpoint of all-cause mortality, stroke or myocardial infarction (36.3 versus 38.0% respectively, p=0.86), though the transcatheter cohort suffered higher rates of moderate/severe aortic regurgitation and requirement for permanent pacing (Thyregod HGH *et al*, 2019). Analysis of the FRANCE-2 Registry suggested the incidence of severe structural degeneration to be 2.5% and of moderate/severe structural degeneration to be 13.3% at 5 years (Didier R *et al*, 2018). Data from the UK TAVI Registry, with a mean follow-up of 5.8 years, demonstrated an incidence of 0.4% for severe structural valve degeneration and 8.7% for moderate structural valve degeneration (Blackman D *et al*, 2019).

Pathophysiology of Bioprosthetic Valve Degeneration

Calcification

Unfortunately, the pathophysiology of bioprosthetic valve degeneration is incompletely understood, largely because of the difficulty in obtaining tissue specimens in early disease. Nonetheless, calcification is the dominant histological feature of explanted degenerated valves. In one series of explanted porcine bioprostheses, more than 50% demonstrated calcific deposits within 3 years of implantation with a preponderance for the commissural and basal regions of the valve cusps, where mechanical stress is greatest (Butany J *et al*, 2001). Calcification may lead to valve stenosis as a consequence of progressive cusp immobility or lead to regurgitation as a consequence of cusp tears, perforation or commissural dehiscence (Schoen F *et al*, 1987; Allard M *et al*, 1995).

Bioprosthetic valve calcification is believed, at least in part, to occur as a consequence of pre-treatment with glutaraldehyde which results in cross-linking of collagen and availability of free aldehyde groups. Phosphorus on free aldehyde groups then interacts with circulating calcium after implantation to initiate calcium phosphate aggregates (Schoen F *et al*. 1999). Devitalisation of tissue during glutaraldehyde fixation also releases calcium and membrane-associated phospholipids from damaged cells which form the nidus for further nucleation of calcium phosphate within the valve cusps. Over time these deposits expand and coalesce, ultimately resulting in valve dysfunction.

Manufacturers have appreciated the less favourable effects of glutaraldehyde fixation and explored alternative cross-linking pre-treatments, such as dye-mediated photofixation and carbodiimide-based fixation. These show promise in the prevention of tissue calcification but have not translated into clinical use (Simionescu DT *et al*, 2004). Instead, most current generation bioprostheses are now treated with anti-mineralisation preparations such as ethanol or alpha-oleic acid. Alpha-oleic acid covalently bonds to residual aldehyde groups and so reduces the binding of calcium (Chen W *et al*, 1994). Intriguingly, observations suggest that some anti-mineralisation treatments protect the valve cusps from calcification but not the aortic wall of stentless valves. This may be because elastin is the principal substrate for calcification in the aorta (Schoen FJ *et al*, 2005).

Beyond the passive initiation of calcification via interaction of circulating calcium and the components of devitalised xenograft tissue, bioprosthetic valve calcification is

thought to be actively mediated by atherosclerotic-like pathways including infiltration of oxidised lipid. Accordingly, the development of structural valve degeneration has been associated with higher levels of plasma low-density lipoprotein-cholesterol and apolipoprotein B (Mahjoub H *et al*, 2013). Bioprosthesis calcification is, furthermore, thought to become orchestrated in a fashion similar to the physiological mineralisation of bone. For example, the regulatory proteins osteopontin, tissue growth factor-alpha and tenascin-C have been demonstrated in calcified porcine bioprostheses as well as in stenotic native aortic valves (Srivasta SS *et al*, 1997).

Other factors predisposing to bioprosthetic valve calcification are thought to be dysregulation of calcium-phosphate metabolism, such as that found in chronic renal disease or parathyroid tumours, and increased valvular mechanical stress, as in the setting of arterial hypertension or patient-prosthesis mismatch (Butany J *et al*, 2001). Small prosthesis size and the aortic position are both associated with greater mechanical stress and accelerated mineralisation (Reul Jr GJ *et al*, 1985). Likewise, various valve design features which result in suboptimal distribution of haemodynamic stress have been found to profoundly affect valve durability. For example, one low profile porcine bioprosthesis had a reduced free edge angle rendering it less effective in dissipating mechanical stress and was discovered to suffer from premature calcification and failure (Vesely I *et al* 2003).

Immune Reaction

A number of studies have presented evidence of a pathway involving immune rejection, inflammation and ultimately calcification of bioprosthetic valves. Whilst

glutaraldehyde fixation reduces xenograft antigenicity, it does not wholly eliminate it (Pibarot *et al*, 2009). Animal model studies show that xenogeneic implants, even when pre-treated with glutaraldehyde, are associated with greater histological evidence of adventitial inflammation, and humoral and cellular immune infiltrates when compared to syngeneic implants. The subsequent extent of calcification correlated with the immune cell infiltrate (Manji RA *et al*, 2006). Similarly, in humans, the role of the immune system response to xenografts is highlighted by histological evidence of accumulation of IgM and IgG, incursion of macrophages, cytokine release, collagen breakdown and tissue calcification (Konakci K *et al*, 2005).

Galactose-alpha1,3-galactose (Gal) has long been considered the most important antigen in porcine tissue with respect to stimulating xenograft rejection in humans. Gal antigens are present on commercially available porcine bioprosthetic valves and after implantation are associated with an increase in circulating anti-Gal host antibodies (Bloch O *et al*, 2011). The Gal-related immune reaction is also linked to calcification. One study compared implantation of pericardium from Gal knock-out pigs and wild type pigs in rats, with the pericardium from Gal knock-out pigs calcifying less than that from wild-type pigs (Lila N *et al*, 2010). The anti-Gal IgM and IgG responses are, however, lower when grafts have undergone fixation and decellularisation (Lim HG *et al*, 2013). Ultimately, elimination of Gal antigens has not been sufficient to prevent rejection in pig organ xenotransplantation as non-Gal antigens also appear to be influential.

Although contentious, if an immune response were implicated in degeneration of porcine and bovine valves, this would help to account for the accelerated structural valve degeneration observed in younger patients, who are more immunologically active. Certainly, the incidence of bioprosthetic valve calcification appears to be strongly associated with age (Reul Jr GJ *et al*, 1985). In those over the age of 65 years, <10% of bioprosthetic valves failed within 10 years whereas in those under the age of 35 years, valve failure was almost uniform by 5 years (Siddiqui RF *et al*, 2009). Higher haemodynamic stresses in more physically active young people and the greater competence of the immune system in young people are both speculated to contribute (Milano A *et al*, 1998).

The counter argument to the role of the immune system in valve degeneration cites experiments in which xenograft valve tissue has been implanted in athymic mice and in filter chambers that prevent host cell contact but allow free diffusion of extracellular fluid. The resulting pattern and extent of calcification in xenograft tissue is no different from that seen when implanted directly into wild-type mice (Levy RJ *et al*, 1983). Antibody infiltrates could therefore be a secondary response to valve damage rather than a cause of degeneration.

Pannus

Bioprosthetic valves undergo rapid endothelialisation after implantation, which helps to protect them from leaflet thrombosis. Pannus refers to the proliferation of host endothelial, fibroblast and myofibroblast cells from the anastomotic margins at the suture line over the prosthesis. This occurs almost invariably to a degree, usually

covering part of the sewing ring of stented valves. However, when pannus spreads over the stent posts and valve cusps themselves this is considered an over-exuberant reaction and can result in prosthesis dysfunction. As the process underlying pannus progresses, collagen deposits mature and lead to thickening, increased stiffness and retraction of tissue. Depending on the pattern of pannus overgrowth, it can therefore impede opening of the cusps resulting in stenosis, cause retraction of one of more cusps resulting in progressive valvular incompetence, or cause adverse redistribution of mechanical stress and consequent cusp tears resulting in acute valvular incompetence (Butany J *et al*, 2001)

Bioprosthetic Valve Thrombosis

Overt prosthetic valve thrombosis is unusual in the case of both patients with bioprosthetic valves and mechanical valves receiving therapeutic anticoagulation, with a reported incidence of 0.1-5.7% per patient year (Freeman R *et al*, 2005). The risk is highest during the first 3 months after implantation, greater when the prosthesis is implanted in the mitral position, and in those patients with atrial fibrillation, severe left ventricular systolic impairment and a history of thromboembolism (Vongpatanasin W *et al*, 1996). Clinically, prosthetic valve thrombosis may present as left ventricular failure, cardiogenic shock or systemic embolism.

Closer scrutiny over the past decade, peaked by the emergence of transcatheter aortic valve implantation and development of 4-dimensional computed tomography, has increased our appreciation of valve thrombosis in bioprosthetic valves. Recognition of bioprosthetic valve thrombosis by transthoracic echocardiography alone is very

limited, detecting only ~13% of cases (Egbe *et al*, 2015). To improve detection, it has been proposed that the combination of a 50% increase in transvalvular gradient from baseline, cusp thickness >2 mm and abnormal cusp mobility on echocardiography are suggestive of valve thrombosis (Egbe *et al*, 2015).

The incidence of thrombosis of transcatheter aortic valves is likely to be at least 0.6%, with the majority occurring within the first year. Around two thirds of patients presented with progressive breathlessness whilst the remaining third were asymptomatic. Most developed valve thrombosis despite dual antiplatelet therapy although the introduction of oral anticoagulation was almost universally successful in restoring normal valve function (Cordoba-Soriano JG *et al*, 2015).

Under normal circumstances, the intact vascular endothelium appropriately regulates vessel tone and favours an antithrombotic state. However, the presence of a foreign biomaterial leads to adhesion of plasma proteins which promotes adhesion and activation of platelets, thrombin generation and activation of the pro-thrombotic complement system (Jaffer IH *et al*, 2015). Altered flow dynamics are also associated with endothelial damage and thrombosis. High wall shear stress conditions trigger platelet activation, whilst the complex interplay of altered flow patterns and blood stasis around the prosthetic valve predisposes to localised thrombosis (Kopanidis A *et al*, 2015). Wall shear stress is greater in the setting of patient-prosthesis mismatch, and this has been noted to alter simultaneously the configuration of circulating von Willebrand factor and activate the coagulation cascade, promoting both bleeding and

thrombosis. In surgical bioprostheses, patient-prosthesis mismatch has been associated with early stenosis-type structural valve degeneration (Flameng W *et al*, 2010).

The incidence of clinically overt bioprosthetic valve thrombosis has been estimated at ~1.46-1.99% (Puri R *et al*, 2017). Recently, 4-dimensional computed tomography has emerged as a valuable tool for the characterisation of bioprosthetic valves with the ability to detect hypoattenuated leaflet thickening and restricted leaflet motion as evidence of valve thrombosis. In a study of 405 patients following transcatheter valve implantation, hypoattenuated leaflet thickening was observed in 7%, and the majority of these cases were asymptomatic. Of note, valve thrombosis was associated with larger valve size (29 mm) and the absence of oral anticoagulation. In combined studies of surgical and transcatheter bioprostheses within the first 3 months after implantation, the incidence of valve thrombosis was 13-14% in transcatheter valves and half this at 4-7% in surgical valves. There was, however, no difference in haemodynamic measures of valve function and the only clinical correlate was an increased incidence of ischaemic cerebrovascular events in those patients with hypoattenuated leaflet thickening (Makkar RR *et al*, 2015; Chakravarty T *et al*, 2017). Another study suggested that transprosthetic gradients increased more rapidly during follow-up in those with CT features of subclinical valve thrombosis (Rashid HN *et al*, 2018). Subclinical leaflet thrombosis might then be a trigger of inflammation and fibrocalcific remodelling of valve cusps ultimately leading to structural valve degeneration, however, further investigation is required in this regard.

FIGURE 1.6.

Macroscopic photography of explanted bioprosthetic valves illustrating mechanisms of structural degeneration

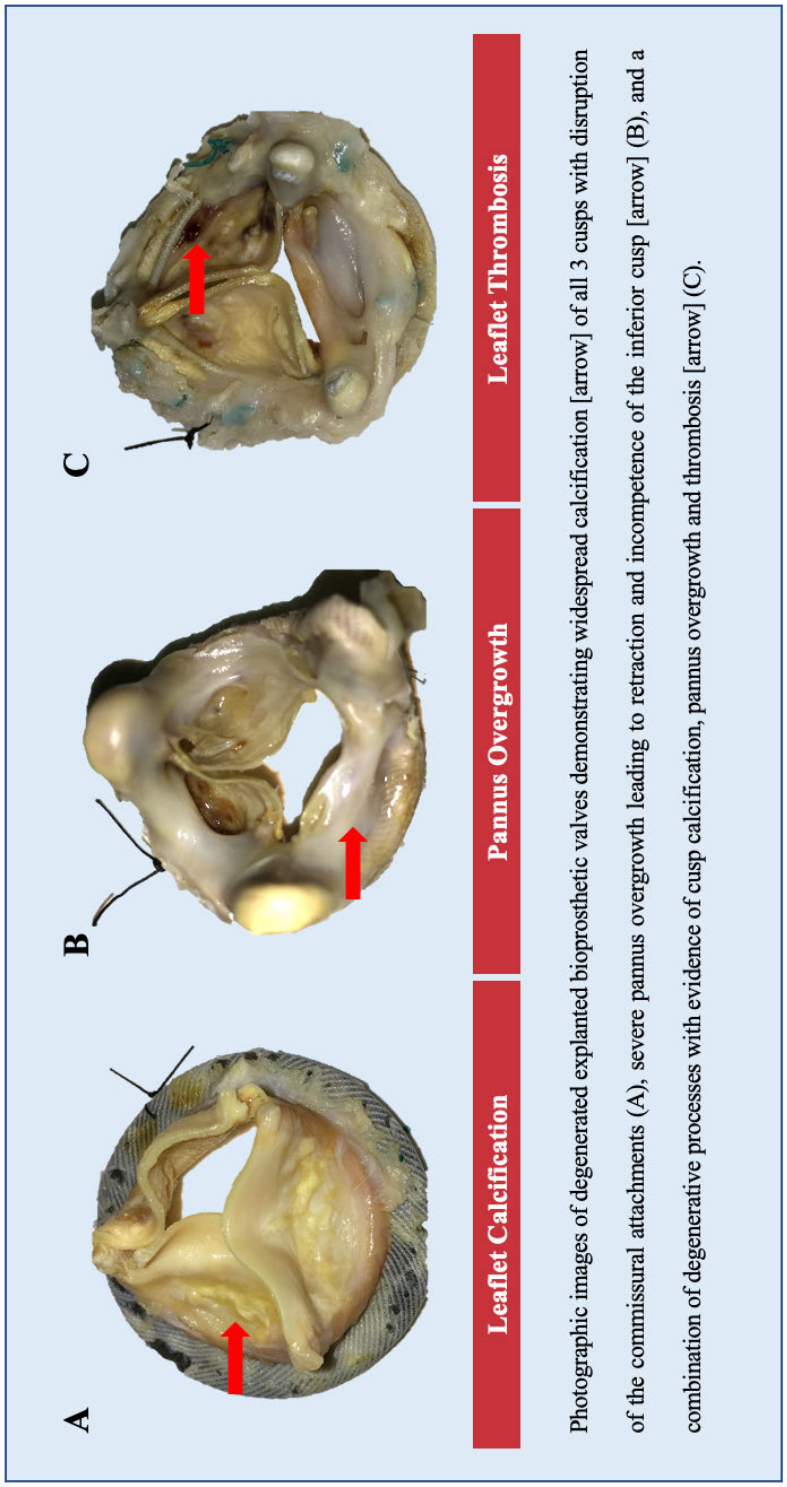

Photographic images of degenerated explanted bioprosthetic valves demonstrating widespread calcification [arrow] of all 3 cusps with disruption of the commissural attachments (A), severe pannus overgrowth leading to retraction and incompetence of the inferior cusp [arrow] (B), and a combination of degenerative processes with evidence of cusp calcification, pannus overgrowth and thrombosis [arrow] (C).

FIGURE 1.7.

Schematic of the mechanisms of bioprosthetic structural valve degeneration

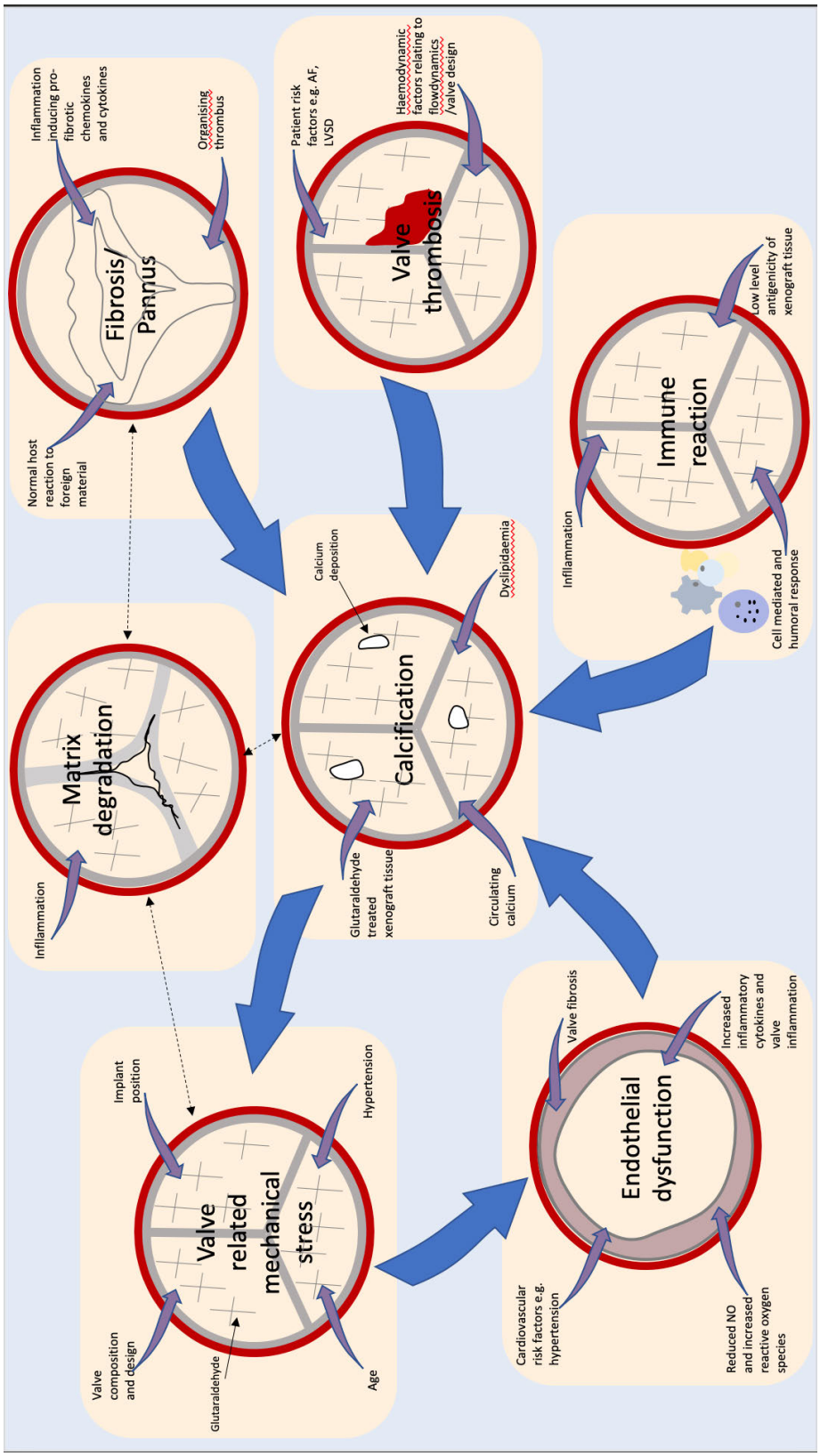

Clinical Imaging of Bioprosthetic Valves

Echocardiography

Transthoracic Doppler echocardiography is the central tool in the assessment of bioprosthetic valves. International guidelines recommend a thorough evaluation be undertaken at baseline and updated in the setting of any new relevant symptoms or clinical signs. Routine surveillance transthoracic echocardiography should then be considered at 5-10 years after valve implantation. Whilst echocardiography is readily accessible and economical, unfortunately image quality is often limited by patient factors and acoustic shadowing from the prosthetic valve. Transoesophageal echocardiography is the next imaging modality of choice when there is reason to suspect prosthetic valve dysfunction or infection. This allows clearer visualisation of the valve cusps and is particularly helpful for localising regurgitant jets. Transoesophageal echocardiography may be able to differentiate infected vegetations from thrombus.

A recent report from the European Association of Cardiovascular Imaging offers recommendations for the assessment of prosthetic valves. First, determining the cause of prosthesis dysfunction is critical and assessment with transthoracic and transoesophageal echocardiography are the mainstays of imaging. Complementary use of computed tomography, fluoroscopy and magnetic resonance imaging should also be considered. Second, echocardiography should include interrogation with Doppler, colour Doppler and in certain instances the use of 3-dimensional echocardiography to better examine cusp pathology and the origin of regurgitant jets. The authors highlight the challenge of assessing the more complex haemodynamics of prosthetic valves,

particularly in some types of mechanical valve, and the potential inaccuracies of estimating the effective orifice area, such as measurement of the left ventricular outflow tract. The Doppler velocity index (peak left ventricular outflow tract velocity / peak aortic jet velocity) is proposed as a particularly helpful measure of prosthetic valve function as there is a linear relationship between the velocity in the outflow tract and implanted valve size. Algorithms are described for the classification of prosthetic valve stenosis, regurgitation and patient-prosthesis mismatch (Lancellotti P *et al*, 2016).

Computed Tomography

Computed tomography is not performed in the routine clinical evaluation of patients with bioprosthetic valves but may provide incremental information to echocardiography when there is a suspicion of valve dysfunction. ECG-gated computed tomography can be undertaken with or without intravenous iodinated contrast medium using a similar protocol to that for computed tomography coronary angiography. If data are acquired throughout the cardiac cycle, then images can be reconstructed during different phases and used to assess motion of the prosthetic valve. Computed tomography may therefore be used to examine the structural integrity of prosthetic valves, to detect leaflet pathology such as calcification, thrombosis or pannus, and to assess the anatomy of the adjacent aorta. Four-dimensional imaging may be used to assess mobility of the valve leaflets, to measure the geometric valve orifice area, and to detect pathological motion of the sewing ring as might suggest dehiscence (Chenot F *et al*, 2010; Lancellotti P *et al*, 2016).

Computed tomography has recently emerged as being of particular value in the assessment of leaflet abnormalities in bioprosthetic valves. Characterisation of tissue density can help to discriminate between pannus and relatively low-density thrombus, with a suggested threshold of 200 Agatston units (Lancellotti P *et al*, 2016). Four-dimensional computed tomography has also contributed greatly to our understanding of leaflet thrombosis in bioprostheses, wherein the combination of >2 mm leaflet thickening and restricted leaflet motion support the diagnosis (Makkar RR *et al*, 2015; Pache G *et al*, 2016).

The limitations of computed tomography include the exposure to ionising radiation and iodine contrast dye, with potential for nephrotoxicity and allergy. Depending on the composition, images may also be degraded by artefact from high density materials present in the construct of a prosthetic valve.

Positron Emission Tomography

Positron emission tomography using the ^{18}F-fluorodeoxyglucose radioisotope has been described in the assessment of suspected prosthetic valve endocarditis and may provide a useful discriminator when other investigations are inconclusive (Nuvoli S *et al*, 2018).

In contrast, ^{18}F-fluoride remains unexplored in the assessment of bioprosthetic valves to date. As described previously, ^{18}F-fluoride positron emission tomography has recently been used to image vascular calcification activity in a range of cardiovascular diseases (Dweck MR *et al*, 2012 b; Forsythe RO *et al*, 2018; Joshi NV *et al*, 2014). It

preferentially signals regions of nascent microcalcification associated with inflammation or tissue degeneration and can be detected before macrocalcification is apparent on computed tomography (Irkle *et al*, 2015). Given that calcification is considered the key pathological process underlying bioprosthetic valve degeneration, we hypothesised that increased ^{18}F-fluoride uptake may identify early subclinical structural valve degeneration before it is visible on either echocardiography or CT and predict subsequent bioprosthetic valve dysfunction.

1.4 SUMMARY

The evolution of aortic stenosis is dominated by progressive valve calcification in the majority, though not all patients. Despite this, the underlying triggers of this process are incompletely understood. There is therefore a mandate for non-invasive assessments that can help to characterise disease mechanisms and evaluate the efficacy of novel therapeutics.

Aortic valve replacement alleviates the bleak prognosis of untreated symptomatic severe aortic stenosis, however, the durability of bioprosthetic valves is finite. The pathogenesis of bioprosthetic valve degeneration is likely to be multi-faceted with calcification as a common end-point but is again not well understood. The natural history of bioprosthetic valve degeneration is such that patients often present late in the disease with acute decompensation. There is therefore an important rationale for assessments that can identify early valve degeneration and predict clinical outcomes.

Novel approaches to contrast-enhanced CT and ^{18}F-fluoride PET-CT will be applied to the assessment of native and bioprosthetic aortic valves to contribute to the understanding and management of aortic stenosis and the structural degeneration of bioprosthetic valves.

1.5 AIMS AND HYPOTHESES

The aims of this thesis are:

1. To investigate the novel use of computed tomography angiography in the assessment of patients with native aortic stenosis and thereby to investigate the relative roles of fibrosis and calcification in the pathogenesis of aortic stenosis (Chapter 3).

2. To establish a methodology for the use of ^{18}F-fluoride PET-CT in the assessment of aortic stenosis and to assess the reproducibility of this technique (Chapter 4).

3. To explore the mechanisms of bioprosthetic valve degeneration in explanted degenerated bioprosthetic valves by assessment with histology and micro-computed tomography/positron emission tomography (Chapter 5).

4. To investigate the utility of ^{18}F-fluoride PET-CT in the detection and prediction of bioprosthetic valve degeneration in a cohort of patients with surgically implanted bioprosthetic aortic valves (Chapter 6).

The hypotheses of this thesis are:

1. Computed tomography angiography can detect both calcification and fibrosis of the aortic valve, and thereby highlight the contribution of fibrosis and calcification in the pathogenesis of aortic stenosis (Chapter 3).

2. ^{18}F-Fluoride positron emission tomography and computed tomography can be established as an accurate and reproducible technique to assess disease activity in aortic stenosis (Chapter 4).

3. Assessment of degenerated bioprosthetic valves with micro-^{18}F-fluoride positron emission tomography and computed tomography, and correlating tissue histology will provide novel insight about the mechanisms of bioprosthetic valve degeneration (Chapter 5).

4. ^{18}F-Fluoride positron emission tomography/computed tomography can be applied to the assessment of bioprosthetic aortic valves to detect and predict structural valve degeneration (Chapter 6).

CHAPTER 2

MATERIALS AND METHODS

2.1 OVERVIEW

The design and methodology of each study is described in detail within the relevant chapters. The following section provides an overview of the patient populations and investigations employed in the course of these studies.

2.2 STUDY POPULATIONS

Two prospectively recruited patient populations form the basis for the work described herein. First, a group of patients with native valve aortic stenosis underwent multi-modality imaging assessment as part of the SALTIRE 2 double-blinded, randomised, placebo-controlled trial. The SALTIRE 2 trial was designed to investigate the ability of calcium modulators, denosumab and alendronic acid, to modify disease progression in aortic stenosis. The primary endpoint was change in CT aortic valve calcium score (CT-AVC) at 2 years and an exploratory secondary endpoint was uptake of ^{18}F-fluoride as assessed by positron emission tomography-computed tomography (PET-CT) at 1 year. A substudy was firstly performed to optimise and establish the reproducibility of ^{18}F-fluoride PET-CT in the assessment of aortic stenosis. An additional group of patients with native aortic valve disease were recruited to an observational imaging study at a collaborating centre (University of Laval, Quebec, Canada). A number of these patients proceeded to aortic valve replacement surgery and donated aortic valve tissue for histological validation.

Second, a group of patients with surgically implanted bioprosthetic aortic valves were recruited at a range of time-points following valve implantation and underwent multi-modality imaging assessment as part of the 18F-FAABULOUS observational cohort study. A cohort of patients with failing bioprosthetic aortic valves undergoing redo-aortic valve replacement surgery donated explanted bioprosthetic valve tissue for micro-PET/CT and histological analysis.

The methodology employed in both of these studies was very similar and is described below.

Ethical Considerations

The SALTIRE 2 and 18F-FAABULOUS research studies were approved by the South-East Scotland Research Ethics Committee and the Administration of Radioactive Substances Advisory Committee (ARSAC) of the United Kingdom. SALTIRE 2 is a clinical trial of an investigational medicinal product and was therefore considered and approved by the Medicine and Healthcare products Regulatory Agency (MHRA) of the United Kingdom. Both SALTIRE 2 and 18F-FAABULOUS were registered on the clinicaltrials.org website (NCT 02132026 and NCT 02304276 respectively) and the conduct was overseen by NHS/University of Edinburgh sponsors. Participants provided prior written informed consent and all studies were performed in accordance with the Declaration of Helsinki.

Recruitment

Patients under the care of the cardiology or cardiothoracic clinical teams at participating centres were firstly identified as potentially suitable study participants and approached by their usual clinical care team. Those who agreed were contacted by the research team and provided with an approved written participant information sheet prior to attending for the first visit.

2.3 STUDY ASSESSMENTS

Study visits were primarily undertaken at the Edinburgh Clinical Research Facility at the Royal Infirmary of Edinburgh. At the first visit, the process of obtaining written informed consent was performed, and the study inclusion and exclusion criteria were confirmed prior to further study involvement. The criteria for each study are detailed below.

SALTIRE 2 Study Eligibility Criteria

For inclusion in the study, participants needed to fulfil the following criteria:

- Age >50 years
- Aortic stenosis with peak aortic jet velocity of >2.5 m/s on Doppler echocardiography
- Grade 2-4 calcification of the aortic valve on echocardiography

Participants did not enter the study if any of the following exclusion criteria were fulfilled:

- Anticipated or planned aortic valve surgery in the next 6 months
- Life expectancy <2 years
- Inability to undergo scanning
- Treatment for osteoporosis with bisphosphonates or denosumab
- Long-term corticosteroid use
- Abnormalities of the oesophagus or conditions, which delay oesophageal/gastric emptying

- Inability to sit or stand for at least 30 minutes
- Known allergy or intolerance to alendronate or denosumab, or any of their excipients
- Hypocalcaemia
- Regular calcium supplementation
- Dental extraction within 6 months
- History of osteonecrosis of the jaw
- Major or untreated cancers
- Poor dental hygiene
- Women of child-bearing potential who have experienced menarche, are pre-menopausal, have not been sterilised or who are currently pregnant
- Women who are breastfeeding
- Renal failure (estimated glomerular filtration rate of <30 mL/min)
- Allergy or contraindication to iodinated contrast
- Inability or unwilling to give informed consent
- Likelihood of non-compliance to treatment allocation or study protocol

18F-FAABULOUS Study Eligibility Criteria

For inclusion in the study, participants must meet the following criteria:

- Ability to give informed consent
- Over 40 years of age
- Cohort 1: patients with a surgically implanted bioprosthetic aortic valve who are due to undergo redo-aortic valve surgery or valve-in-valve transcatheter valve implantation for bioprosthetic valve failure

- Cohort 2: patients with a surgically implanted bioprosthetic aortic valve, implanted 1 month, 2 years, 5 years or 10 years prior to study recruitment and without known evidence of valve dysfunction or degeneration.

Participants did not enter the study if any of the following exclusion criteria were fulfilled:

- Inability to give informed consent
- Pregnancy
- Breastfeeding
- Claustrophobia
- Allergy to iodinated contrast
- Liver failure
- Chronic kidney disease (with estimated glomerular filtration rate <30 mL/min/1.73 m^2)
- Paget's disease
- Metastatic malignancy
- Inability to tolerate the supine position

Clinical History

Anonymised participant data was entered into case record forms with demographic details including date of birth, sex and ethnicity. Participants were then asked questions in relation to their current symptoms, in particular their experience of breathlessness (according to the New York Heart Association classification), ankle swelling, angina (according to the Canadian Cardiovascular Society classification),

palpitation, pre-syncope and syncope. Details of significant past medical history were recorded with particular reference to history of cardiac disease, details of previous cardiac surgery or procedures, history of hypertension, dyslipidaemia, diabetes, respiratory disease, renal disease, liver disease, cerebrovascular disease or malignancy. Participants were also asked to provide information about smoking habit and alcohol intake. Current medication and history of adverse or allergic medication reactions were documented.

Clinical Examination

Each participant had their height and weight recorded, which was then used to calculate body mass index and surface area. Heart rate and blood pressure (by automated sphygmomanometry) were measured. A standardised cardiovascular clinical examination was performed in each case with the participant positioned at 45 degrees in a semi-reclined position. The rate, regularity, volume and character of the pulse, the height and characteristics of the jugular venous pressure, the location and character of the left ventricular apex beat, and fluid status were assessed. Heart sounds were evaluated by auscultation with additional sounds and murmurs being noted. The lung fields were auscultated for evidence of inspiratory crepitations which might signify pulmonary oedema.

Venesection

Venesection was performed at stipulated points according to study protocol and undertaken in conjunction with peripheral venous cannulation where this was required. Up to 40ml of venous blood was withdrawn and samples used to measure the full blood

count, renal biochemistry, liver function tests, lipid profile, glucose and cardiac enzymes.

Electrocardiography

Participants were all assessed with a 12-lead electrocardiogram (ECG), which was printed and filed in the case record. The ECG was examined for features consistent with arrhythmia, conduction disease, ischaemia, left ventricular hypertrophy and left ventricular strain. Left ventricular hypertrophy was diagnosed using the Romhilt-Estes criteria (5 points diagnostic; 4 points probable): any one of R or S in limb leads >20 mm, S in V1 or V2 > 30 mm, R in V5 or V6 > 30 mm = 3 points; ST-T vector opposite to QRS without digoxin = 3 points or ST-T vector opposite to QRS with digoxin = 1 point; negative P wave in V1 > 1 mm depth and > 0.04 s = 3 points; left axis deviation (axis -30^{o} or more) = 2 points; QRS duration > 0.09 s = 1 point; delayed intrinsicoid deflection V5 or V6 > 0.05 s = 1 point. Left ventricular strain was diagnosed if there was ST depression and T wave inversion in the anterolateral chest leads.

One study comparing ECG-based approaches for the diagnosis of left ventricular hypertrophy has suggested that the Romhilt-Estes criteria, using a threshold of 4 points, has a sensitivity of 11.9% (95% confidence interval 5.3-22.2%) and specificity of 96.7% (95% confidence interval 88.5-99.6%) for the detection of left ventricular hypertrophy as defined by echocardiography when left ventricular mass is corrected for body surface area and sex-specific thresholds are employed. (Morrison I *et al*, 2007, Anatol J Cardiol)

2.4 ECHOCARDIOGRAPHY

Physics of Echocardiography

The first clinical application of ultrasound was in diagnostic brain imaging in the 1930s, whereby a separate transmitter and receiver were used to detect transmission of ultrasound waves through the head. Modern day cardiac ultrasound is based upon detection of the reflection of ultrasound waves by a single transducer (both transmitter and receiver) and originated in 1953 in Sweden, later being termed echocardiography. Ultrasound refers to sound waves with a frequency >20 kHz and in echocardiography transducers work using the piezoelectric effect. Piezoelectric crystals change shape when an electrical voltage is applied and can be made to oscillate rapidly by applying an alternating voltage, thereby generating ultrasound. As ultrasound travels through the body, each tissue has a different acoustic impedance which results in varying degrees of reflection as ultrasound waves meet tissue boundaries. Returning ultrasound waves will then cause the piezoelectric crystals to oscillate and so generate an electrical voltage which can be detected.

The Doppler effect describes how an observer perceives a difference in the wavelength or frequency of a sound wave depending on movement of the source relative to them. For example, if a source is moving towards the observer then the sound wave wavelength shortens and frequency increases, with the converse also being true. The difference in frequency between the transmitted and returning ultrasound beams is used to calculate the Doppler shift. By this principle, Doppler echocardiography allows characterisation of the direction and velocity of blood flow in the heart and great

vessels, which is fundamental to the assessment of valve function. The Doppler effect can also be used to measure movement of the myocardium (tissue Doppler imaging) and help in the assessment of left ventricular systolic and diastolic function.

Image Acquisition

Transthoracic echocardiography is the principal non-invasive imaging method for assessment of aortic valve heart disease. Standard echocardiographic assessment involves the use of ultrasound to produce 2-dimensional images in a number of anatomical planes with high spatial and temporal resolution. In addition, the use of colour flow, pulsed and continuous wave Doppler facilitates a detailed assessment of native and prosthetic valve function. The aortic jet velocity can be measured from continuous wave Doppler aligned to blood flow through the aortic valve, which can be used to derive the peak and mean aortic valve gradients. The estimated aortic valve area can also be calculated from the continuity equation (aortic valve area = [left ventricular outflow tract velocity-time integral x left ventricular outflow tract area] / aortic valve velocity-time integral).

Comprehensive transthoracic echocardiography was performed at intervals in all study participants. Echocardiography was performed by a single experienced British Society of Echocardiography-accredited sonographer using a single scanner (Affiniti 70, Philips Medical Systems, The Netherlands) according to international guidelines (Lancelloti P *et al,* 2016) (Zoghbi W *et al*, 2009). Left ventricular outflow tract diameter was measured from the inner edge of the septal endocardium to the inner edge of the anterior mitral valve leaflet in mid-systole. Left ventricular outflow tract

velocity-time integral was measured in the apical 5-chamber view using pulsed-wave Doppler positioned just proximal to the aortic valve. Aortic valve peak gradient, mean gradient and peak aortic jet velocity were calculated from the aortic valve velocity-time integral, measured using a continuous wave Doppler. The aortic valve velocity-time integral was sampled from the apical, suprasternal and right parasternal position using both the standard phased array probe and standalone pencil probe. Mean values were taken from 3 measurements when subjects were in sinus rhythm and from 5 measurements if atrial fibrillation was present. This was the approach used in the assessment of both native aortic valve and prosthetic aortic valve function.

Aortic valve regurgitation was graded as mild, moderate or severe according to guideline recommendation on the basis of visual appraisal of colour flow mapping in multiple acoustic planes. In addition, the pressure half time (ms), vena contracta width (cm), regurgitant volume (mL), regurgitant fraction (%), regurgitant jet width/left ventricular outflow tract diameter, and evaluation of aortic flow reversal in diastole were all used as appropriate to help guide severity assessment.

Reproducibility

Echocardiography in the assessment of aortic valve disease is highly reproducible when performed by experienced observers. In a study of 150 patients with moderate aortic stenosis, the intra-observer variation and reproducibility coefficients were 1.88% and 0.16 et al respectively for peak aortic jet velocity, and 2.08% and 0.14 et al for LVOT velocity/peak aortic jet velocity, whilst inter-observer variation and reproducibility coefficients were 2.00% and 0.14 et al for peak aortic jet velocity, and

2.08% and 0.14 et al for LVOT velocity/peak aortic jet velocity (Moura L et al, 2011, Rev Port Cardiol). It appears to be more reproducible to measure the peak of a Doppler trace rather than the velocity time integral, so peak aortic jet velocity and the ratio of left ventricular outflow tract velocity to peak aortic jet velocity offer the best variability and reproducibility amongst measures of aortic stenosis severity. In another study, 25 observers independently reviewed Doppler tracings from 20 patients with aortic stenosis and demonstrated the superior reproducibility of measuring peak velocity rather than velocity time integral (coefficient of variation 10.1% vs. 18.0% for LVOT pulsed wave Doppler, $p<0.001$) (coefficient of variability 4.0% vs. 10.2% for peak aortic jet velocity continuous wave Doppler, $p<0.001$) (Sacchi S *et al*, 2018). We have also previously demonstrated excellent reproducibility of echocardiography in the assessment of aortic stenosis specifically in our centre, which can be enhanced by the use of contrast agent in patients with suboptimal image quality (Smith LA *et al*, 2004).

FIGURE 2.1.

Transthoracic echocardiography in the assessment of aortic stenosis.

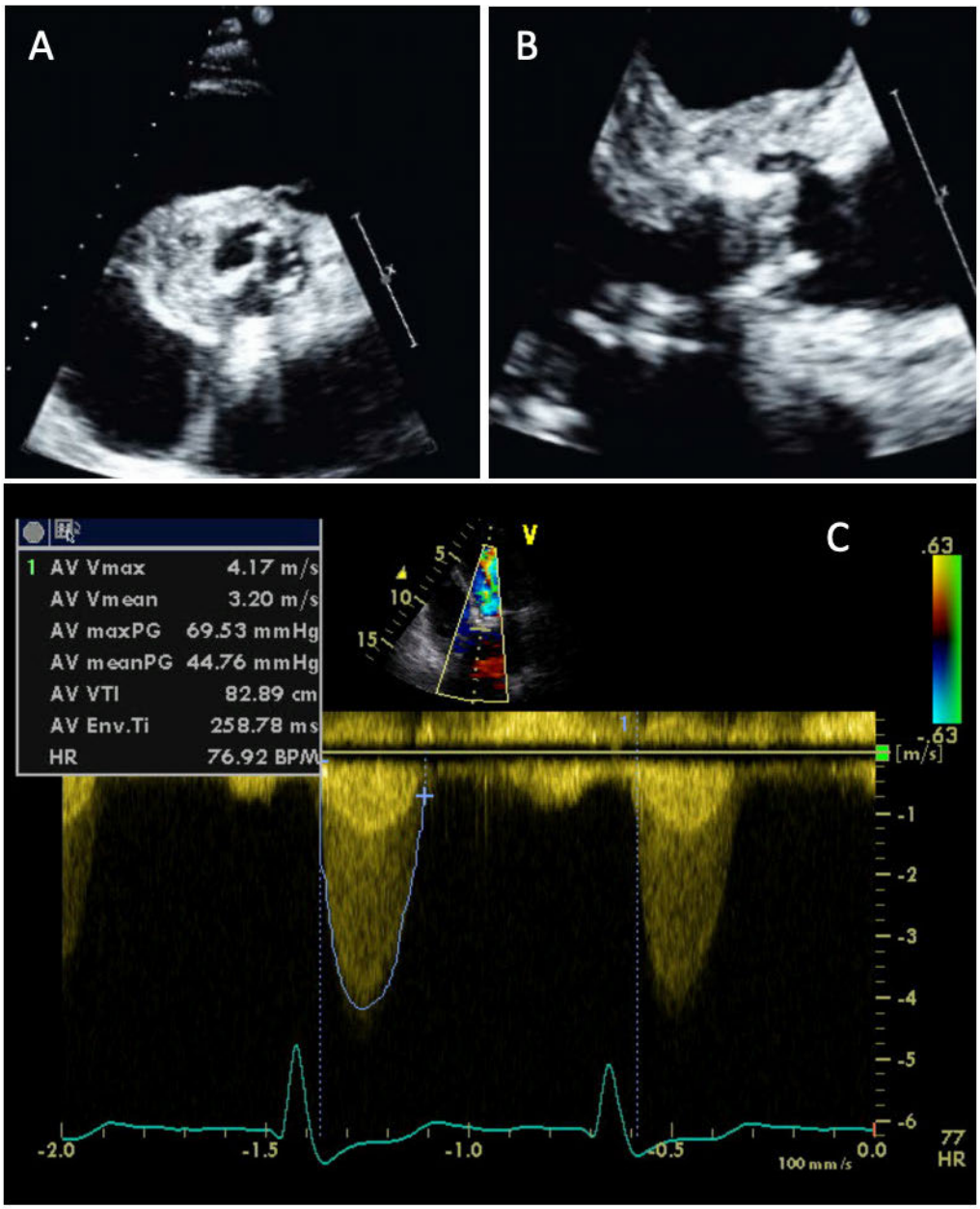

Figure 2.1. Images from a transthoracic echocardiogram of a patient with aortic stenosis showing severe fibrocalcific thickening of a trileaflet aortic valve in the parasternal short axis (A) and parasternal long axis (B), and a continuous wave Doppler profile aligned to the aortic valve in the apical 5-chamber view with measurements consistent with severe aortic stenosis (C).

2.5 COMPUTED TOMOGRAPHY

Physics of Computed Tomography

X-ray, or Rontgen radiation, is a highly penetrative form of electromagnetic radiation emitted when accelerated electrons collide with a target anode. Conventional clinical radiography is the product of an X-ray photon beam being attenuated to varying degrees depending on the density of tissue through which it passes, and results in a 2-dimensional projection of a 3-dimensional structure. Computed tomography (CT) is based upon the principle of conventional radiography that different tissues can be distinguished by their relative ability to absorb photons (attenuation coefficients). However, the detectors of a CT scanner do not produce an image but rather measure the passage of a thin (1-10 mm) X-ray beam through the body. In modern CT scanners, one or more X-ray photon beams and detector rays are mounted on a rapidly rotating gantry and the information from the intersection of beams is used to generate cross-sectional (tomographic) images. The cross-sectional area created by the intersection of 2 beams is referred to as a pixel and is multiplied by slice width to produce voxels, producing a matrix of up to 1024 x 1024 voxels. The attenuation coefficient is calculated for each voxel and converted to Hounsfield scale (HU). Cross-sectional images are then digitally ‘stacked’ to create a 3-dimensional reconstruction of the scanned volume. Thus, CT can provide a detailed anatomical assessment of the internal organs, blood vessels, soft tissue and skeleton.

Image Acquisition

Participants were imaged using a hybrid 128-slice PET/CT scanner (Biograph mCT, Siemens Medical Systems, Erlangen, Germany). If the resting heart rate prior to scanning was > 60 /min, medication (usually betablockade) was administered as appropriate to suppress the heart rate with a view to optimising image quality and limiting radiation exposure. Participants were asked to lie supine with both hands above the head and attached to a 3-lead ECG monitor. Non-contrast CT was centred on the aortic valve and acquired with electrocardiogram-gating during held expiration (40 mAs/rot [CareDose], 120 kV tube voltage, pitch 0.24, field of view 210 mm). Contrast-enhanced CT angiography was timed to obtain peak arterial enhancement in the aortic root, with a 20-mL test bolus of contrast given to determine the appropriate trigger delay and, depending on body mass index, 80-100 mL of contrast (400 mgI/mL; Iomeron, Bracco, Milan, Italy) administered for the acquisition. This was performed with either prospective (heart rate <60 /min) or retrospective (heart rate >60 min) electrocardiogram-gating during held expiration (330 ms rotation time, 100-120 kV tube voltage, 160-245 mA tube current and 3.8 mm/rotation table feed).

All scans were supervised by experienced radiographers and a medical practitioner. Patient radiation exposure was recorded and periodically reviewed by the medical physics department. Patients were observed for at least 5 min after scanning for evidence of contrast-related reactions before their venous cannula was removed and they were released from the department. All scans were reported by a consultant radiologist and incidental findings were acted upon as appropriate.

Aortic Valve Calcium Scoring

Image Reconstruction

Non-contrast CT images in the scanned volume were reconstructed in diastole in the axial plane with a 3-mm slice thickness, using a B35f kernel and standard filtered back projection reconstruction algorithm.

Image Analysis

Aortic valve calcification was assessed using the dedicated CT Vscore^{TM} application within the Vitrea Advanced analysis software (Vitrea Advanced, Vital Images, Minnetonka, USA). Aortic valve calcification was manually selected on 3-mm axial slices through the valve and surrounding structures. Beginning at the base of the valve, careful attention was paid to distinguish calcification of the aortic valve from that of other structures including the mitral annulus, left ventricular outflow tract and coronary arteries. If confluent calcification extended into the ascending aorta, the ostium of the left coronary artery was used as the anatomical limit beyond which calcification was excluded. Calcification was defined on the Hounsfield scale as at least 3-4 adjacent pixels with a radiodensity ≥ 130 HU. The calcium score was calculated in Agatston Units (AU) by applying an arbitrary weighted density score (130-199 HU = 1; 200-299 HU = 2; 300-399 HU = 3 and ≥ 400 HU = 4) and then multiplying by the area (mm^3). Aortic valve calcium volume and CT-aortic valve calcium score (CT-AVC) (Agatston Units, AU) were recorded.

The measurement of CT-AVC in patients with aortic stenosis is repeatable, with very good inter-observer reproducibility (median CT-AVC 1207 AU, mean difference 0%,

[limits of agreement -6 to 5%]) and intra-observer scan-rescan reproducibility (median CT-AVC 1149, mean difference 2% [limits of agreement -12 to 16%]) (Jenkins WSA *et al*, 2018). This has similarly been demonstrated for measurement of aortic valve calcium volume (correlation coefficient r=0.99, median interscan variability 7.9%, repeatability coefficient 237.8 mm3, limits of agreement −393 to 559 mm^3). As expected, proportional bias is evident whereby scan-rescan differences are greater in patients with higher calcium burden (Messika-Zeitoun D *et al*, 2004).

CT Angiography

Image Reconstruction

Contrast-enhanced CT images in the scanned volume were reconstructed in diastole with a 1 mm slice thickness, using a B35f kernel and standard filtered back projection reconstruction algorithm.

Image Analysis

Analyses were performed using an OsiriX workstation (OsiriX version 8.0.3 64-bit; OsiriX Imaging Software, Geneva, Switzerland). The diastolic sequence offering the best image quality was selected and a 3-dimensional multi-planar reconstruction was re-oriented to the short axis plane of the aortic valve. This allowed measurement of the dimensions of the aortic valve annulus and assessment of valve pathology such as leaflet calcification or non-calcific leaflet thickening. In the evaluation of patients with bioprosthetic aortic valves, CT scans were determined to be abnormal if there was evidence of circumferential pannus extending into the valve cusps, spotty leaflet

calcification (<3 mm) (Motoyama S *et al*, 2007), large leaflet calcification (≥3 mm) or non-calcific thickening (≥2 mm) (Figure 2.2).

In the evaluation of patients with native aortic valve stenosis, quantification of aortic valve calcium volume and non-calcific leaflet volume were quantified using SliceOmatic (Tomovision, Magog, Canada). Using re-oriented short axis images, the region-growing tool was employed to select voxels within a defined range of attenuation values. The lower threshold for detection of calcium was 3 standard deviations of the Hounsfield units within the blood pool region of interest above mean blood pool attenuation. For non-calcific leaflet tissue, a fixed lower threshold of 30 HU was employed to exclude artifact (e.g. photon starvation adjacent to dense calcification). The upper threshold for non-calcific tissue was calibrated to blood pool. Using these thresholds, areas of calcium and non-calcific leaflet thickening were assessed and quantified. Each adjacent 3-mm slice was assessed so that the whole volume of the valve was covered, with care to avoid regions of calcification in the aorta and coronary arteries.

FIGURE 2.2

CT to detect leaflet pathology in the assessment of bioprosthetic valves.

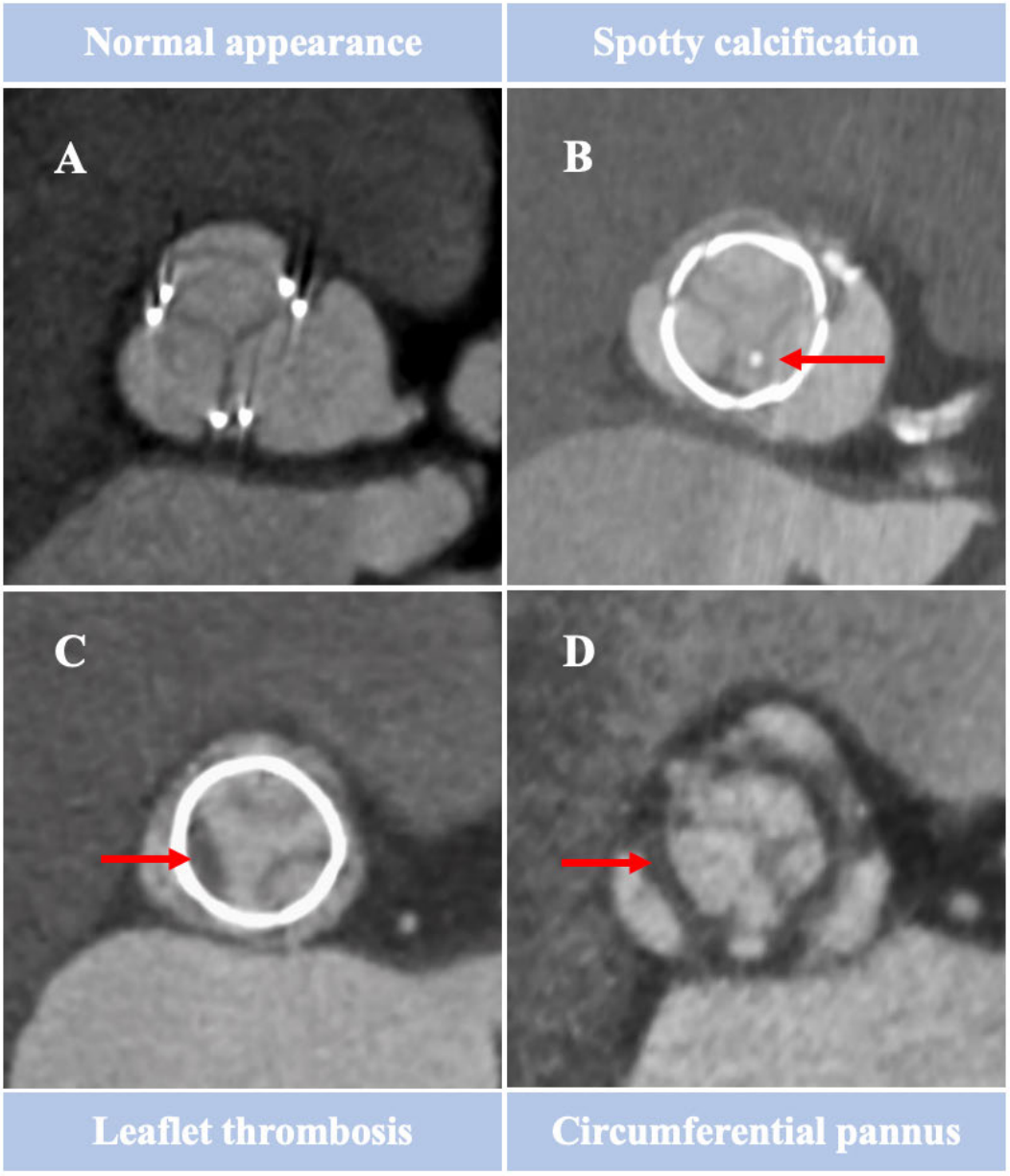

Figure 2.2. CT can be used to identify bioprosthetic valve leaflet pathology *in vivo*, for example, normal appearance of a bioprosthetic valve (A), an isolated calcific nodule (B), hypoattenuation leaflet thickening implying leaflet thrombosis (C) and a circumferential rim of low attenuation consistent with pannus (D).

2.6 ^{18}F-FLUORIDE POSITRON EMISSION TOMOGRAPHY / COMPUTED TOMOGRAPHY

Physics of Positron Emission Tomography

Positron emission tomography (PET) is a non-invasive medical imaging technique that permits the detection and quantification of active metabolic processes in the human body. The positron is released by unstable positron-emitting nuclei, such as ^{18}F-fluoride, following radioactive decay of a proton to a neutron (beta decay). The positron travels a short distance (millimetres) before colliding with an electron, resulting in annihilation of both particles and the release of two photons directed at nearly 180º degrees to one another with a fixed energy of 511 keV. That the origin of these tangential photons may be localised to a 'line of coincidence' using a ring of detectors encircling a patient forms the basic principle of clinical PET imaging. From the accumulation of events detected over a period of time, the originating point of these collisions can be computed, and a 3-dimensional image reconstructed.

Radioactive PET tracers comprise a positron emitter and a molecular vehicle selected to interact with a metabolic process of interest. The tracer is injected into an individual and the PET scanner detects emitted radiation to localise and to quantify the pathophysiological process in question. The resolution of clinical PET imaging is restricted by the distance that the emitted positron travels before annihilation, with modern clinical PET cameras achieving a resolution of ~2.36 mm (Moses *et al*, 2011) which compares with ~0.5 mm for modern CT scanners. We have combined PET with CT imaging by using a hybrid scanner where both technologies are incorporated in the

same gantry and scanning modalities can be performed sequentially with the patient lying in the same position. This allows an attenuation correction CT scan to be performed in order to adjust PET data according to the density and volume of tissue through which photons have travelled. Hybrid scanning also permits co-registration of PET and CT images so that functional data from PET tracer uptake can be combined with detailed anatomical information from CT. Radiation exposure is greater by virtue of performing both imaging modalities but remains modest, in the region of 5 milliSieverts using conventional tracers.

FIGURE 2.3.

Principles of positron emission tomography

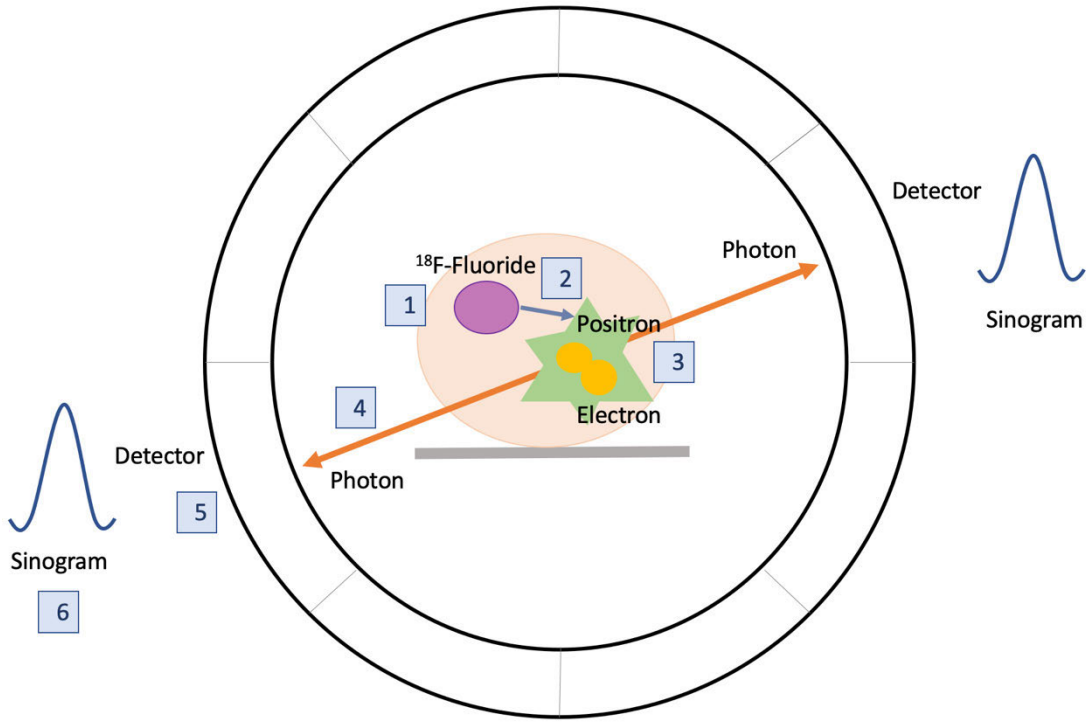

Figure 2.3. 1. ^{18}F-Fluoride binds to hydroxyapatite in the cardiovascular system and skeleton. 2. Beta decay of ^{18}F-fluoride results in release of a positron. 3. After travelling a short distance (millimetres), the positron collides with its anti-particle, an electron, which results in an annihilation reaction. 4. The annihilation reaction releases two photons with a fixed energy of 511 keV in opposite directions (180 degrees) to one another. 5. This activity is sensed by a ring of detectors which convert the signal into an electronic pulse. Two electronic pulses detected in coincidence confirms the presence of an annihilation reaction somewhere along the line of response. 6. This data is converted into a series of sinograms for each projection angle.

Radiotracer Manufacture

^{18}F-Fluoride was synthesised in the on-site cyclotron in the Edinburgh Imaging facility at the University of Edinburgh by radiochemistry staff. ^{18}F-Fluoride is produced primarily by proton irradiation of ^{18}Oxygen, a stable naturally occurring isotope of oxygen, in aqueous $H_2{}^{18}O$. Radioisotope was produced on the day of administration and quality assurance checks were satisfied prior to approval for human use.

Image Acquisition

As already described, participants' height and weight were measured to facilitate correct setup of the scan, and a peripheral venous cannula was inserted. If the resting heart rate prior to radioactive tracer injection was > 60 /min, 25-50 mg oral metoprolol was administered where safe and appropriate to suppress the heart rate. Participants were transferred to a lead-lined uptake room under video surveillance where a target dose of 125 MBq of ^{18}F-sodium fluoride was administered intravenously by PET-trained radiographers, with an expected effective radiation dose of 3 mSv. Pharmacokinetic modelling has previously demonstrated that 60 min post-administration provides optimal vascular tissue contrast resolution (Irkle *et al*, 2015). Therefore, on approaching 60 min following tracer administration, participants were asked to empty their bladder in dedicated facilities and transferred to the scanner. They were asked to lie supine with both hands above their head and were attached to a 3-lead ECG monitor.

^{18}F-Fluoride PET/CT of the thorax was performed using a hybrid 128-slice PET/CT scanner (Biograph mCT, Siemens Medical Systems, Erlangen, Germany). An

attenuation correction CT scan was performed initially (without contrast enhancement, 120 kV, 50 mA, slice thickness 5 mm, increment 3 mm). PET data was then acquired in 3-dimensional list mode over a single 30-min bed position centred over the aortic valve. A simultaneously acquired ECG allowed segregation of PET data into 4 phases according to the R-R interval. Immediately after the PET scan, an ECG-gated, contrast-enhanced CT angiogram was performed for co-registration with PET. The acquisition protocol for CT has been described above.

Image Reconstruction

Static PET images were reconstructed with correction applied for attenuation, dead time, scatter and random coincidences, using an optimised iterative reconstruction algorithm (Siemens Ultra-HD; TrueX + time of flight, matrix 200, zoom 1; Gaussian filter).

Image Analysis

Analyses were performed using an OsiriX workstation (OsiriX version 8.0.3 64-bit; OsiriX Imaging Software, Geneva, Switzerland). In order to counteract the significant motion during the cardiac cycle, ECG-gated contrast-enhanced CT images were reconstructed in diastole using 1-mm slices. For this purpose, list mode PET data was also configured to the ECG and used to reconstruct at 25% intervals of the cardiac cycle with diastolic data determined as that acquired between 50 and 75% of the R-R interval. Diastolic PET and CT reconstructions were reoriented to the short axis plane of the aortic valve (native or bioprosthetic), fused and carefully co-registered in all 3 planes using the 2-D orthogonal tool. Key points of reference for co-registration were

the sternum, vertebrae, blood-pool in the left ventricle (based upon the high ^{18}F-fluoride activity in the blood relative to the surrounding myocardium), the ascending aorta and the aortic arch.

Regions of interest in the native or bioprosthetic aortic valve were manually selected to generate maximum and mean standardised uptake values (SUV). The SUV is the decay-corrected tissue concentration of a tracer divided by the injected dose per body weight; each image voxel represents a SUV that is derived during image reconstruction. SUVs were corrected for residual blood pool activity, measured with a 2 cm^2 region of interest drawn on 3 contiguous slices in the right atrium from the level of the right coronary ostium, to produce a tissue-to-background ratio (TBR). Cardiovascular PET imaging may be hampered by both cardiorespiratory motion and proximity to the blood pool. These factors amount to potential sources of error when quantifying the radiotracer signal within a cardiovascular tissue of interest, making the use of TBR quantification preferential over SUV alone. Both a 'whole valve' approach and a 'most diseased segment' (MDS) approach to measuring tracer activity in the tissue of interest were explored, and the refinement of this technique is described in Chapter 4.

The reproducibility of the quantification of ^{18}F-sodium fluoride in the aortic valve has previously been examined, optimised by the reorientation of PET/CT images into the short axis plane of the valve and by the use of mean TBR values. Using this method, good repeatability has been demonstrated with narrow limits of agreement (±0.20) and

intraclass coefficients for both intra-observer and inter-observer reproducibility > 0.95 (Dweck *et al*, 2012).

FIGURE 2.4.

Methodology for co-registration of positron emission tomography and contrast computed tomography in bioprosthetic aortic valves.

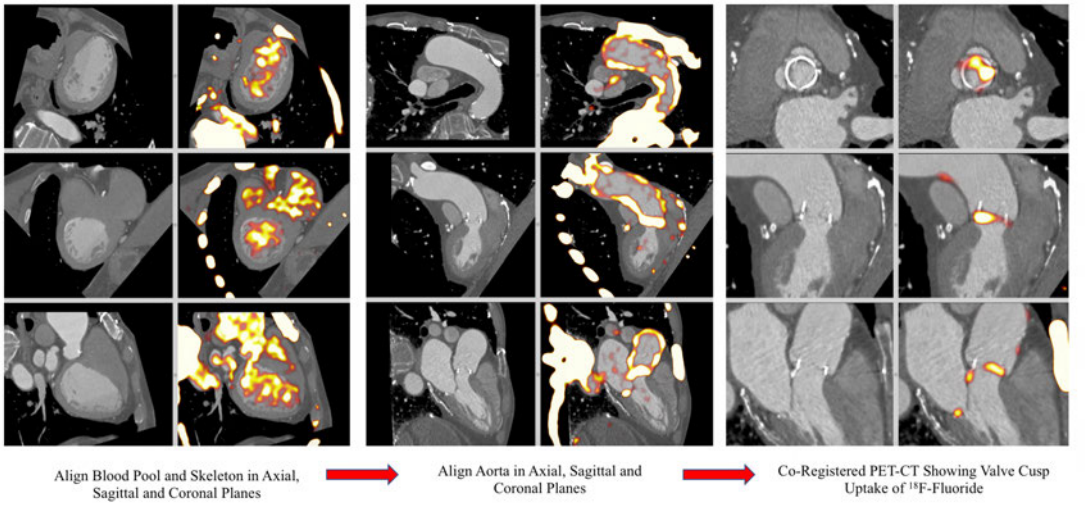

Figure 2.4. Careful alignment of PET tracer uptake in the cardiac blood pool with contrast-enhanced CT images (already re-orientated into the short axis of the aortic valve) was performed in 3 planes (left). This was possible because of high ^{18}F-fluoride activity in blood pool compared to the myocardium. Subsequently PET tracer uptake in the ascending aorta and aortic arch (centre) was aligned with the CT and final refinement of co-registration was performed according to landmarks around the aortic valve such as the coronary arteries and mitral valve annulus.

2.7 MICRO-^{18}F-FLUORIDE POSITRON EMISSION TOMOGRAPHY / COMPUTED TOMOGRAPHY

Micro-PET/CT describes the use of a pre-clinical scanner for molecular or functional imaging of biochemical processes on a miniaturised scale. This facilitates imaging of anaesthetised small animal subjects or *ex-vivo* tissue. The fundamental resolution of a pre-clinical PET scanner (0.67 mm full width at half maximum) is superior to that of a clinical PET scanner (1.83 mm full width at half maximum). Micro-PET/CT was performed to explore the mechanisms of bioprosthetic aortic valve degeneration, allowing correlation between high resolution images and histological analyses.

Explanted degenerated aortic valve bioprostheses were obtained with written consent from patients undergoing repeat surgical aortic valve replacement for bioprosthetic valve failure. Valves were weighed, photographed and their macroscopic features documented. *Ex-vivo* micro-PET/CT was performed with a nano-PET-CT scanner (Mediso, Hungary) before undergoing histological evaluation. A series of scans using variations in acquisition parameters and scanning mediums were undertaken to arrive at the optimal method. Explanted valves were incubated with 2 MBq ^{18}F-fluoride for 20 min and PET data were acquired over a 30-min bedtime using 1:5 coincidence mode. A micro-CT was then acquired (semi-circular full trajectory, maximum field of view, 720 projections, 70 kVp, exposure 300 ms and 1:1 binning) for attenuation correction and anatomical co-registration. PET data were reconstructed using Mediso's iterative Tera-Tomo 3D algorithm and the following settings: 4 iterations, 6 subsets, full detector model, normal regularization, spike filter on, voxel size 0.6 mm,

400-600 keV energy window. Analysis was performed using PMOD (PMOD Technologies, Switzerland) to localise and quantify ^{18}F-fluoride activity and calcification on CT.

2.8 HISTOLOGICAL VALIDATION

To characterise the pathophysiology underlying the imaging observations made in these investigations, excised native aortic valve tissue and bioprosthetic valve tissue was obtained for histological examination. All patients provided prior written informed consent. These analyses were performed by collaborating groups at the University of Laval (Quebec, Canada), the University of British Columbia (Vancouver, Canada) and the CVPath Institute (Gaithersburg, Maryland, USA).

In patients undergoing aortic valve replacement, the aortic valve (native or bioprosthetic) was excised at the time of surgery and the integrity of the valve structure was preserved wherever possible. Explanted valve specimens were fixed in 10% w/v buffered formalin phosphate (Fisher Chemical SF100-20) pending histological analysis. Heavily calcified samples were treated with fixative decalcifier to facilitate sectioning (Fisher Chemical, Cal-Ex II, CS511-1D). Leaflets were detached from the base of the valve and marked with tissue dye fixed with acetic acid to maintain orientation. Each leaflet was processed then sectioned into 2-4 mm sections and embedded in paraffin sequentially to yield 7-8 tissue cross-sections per leaflet. Paraffin sections (4 μm) were used for histology and immunohistochemistry (IHC). Tissue was sectioned and stained for architecture (haematoxylin and eosin, Movat pentachrome, Verhoeff-van Gieson), calcium phosphate (von Kossa, Alizarin red), thrombus and fibrosis (Movat Pentachrome), and collagen (Picrosirius red). Visual assessment was performed by experienced pathologists and reported.

Histology Tissue Staining Protocols

Haematoxylin and Eosin: Eosin is an acidic dye which stains basic structures pink, such as cytoplasm or extracellular fibres. Haematoxylin is a basic dye which stains acidic structures, such as nuclei, a purple-blue colour. Tissue sections were deparaffinised using heat and immersion in xylene. Sections were then hydrated by passing through decreasing concentrations of alcohol before firstly being stained with haematoxylin for 3-5 min. Sections were washed under running water for several minutes, treated in 1% hydrochloric acid alcohol, washed, treated in ammonia and then washed again prior to staining with eosin for 10 minutes. Finally, tissue sections were washed in running water, dehydrated in increasing concentrations of alcohol, cleared in xylene and mounted in mounting media ready for microscopy.

Movat Pentachrome: This is a five-colour stain which highlights the constituents of connective tissue, with nuclei and elastin staining black, collagen staining yellow, mucin staining blue, fibrin staining bright red and muscle staining red. Tissue sections were deparaffinised and hydrated as above. Tissue was subject to a Bouins mordant, heated in a microwave and rested for 10 min. After washing in cold running water, sections were treated in sodium thiosulphate for 5 min then again washed and stained with 1% Alcian Blue for 20 min. After a wash, sections were placed in preheated alkaline alcohol for 10 min, again rinsed then treated in Movat's Weigerts for 1 hour. A further wash was followed by treatment in Crocein scarlet/acid fuchsin for 1 minute, a rinse, treatment in 5% phosphotungstic acid for 5 minutes, transfer to 1% acetic acid for 5 min, a rinse, dehydration in increasing concentrations of alcohol and then treatment in alcoholic saffron for 20 min. A final rinse with 2 changes was performed

in 100% ethanol before clearing in xylene and mounting in mounting media for microscopy.

Verhoeff-van Gieson: This method stains collagen red, nuclei blue, erythrocytes and cytoplasm yellow, and elastin blue/black. Tissue sections were deparaffinised and hydrated to distilled water, then stained in Verhoeff's solution for 1 hour. After a tap water rinse, sections were differentiated in 2% ferric chloride for 1-2 min then washed in several changes of tap water to stop differentiation. Sections were treated in 5% sodium thiosulphate for 1 min, rinsed in tap water, then counter-stained with van Gieson's solution for 3-5 min. Finally, sections were dehydrated through increasing concentrations of alcohol, cleared in xylene and mounted in mounting medium.

Von Kossa: Silver ions bind phosphate ions and undergo photochemical degradation to visualise silver deposits as a metallic silver colour on microscopy. Tissue sections were deparaffinised and hydrated as above, then immersed in 5% aqueous silver nitrate. Sections were then exposed to ultraviolet light for 20 min, washed in distilled wated then treated with 2% sodium thiosulphate for 2 min. After rinsing, sections were counter-stained with 1% neutral red for 2 min. They were then dehydrated in alcohol, cleared in xylene and mounted in mounting medium.

Alizarin Red: This stain binds calcium to form a lake pigment that is orange-red in colour. Mounted tissue sections were deparaffinised and hydrated. Sections were stained with the Alizarin red solution for up to 5 min under microscope observation

then dried and blotted. Sections were dehydrated in acetone, then acetone-xylene, cleared in xylene and mounted in mounting medium.

Picrosirius Red: In bright field microscopy this stains collagen red and nuclei, cytoplasm and muscle fibres yellow. Tissues sections were deparaffinised and hydrated. Nuclei were stained with Weigert's haematoxylin for 8 min, then thoroughly rinsed in running water. Sections were stained with picrosirius red for 1 hour then washed in 2 changes of acidified water and dried. Finally, slides were dehydrated, cleared in xylene and mounted in mounting medium.

2.9 STATISTICAL ANALYSIS

Baseline characteristics are reported as number (percentages) for categorical variables and mean ± standard deviation or median [interquartile range] for continuous variables depending on whether variables were normally distributed. Categorical data were compared using chi-squared or Fisher's exact tests. Continuous variables were transformed where not normally distributed. The point-biserial correlation coefficient was used to measure the strength and direction of the association between one dichotomous variable and one continuous variable. One-way ANOVA was used to compare continuous data across multiple factors, with post-hoc analysis using the Bonferonni test where appropriate. The Student's *t*-test or Mann-Whitney U test were used to compare continuous outcomes between two independent groups depending on whether they were or were not normally distributed, respectively. The Student's *t*-test or Wilcoxon signed-rank test were employed to compare paired variables. Two-tailed Pearson's correlation analysis was performed to investigate the strength of linear relationship between two variables, for example, between ^{18}F-fluoride uptake and echocardiographic measures of valve function. Multivariable analysis was performed, for example, to assess the predictors of deterioration in bioprosthetic valve dysfunction. Reproducibility was analysed and presented using Bland-Altman analyses and intraclass correlation coefficients (ICC). Statistical analysis was undertaken using IBM SPSS Statistics 23 or Graph Pad Prism 6 (GraphPad Software Inc., California USA) and significance was taken at the two-sided 5% level ($p<0.05$).

CHAPTER 3

CONTRAST-ENHANCED COMPUTED TOMOGRAPHY IN THE ASSESSMENT OF AORTIC STENOSIS

Cartlidge TRG, Bing R, Kwiecinski J, Guzzetti E, Pawade TA, Doris MK, Adamson PD, Massera D, Lembo M, Peeters FECM, Couture C, Berman DS, Dey D, Slomka P, Pibarot P, Newby DE, Clavel MA, Dweck MR. Contrast-enhanced computed tomography assessment of aortic stenosis. *Heart* 2021; in press.

3.1 ABSTRACT

Background

Computed tomography (CT) aortic valve calcium scoring is an emerging marker of disease severity in patients with aortic stenosis but ignores the substantial contribution of valvular fibrosis.

Objectives

To assess aortic valve fibro-calcific burden using contrast-enhanced CT in patients with aortic stenosis.

Methods

Patients with and without aortic stenosis (38 normal, 39 mild, 78 moderate, 26 severe) underwent echocardiography, CT aortic valve calcium score and contrast-enhanced CT. Volumes of calcific and non-calcific (fibrosis) valve tissue were quantified and indexed to annulus area, using Hounsfield unit thresholds calibrated against blood-pool radiodensity. The fibro-calcific ratio assessed the relative contributions of valve fibrosis and calcification. The fibro-calcific burden (sum of indexed non-calcific and calcific volumes) was determined and validated against *ex-vivo* valve weight.

Results

Contrast-enhanced CT calcium volumes correlated closely with CT calcium score ($r=0.86$, $p=<0.001$), and moderately with peak aortic-jet velocity on echocardiography ($r=0.57$ $p<0.001$). Non-calcific leaflet volumes were similar to calcific volumes in patients with aortic stenosis (79 [52-100) *versus* 75 [40-138] mm^3/cm^2, $p=0.209$).

Fibrosis predominated in mild stenosis while calcification dominated in severe disease (fibro-calcific ratio: 1.33 [0.91-2.4]) *versus* 0.53 [0.35-1.05] respectively; p=0.001). Males exhibited more valve calcium than fibrosis, with the reverse true for females (fibro-calcific ratio: 0.89 [0.45-1.54] *versus* 1.49 [0.82-5.74] respectively; p=0.001). The fibro-calcific burden demonstrated the strongest correlation with peak aortic-jet velocity (r=0.71, p<0.001), especially in women (r=0.77, p=0.001) where it outperformed CT calcium score (r=0.27, p=0.216) (p=0.027). The fibro-calcific burden correlated closely with *ex vivo* valve weight (r=0.88, p<0.001), providing a closer association than CT calcium score, especially in women.

Conclusions

Aortic valve fibrosis is a major contributor to the evolution of aortic stenosis particularly in women. Fibro-calcific burden outperforms aortic valve calcium score as a measure of disease severity and could add value in patients with discordant findings or low-flow states on echocardiography.

3.2 INTRODUCTION

The pathogenesis of aortic stenosis involves an initiation phase characterised by mechanical injury, lipid deposition and a localised inflammatory response, followed by a propagation phase wherein progressive valve fibrosis and calcification promote worsening valvular stenosis (Pawade TA *et al*, 2015).

Recent guidelines have recommended non-contrast CT calcium scoring of the aortic valve (CT-AVC) as an additional method of assessing aortic stenosis severity when echocardiographic measurements are discordant (Baumgartner H *et al*, 2017). This recommendation is based upon data demonstrating the diagnostic accuracy of CT-AVC and its powerful prediction of both disease progression and clinical events (Clavel MA *et al*, 2013; Clavel MA *et al*, 2014; Pawade TA *et al*, 2018). However, CT-AVC has several important limitations. First, it offers little detail about valve morphology and is unable to localise the anatomical distribution of calcium in the valve and surrounding structures. Second, CT-AVC cannot quantify fibrosis, an important contributor to valve stenosis and can therefore misclassify disease severity, particularly amongst young women and those with bicuspid valves (Shen M *et al*, 2016; Simard L *et al*, 2016). Third, it demonstrates only moderate associations with hemodynamic severity on echocardiography and different severity thresholds are required in the two sexes, with women consistently demonstrating lower calcium burden for a given degree of valvular stenosis, even after correction for body size (Clavel MA *et al*, 2013; Clavel MA *et al*, 2014; Pawade TA *et al*, 2018).

Contrast CT angiography is widely used to assess and to quantify both calcific and non-calcific plaques in the coronary vasculature (Dweck MR *et al*, 2016). In the present study, we aimed to apply a similar approach to the aortic valve, allowing evaluation of the aortic valve calcium burden but also non-calcific leaflet thickening as a marker of valve fibrosis. We hypothesised that this technique would provide novel insights into the pathogenesis of aortic stenosis and improve the quantification of disease severity.

3.3 METHODS

Study Population

Individuals over the age of 50 years with mild, moderate and severe aortic stenosis were prospectively recruited from the Edinburgh Heart Centre. This was a substudy of the SALTIRE 2 randomised controlled trial of novel drug treatments in aortic stenosis (NCT 02132026) and patient eligibility was defined by the inclusion and exclusion criteria for this study, detailed below. Written informed consent was obtained from all participants. The study was approved by the South East Scotland Research Ethics Committee, the Medicine and Healthcare products Regulatory Agency (MHRA) of the United Kingdom and conducted in accordance with the Declaration of Helsinki. Volunteers without clinical or imaging evidence of aortic valve disease were recruited from a coronary heart disease population to provide a control cohort (NCT 02110303).

Study Patient Selection Criteria

Inclusion Criteria

For inclusion in the study, participants should fulfil the following criteria:

Age > 50 years; peak aortic jet velocity >2.5 m/s on Doppler echocardiography; grade 2-4 calcification of the aortic valve on echocardiography.

Exclusion Criteria

Participants will not enter the study if any of the following exclusion criteria are fulfilled:

Women of childbearing potential who are premenopausal, have not been sterilised or who are currently pregnant; women who are breastfeeding; renal failure (estimated glomerular filtration rate of <30 mL/min); inability to undergo scanning; allergy or contraindication to iodinated contrast; inability or unwilling to give informed consent; likelihood of non-compliance to treatment allocation or study protocol; anticipated or planned aortic valve surgery in the next 6 months; life expectancy less than 2 years; treatment for osteoporosis with bisphosphonates or denosumab; known allergy or intolerance to alendronate or denosumab, or any of their excipients; abnormalities of the oesophagus or conditions, which delay oesophageal/gastric emptying; inability to sit or stand for at least 30 minutes; hypocalcaemia; regular calcium supplementation; dental extraction within 6 months; long term corticosteroid use; history of osteonecrosis of the jaw; poor dental hygiene.

Study Assessments and Data Collection

Potential participants with aortic stenosis were approached by the clinical team and attended for an initial visit with clinical evaluation and Doppler echocardiography to assess the severity of aortic stenosis. Participants fulfilling the eligibility criteria were then invited to undergo baseline clinical assessment, electrocardiography (ECG), non-contrast CT-AVC and contrast-enhanced CT angiography. Randomization to investigational treatment or placebo was undertaken at a subsequent visit outwith the remit of this study.

Image Analysis

Doppler Echocardiography

A comprehensive echocardiographic assessment was performed at baseline by a single experienced British Society of Echocardiography (BSE)-accredited sonographer using a standardised protocol (Bushra R *et al*, 2012). The principal measure of hemodynamic aortic stenosis severity was the peak aortic-jet velocity but mean gradient, aortic valve area (calculated using the continuity equation) and indexed aortic valve area were also recorded. Aortic valve Doppler measurements were routinely assessed from the apex, suprasternal notch and right sternal edge. Mean values were taken from 3 measurements when subjects were in sinus rhythm and from 5 measurements when in atrial fibrillation.

Computed Tomography

Baseline CT imaging was performed on a 128-detector CT scanner (Biograph mCT, Siemens). Electrocardiography (ECG)-gated non-contrast CT-AVC and contrast-enhanced CT angiography were performed in diastole and held expiration. Prior to scanning, participants were given 25 mg of oral metoprolol if their resting heart rate was >65 beats/min in the absence of any contraindication.

All CT analyses were performed blinded to the echocardiographic assessments of aortic stenosis severity. CT-AVC was quantified by an experienced operator (TP) using dedicated software (Vitrea Advanced; Toshiba Systems) on axial views, with care taken to exclude calcium originating from the ascending aorta, left ventricular outflow tract, and coronary arteries (Pawade TA *et al*, 2018; Pawade TA *et al*, 2020). The calcium score was recorded in Agatston units.

Contrast-enhanced CT analysis was performed using an OsiriX workstation (OsiriX version 8.0.3 64-bit; OsiriX Imaging Software, Geneva, Switzerland). ECG-gated contrast-enhanced CT images were reconstructed in diastole. A multi-planar reconstruction was re-oriented into the exact short-axis (*en face*) plane of the aortic valve as described previously and, using the aortic valve annulus as the reference slice, resliced in 3-mm increments through the valve (Gurvitch *et al*, 2014; Achenbach S *et al*, 2012; Pawade TA *et al*, 2016). This slice thickness was selected to remain consistent with non-contrast CT calcium scoring. Blood pool contrast attenuation was sampled within a 2 cm^2 circular region of interest positioned in the center of the lumen of the aortic root at the level of the sinotubular junction (Hounsfield Units, HU). Care was taken to exclude aortic wall calcifications.

In the second part of the analysis, quantification of the aortic valve calcium volume and non-calcific leaflet volume was performed using SliceOmatic (Tomovision, Magog, Canada). Contrast-enhanced short-axis CT images of the valve were transferred to SliceOmatic as high dynamic range (HDR) files. The region-growing tool was used to select voxels within a defined range of attenuation values (HU) for valvular calcium and non-calcific leaflet thickening. The lower threshold for detection of calcium was determined as 3 standard deviations above the mean blood pool attenuation. For non-calcific leaflet thickening, a fixed lower threshold of 30 HU was employed to exclude artifacts (e.g. areas of photon starvation adjacent to dense calcification). The upper threshold for non-calcific valve thickening was calibrated to the mean blood pool attenuation according to an equation derived from analysis of a derivation cohort comprising 100 patient scans. Two independent observers titrated

the upper threshold for non-calcific leaflet thickening starting at 200 HU and adjusting by increments of 25 HU in either direction until the margins of the 3 aortic valve cusps were delineated without any highlighting of the blood pool. When this visually determined upper threshold (x) was plotted against the mean blood pool attenuation (y) in the derivation cohort, a strong linear relationship was identified (r^2=0.902, p<0.001) with the equation: x = 41.46 + 0.42(y). Using these HU thresholds, areas of calcium and non-calcific leaflet thickening in the valve were assessed and quantified on co-axial *en face* views. Each adjacent 3-mm slice was assessed so that the whole volume of the valve was covered. Care was taken to avoid areas of calcification in the aorta and coronary arteries. This was easier to accomplish than on non-contrast CT-AVC scans, given the superior anatomical detail provided by contrast CT and the ability to align with the true plane of the valve.

Indexing to Aortic Annulus Area

Calcific and non-calcific leaflet volumes were indexed to the annulus area determined by contrast-enhanced CT. This method is repeatable and widely used to size transcatheter aortic valves pre-procedure (Gurvitch *et al*, 2014; Achenbach S *et al*, 2012). These indexed volumes for calcific and non-calcific valve thickening were then used for all subsequent comparisons and analyses.

Reproducibility

Measurements of calcific and non-calcific leaflet volumes were performed independently in 20 patients by two experienced operators (TC, JK) in order to assess inter-observer reproducibility. For this purpose non-calcific and calcific volumes were

not indexed to aortic valve area as the reproducibility of annular dimensions measured by CT angiography has been well described (Gurvitch *et al*, 2014; Achenbach S *et al*, 2012).

Fibro-Calcific Ratio and Fibro-Calcific Burden

Using the contrast-enhanced indexed CT calcium volumes and the non-calcific leaflet volumes, we explored two novel imaging measures. The fibro-calcific ratio was derived by dividing the non-calcific by the calcific indexed leaflet volumes. A ratio >1.0 indicated a predominance of non-calcific (fibrotic) disease in the valve, whilst a ratio ≤1.0 indicated predominant calcification. The fibro-calcific burden was derived by addition of the indexed calcific and non-calcific leaflet volumes to provide an overall marker of disease burden.

Validation of the Fibro-calcific Burden

The fibro-calcific burden was validated as a marker of aortic stenosis severity in two ways. First, the fibro-calcific burden was validated against *ex vivo* valve histology and valve weight using a separate patient population with severe aortic stenosis from Quebec, Canada. These subjects underwent contrast-enhanced, ECG-gated CT <3 months prior to surgical aortic valve replacement. Image analysis with quantification of calcific and non-calcific leaflet volumes was performed as described above. Aortic valves were excised at the time of surgery and examined by a single pathologist who was blinded to the CT. The valve cusps and any accompanying small fragments were removed from 4-(2-hydroxyethyl)-1-piperazineethanesulfonic acid solution, placed on absorbing paper, and then weighed on laboratory scales with a tolerance of ±0.01 g.

Additionally, sections of three leaflet of the valves were sliced and then stained with Masson Trichrome and/or Verhoeff-Van Giesson staining to assess regions of fibrosis and calcification within the valve as well as other potential components such as thrombus or lipid. Areas of non-calcific leaflet thickening observed on the CT were targeted to assess the histological composition in these regions.

Second, our study cohort findings were independently and externally validated in a further cohort of 39 patients with aortic stenosis (Université Laval, Quebec, Canada) who underwent Doppler echocardiography and ECG-gated contrast-enhanced CT angiography within the same episode of care (<3 months apart). Observers from Quebec (EG, MC) were initially trained in the image analysis methodology in Edinburgh before performing a local independent analysis on their validation cohort, with comparisons made between CT and echocardiography assessments of disease severity. Again, CT analysis was performed blinded to echocardiographic data.

Statistics and Data Analysis

Baseline characteristics are reported as number (percentages) for categorical variables and mean ± standard deviation or median [interquartile range] for continuous variables as appropriate. Where not normally distributed, continuous variables were $\log_{10}$ transformed. One-way analysis of variance was used to compare continuous data across multiple factors, with post-hoc analysis using the Bonferroni correction where appropriate. The Student's *t*-test or Mann-Whitney U test were used to compare continuous outcomes between two independent groups depending on whether they were normally distributed. Two-tailed Pearson's correlation (where data were

normally distributed) and Spearman's rank correlation coefficient (where data were not normally distributed) were performed to assess the relationship between CT-AVC Agatston score, contrast CT calcium volume, non-calcific leaflet thickening volume and echocardiographic measures of aortic stenosis severity. Comparison of the strength of association between a variable and two linear predictors was made by applying Fisher's Z transformation to the Pearson correlation coefficients. Statistical analysis was undertaken using IBM SPSS Statistics 23 and significance was taken at the two-sided 5% level ($p<0.05$).

3.4 RESULTS

Baseline Characteristics of Study Population

A total of 143 volunteers (20% female) with aortic stenosis (39 mild, 78 moderate, 26 severe disease) attended for baseline study assessment. Participants were relatively elderly (age 72±8 years) with a high prevalence of treated hypertension (67%), known coronary artery disease (36%), type 2 diabetes mellitus (21%) and smoking habit (34%) (Table 3.1). Thirty-eight participants (50% female, age 65±8 years) without evidence of aortic valve stenosis or sclerosis comprised the control group.

TABLE 3.1.

Patient baseline characteristics.

POPULATION CHARACTERISTICS	
Total subjects	143
Age (years)	72 ± 8
Female (%)	28 (19.9)
Medical History	
Hypertension (%)	96 (67.1)
Diabetes (%)	30 (21.0)
Coronary Artery Disease (%)	51 (35.7)
Smoking (%)	49 (34.3)
Dyslipidaemia (%)	74 (51.7)
Medication	
Statin (%)	91 (63.6)
ACEi (%)	49 (34.3)
ARB (%)	26 (18.2)
Beta-Blocker (%)	53 (37.1)
Antiplatelet (%)	73 (51.0)
Warfarin (%)	19 (13.3)
Echocardiography	
LV Systolic Dysfunction (%)	6 (4.2)
Bicuspid Aortic Valve (%)	6 (4.2)
LVOT Area (cm^2)	3.14 [3.14-3.80]
Aortic Valve Peak Velocity (I)	3.36 [2.89-3.85]
Aortic Valve Mean Gradient (mmHg)	23.3 [17.7-31.7]
Aortic Valve Area (cm^2)	1.05 [0.86-1.27]
Computed Tomography	
Annulus Area (cm^2)	4.62 [4.02-5.25]
Bicuspid Aortic Valve (%)	13 (9.1)
Agatston Score (AU)	1189 [671-2257]
Non-Contrast CT Calcium Volume (mm^3)	978 [583-1777]
Contrast CT Calcium Volume (mm^3)	351.6 [170.2-778.9]
Non-Calcific Leaflet Volume (mm^3)	353.3 [228.9-511.1]
Fibro-calcific burden (mm^3)	772.4 [456.2-1196.8]

Abbreviations: ACEi: angiotensin-converting enzyme inhibitor, ARB: angiotensin receptor blockade, CT: computed tomography, LV: left ventricle, LVOT: left ventricular outflow tract.

Annulus Area Measured by Contrast-Enhanced CT

The area of the aortic valve annulus measured by CT across the study population was 4.60 [4.01-5.30] cm^2, with males having larger annular dimensions than females (males: 4.76 [4.21-5.44] *versus* females: 3.51 [3.19-4.17] cm^2, $p<0.001$). There was a moderate correlation between measurements of annulus area by CT and LVOT area by echocardiography ($r=0.68$, $p<0.001$), although there was a tendency for echocardiography to underestimate the area when compared to CT (LVOT area by echocardiography: 3.14 [3.14-3.80] *versus* annulus area by CT: 4.62 [4.02-5.25] cm^2, $p<0.001$).

Aortic Valve Calcification

In the control group, no aortic valve calcification was observed on either the contrast-enhanced or non-contrast CT scans. In the aortic stenosis cohort, the median indexed aortic valve contrast-enhanced CT calcium volume was 75 [40-138] mm^3/cm^2 (Figure 3.1). There was excellent inter-observer reproducibility (intraclass correlation coefficient [ICC] [average measures]: 0.95 (95% confidence interval [CI] 0.88 to 0.98), $p<0.001$). Indexed contrast CT calcium volumes doubled with each increase in aortic stenosis severity class (mild: 42 [20-67] mm^3/cm^2, moderate: 80 [42-157] mm^3/cm^2 and severe: 154 [96-234] mm^3/cm^2) (Figure 3.2). Indexed contrast-enhanced CT calcium volumes correlated closely with non-contrast CT-AVC ($r=0.86$, $p<0.001$), with the two measures demonstrating similar moderate correlations with peak aortic-jet velocity ($r=0.57$ and $r=0.60$ respectively, both $p<0.001$). Males displayed higher indexed calcium volumes on contrast-enhanced CT than females, an observation that persisted after adjusting for peak aortic-jet velocity (males: 26 [16-48] *versus* females:

9 [4-18] $mm^3/cm^2/ms$-1, $p<0.001$). In men, echocardiographic measures of aortic severity demonstrated a moderate correlation with indexed calcific CT volumes (peak aortic-jet velocity: $r=0.52$, $p=0.001$), whereas no correlation was observed in women (peak aortic-jet velocity: $r=0.16$, $p=0.463$; Table 3.2).

Non-Calcific Valve Thickening

In the control cohort, our novel image analysis approach detected the edge of the leaflets, providing a median non-calcific leaflet volume of 30 [20-43] mm^3/cm^2 with no gender difference (males: 27 [21-39] *versus* females: 33 [19-43] mm^3/cm^2, $p=0.184$). In patients with aortic stenosis, indexed non-calcific leaflet volumes were more than double those in the control cohort (79 [52-100] mm^3/cm^2, $p<0.001$) and similar to the measured indexed volumes of valvular calcium (79 [52-100] *versus* 75 [40-138] mm^3/cm^2, $p=0.209$) (Figures 3.1 and 3.2). Quantification of indexed non-calcific leaflet volume demonstrated excellent inter-observer reproducibility (ICC [average measures]: 1.00 (95% CI 0.99 to 1.00), $p<0.001$). There was a progressive increase in the indexed non-calcific leaflet volume with increasing aortic stenosis severity, although this was more gradual than for the indexed calcific volumes (mild: 62 [42-88] mm^3/cm^2; moderate: 81 [56-111] mm^3/cm^2; and severe: 85 [64-106] mm^3/cm^2; $r=0.22$, $p=0.012$). Whilst only a weak correlation was observed between indexed non-calcific valve thickening and echocardiographic measurements in men, a moderate correlation was observed in women (Table 3.2).

FIGURE 3.1.

Contrast-enhanced computed tomography in aortic stenosis: detection of valve calcification and fibrosis.

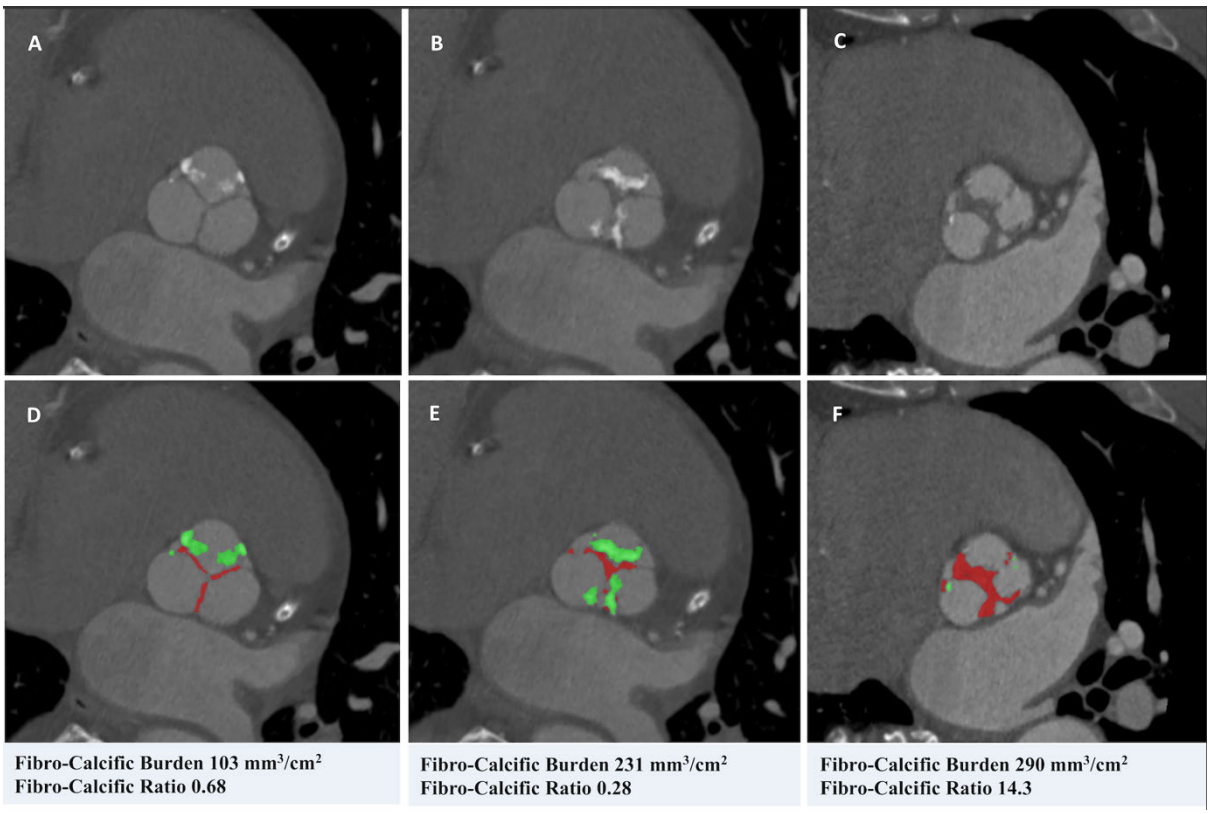

Figure 3.1. Contrast-enhanced CT images in the *en face* plane of the aortic valve **(A-C)** with calcium highlighted in green and non-calcific fibrotic leaflet thickening highlighted in red **(D-F)**. The total fibro-calcific burden (mm^3/cm^2) and the fibro-calcific ratio are presented beneath.

FIGURE 3.2.

Calcific and Non-Calcific Aortic Valve Volumes.

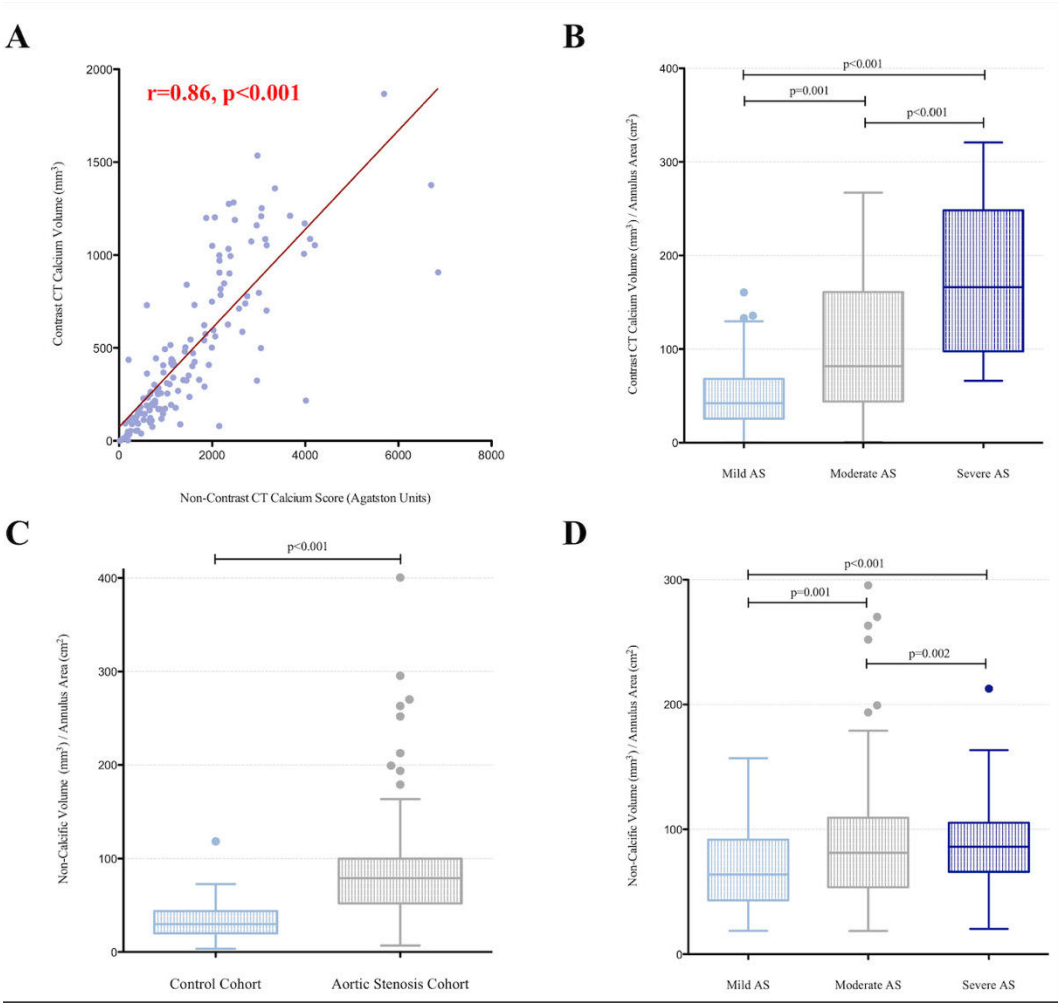

Figure 3.2. Scatter plot illustrating the close correlation between CT-AVC (Agatston Score) and contrast-enhanced CT calcific volume **(A)** (r=0.86, p<0.001). Tukey boxplot demonstrated a progressive increase in the indexed calcific volume with progressive aortic stenosis severity class **(B)**, a comparison of the non-calcific volume in volunteers without aortic valve disease (control cohort) *versus* patients with aortic stenosis **(C)** and the indexed non-calcific leaflet volumes also increasing with aortic stenosis severity class **(D)**.

TABLE 3.2.

Association between CT and echocardiographic assessments in aortic stenosis.

	PEAK VELOCITY	MEAN GRADIENT
CT-AVC (Agatston score) All	r=0.51 p<0.001*	r=0.52 p<0.001*
CT-AVC (Agatston score) Men	r=0.57 p<0.001*	r=0.60 p<0.001*
CT-AVC (Agatston Score) Women	r=0.27 p=0.216	r=0.37 p=0.074
Calcific volume (indexed to annulus area) All	r=0.44 p<0.001*	r=0.43 p<0.001*
Calcific volume (indexed to annulus area) Men	r=0.52 p<0.001*	r=0.52 p<0.001*
Calcific volume (indexed to annulus area) Women	r=0.16 p=0.463	r=0.10 p=0.691
Non-calcific volume (indexed to annulus area) All	r=0.30 p=0.001*	r=0.27 p=0.004*
Non-calcific volume (indexed to annulus area) Men	r= 0.25 p=0.013*	r=0.19 p=0.076
Non-calcific volume (indexed to annulus area) Women	r=0.49 p=0.017*	r=0.60 p=0.005*
Fibro-calcific burden All	r=0.71 p<0.001*	r=0.70 p<0.001*
Fibro-calcific burden Men	r=0.68 p<0.001*	r=0.67 p<0.001
Fibro-calcific burden Women	r=0.77 p<0.001*	r=0.85 p<0.001*

Pearson correlation coefficients derived from transformed (log10) data.

Fibro-Calcific Ratio

The ratio of the non-calcific to calcific leaflet volumes across the cohort of patients with aortic stenosis was 1.04 [0.48-1.79]. However, this fibro-calcific ratio varied depending on the severity of aortic stenosis. Fibrotic tissue predominated (1.33 [0.91-2.4]) in patients with mild aortic stenosis, was similar to calcium in those with moderate stenosis (0.98 [0.47-1.78]) and played a more minor role in those with severe stenosis (0.53 [0.35-1.05]) (Figure 3.3). The fibro-calcific ratio also differed with respect to sex, with males exhibiting proportionally more calcific than non-calcific leaflet thickening and females demonstrating the reverse (males: 0.89 [0.45-1.54] *versus* females: 1.49 [0.82-5.74], p=0.001). This sex-difference remained after correcting for peak aortic-jet velocity (males: 0.26 [0.12-0.49] *versus* females: 0.31 [0.13-0.61] ratio/ms-1, p=0.001). We did not demonstrate a statistical association between the fibro-calcific ratio and patient age (r=-0.10, p=0.248) though when patients were divided into quartiles according to age the youngest quartile did exhibit the highest ratio (quartile 1: 0.39 [0.25-0.84]; quartile 2: 0.23 [0.12-0.54]; quartile 3: 0.29 [0.18-0.53]; quartile 4: 0.31 [0.13-0.61] ratio/ms-1, p=0.118). Similarly, we did not demonstrate a statistical difference in the ratio observed in patients with tricuspid or bicuspid valves after correcting for stenosis severity although there was an apparent tendency for a lower ratio in those with a bicuspid valve (0.31 [0.15-0.57] *versus* 0.11 [0.09-0.43] ratio/ms-1 respectively, p=0.115).

FIGURE 3.3.

The Fibro-Calcific Ratio.

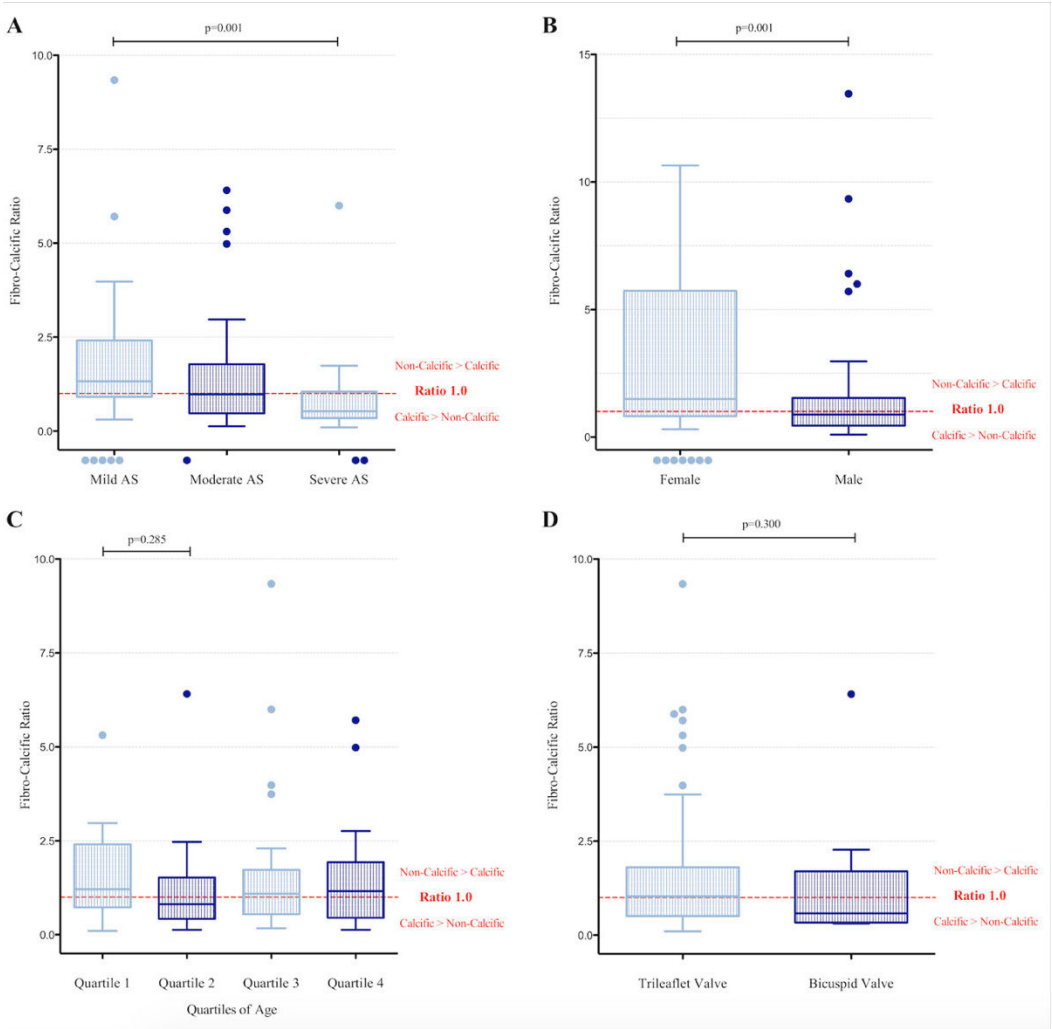

Figure 3.3. Tukey boxplots of the fibro-calcific ratio grouped by aortic stenosis disease severity class **(A)**, by sex **(B)**, by quartiles according to age (quartile 1 being the youngest and quartile 4 the eldest) **(C)** and by cusp morphology (trileaflet versus bicuspid valves) **(D)**. Note that the ratio decreases with progressive aortic stenosis severity class and is higher in women than men but does not demonstrate a clear difference according to patient age or valve morphology.

Fibro-Calcific Burden

Non-calcific and calcific leaflet volumes were combined and indexed to annulus area to produce the fibro-calcific burden as a marker of the total disease severity. The fibro-calcific burden across the whole cohort was 172 [112-243] mm^3/cm^2 (compared to 30 [20-43] mm^3/cm^2 in the control cohort; $p<0.001$) and there was a progressive increase in this burden with increasing aortic stenosis severity (mild: 110 [77-150] mm^3/cm^2; moderate: 191 [119-253] mm^3/cm^2; and severe: 230 [196-333] mm^3/cm^2; $p<0.001$) (Figure 3.4). The fibro-calcific burden demonstrated a strong correlation with all echocardiographic measures of aortic stenosis severity (peak aortic-jet velocity: $r=0.71$ $p<0.001$), comparing favorably with traditional non-contrast CT-AVC assessments ($r=0.60$, $p<0.001$; Table 3.2). The fibro-calcific burden appeared to be of particular value in women, where it demonstrated a much closer association with hemodynamic echocardiographic assessments (peak aortic-jet velocity: $r=0.77$, $p=0.001$; mean gradient: $r=0.85$, $p=0.001$) than was observed for CT-AVC (peak aortic-jet velocity: $r=0.27$, $p=0.22$; mean gradient: $r=0.37$, $p=0.074$; Table 3.2; Figure 3.5).

FIGURE 3.4.

Fibro-Calcific Burden (combined non-calcific and calcific leaflet volumes indexed to annulus area) and its association with aortic stenosis severity compared with non-contrast CT calcium scoring.

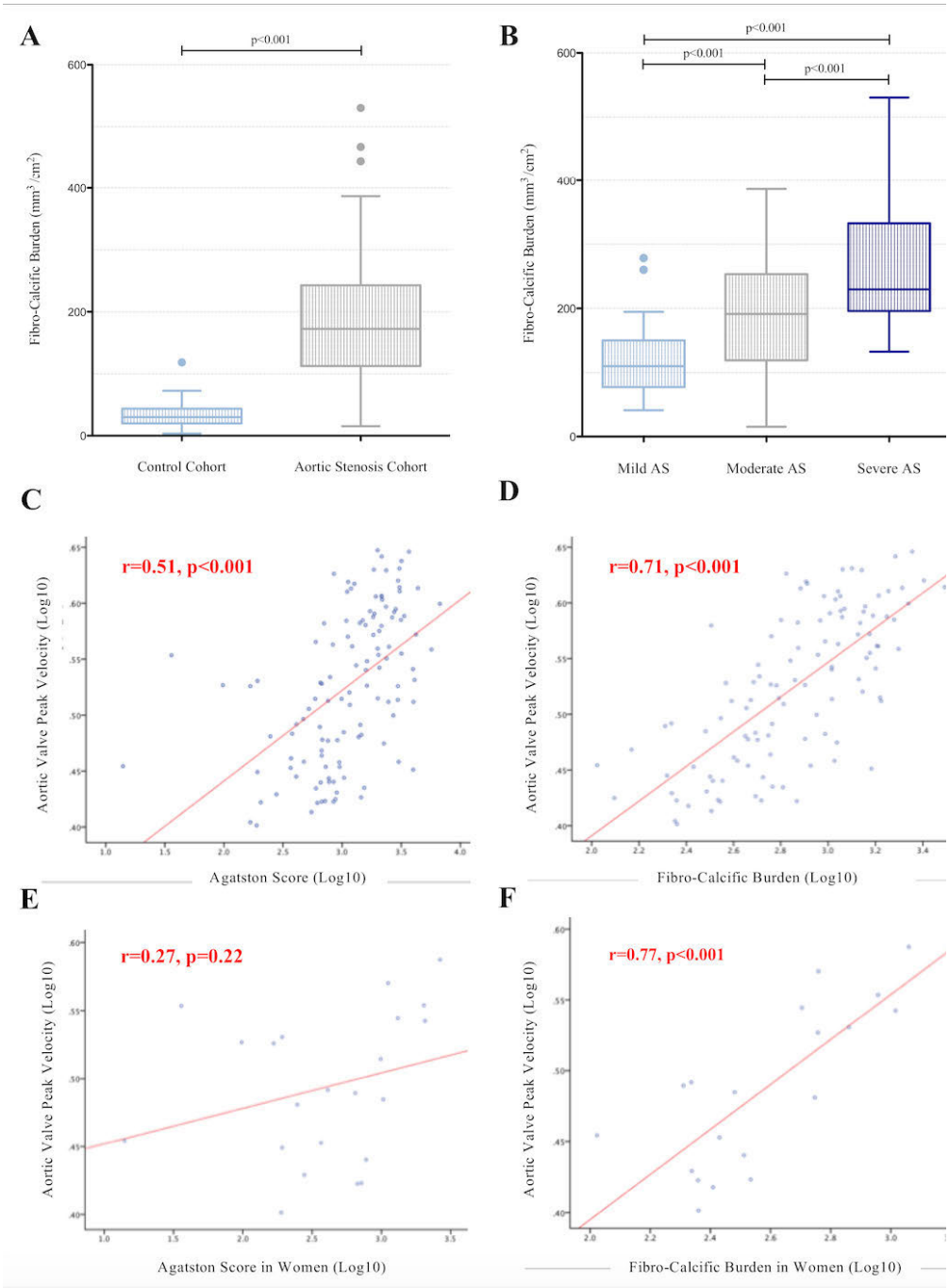

Figure 3.4. Tukey boxplots of the total fibro-calcific burden (mm^3/cm^2) comparing values in the control cohort without aortic valve disease *versus* the cohort with aortic stenosis **(A)** and grouped by aortic stenosis severity class **(B)**. Scatter plots illustrating the correlation of aortic valve peak velocity with both non-contrast CT-AVC ($r=0.51$, $p<0.001$) **(C)** and the improved association with the fibro-calcific burden ($r=0.71$, $p<0.001$) **(D)** across the whole population. When women with aortic stenosis were selected, there was no significant association between peak velocity and CT-AVC ($r=0.27$, $p=0.22$) **(E)** but the fibro-calcific burden offered a strong positive correlation ($r=0.77$, $p<0.001$) **(F)**, similar to that in the population as a whole.

FIGURE 3.5.

Case illustration of utility of the fibrocalcific burden in assessment of aortic stenosis.

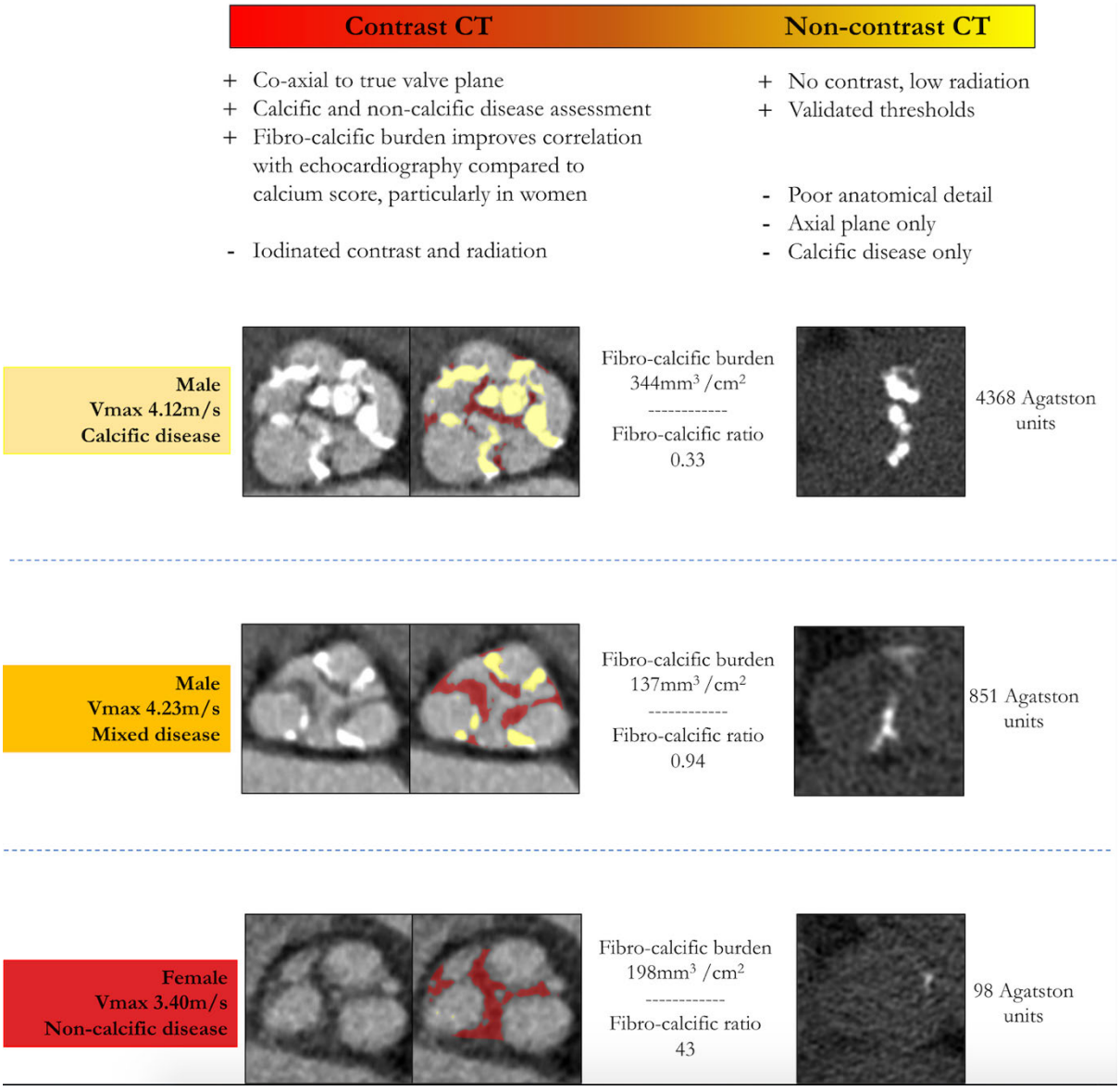

Figure 3.5. Summary figure illustrating the comparison of the relative strengths and weakness of contrast and non-contrast computed tomography for the assessment of aortic stenosis disease burden and severity. The top patient example demonstrates

severe, predominantly calcific aortic stenosis with a corresponding high Agatston score. The calcium was distributed over multiple axial slices on CT-AVC and is more readily appreciated from the *en face* contrast-enhanced images. The middle example is of severe concordant aortic stenosis with mixed fibro-calcific disease but an Agatston score well below the threshold for severe disease. The bottom example demonstrates moderate, fibrotic aortic stenosis with only trivial calcification.

External Validation of Fibro-Calcific Burden

Twenty-five patients with severe aortic stenosis awaiting surgical aortic valve replacement underwent contrast-enhanced CT and subsequent analysis of the explanted aortic valve. There was a very strong correlation between the combined fibro-calcific burden and aortic valve weight ($r=0.88$, $p<0.001$). The valve weight demonstrated a closer ($p=0.03$) association with the combined fibro-calcific burden ($r=0.87$, $p=0.002$) than with CT-AVC alone ($r=0.76$, $p=0.009$). An interaction was observed between fibro-calcific burden and sex with respect to the prediction of valve weight, with a closer association between fibro-calcific burden and weight in women than in men ($p=0.04$). Finally, histological examination confirmed the presence of valve fibrosis in spatial correlation with areas of non-calcific leaflet thickening observed on CT (Figure 3.6). By contrast there was no thrombus or gross lipid deposition observed in these areas.

In the external validation cohort, 39 patients (10 women and 29 men) (Table 3.3) underwent a contrast-enhanced ECG-gated CT and Doppler echocardiography. Correlations between the indexed calcific or non-calcific leaflet volumes and the mean gradient on echocardiography were similar to that observed in the original cohort (calcium volume: $r=0.74$, $p<0.001$; non-calcific volume: $r=0.44$, $p=0.005$). The correlation with echocardiographic assessments of aortic stenosis severity (mean gradient) was better for the fibro-calcific burden ($r=0.78$, $p<0.001$) than CT-AVC ($p=0.005$). Similar results were seen when peak aortic-jet velocity was used as the echocardiographic measure of aortic stenosis severity (Table 3.3).

FIGURE 3.6.

Comparison between contrast CT analysis and histologic examination.

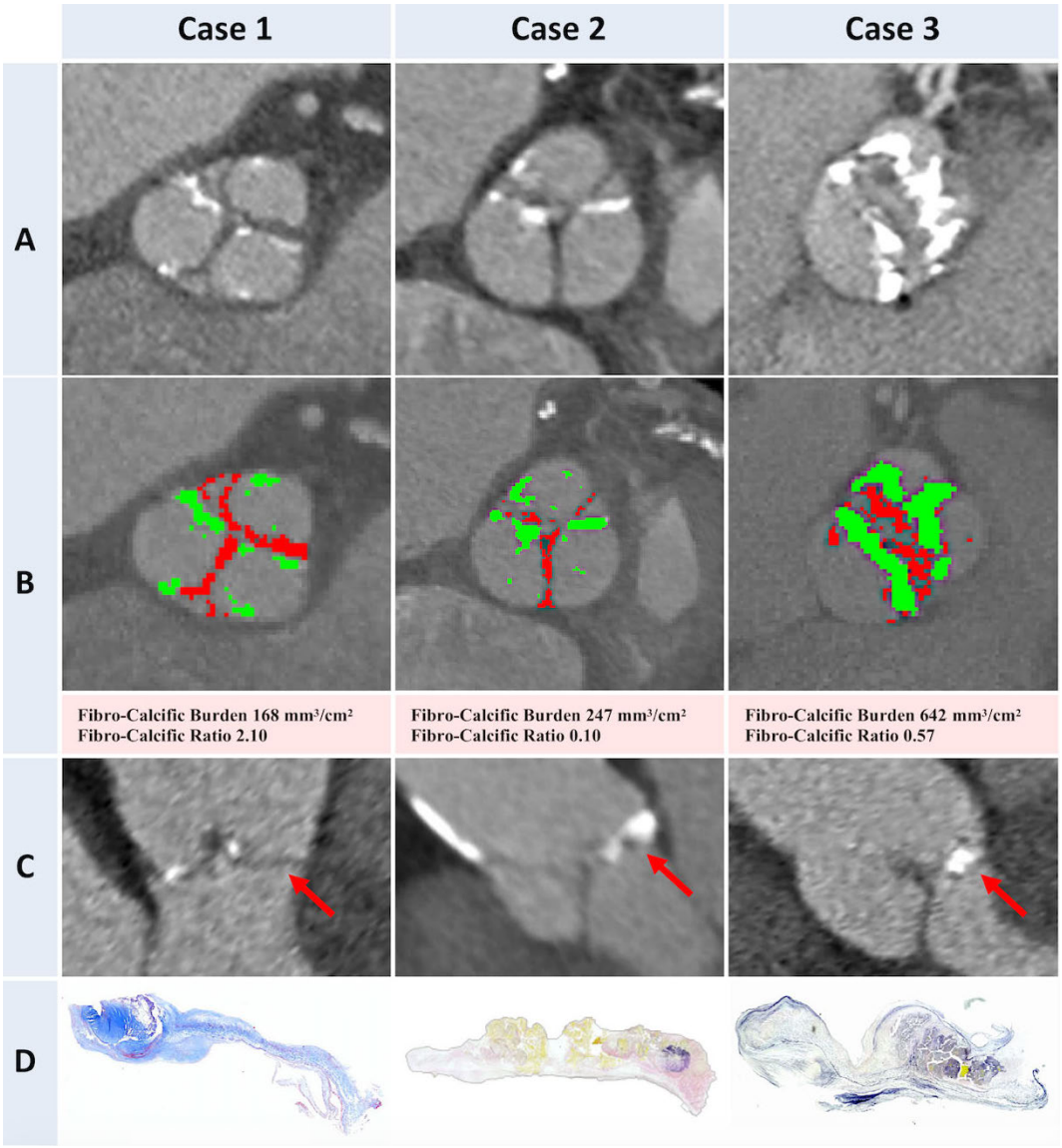

Figure 3.6. Case 1. A tricuspid aortic valve from a woman with a large amount of fibrosis (red) compared to calcification (green) on CT. Histology confirms a preponderance of fibrosis in the valve consistent with the CT findings with no clear

evidence of valve thrombosis or lipid infiltration. Trichrome Masson staining: blue sections represent collagen; red/purple represents calcium.

Case 2. A tricuspid aortic valve from a man with a small amount of fibrosis compared to calcification (from the 3 CT slices containing the aortic valve this one was the only one with significant fibrosis). This was again confirmed on histological analysis of the valve leaflet. Verhoeff-Van Giesson staining: Black represents elastic fibres, pink collagen fibres, and yellow calcium.

Case 3. A bicuspid aortic valve from a man with both extensive fibrosis and calcification in the valve. Findings were again confirmed on histology with the spatial distribution of calcium and fibrosis on histology appearing similar to the calcific and non-calcific leaflet thickening on CT (Verhoeff-Van Giesson staining).

TABLE 3.3.

Patient Characteristics of Validation Cohort from Universite Laval, Canada.

POPULATION CHARACTERISTICS	
Total subjects	39
Age (years)	65.9±10.4
Female n (%)	10 (26)
Medical History	
Hypertension (%)	25 (64)
Diabetes (%)	9 (23)
Coronary Artery Disease (%)	17 (44)
Smoking (%)	12 (31)
Dyslipidaemia (%)	23 (59)
Medication	
Statin (%)	24 (62)
ACEi (%)	14 (36)
ARB (%)	7 (18)
Beta-Blocker (%)	14 (36)
Antiplatelet (%)	28 (72)
Warfarin (%)	1 (3)
Echocardiography	
LV Systolic Dysfunction (%)	2 (5)
Bicuspid Aortic Valve (%)	15 (38)
Aortic Valve Mean Gradient (mmHg)	27.7±12.4
Aortic Valve Area (cm^2)	1.44±0.35
Computed Tomography	
Annulus Area (cm^2)	5.36±1.17
Contrast CT Calcium Volume (mm^3/cm^2)	86.5 [14.5-225.1]
Non-Calcific Leaflet Volume (mm^3/cm^2)	62.3 [12.6-101.2]

Abbreviations: ACEi: angiotensin-converting enzyme inhibitor, ARB: angiotensin receptor blockade, CT: computed tomography, LV: left ventricle, LVOT: left ventricular outflow tract.

3.5 DISCUSSION

For the first time, we describe a novel method of CT analysis that allows assessment of both valve calcification and non-calcific leaflet thickening (fibrosis) in patients with aortic stenosis (Figure 3.5). This has provided unique insights into the underlying pathophysiology of aortic stenosis, with fibrosis appearing to predominate in women and patients with mild stenosis, whilst calcification dominated in men and those with advanced severe disease. Moreover, we propose a novel anatomical measure of aortic stenosis severity, the fibro-calcific burden, that incorporates both fibrotic and calcific valve thickening. This novel summary measure demonstrates excellent agreement with echocardiographic assessments of hemodynamic disease severity and valve weight that were superior to CT-AVC alone. Given the widespread use of contrast CT in the assessment of patients with aortic stenosis (such as transcatheter aortic valve replacement planning), the fibro-calcific burden could be readily adopted into routine clinical practice, providing an alternative assessment of aortic stenosis severity for patients with uncertain disease severity.

Discordant echocardiographic assessments of aortic stenosis severity are observed in around a third of patients (Clavel MA *et al*, 2013; Minners J *et al*, 2010), leading to diagnostic uncertainty about true disease severity. Non-contrast CT-AVC has emerged as an attractive alternative imaging approach in these patients providing an anatomic assessment of disease severity independent of flow that is now recommended by international guidelines (Baumgartner H *et al*, 2017). Sex-specific CT-AVC thresholds for severe aortic stenosis have been developed that may indirectly correct

for the increased valve fibrosis observed in women and which generally offer good diagnostic accuracy compared to echocardiography (area under the curve of ~0.90) (Pawade TA *et al*, 2018). However, as CT-AVC becomes more widely established, it is important to recognise that by ignoring valve fibrosis CT-AVC may in certain cases underestimate aortic stenosis severity. Indeed, reports have emerged in the literature of patients with concordant severe aortic stenosis yet low CT calcium scores, especially in young women (Shen M *et al*, 2016). Moreover, differentiation of valvular calcification from calcification of the aorta, left ventricular outflow tract, mitral valve annulus and coronary arteries can be challenging on axial non-contrast CT-AVC images. There is therefore a clear rationale for exploring alternative anatomic assessment of aortic stenosis. In particular, contrast-enhanced CT angiography offers a potential solution to each of these problems with the added advantage of current widespread use for transcatheter aortic valve replacement planning.

Our study has several important strengths. First, we prospectively recruited patients across the spectrum of aortic stenosis severity as well as control subjects with normal aortic valves. Each participant underwent systematic multi-modality imaging assessments including ECG-gated non-contrast CT, contrast-enhanced CT and Doppler echocardiography with the rigor employed by a regulated double blind randomised controlled trial. The novel image analysis protocol here proposes the use of flexible thresholds for defining calcific and non-calcific valve thickening based upon contrast load at the sinotubular junction and makes use of approaches for finding the true aortic valve plane and sizing the aortic annulus that are well established in the transcatheter aortic valve replacement field. This has allowed the development of a

robust and reproducible method for quantifying both calcific and non-calcific valve thickening that has helped highlight the importance of fibrosis in the pathogenesis of aortic stenosis. Moreover, this study has established the fibro-calcific burden as a promising anatomic measure of aortic stenosis severity which we have validated against hemodynamic assessments on echocardiography, CT-AVC and *ex vivo* valve weights across two independent international patient cohorts.

Progressive valve stiffening and narrowing in aortic stenosis occurs due to both fibrosis and calcification, although previous imaging approaches have focused almost exclusively on the latter (Dweck MR *et al*, 2012 a). Contrast-enhanced CT allows quantification of valvular calcium with a close association with CT-AVC, the current gold standard. However, we have also used contrast CT to measure the volume of non-calcific valve thickening as a surrogate of fibrosis, allowing calculation of the fibro-calcific ratio and providing an insight into the relative contributions of these pathological processes at different stages of disease. When examining the aortic stenosis cohort as a whole, the volumes of calcific and non-calcific valve thickening were similar (fibro-calcific ratio 1.04 [0.48-1.79]) highlighting the important contribution that fibrosis makes to the pathology of aortic stenosis. Here we make the assumption that non-calcific valve thickening represents valve fibrosis. We deliberately selected a lower boundary threshold of 30 HU to define non-calcific leaflet thickening since attenuation levels below this level may include thrombosis rather than fibrosis. Our assumptions are strongly supported by previous histological data demonstrating the predominance of fibrosis and calcification in aortic stenosis

(Yetkin E *et al*, 2009; Hinton RB *et al*, 2006), and are further confirmed by our own correlative *ex vivo* and histological assessments (Figure 3.6).

The fibro-calcific ratio is not fixed but is instead highly variable. In mild aortic stenosis, fibrosis was the dominant finding, in moderate aortic stenosis there appeared to be a balanced contribution, while in severe disease calcification predominated. This suggests early disease begins with a fibrotic response that progressively calcifies leading to the development of hemodynamically significant disease. Interestingly, the fibro-calcific ratio also exhibited a clear sex discrepancy with calcification predominating in men (0.89 [0.45-1.54]) and fibrosis the predominant process in women (1.49 [0.82-5.74]). These observations have important clinical implications, indicating that the factors driving aortic stenosis progression both evolve with time and are different in men and women. The development of effective medical therapies will depend on understanding the mechanisms underlying these observations and potentially tailoring pharmacological interventions according to sex, disease severity and the predominant pathological processes observed on imaging.

We explored the fibro-calcific burden as a novel anatomic measure of aortic stenosis severity. Differentiation of pathology in the valve from surrounding structures is easier than with CT-AVC, because contrast CT allows analysis on high-resolution images in the true plane of the valve. Reproducibility of measurements was therefore excellent. The fibrocalcific score was nearly 6-fold higher in patients with aortic stenosis compared to control subjects and increased steadily with progressive disease severity. Indeed, the fibro-calcific burden demonstrated a close association with

echocardiographic measurements of hemodynamic severity, outperforming CT-AVC. This was particularly true in women, in whom the CT-AVC demonstrated a disappointing association with peak aortic-jet velocity that improved considerably (similar to that observed in men) when using the fibro-calcific burden as the CT assessment. Similar findings were observed in an external independent validation cohort. Finally, we validated the CT fibro-calcific score against the valve weights of 25 explanted valves from patients who had undergone CT imaging shortly before surgical aortic valve replacement. Once again, the fibro-calcific score demonstrated a closer association with valve weight than CT-AVC even though these patients all had severe stenosis, a stage of the disease where calcium predominates.

The fibro-calcific burden holds major promise as an alternative anatomic assessment of aortic stenosis severity to complement echocardiography and CT calcium scoring. CT angiography is already widely performed in many centres, for example, as part of the routine pre-procedure assessment for transcatheter valve implantation and many clinicians have already developed corresponding expertise in reading these scans. There is therefore considerable potential for the fibro-calcific burden to be rapidly adopted into routine clinical practice within established patient pathways. However, further work is now required to validate the fibro-calcific burden in large patient populations, to establish its prognostic value and to provide robust thresholds that can be used in clinical practice to identify patients with severe and non-severe aortic stenosis.

We should acknowledge some limitations of our study. Our image analysis method is time consuming (~45 min) relying upon multiple steps and transfer of data between different software packages. An integrated software solution that can facilitate more rapid image analysis whilst maintaining accuracy and reproducibility would be welcome and help accelerate uptake of this approach. In addition, image analysis is challenging in scans at the upper and lower extremes of blood-pool contrast load and there is likely scope to refine how we calculate and administer intravenous iodinated contrast media and acquire the images.

In conclusion, CT angiography allows robust and reproducible quantification of both valve leaflet fibrosis and calcification in patients with aortic stenosis. This has provided key pathophysiological insights, highlighting the importance of non-calcific valve thickening, particularly among women and patients with mild aortic stenosis. Moreover, the fibro-calcific burden provides a novel assessment of aortic stenosis severity that offers closer agreement with echocardiographic assessments and valve weight than CT-AVC. Further work is now required to validate the fibro-calcific burden, and to establish both its prognostic value and clear thresholds that can be used to differentiate severe from non-severe disease. This novel imaging method may provide an invaluable tool to confirm aortic stenosis severity in patients with discordant echocardiographic measurements or low-flow states.

CHAPTER 4

OPTIMISATION AND REPRODUCIBILITY OF AORTIC VALVE ^{18}F-FLUORIDE POSITRON EMISSION TOMOGRAPHY IN PATIENTS WITH AORTIC STENOSIS

Pawade TA, Cartlidge TRG, Jenkins WSA, Adamson PD, Robson P, Van Beek EJR, Fletcher A, Tuck S, Newby DE, Dweck MR. Optimization and reproducibility of aortic valve 18F-fluoride positron emission tomography in patients with aortic stenosis. *Circ Cardiovasc Imaging.* 2016;**9**:e005131.

4.1 ABSTRACT

Objective

^{18}F-Fluoride positron emission tomography (PET) and computed tomography (CT) can measure disease activity and progression in aortic stenosis. We aimed to optimise imaging methodology, analysis and scan-rescan reproducibility.

Methods

Fifteen patients with aortic stenosis underwent ^{18}F-fluoride PET-CT on two occasions. We compared non-gated PET and non-contrast CT with a modified approach that incorporated contrast CT and ECG-gated PET. We explored a range of image analysis techniques including estimation of blood pool activity at differing vascular sites and a most-diseased segment (MDS) approach.

Results

Contrast-enhanced ECG-gated PET-CT provided superior spatial localization of ^{18}F-fluoride uptake that permitted localization to individual valve leaflets. Indeed, uptake was most commonly observed at sites of maximal mechanical stress, the leaflet tips and the commissures. Scan-rescan reproducibility was markedly improved using enhanced analysis techniques leading to a reduction in variability from ±25% to <±10% (tissue-to-background MDS: mean value 1.55, difference 0.05, limits of agreement -0·10 to 0·20).

Conclusion

Optimised ^{18}F-fluoride PET-CT provides excellent spatial localization and scan-rescan reproducibility. It is estimated that a clinical trial powered at 95% would require a sample size of 46 patients to demonstrate a 10% reduction in ^{18}F-Fluoride uptake (assuming an alpha error of probability of 0.05). This technique holds major promise as a real-time marker of disease activity in aortic stenosis and is ready to be used as a biomarker end-point in clinical trials of novel therapies in aortic stenosis.

4.2 INTRODUCTION

Aortic stenosis is the most common form of valve disease in the western world and a major health care burden that is set to treble by 2050. However, we currently lack any disease-modifying therapies. Calcification appears to be the predominant pathological process driving disease progression leading to major interest in novel treatment strategies aimed at reducing calcification activity in the valve (Pawade TA *et al*, 2015). However, assessing the efficacy of new therapies requires large trials with prolonged follow-up to demonstrate an impact on disease progression and clinical end-points (Rossebo AB *et al*, 2008). A non-invasive imaging technique capable of measuring calcification activity in the valve would be highly desirable to assess treatment efficacy in phase 2 clinical trials.

^{18}F-Fluoride is a positron-emitting radiotracer that binds to regions of newly developing microcalcification beyond the resolution of computed tomography (Irkle A *et al*, 2015). It is readily taken up by the valves of patients with aortic stenosis and on histology, correlates with markers of calcification activity (Dweck MR *et al*, 2014)). Importantly this technique predicts disease progression both with respect to echocardiography and CT calcium scoring as well as adverse cardiovascular events (Dweck MR *et al*, 2014; Dweck MR *et al*, 2012 b; Jenkins WSA *et al*, 2014). ^{18}F-Fluoride positron emission tomography (PET) imaging therefore holds major promise as a marker of calcification activity in aortic stenosis and is an exploratory end-point in a randomised controlled trial of therapies targeting calcium metabolism (NCT02132026). Here, we sought to optimise ^{18}F-fluoride PET scanning of the aortic

valve and to assess the scan-rescan reproducibility of this technique to inform its future application as a biomarker of calcification activity in clinical trials.

4.3 METHODS

Study Population

Patients aged over 50 years with asymptomatic mild, moderate and severe calcific aortic stenosis were recruited from the Royal Infirmary of Edinburgh. Exclusion criteria included renal failure and women of childbearing potential, as detailed below. This study was approved by the Scottish Research and Ethics Committee and the Medicines and Healthcare products Regulatory Authority (MHRA) of the United Kingdom. All patients gave written informed consent and research was performed in accordance with the Declaration of Helsinki.

Inclusion Criteria

Age > 50 years; peak aortic jet velocity > 2.5 m/s on Doppler echocardiography; grade 2-4 calcification of the aortic valve on echocardiography.

Exclusion Criteria

Women of childbearing potential who are premenopausal, have not been sterilised or who are currently pregnant; women who are breastfeeding; renal failure (estimated glomerular filtration rate of <30 mL/min); inability to undergo scanning; allergy or contraindication to iodinated contrast; inability or unwilling to give informed consent; likelihood of non-compliance to treatment allocation or study protocol; anticipated or planned aortic valve surgery in the next 6 months; life expectancy less than 2 years; treatment for osteoporosis with bisphosphonates or denosumab; known allergy or intolerance to alendronate or denosumab, or any of their excipients; abnormalities of

the oesophagus or conditions, which delay oesophageal/gastric emptying; inability to sit or stand for at least 30 minutes; hypocalcaemia; regular calcium supplementation; dental extraction within 6 months; long term corticosteroid use; history of osteonecrosis of the jaw; poor dental hygiene.

Initial Image Acquisition and Analysis

Each patient underwent ^{18}F-fluoride positron emission tomography (PET) and computed tomography (CT) scanning on two occasions less than 3 months apart. Patients were given 25 mg of oral metoprolol if their resting heart rate was >65 beats/min before being administered 125 MBq of ^{18}F-fluoride intravenously. After 60 min, patients were imaged with a hybrid PET and CT scanner (Biograph mCT, Siemens). Attenuation-correction CT scan was performed before acquisition of PET data in list mode using a single 30-min bed position centred on the valve in three-dimensional mode. Finally, ECG-gated aortic valve CT calcium scoring and contrast-enhanced CT angiography were performed in diastole and in held expiration.

CT calcium scoring was performed by an experienced operator using dedicated software (Vitrea Advanced, Toshiba systems) on axial views, with care taken to exclude calcium originating from the ascending aorta, left ventricular outflow tract and coronary arteries. The calcium score was recorded in Agatston Units (AU).

PET analysis was performed using an OsiriX workstation (OsiriX version 3.5.1 64-bit; OsiriX Imaging Software, Geneva, Switzerland). As previously reported, regions of interest were drawn around the perimeter of the valve on the fused non-gated PET

and non-contrast CT images (Dweck MR *et al*, 2012 b). These generated mean and maximum standard uptake values (SUV) for each slice. Averaging these values across the entire valve produced whole valve SUV_{mean} and SUV_{max} values respectively. These SUV values were then corrected for blood pool activity to generate tissue-to-background ratio (TBR): whole-valve $I_{,}$ and TBR_{max}. The blood pool uptake was determined using SUV_{mean} values averaged from across ROIs drawn on 5 contiguous slices in the brachiocephalic vein. For consistency the most caudal ROI was positioned at the point where the innominate vein joined the brachiocephalic vein (Dweck MR *et al*, 2012 b).

To optimise the spatial resolution and scan-rescan reproducibility of ^{18}F-fluoride PET/CT imaging, we assessed different approaches to both image acquisition and image analysis.

Optimisation of PET Image Acquisition

Contrast CT of Aortic Valve

Our original technique required the reorientation and co-registration of non-contrast CT images of the aortic valve. This technique posed several challenges, particularly with respect to getting into the true plane of the valve and accurately defining its perimeter. Moreover, the structure of individual leaflets was not visible on these scans precluding more detailed localization of ^{18}F-fluoride uptake. Contrast CT offered potential solutions to these challenges given its superior anatomical detail and the well-established methodology for finding the true plane of the valve (Litmanovich DE *et al*, 2014) (Figure 4.1).

ECG-Gated PET Data

PET is susceptible to motion, limiting accurate co-registration and the spatial assessment of PET activity within the valve. As a solution, we employed electrocardiogram (ECG) gating of list mode PET data. These data were reconstructed into 4 gates at 25% intervals of the cardiac cycle. Only data acquired between 50 and 75% of the RR interval were assessed because this period corresponds with diastole when cardiac motion is at a minimum. Given that three quarters of the PET data are therefore discarded, the bedtime was increased to 30 min in an attempt to preserve signal-to-noise.

Optimisation of PET Image Analysis

Measurement of Blood Pool Activity

The stability of blood pool measurements in the SVC for ^{18}F-fluoride based tracers has recently been questioned (Chen W *et al*, 2015) and we were concerned about variation in the measured blood-pool activity at different levels of the brachiocephalic vein. We reasoned that this may be explained by the relatively small diameter of this vein rendering it susceptible to partial volume effects, amplified by the very low PET signal in surrounding lung tissue (especially in the cranial aspects of the brachiocephalic vein). We hypothesised that sampling blood-pool activity from the centre of the right atrium (a much larger structure) may improve the ease and accuracy with which these measurements could be made and the consequent scan-rescan reproducibility. Using the same co-registered PET and CT images of the heart, re-orientated to the plane of the valve, a 2-cm^2 ROI was drawn in the centre of the right atrium at the level of the right coronary ostium and again in the same position one slice superiorly. Averaging

the mean SUV for these two slices gave an alternative measure of blood-pool activity, which was used to correct valvular uptake measurements using two different approaches. First, we used the conventional method of dividing aortic valve SUV measurements by the blood-pool to generate TBR values. Secondly we subtracted the blood-pool value from the valvular uptake, to generate the corrected aortic valve SUV (cSUV) as described recently (Chen W *et al*, 2015).

Most -diseased Segment and Whole Valve Approach

One of the biggest difficulties in quantifying uptake in the valve is defining its limits in the z plane. To overcome this challenge, our original whole valve technique was compared to a 'most-diseased segment' (MDS) approach where the two contiguous slices with the highest SUV values (frequently in the centre of the valve) were averaged to generate $SUV_{MDSmean,}$ SUV_{MDSmax} and corresponding TBR values. This is similar to the approach previously used for quantifying ^{18}F-fluorodoexyglucose uptake in carotid and aortic atheroma (Fayad ZA *et al*, 2011).

Spatial Resolution and Scan-Rescan Reproducibility

The effect of our modifications on spatial resolution and scan-rescan reproducibility were then assessed in comparison with the original approach. First, we assessed the ability of the technique to localise increased ^{18}F-fluoride activity to individual valve leaflets and their different regions. This was done visually using a standardised method for windowing the fused PET/CT images that incorporated the blood pool activity in RA as the minimum. Kappa statistics were then used to quantify agreement as to the

presence or absence of increased ^{18}F-fluoride uptake in individual leaflets between the baseline and repeat scans.

Second, we determined the scan-rescan reproducibility of ^{18}F-fluoride PET quantification in the valve using the various approaches. The paired scans for each patient were analysed by two experienced observers in a random order at least 2 weeks apart to minimise recall bias.

Statistical Analysis

Continuous variables were expressed as mean ± standard deviation. For normally distributed data, Student's *t*-tests were used to assess differences between mean values. Data underwent logarithmic transformation where necessary. To determine a relationship between continuous variables, the Pearson's correlation coefficients were used. Scan-rescan, intra-observer and inter-observer reproducibility for both CT calcium scoring and PET uptake were analysed and presented using Bland-Altman analyses and intraclass correlation coefficients (ICC). Statistical significance was defined as two-sided $P<0.05$.

4.4 RESULTS

Patient Characteristics

Fifteen patients (73±9 years, 67% male) had 2 scans within a 13-week period (13 patients had repeat scanning within 8 weeks). Seven patients had mild aortic valve disease, 4 had moderate and 4 had severe aortic stenosis (Table 4.1). There were no differences in ^{18}F-fluoride doses between the two visits (123±8 and 125±4 MBq, P=0·49). The mean total radiation dose per patient for the two scans was 28.9±13 mSV.

Altered PET Acquisition and Image Quality

Contrast CT imaging of the valve appeared to provide much clearer anatomical detail of the leaflets and valve structure compared to non-contrast CT (Figure 4.2). This made it technically easier to get into the true plane of the valve and allowed more accurate regions of interest to be drawn around its perimeter (Figure 4.1 and 4.2). Co-registration with ECG-gated PET data then allowed localization of ^{18}F-fluoride uptake to individual leaflets and their different regions, which was previously impossible using non-contrast CT and non-gated PET. Most commonly increased activity was observed across all three coronary cusps (n=10), it involved two cusps in 4 patients, and was isolated to one cusp in just 1 patient. The non-coronary cusp was involved in all patients apart from that latter case. Activity was most frequently observed at the valve commissures, and specifically at the points where the valve cusps meet the aortic ring (n=10) and at the tips where the leaflets coapt during diastole (n=8) (Figure 4.2).

TABLE 4.1.

Patient Characteristics.

Characteristics	Average ±SD
Age (years)	73±7
Male (%)	67
Body Mass Index (kg/m^2)	30±6
BSA (m^2)	1.95±0.2
Mean Arterial Pressure (mmHg)	100±9.3
Breathlessness (%)	47
Chest pain (%)	27
Syncope (%)	7
Interval between scans (weeks)	5±3
Heart rate (/min)	61±8
^{18}F-Fluoride Dose Received	120±13
Hypertension (%)	73
Previous CABG/PCI (%)	33
Liver Disease (%)	7
Rheumatic Fever (%)	0
Previous MI (%)	20
Current/ex-smoker (%)	40
Hypercholesterolemia (%)	67
Diabetes (%)	27
Renal Disease (%)	0
TIA/CVA (%)	13
Serum Creatinine (mg/dL)	74±11
GFR (mL/min/1.73 m^2)	115±21
ACE inhibitors (%)	47
AIIRB (%)	7
Beta Blockers (%)	40
Statins (%)	60
AV jet velocity (I)	3.48±0.5
AV mean gradient (mmHg)	27±10

FIGURE 4.1.

Creation of Co-registered En Face Short-Axis PET/CT Images of the Aortic Valve.

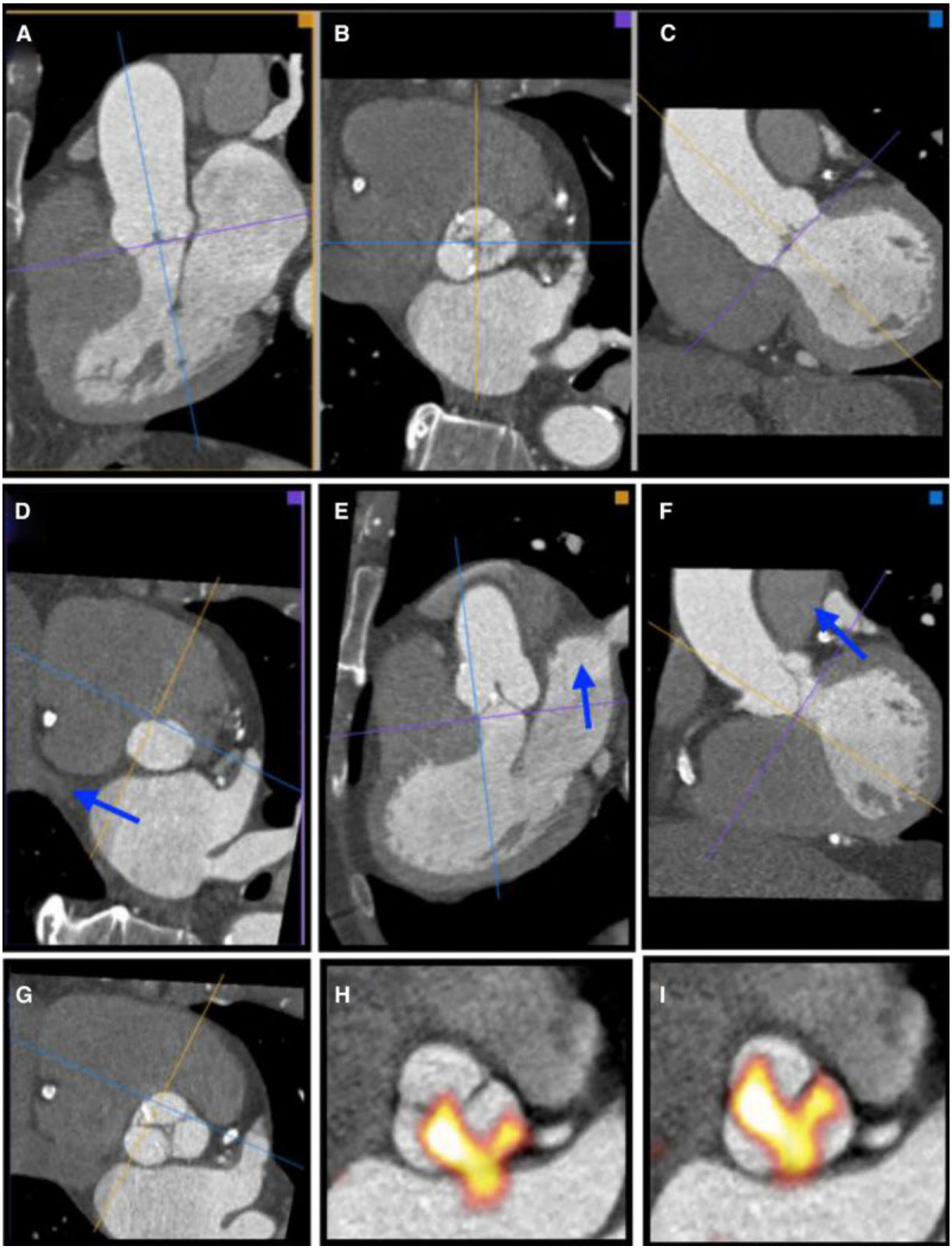

Figure 4.1. Creation of planar en-face valve images using CT angiography was achieved as follows. First, the CT angiogram is reorientated to get into the approximate plane of the aortic valve by lining up the axial cross hair (purple in this example) using the images in the coronal (a) and sagittal planes (c). This creates an approximate cross sectional image of the aortic valve in the axial frame (b). Scrolling down in the axial frame, the centre of the crosshairs is then placed over the exact point at which the right coronary cusp disappears, identifying the base of that leaflet (d). Similarly, the base of the non-coronary cusp is identified and orthogonal planes adjusted so that the purple plane goes through the base of both these two cusps (d). Finally, the base of the left coronary cusp is found by rotation of the axial cross hairs so that first the cusp comes into view. The image is then slowly rotated in the opposite direction until the point where the leaflet first disappears (the base) is again found (f). This produces an en face image of the valve aligned with the base of all three leaflets (g). Adjacent 3-mm slices are then created in that plane and used for subsequent assessment. These slices are fused with the ^{18}F-Fluoride PET images (h) and careful co-registration performed in 3-dimensions to ensure accurate alignment between the PET and CT images (i).

FIGURE 4.2.

Improved Localisation of PET Signal Within the Aortic Valve and its Leaflets.

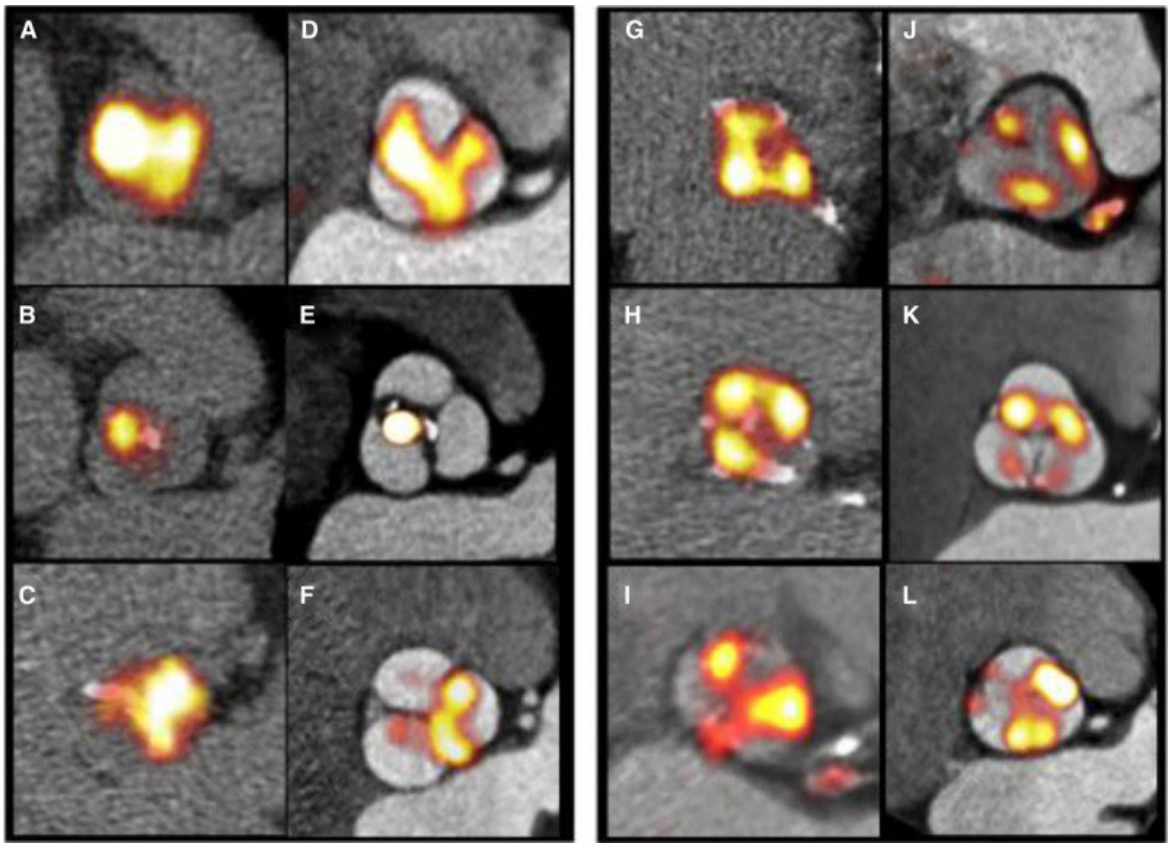

Figure 4.2. Paired non-gated, non-contrast PET/CT scans (original approach: A-C, G-I) and gated, contrast-enhanced PET/CT images (final approach: D-F, J-L). Images demonstrate the typical distribution of the tracer uptake within the valve at sites of increased mechanical stress i.e. at the leaflet tips (D-F) and at the commissures (J-L).

There was good scan-rescan and intraobserver agreement as to the presence or absence of increased ^{18}F-fluoride activity within individual valve cusps with an overall kappa statistics of 0.70 (95% CI 0.48 to 0.91). This agreement was excellent in the non- and right coronary cusps but was more difficult in the left coronary cusp perhaps due to adjacent uptake in the left main stem, aorta and other valve cusps (Tables 4.2 and 4.3).

Effect of Altered Image Analysis on PET Reproducibility

Interobserver and intra-observer reproducibility was excellent with no fixed or proportional biases for the various ^{18}F-fluoride uptake measurements as previously reported. ICC values were all >0.95 (Dweck MR *et al*, 2012 b).

The scan-rescan reproducibility of our original approach produced an error of approximately ±25% for each of the different SUV measurements (Table 4.4). Scan re-scan reproducibility for TBR measurements were also disappointing with an error of ±60%.

Blood pool measurements

The poor reproducibility of the original TBR values compared to SUV suggested a problem with measuring blood-pool activity in the brachiocephalic vein. Indeed a step-wise and non-physiological reduction in these blood pool measurements was observed on moving cranially up the axial slices away from the heart and into the lung. On average a 20% difference in values was observed between the top and bottom slices but this difference could be as high as 66%. By comparison blood-pool sampling from the right atrium was easier to perform, allowed larger regions of interest to be drawn

and was consistent, demonstrating a <1% difference in measurements acquired on adjacent slices (Figure 4.3). Even with the new approach, variation remained in the ^{18}F-fluoride blood pool PET activity observed in different patients (blood pool SUV 1.10±0.35).

Sampling the blood pool in the right atrium led to a substantial improvement in the scan-rescan reproducibility of all our TBR measurements. Indeed after implementing this approach the reproducibility of our TBR values consistently outperformed those for SUV values with percentage errors of between 20 and 25% for both mean and maximum values. In contrast, the approach of subtracting the blood pool uptake from the tissue SUV to produce cSUV measures did not greatly improve reproducibility resulting in percentage errors of ±40% (Table 4.4).

MDS Approach

The MDS technique improved the technical ease of image analysis, removing the difficulty in deciding upon the upper and lower limits of the valve in the z plane. This translated into further improvements in scan-rescan reproducibility for mean TBR values. Indeed the percentage error for $TBR_{MDSmean}$ measurements was reduced to <10%. Similarly maximum values were optimised upon addition of the MDS approach (percentage errors TBR_{MDSmax} ±18%) as were the SUV measurements (percentage errors: $SUV_{MDSmean}$ ±24%, SUV_{MDSmax} ±30%; Table 4.3).

Final Approach: Addition of Contrast-CT and ECG-gated PET

After the addition of contrast CT and ECG-gated PET data, the reproducibility for our $TBR_{MDSmean}$ measurement remained excellent with a percentage error of <10% and an ICC value of 0.95 (Figure 4.4). This was the best performing measure of the different approaches tested and was again superior to the equivalent $SUV_{MDSmean}$ value (percentage error ±34%). It also outperformed the measurements quantifying maximum ^{18}F-fluoride uptake in the valve, which were less reproducible after the addition of gated-PET and contrast-CT (percentage errors SUV_{MDSmax} ±49% and TBR_{MDSmax} ±36% respectively) (Table 4.4).

Study Populations and Sample Sizes

The excellent reproducibility of our valvular TBR_{MDSmax} PET measurements means that relatively few patients would be required to demonstrate a reduction in ^{18}F-fluoride activity secondary to a drug intervention. Assuming 95% power and an alpha error probability of 0.05, we estimate that 46 patients in each arm would be required to demonstrate a 10% reduction in ^{18}F-fluoride PET activity (TBR_{MDSmax}), 16 patients would be required for a 20% reduction and 9 patients would be required for a 30% reduction (Figure 4.4).

TABLE 4.2.

Scan-rescan and intra-observer reproducibility for presence or absence of ^{18}F-fluoride uptake.

	Right coronary Cusp			Non Coronary Cusp			Left Coronary Cusps		
Scan	**1a**	**1**	**2**	**1a**	**1**	**2**	**1a**	**1**	**2**
1	+	+	+	+	+	+	+	+	-
2	+	+	+	+	+	+	+	+	+
3	+	+	+	-	+	+	-	+	-
4	+	+	+	+	+	+	+	+	+
5	+	+	+	+	+	+	+	+	+
6	+	+	+	-	-	-	-	-	-
7	+	+	+	+	+	+	+	+	+
8	-	-	-	+	+	+	+	+	+
9	+	+	+	+	+	+	+	+	+
10	+	+	+	+	+	+	+	+	+
11	-	-	-	+	+	+	+	+	+
12	+	+	-	+	+	+	-	-	-
13	+	+	+	+	+	+	+	+	+
14	+	+	+	+	+	+	+	-	+
15	+	+	+	+	+	+	+	+	+

Table 4.2. Presence or absence of ^{18}F-Fluoride PET signal is denoted (+ and – respectively) for each individual valve leaflet. The distribution of ^{18}-Fluoride signal on scan 1 images (1a) were reassessed (1b) to assess intra-observer reproducibility and compared to scan 2 (2) to determine scan-rescan reproducibility.

TABLE 4.3.

Kappa statistics for interobserver and scan-rescan agreement for ^{18}F-Fluoride PET signal distribution.

	Overall	**Right Coronary Cusp**	**Non Coronary Cusp**	**Left Coronary Cusps**
Interobserver Agreement	**0.73** (SE 0.15, 95% CI 0.44 to 1.00)	**1.00 (SE 0.00, 95% CI 1.00 to 1.00)**	**0.63** (SE 0.33, 95% CI -0.01 to 1.00)	**0.58 (SE 0.26, 95% CI** 0.07 to 1.00)
Scan-rescan Agreement	**0.66** (SE 0.16, 95% CI 0.36 to 0.97)	**0.76 (SE 0.22, 95% CI** 0.32 to 1.00)	**1.00 (SE 0.00, 95% CI 1.00 to 1.00)**	**0.44 (SE 0.27, 95% CI** -0.08 to 0.97)

SE: Standard Error, CI Confidence Intervals.

FIGURE 4.3.

Measuring Blood Pool Activity in the Brachiocephalic vein and the right atrium.

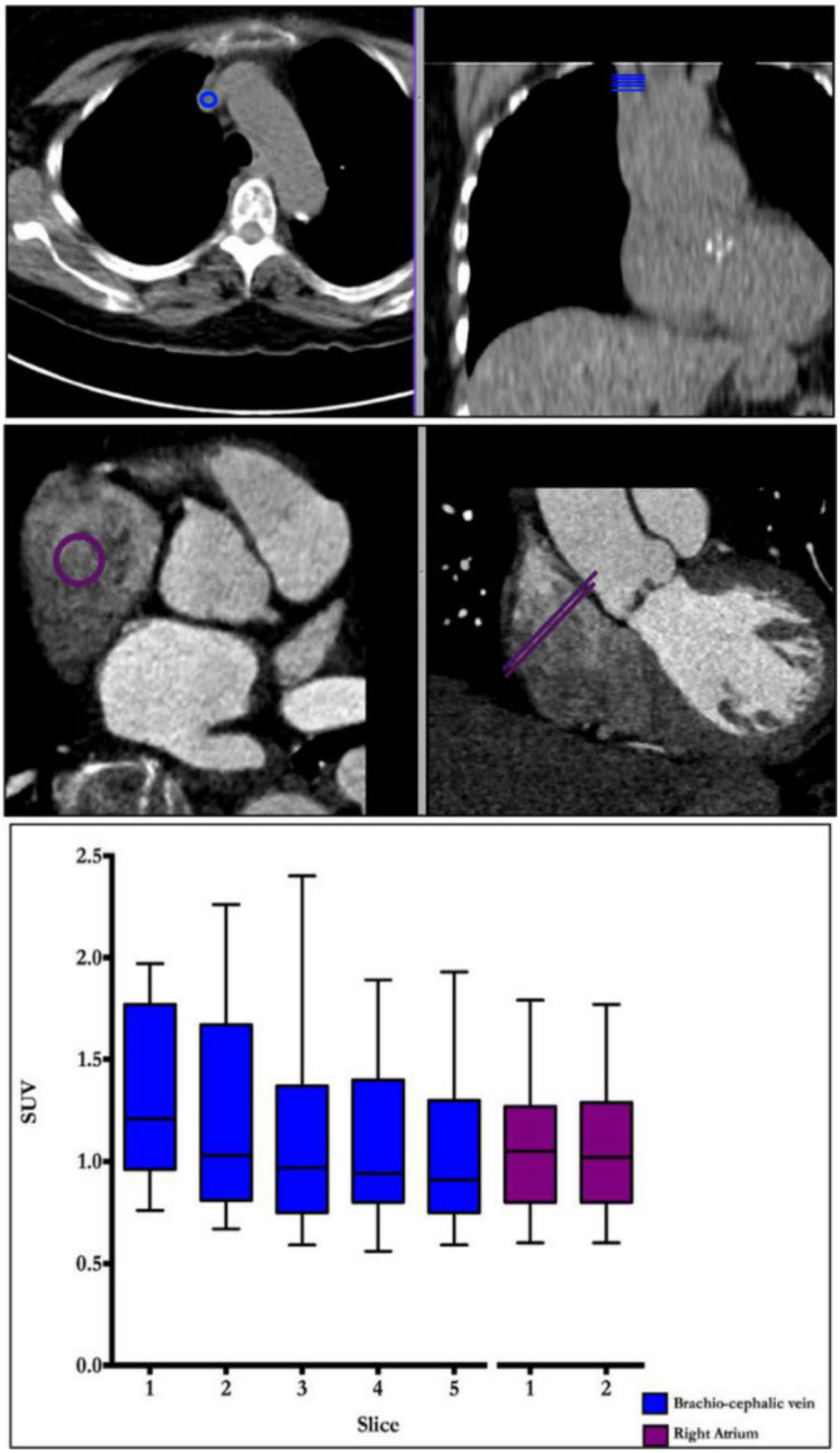

Figure 4.3. Regions of interest for measuring blood pool activity in the brachiocephalic vein (top) and right atrium (bottom) are shown in the en-face of the valve (left) and coronal (right) planes. Note that the right atrium is a much larger structure allowing for larger regions of interest with less potential for partial volume artifact problems related to poor registration. Tukey plot demonstrates mean SUV values for 5 contiguous slices from brachiocephalic (blue) and 2 from the right atrium (purple). Note the variation in brachiocephalic vein measurements between those taken most caudally versus those taken most cranially.

TABLE 4.4.

Bland-Altman values and percentage errors for each stepwise change to the image acquisition and analysis technique.

	MEAN VALUES				MAXIMUM VALUES			
	Ave	AD	LOA	Error (±%)	Ave	AD	LOA	Error (±%)
ORIGINAL APPROACH *WHOLE VALVE, UNGATED PET, NON CONSTRAST CT*								
ORIGINAL Standard Uptake Value	1.53	0.00	-0.39 to 0.37	**25**	1.96	0.09	-0.61 to 0.42	**26**
ORIGINAL Tissue to Background Ratio (using brachiocephalic)	1.44	0.04	-0.93 to 0.84	**61**	1.87	0.16	-1.34 to 1.05	**64**
RA BLOOD POOL CORRECTION								
corrected Standard Uptake Value (cSUV) (subtracting RA)	0.43	0.00	-0.19 to 0.17	**42**	0.86	0.10	-0.43 to 0.24	**39**
Tissue to Background Ratio (using RA)	1.42	0.03	-0.30 to 0.37	**24**	1.84	0.06	-0.46 to 0.33	**21**
Most Diseased Segment APPROACH								
Standard Uptake Value	1.65	0.00	-0.40 to 0.39	**24**	2.17	0.16	-0.82 to 0.50	**30**
Tissue to Background Ratio (using RA)	1.55	0.00	-0.14 to 0.16	**10**	2.02	0.14	-0.50 to 0.22	**18**
FINAL APPROACH *RA BLOOD POOL, Most Diseased Segment, GATED PET, CONTRAST CT*								
FINAL Standard Uptake Value	1.66	0.04	-0.61 to 0.52	**34**	2.52	0.27	-1.5 to 0.96	**49**
FINAL Tissue to Bound Ratio (using RA)	1.55	0.05	-0.10 to 0.20	**10**	2.39	0.11	-0.97 to 0.75	**36**

Ave: Average Value, AD: Average Difference, LOA: Limits of Agreement, CT: Computed Tomography, PET: Positron Emission Tomography, RA: Right Atrium.

FIGURE 4.4.

Scan-rescan Reproducibility for ^{18}F-Fluoride PET quantification in the aortic valve with consequent sample size estimates.

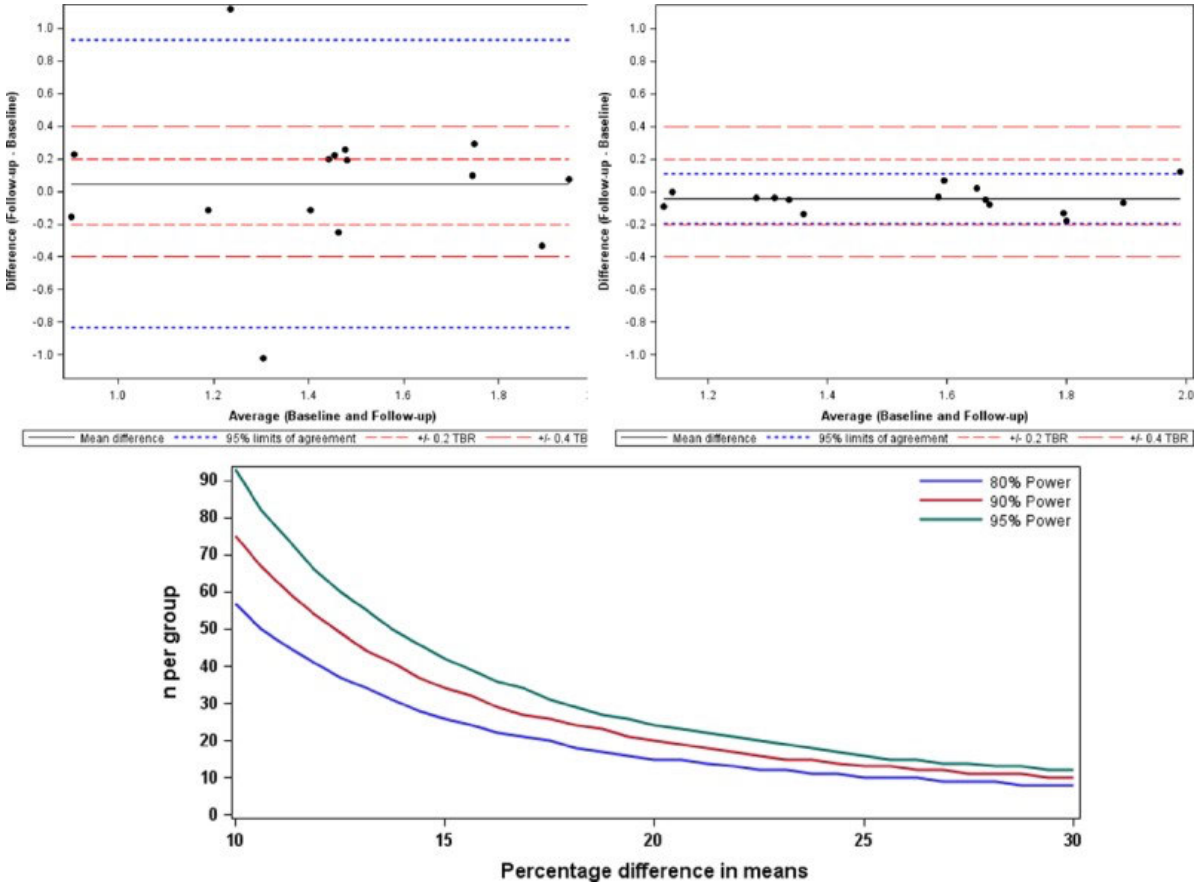

Figure 4.4. Bland Altman plots of scan-rescan reproducibility for $TBR_{MDSmean}$ measurements using the original image analysis and acquisition methods (left) and then using final method (right). Percentage error for the final technique is less than ±10%. Graph (below) showing sample size estimates needed to power clinical trials: 95% power, assuming 2-sided significance and an alpha error of probability of 0.05. These data suggest relatively few patients would be required to demonstrate the effects of novel therapies on calcification activity as measured using ^{18}F-fluoride PET.

4.5 DISCUSSION

In this study we have systematically investigated the acquisition and analysis of ^{18}F-fluoride PET imaging of the aortic valve. First, we have improved the spatial localization of tracer uptake using ECG-gated PET data and contrast CT imaging, so that activity can now be localised to individual leaflets and regions within those leaflets. This has demonstrated that calcification activity is most commonly observed at sites of maximal mechanical stress: in particular in regions of leaflet coaptation and at the commissures. Second, we have improved the scan-rescan reproducibility ultimately demonstrating excellent agreement statistics for repeat $TBR_{MDSmean}$ measurements in the valve (percentage error ±10%). This has important implications for application to future clinical trials, indicating that ^{18}F-fluoride might provide a useful imaging end-point of drug efficacy, requiring relatively few patients in order to demonstrate reductions in valvular calcification activity.

In this study we have modified our previous image acquisition protocol to include contrast-enhanced CT imaging of the aortic valve, thereby providing greater definition of the individual valve leaflets and their components. Moreover we have included ECG-gated PET data to reduce the effects of cardiac motion and more accurately localise the pattern of activity on to the valve. The combined effect of these changes has been to improve the spatial localization of PET activity within the valve, which after accurate 3-dimensional co-registration, is now possible within specific regions of individual leaflets. This has demonstrated that ^{18}F-fluoride activity predominantly localises to sites of increased mechanical stress within the valve, supporting

mechanical injury as a key driver to the disease process. For example ^{18}F-fluoride activity was observed at the tips of the valve leaflets exactly at the sites of leaflet coaptation during valve closure. Additionally uptake was observed at the valve commissures where mechanical stress is concentrated before being transferred to the aortic wall (Aikawa E *et al*, 2007; Deck JD *et al*, 1988). Whilst these findings need to be confirmed in larger studies, they here provide key insight into the triggers to calcification activity in aortic stenosis and the importance of mechanical injury. Recent data have indicated that the relationship between the valve calcium burden and hemodynamic obstruction is not perfect. The ability of PET to accurately localise calcification activity may be useful in trying to understand whether calcium formation at different sites of the valve have different hemodynamic impacts.

We have modified our image analysis protocol, optimizing the scan-rescan reproducibility of ^{18}F-fluoride imaging in the aortic valve using several different approaches. To date, it has been standard practice for ^{18}F-fluorodeoxyglucose PET to measure the blood pool SUV in the brachiocephalic vein (Tawakol A *et al*, 2006). This has the benefit of avoiding contamination of myocardial ^{18}F-fluorodeoxyglucose uptake that would overestimate the blood pool activity. However, this would not be the case for ^{18}F-fluoride which has no background myocardial uptake. We therefore measured blood pool activity in both the right atrium and the brachiocephalic vein. Measurements in the right atrium are easily performed on the en face images of the valve and resulted in much more consistent blood-pool measurements. Moreover this approach led to a dramatic improvement in the scan-rescan reproducibility of our TBR measurements such that they then outperformed equivalent SUV measures. Thus it

appears important to correct for variations in background blood pool activity that can occur between scans perhaps due to minor changes in renal function, tracer dose and pharmacokinetics. We believe that sampling the blood-pool activity in the right atrium improved reproducibility because these measurements are less susceptible to the partial volume effects of adjacent lung tissue and because any minor inaccuracies in co-registration with the PET signal will not have a great impact.

Chen *et al* recently surmised that subtracting the blood pool from tissue SUV would improve accuracy because blood activity appears to add to vascular wall activity due to spatial blurring of PET images (Chen W *et al*, 2015). However our study findings did not support this and their approach produced lower TBR values thereby increasing the percentage error of our repeat measurements.

Another major improvement in reproducibility was obtained using the most diseased segment (MDS) approach: measuring activity in the two hottest adjacent slices in the valve, rather than attempting to sample the entire valve. The major advantage of this technique is that it removes the considerable difficulty in deciding the limits and boundaries of the valve. Such uncertainty can lead to major differences in valve measurements because uptake is much lower at the extremes of the valve where the volume of tissue is small and inclusion of extraneous tissue will dilute down mean values.

This is the first study to assess scan-rescan reproducibility for ^{18}F-fluoride uptake in the aortic valve. This is important in order to validate this marker for serial

investigations as well as to estimate sample sizes for future clinical trials of novel therapeutic interventions. However we can now report $TBR_{MDSmean}$ measurements, made using our optimised image acquisition and analysis protocols, quantify valvular ^{18}F-fluoride activity with excellent reproducibility and less than a 10% percentage error. We have already shown that the $TBR_{MDSmean}$ can predict disease progression and clinical events in patients with aortic stenosis (Jenkins WSA *et al*, 2015). Our data now demonstrate that it is a robust end-point with which to detect reductions in calcification activity due to novel therapies. We have also provided an estimate of the sample sizes required at different levels of estimated drug effects. As a result of the excellent scan-rescan reproducibility, PET imaging requires few subjects to show significant differences between groups: less than 50 patients in each group to detect a 10% reduction in ^{18}F-fluoride activity. However whilst these estimates provide a framework for minimum sample sizes, they should be interpreted with a degree of caution, because they assume a perfect agreement between changes in the $TBR_{MDSmean}$ signal and underlying changes in valve calcification activity. This may not be the case. Whilst previous studies have indicated that ^{18}F-fluoride uptake correlates with histological markers of calcification activity and accurately predicts the progression in the CT calcium score, we currently lack data to show that ^{18}F-fluoride is modifiable with drug therapy. Largely this is because no drug has yet demonstrated an ability to reduce disease activity in aortic stenosis and we lack reliable animal models of this condition. However the ability of medication directly targeting valve calcification activity to reduce aortic stenosis progression and the ^{18}F-fluoride signal is the subject of an ongoing randomised control trial (NCT02132026) and we await the results with interest.

In this manuscript, "mean" measures of PET uptake demonstrated improved reproducibility compared to "maximum" measures. In particular ECG-gating of the PET data appeared to have a detrimental effect on the reproducibility of our maximum measures. Given that gating discards 75% of the PET data, and increases noise in the image, this is perhaps unsurprising for a technique that relies on a single voxel within an ROI. It is possible that advanced image analysis approaches that models and corrects for both cardiac and respiratory motion without discarding any PET data would improve the reproducibility of TBR_{MDSmax} measurements as has recently been described for coronary ^{18}F-fluoride activity (Rubeaux M *et al*, 2015). This should be explored because it remains possible that TBR_{MDSmax} values may be more sensitive to change and therefore better able to detect the effects of disease modifying therapies.

In conclusion, we have optimised ^{18}F-fluoride PET imaging in the aortic valve. Excellent localization of the PET signal within the aortic valve is now possible, with uptake observed in regions of maximal mechanical stress. Moreover quantification of valvular ^{18}F-fluoride uptake is now possible with excellent scan-rescan reproducibility. ^{18}F-Fluoride PET holds major promise as a method to better understand calcification activity in aortic stenosis and as a surrogate endpoint in clinical trials assessing the efficacy of potential therapeutic interventions.

CLINICAL PERSPECTIVES

^{18}F-Fluoride is being increasingly used as a research tool to study vascular calcification activity, binding preferentially to regions of newly developing microcalcification beyond the resolution of CT (Irkle A *et al*, 2015). In aortic stenosis there is a close association between valvular ^{18}F-fluoride uptake and calcification activity on histology (alkaline phosphatase staining), with the pattern of PET uptake ultimately predicting where new macroscopic deposits of calcium will develop on CT (Dweck MR *et al*, 2014). Indeed baseline ^{18}F-fluoride PET imaging is a good predictor of disease progression after both 1 and 2 years, as assessed aortic valve CT calcium score and Doppler echocardiography (Dweck MR *et al*, 2014; Jenkins WSA *et al*, 2015). ^{18}F-Fluoride PET therefore acts as a marker of disease activity in aortic stenosis with major potential to improve our understanding of the role of calcification in aortic stenosis. ^{18}F-Fluoride is also being considered as an end-point in studies of novel therapies for this condition, because any reduction in calcification activity is likely to be detectable earlier than on standard measures of disease progression (e.g. echocardiography or CT calcium scoring which take at least 2 years to detect a difference) (Pawade TA *et al*, 2015). This would speed up phase 2 trials of new medication and reduce costs, potentially expediting the development of these much needed drugs.

CHAPTER 5

^{18}F-FLUORIDE POSITRON EMISSION TOMOGRAPHY- COMPUTED TOMOGRAPHY AND HISTOPATHOLOGY OF EXPLANTED BIOPROSTHETIC VALVES

Cartlidge TRG, Doris MK, Sellers SL, Pawade TA, White AC, Pessotto R, Kwiecinski J, Fletcher A, Alcaide C, Lucatelli C, Densem C, Rudd JHF, van Beek EJR, Tavares A, Virmani R, Berman D, Leipsic JA, Newby DE, Dweck MR. Detection and prediction of bioprosthetic aortic valve degeneration. *J Am Coll Cardiol.* 2019;**73**:1107-1119.

5.1 ABSTRACT

Background

There are an increasing number of people living with bioprosthetic heart valves, however, the pathophysiology of bioprosthetic valve degeneration is complex and poorly understood. Calcification is a key feature of failed bioprosthetic valves and ^{18}F-fluoride has been described as a marker of calcification activity in other cardiovascular pathology.

Objectives

To investigate mechanisms of bioprosthetic valve degeneration and establish the histological correlates of ^{18}F-fluoride binding in bioprosthetic valve tissue.

Methods

We examined 16 explanted degenerated bioprosthetic valves *ex vivo* using a unique combination of histopathology, ^{18}F-fluoride micro-PET and CT.

Results

Calcification was the most prevalent pathological feature (in 87%), whilst thrombus (40%) and extension of pannus onto the cusps (47%) were other common findings in this series of degenerated valves. All valves exhibited ^{18}F-fluoride uptake on PET, with a strong positive correlation between ^{18}F-fluoride activity and calcium burden measured by CT (maximum standardised uptake value [SUV] *versus* total calcium volume: r=0.73, p=0.0031). ^{18}F-Fluoride uptake was highest in regions of leaflet

calcification but was also present in regions where histology demonstrated organised thrombus, fibrosis and markers of matrix degradation.

Conclusion

Here we demonstrate that ^{18}F-fluoride uptake is a consistent feature of bioprosthetic valve degeneration which correlates with calcification but also with other features of valve degeneration in the absence of calcium. ^{18}F-Fluoride PET/CT therefore holds promise in the preclinical and clinical setting to help elucidate the pathophysiology of valve degeneration and assess the efficacy of developments in valve technology to reduce calcification and improve durability.

5.2 INTRODUCTION

The expansion in implantation of bioprosthetic heart valves over recent years reflects two key advantages of bioprosthetic over mechanical valves. First, bioprosthetic valves have low thrombogenicity and are not therefore associated with the requirement for longterm anticoagulation that is mandated with mechanical valves. Second, bioprosthetic valves can be crimped and mounted on an expandable stent for percutaneous transcatheter delivery or rapid surgical implantation. This feature has extended the availability of aortic valve intervention to high risk surgical candidates and those with specific technical contra-indications to cardiac surgery.

Durability of Bioprosthetic Valves

Since the emergence of bioprosthetic heart valves in the 1970s, technology has developed to overcome a variety of biomechanical problems ranging from premature tissue failure to stent fractures (Wheatley *et al*, 1987). Similarly, the performance and durability of xenograft tissue has incrementally improved with careful selection of porcine or bovine pericardial tissue, glutaraldehyde fixation to reduce antigenicity and increase tissue strength, and anti-mineralisation treatments. Nevertheless, the longterm durability of bioprosthetic aortic valves is finite and valve failure may result from structural valve degeneration, valve thrombosis or prosthetic valve infective endocarditis. Of these complications the most common mode of failure is structural valve degeneration, with actuarial estimates of reoperation for structural valve degeneration at 20 years ~46% in those under 60 years old at the time of implantation (Johnston DR *et al*, 2015).

Pathophysiology of Structural Valve Degeneration

Structural valve degeneration is incompletely understood but postulated mechanisms include dystrophic calcification, injury resulting from adverse mechanical stress, immune reactivity, subclinical leaflet thrombosis, and an inflammatory process with similarities to atherosclerosis. Dystrophic calcification of bioprosthetic valves results from the devitalisation of cells during glutaraldehyde fixation, thereby providing a substrate for passive nucleation of calcium phosphate on the plasma membrane, cellular organelles and apoptotic bodies (Simionescu A *et al*, 2004). Calcium phosphate may also precipitate around the fibrous components of bioprosthetic valve tissue, such as the structural spaces around type 1 collagen called 'hole zones'. These hole zones are usually shielded by proteoglycans, however, as these degrade and collagen is damaged by the effects of mechanical stress, oxidative stress and enzymatic activity, there is increased potential for calcification (Lovekamp JJ *et al*, 2006). Elastin is also degraded by mechanical injury and proteolysis, so offering another site for neocalcification (Simionescu A *et al*, 2004).

Bioprosthetic valves lack the distinctive layers and regenerative properties of the native aortic valve, and are therefore more susceptible to adverse mechanical stress (Dalgliesh AJ *et al*, 2019). Mechanical load and calcification appear to be closely related, with calcium deposits often described at sites of peak mechanical stress at the leaflet margins and attachments to the valve frame. The cumulative effects of mechanical stress can result in delamination (e.g. cracking) of fibrous components, deterioration of the extracellular matrix with proteolysis and loss of glycosaminoglycans, and calcification of damaged collagen and elastin fibres. As

valve cusps become increasingly non-compliant, this exaggerates mechanical stress further and causes progressive structural degeneration (Sacks MS *et al*, 2015).

Following implantation, prosthetic valves (both mechanical and bioprosthetic) trigger a foreign body reaction with infiltration of endothelial cells, myofibroblasts and immune cells (Teshima H et el, 2003). This is commonly initiated at sites where host and prosthetic material come into contact such as the suture line, leading to a fibrovascular tissue proliferation commonly referred to as pannus. There is evidence that increased expression of transforming growth factor ß (TGF- ß) and its type 1 receptor by myofibroblasts are important in mediating the proliferation of pannus (Teshima H et el, 2003). Though pannus formation may be protective against thrombosis and mechanical abrasion, overgrowth of pannus can be harmful by causing valve stenosis or regurgitation, and may also be a trigger for valve calcification.

The immune reaction to bioprosthetic valve implantation is not fully understood but may be an important factor in structural degeneration. Infiltrates of immune cells are a common feature of explanted degenerated valves, as are high levels of IgM, IgG and C4d complement fragment (Nair V *et al*, 2012). Macrophages promote destruction of tissue by generating reactive oxidative species and calcium binding proteins such as osteopontin and osteonectin (New SE *et al*, 2013). In addition, high levels of macrophage-derived proteolytic enzymes, such as MMP-9 and plasminogen, are associated with phagocytosis and destruction of the extracellular matrix (Simionescu A *et al*, 1996 a). In animal studies, glutaraldehyde-treated xenogeneic implants suffer from more severe inflammation and tissue destruction then syngeneic implants and

there is a direct correlation between intensity of inflammation and severity of implant calcification (Manji RA *et al*, 2006). In further support of a causal immunological role, recipients of xenograft valves are found to have increased titres of antibodies to animal carbohydrates and animal proteins, including galactose-œ-1,3-galactose (œ-Gal), porcine albumin and type 4 collagen (Bloch O *et al*, 2011; Boër U *et al*, 2017). Xenograft valves also deteriorate more rapidly in younger subjects who are known to have greater immune reactivity whereas homografts which have lower immunogenicity are more durable (Bell D *et al*, 2019).

There appear to be some similarities between native vascular atherosclerosis and features of degenerated bioprosthetic valves. For example, tissue from explanted valves exhibits lipid deposition, with oxidised low-density lipoprotein (LDL) and foam cells analogous to those seen in atherosclerosis (Simionescu A *et al*, 1996 b). Clinical studies reveal a correlation between the incidence of structural valve degeneration and features of adverse lipid metabolism, such as an increasing ratio of low-density to high-density lipoprotein cholesterol (Nsaibia MJ *et al*, 2016). The driver to lipid deposition in bioprosthetic valves is not well explained but it has been postulated that LDL may become entangled with glycosaminoglycans in leaflet tissue (Shetty R *et al*, 2009).

Overt valve thrombosis is classified out with structural valve degeneration (Dvir *et al*, 2018), however, there is evidence that subclinical leaflet thrombosis contributes to valve degeneration. This may be initiated by deposition of thrombogenic proteins such as fibrinogen, which has been found to be widely distributed in explanted valve tissue

(Sakaue T *et al*, 2018). Recurrent leaflet thrombosis may then trigger chronic inflammation, infiltration of leucocytes and ultimately provide a nidus for calcification (Sakaue T *et al*, 2018).

Across the various pathways of bioprosthetic valve structural degeneration described here, calcification is a key common pathway and the most frequently identified histological feature of valve failure. Calcification is therefore an attractive target for investigative markers of disease progression. Micro-positron emission tomography/computed tomography (PET/CT) describes the use of a pre-clinical scanner for molecular or functional imaging of biochemical processes on a miniaturised scale. ^{18}F-fluoride PET/CT has previously been utilised to identify micro-calcification in native aortic stenosis and carotid artery atherosclerosis (Dweck MR *et al*, 2015; Irkle A *et al*, 2015). We therefore hypothesised that micro-^{18}F-fluoride PET/CT could be used to study mechanisms of structural valve degeneration in explanted bioprosthetic valves, allowing correlation between high resolution imaging and histological analysis.

PET/CT of Bioprosthetic Valves

Micro-PET/CT imaging of bioprosthetic heart valves is a novel field and presents a number of technical challenges. Despite the excellent spatial resolution of modern pre-clinical PET/CT, bioprosthetic valves are associated with a range of artefacts due to the radio-opaque and metal components of the prostheses. Compounding this, there are considerable differences in the composition of bioprosthetic valves. For example, the Edwards Lifesciences Perimount series is designed around a cobalt-chromium

alloy stent with stainless steel wire frame whilst the Medtronic Mosaic and Hancock series are built around a flexible acetyl homopolymer stent frame. CT artefacts particularly encountered during imaging of bioprosthetic valves include beam hardening, photon starvation and partial volume artefact.

Beam hardening is the result of low energy photons being absorbed during passage of the X-ray beam through dense material, thereby increasing the mean energy of the beam and reducing the rate at which it is attenuated. If the X-rays pass through a dense cylindrical object then this can produce 'cupping artefacts', or if material in the scanned sample contains very heterogenous material then beam hardening varies with the tube position and can created dark bands and streak artefacts. The latter can occur with dense mineralised tissue, prosthetic material or contrast medium. Strategies for minimising beam hardening artefact include filtration with a metallic material to 'pre-harden' the beam. In clinical scanners, phantoms can be used to calculate calibration corrections and iterative beam hardening correction algorithms can be applied.

Photon starvation artefact is the effect of an X-ray beam passing through highly attenuating material, such that insufficient photons reach the detector in certain projections. The reconstruction process has the effect of further amplifying the artefact, producing horizontal streaks in the image. Increasing the tube current can be used to help address this problem, though at the expense of a higher radiation dose. Adaptive filtration techniques may also be used to help smooth these artefacts in clinical imaging.

Partial volume CT artefact occurs when a dense object in the periphery of the scanned volume partially protrudes into the x-ray beam in certain alignments of the beam but not others. The inconsistencies between different projections can result in shading artefacts appearing in the image. This may be mitigated by minimising the acquisition section width.

Micro-PET is similarly subject to artefactual inaccuracies. First, partial volume effect arises when the size of a region or object is less than twice that of the full width at half maximum, a reflection of the upper limit of resolution of PET imaging. In this setting, the activity in the region of interest may be underestimated whilst activity in adjacent regions may appear to be artificially increased due to spill over. Second, CT attenuation correction (according to Hounsfield units) is routinely used in PET imaging to characterise tissue and apply a scale factor to the PET signal. This usually works well in clinical imaging, however, these algorithms tend to over-correct in the presence of high density material such as contrast agent or metallic objects. Artefact resulting from CT attenuation correction errors may therefore suggest high PET activity in regions where that is not the case. We planned to optimise our image acquisition protocol to minimise the impact of these potential artefacts and recognised the requirement to interpret our data accordingly.

5.3 METHODS

Study Population

Explanted degenerated bioprosthetic valves were obtained with written informed consent from patients undergoing redo-valve replacement surgery. Valves were weighed, photographed and their macroscopic features documented. Autoradiography and histological correlation were performed with one valve. All other valves were assessed by ^{18}F-fluoride positron emission tomography (PET), micro-computed tomography (CT) and histological examination.

Classification of Features of Structural Valve Degeneration

Using a combination of visual examination, micro-CT and histology, pathological features of bioprosthetic valve degeneration were noted and classified according to published criteria (Table 5.1) (Butany J *et al*, 1992; Butany J *et al*, 2007; Schoen RJ *et al*, 1987; Isihara T *et al*, 1981).

TABLE 5.1.

Classification of features of bioprosthetic valve degeneration

(Butany J *et al*, 1992; Butany J *et al*, 2007; Schoen RJ *et al*, 1987; Isihara T *et al*, 1981).

Grading of Pannus	Grade 0	No pannus
	Grade 1	Mild and involving part of the circumference of the valve ring
	Grade 2	Moderate and extending up to 2mm onto the surface of the cusp
	Grade 3	Severe and extending beyond 2 mm onto the surface of the cusp
	Grade 4	Very severe and surrounding the flow and nonflow surfaces of the cusp, causing the cusp to shorten
Grading of Calcification	Grade 0	No calcification
	Grade 1	Small, isolated calcific nodules
	Grade 2	Moderate, patchy nodules up to 1 mm in length
	Grade 3	Severe nodules up to 2mm in length
	Grade 4	Very severe, diffuse nodules capable of puncturing through the cusp surface
Grading of Tears	Type I	Linear tears involving the free edge of cusp
	Type II	Linear tears running parallel to the sewing ring, along the basal regions of cusp
	Type III	Large round or oval perforations occupying the central regions of the cups
	Type IV	Small pinhole like fenestrations in the cusp
Grading of Thrombus	Grade 0	No thrombus
	Grade 1	1A. Mild on one surface or 1B. both surfaces
	Grade 2	2A. moderate and extending up to 2mm on one surface or 2B. both surfaces of cusp
	Grade 3	Severe and extending beyond 2mm on either surface, causing restricted cusp mobility

Autoradiography

As we were exploring the novel application of ^{18}F-fluoride PET in the assessment of bioprosthetic valve degeneration, we first performed autoradiography to characterise the relationship between ^{18}F-fluoride binding and histological markers of calcification in bioprosthetic valves. Non-decalcified valve tissue was cooled in dry ice and then sectioned using a cryostat (CM1520 Wetzlar, Germany). Sections for autoradiography were mounted on Superfrost slides (Gerhard Menzel, Braunschweig, Germany) before treatment with spray fixative. Sections were bathed in a solution of ^{18}F-fluoride (1 kBq/mL) for 60 min, and then rinsed with PBS. A freshly blanked phosphor screen was then placed over the slides and an overnight exposure was acquired. The screen was subsequently read using a FujiFilm FLA-5100 Fluorescent Image Analyser (Raytek Scientific Limited, Sheffield, UK). Sections adjacent to those used for autoradiography were examined for calcium orthophosphate using Von Kossa's stain. These were manually registered and assessed for co-localisation with ^{18}F-fluoride uptake.

^{18}F-Fluoride Positron Emission Tomography and Computed Tomography

Explanted bioprosthetic valves were preserved in 10% w/v buffered formalin phosphate (Fisher Chemical SF100-20) after explantation. Prior to imaging, valves were rinsed in phosphate-buffered saline (PBS) then incubated in 20 mL of 100 kBq/mL ^{18}F-fluoride (target activity 2 MBq) for 20 min at 20^{o} Celsius. Valves were rinsed in PBS on a further 2 occasions before being mounted in a plastic universal container for scanning. PET data were acquired over a 30 min bed time using 1:5 coincidence mode. A micro-CT was acquired (full semi-circular full trajectory,

maximum field of view, 720 projections, 70 kVp, exposure 450 ms and 1:4 binning) for attenuation correction and anatomical co-registration. PET data were reconstructed using Mediso's iterative Tera-Tomo 3D algorithm and the following settings: 4 iterations, 6 subsets, full detector model, normal regularization, spike filter on, voxel size 0.6 mm, 400-600 keV energy window.

Optimisation of Image Acquisition

As this constitutes the first reported use of ^{18}F-fluoride micro-PET/CT in the assessment of bioprosthetic valves, a series of scans using variations in acquisition parameters and scanning mediums were undertaken to determine an optimal approach. The CT tube voltage was adjusted and a subjective assessment was made of image quality. Images of a unused control valve (Edwards Lifesciences 25mm Perimount) were acquired by independently varying tube voltage (35, 50 and 70 kVp) and exposure time (300ms and 450ms). It was determined that a tube voltage of 70 kVp with 450ms exposure provided the best image quality by minimising beam hardening artefact from the high density material in the valve.

Different scanning mediums were also investigated. The control valve was scanned immersed in PBS, in varying concentrations of iodinated contrast medium (10%, 20% and 50%), and without liquid scanning medium. From subjective assessment, there was some reduction in CT beam hardening artefact when using higher concentrations of contrast medium, however, this also resulted in anatomical detail being obscured and a reduced ability to detect tissue calcification. There was concern that scanning without liquid medium may result in tissue damage, however, this ultimately provided

the best anatomical detail and did not negatively impact on subsequent histological analyses.

Image Analysis

Analysis of PET/CT was performed using PMOD (PMOD Technologies, Switzerland) and OsiriX (OsiriX version 8.0.3 64-bit; OsiriX Imaging Software, Geneva, Switzerland). A bespoke tool was used to measure calcium volume in the valve cusps, taking care to exclude calcification of the sewing ring and the valve ring itself. The micro-PET and CT series were reorientated and fused. ^{18}F-Fluoride uptake in the valve cusps by various methods including the whole valve mean, the most diseased segment mean, and the maximum standardised uptake values (SUV).

Histological Validation

To characterise the pathophysiology underlying the imaging observations made in these investigations, bioprosthetic valve tissue underwent histological examination. These analyses were performed by collaborating groups at the University of British Columbia (Vancouver, Canada) and the CVPath Institute (Gaithersburg, Maryland, USA).

In patients undergoing redo-valve replacement surgery, the bioprosthetic valve was excised at the time of surgery and the integrity of the valve structure was preserved. Explanted valve specimens were fixed in 10% w/v buffered formalin phosphate (Fisher Chemical SF100-20) pending histological analysis. Heavily calcified samples were treated with fixative decalcifier to facilitate sectioning (Fisher Chemical, Cal-Ex

II, CS511-1D). Leaflets were detached from the base of the valve and marked with tissue dye to maintain orientation. Each leaflet was processed then sectioned into 2-4 mm sections and embedded in paraffin sequentially to yield 7-8 tissue cross-sections per leaflet. Paraffin sections were used for histology. Sections were stained for architecture (haematoxylin and eosin, Movat pentachrome), calcium phosphate (von Kossa), thrombus and fibrosis (Movat Pentachrome). Visual assessment was performed and reported by experienced pathologists.

Tissue Staining Protocols

Haematoxylin and Eosin

Eosin is an acidic dye which stains basic structures pink, such as cytoplasm or extracellular fibres. Haematoxylin is a basic dye which stains acidic structures, such as nuclei, a purple-blue colour. Tissue sections were deparaffinised using heat and immersion in xylene. Sections were then hydrated by passing through decreasing concentrations of alcohol before firstly being stained with haematoxylin for 3-5 min. Sections were washed under running water for several minutes, treated in 1% hydrochloric acid alcohol, washed, treated in ammonia and then washed again prior to staining with eosin for 10 minutes. Finally, tissue sections were washed in running water, dehydrated in increasing concentrations of alcohol, cleared in xylene and mounted in mounting media ready for microscopy.

Movat Pentachrome

This is a five-colour stain which highlights the constituents of connective tissue, with nuclei and elastin staining black, collagen staining yellow, mucin staining blue, fibrin

staining bright red and muscle staining red. Tissue sections were deparaffinised and hydrated as above. Tissue was subject to a Bouins mordant, heated in a microwave and rested for 10 min. After washing in cold running water, sections were treated in sodium thiosulphate for 5 min then again washed and stained with 1% Alcian Blue for 20 min. After a wash, sections were placed in preheated alkaline alcohol for 10 min, again rinsed then treated in Movat's Weigerts for 1 hour. A further wash was followed by treatment in Crocein scarlet/acid fuchsin for 1 minute, a rinse, treatment in 5% phosphotungstic acid for 5 minutes, transfer to 1% acetic acid for 5 min, a rinse, dehydration in increasing concentrations of alcohol and then treatment in alcoholic saffron for 20 min. A final rinse with 2 changes was performed in 100% ethanol before clearing in xylene and mounting in mounting media for microscopy.

Von Kossa

Silver ions bind phosphate ions and undergo photochemical degradation to visualise silver deposits as a metallic silver colour on microscopy. Tissue sections were deparaffinised and hydrated as above, then immersed in 5% aqueous silver nitrate. Sections were then exposed to ultraviolet light for 20 min, washed in distilled wated then treated with 2% sodium thiosulphate for 2 min. After rinsing, sections were counter-stained with 1% neutral red for 2 min. They were then dehydrated in alcohol, cleared in xylene and mounted in mounting medium.

5.4 RESULTS

Explanted Degenerated Bioprosthetic Valves

Sixteen explanted bioprosthetic valves were obtained for *ex vivo* investigation. These comprised porcine and bovine pericardial stented valves of a variety of models produced by four different manufacturers (Table 5.2). One bovine pericardial valve was investigated by ^{18}F-fluoride autoradiography and histopathology. The other fifteen valves were assessed by macroscopic inspection, micro-computed tomography (CT), ^{18}F-fluoride positron emission tomography (PET) and histopathology. Features of bioprosthetic valve degeneration were documented including cusp tears and perforations, valve frame distortion, cusp calcification, fibrosis and thrombus formation. Calcium volume was measured by CT and ^{18}F-fluoride tracer uptake was quantified by PET. Morphological findings were graded according to published criteria (Table 5.1) and the results are summarised below (Tables 5.2 and 5.3).

TABLE 5.2. Characteristics of explanted bioprosthetic valves, measures of ^{18}F-fluoride PET activity and CT calcium volume.

Valve ID	Model	Leaflet Tissue	Age	Sex	Weight	Total Mean SUV	Maximum SUV	MDS Mean SUV	Peak SUV	Calcium Volume (mm^3)
1	Medtronic Mosaic	Porcine valve	76	F	3.8	10574.2	4290.0	182.4	170.4.0	*
2	CE Porcine	Porcine valve	78	F	3.7	277250.9	673557.3	8191.3	10249.0	*
3	CE Porcine	Porcine valve	59	M	4.3	815830.8	637065.2	39844.4	19571.6	*
4	CE Perimount	Bovine pericardium	76	M	3.6	192683.9	291225.8	7826.0	4034.0	*
5	CE Porcine	Porcine valve	75	M	5.4	1362562.6	547390.1	48655.4	21077.4	*
6	Sorin Mitroflow	Bovine pericardium	77	F	2	753609.1	582924.5	27837.1	20670.2	*
7	CE Porcine	Porcine valve	37	M	4.2	2180574.1	333604	14425.9	13430.3	310
8	St Jude Trifecta	Porcine pericardium	78	F	5	958456.6	1158552.1	43373.3	61190.4	448
9	CE Perimount	Bovine pericardium	37	F	6	419790.5	271810.0	16650.5	12264.1	94
10	CE Perimount	Bovine pericardium	51	M	6	313731.5	256620.0	13069.5	7633.2	152
11	CE Perimount	Bovine pericardium	61	F	7.6	461228.8	547049.9	14445.7	10162.6	331
12	CE Perimount	Bovine pericardium	54	F	3.1	157859.5	74276.4	4489.3	6723.7	7
13	Sorin Mitroflow	Bovine pericardium	49	M	4.9	12649.5	621597.8	12649.5	10100.6	285
14	CE Porcine	Porcine valve	80	M	3.4	290843.0	136230.9	13995.4	8852.3	7
15	Medtronic Hancock	Porcine valve	69	F	6.7	357448.7	358450.6	12572.4	9589.4	54

TABLE 5.3. Summary of macroscopic, histopathology, micro-CT and micro-PET findings from explanted bioprosthetic valves

Valve ID	Cusp Tear (Type 1-4)	Pannus (Grade 0-4)	Thrombus (Grade 0-3)	Calcification (Grade 0-4)	Histopathology	Micro-CT	Micro-PET ^{18}F-Fluoride Activity
1	4	1	2B	3	Mild fibrous thickening all cusps Organised thrombus all cusps Cusp 3 Ca	Non-calcific cusp thickening Localised Ca Cusp 3	Valve ring pannus – mild Cusp 3 Ca – high Thrombus – localised high
2	2	1	0	2	Mild fibrous thickening all 3 cusps Cusp 3 Ca No thrombus	Non-calcific cusp thickening Localised Ca cusp 3	Valve ring pannus – mild Cusp 3 Ca – high
3	4	1	0	4	Mild fibrous thickening cusps 1 & 2 Severe nodular Ca cusp 3 No thrombus	Severe Ca cusp 3	Valve ring pannus – mild Cusp 3 Ca – high
4	1	1	0	0	Moderate fibrous thickening No calcium No thrombus	Non-calcific cusp thickening No cusp Ca	Valve ring pannus – mild Cusps – mild diffuse,
5	2	1	0	4	No significant fibrosis Full thickness intrinsic Ca all cusps No thrombus	Severe nodular Ca in all cusps	Regions of Ca in all cusps – very high
6	1	1	0	4	Mild fibrous thickening all 3 cusps Full thickness intrinsic Ca all cusps No thrombus	Non-calcific cusp thickening Severe Ca in all cusps	Regions of Ca in all cusps – very high
7	1	2	1B	4	No significant fibrosis Calcification cusp 1 Organised thrombus cusps 1 & 2	Severe diffuse Ca cusp 1	Cusp 1 Ca – very high Regions of Ca in other cusps – high

8	1	3	0	4	No significant fibrosis Severe intrinsic Ca cusp 1 & 3 No thrombus	Ca within pannus Severe Ca cusp 1 & 3	Regions of pannus – very high Cusp 1 & 3 Ca – very high
9	-	4	0	4	Severe fibrous thickening all cusps Severe intrinsic Ca cusp 1 No thrombus	Non-calcific cusp thickening Diffuse Ca cusp 1 & 2 Ca within pannus	Cusp 1 & 2 pannus / Ca – very high Cusp 3 pannus (no Ca) – very high
10	-	4	1B	4	Severe intrinsic Ca all cusps Severe fibrous thickening cusp 3 Mild organised thrombus all cusps	Non-calcific cusp thickening, severe cusp 3 Diffuse Ca all cusps	All cusps regions of Ca – very high Cusp 3 pannus with Ca – very high
11	1	1	2B	4	No significant fibrosis Intrinsic Ca all cusps, severe cusp 1 Organised thrombus cusp 3	Diffuse Ca all cusps, max commissures	All cusps regions Ca- very high Thrombus base cusp 3 – mild
12	-	2	0	0	Fibrous thickening cusp 2 & 3 Organised thrombus cusp 2 No calcium	Fibrotic nodule cusp 3 Calcified pannus around valve ring	All cusps, commissures – mild Pannus base cusp 3 – high
13	2	1	1A	4	Fibrous thickening all cusps Organised thrombus cusp 1 No calcium	Non-calcific cusp thickening, severe in cusp 2 Severe diffuse Ca cusps 1 & 3	Regions Ca cusps 1 & 2 – very high Fibrotic thickening/thrombus cusp 3 – high
14	3	4	0	3	Fibrous thickening all cusps No calcium No thrombus	Non-calcific thickening all cusps Calcified pannus cusp 1 & 3	Circumferential pannus – high Ca within pannus cusp 1 – very high
15	1	2	2A	4	Severe intrinsic Ca all cusps Fibrous thickening all cusps Organised thrombus cusp 1	Large calcific nodule cusp 1 Small Ca deposits cusps 2 & 3	Regions Ca all cusps – very high Regions non-calcific thickening base of all cusps – high

Autoradiography

A bovine pericardial stented aortic valve (Edward's Lifesciences Perimount) was explanted during repeat aortic valve replacement surgery for symptomatic severe prosthetic valve stenosis. Diffuse nodular calcification of the valve cusps was visible on gross assessment. On autoradiography, binding of ^{18}F-fluoride to valve tissue was found to co-localise with visually apparent calcification and evidence of structural calcium phosphate on von Kossa staining (Figure 5.1).

FIGURE 5.1.

Autoradiography and histology of an explanted bioprosthetic aortic valve.

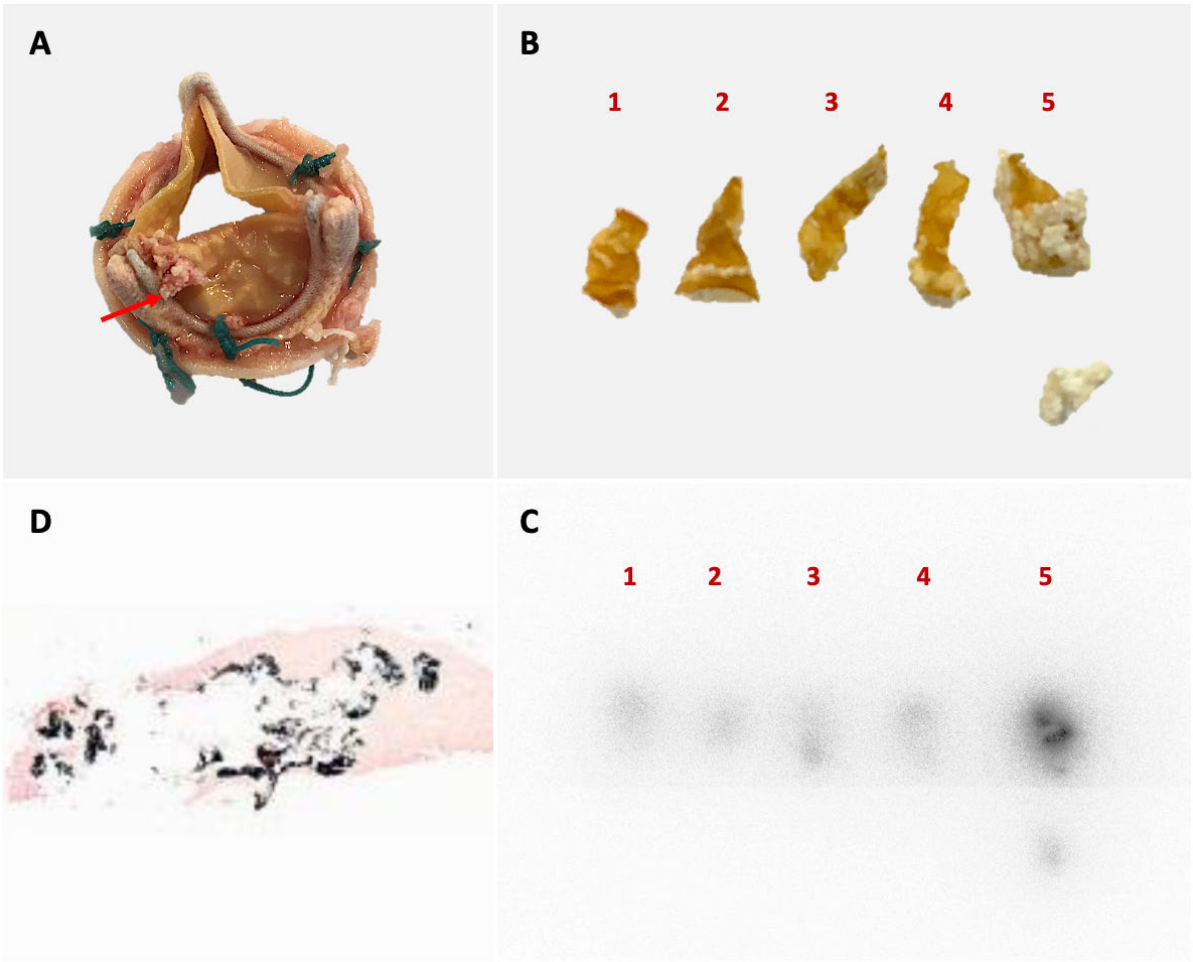

Figure 5.1. A. Photograph of an explanted bovine pericardial bioprosthetic aortic valve with a large calcific nodule close to a commissural attachment (red arrow) **B**. Tissue sections from the valve cusps with a large calcific nodule on section 5 **C**. Autoradiography of corresponding tissue sections (1-5) demonstrating ^{18}F-fluoride uptake in all samples, with the highest signal in section 5 **D.** Von Kossa stain confirming severe intrinsic calcification penetrating the cusp surface (black).

Calcification

Calcification was often presumed on visual inspection, though this alone did not offer a reliable indication of the presence of calcification and in 2 notable cases it was not substantiated by findings from CT or histology (valves 4 and 12). CT detected cusp calcification in 13 valves (87%) and histology identified cusp calcification in 11 valves (73%), all of which had calcium clearly apparent on CT. CT therefore appeared to offer greater sensitivity for the detection of tissue calcification than histology. Tissue histology revealed a typical pattern of intrinsic cusp calcification, with calcium aggregates developing in the central region of the cusp and ultimately penetrating the cusp surface in severe cases (e.g. valves 1, 5, 6, 8, 9, 10, 11 and 15). ^{18}F-Fluoride uptake assessed by micro-PET correlated spatially with calcification seen on CT and histology, and was associated with the highest tracer activity when compared to healthy cusp tissue and other features of tissue degeneration (e.g. valves 1, 5, 6, 8, 9, 10, 11, 15).

Pannus

Pannus had a characteristic appearance, typically covering the valve sewing ring in a circumferential pattern and extending to a variable degree over the surfaces of the valve cusps. Pannus was a universal finding (100%) affecting the valve sewing ring and involved the valve cusps in 7 out of 15 cases (47%). In severe cases, there was significant encroachment causing restricted cusp mobility and cusp retraction (e.g. valves 9 and 10). This could be a mechanism of valve stenosis and/or valve incompetence. CT was able to differentiate between regions of calcific and non-calcific cusp thickening, and in several cases identified calcium deposits within

regions of mature pannus (e.g. valves 8, 9 and 14). Histology samples from regions of pannus confirmed fibrous cusp thickening, with and without associated calcification. ^{18}F-Fluoride PET uptake was increased in regions of pannus affecting both the valve sewing ring and cusps, even in the absence of calcification, (e.g. valves 1, 4, 9, 12, 13). This advocates pannus as a potential driving factor in bioprosthetic valve calcification.

Thrombus

Thrombus was also a prevalent finding, identified by histology in 6 out of 15 valves (40%). When present it tended to be minor and localised (grade 1 in 3 cases, grade 2 in 3 cases), and was unlikely to account for significant valve dysfunction. In 2 cases thrombus was seen in association with more significant cusp thickening and increased ^{18}F-fluoride uptake, both in the absence of cusp calcification (e.g. valve 1, cusp 2) and presence of cusp calcification (e.g. valve 15, cusp 1).

^{18}F-Fluoride Positron Emission Tomography

Increased uptake of ^{18}F-fluoride was frequently seen co-localising to the rim of pannus covering the valve sewing ring, to regions of fibrotic cusp thickening (e.g. valve 9, cusp 3), and to regions where histology identified organised thrombus in the absence of calcification (e.g. valve 1, cusp 2). The areas of highest tracer uptake correlated with CT and histological evidence of calcification. Valve cusp ^{18}F-fluoride activity was quantified and found to correlate with calcium volume as measured by CT (maximum standardised uptake value [SUV] *versus* total calcium volume: r=0.73, p=0.0031) (Figure 5.2).

FIGURE 5.2.

Association between ^{18}F-fluoride uptake by PET and total calcium volume by CT.

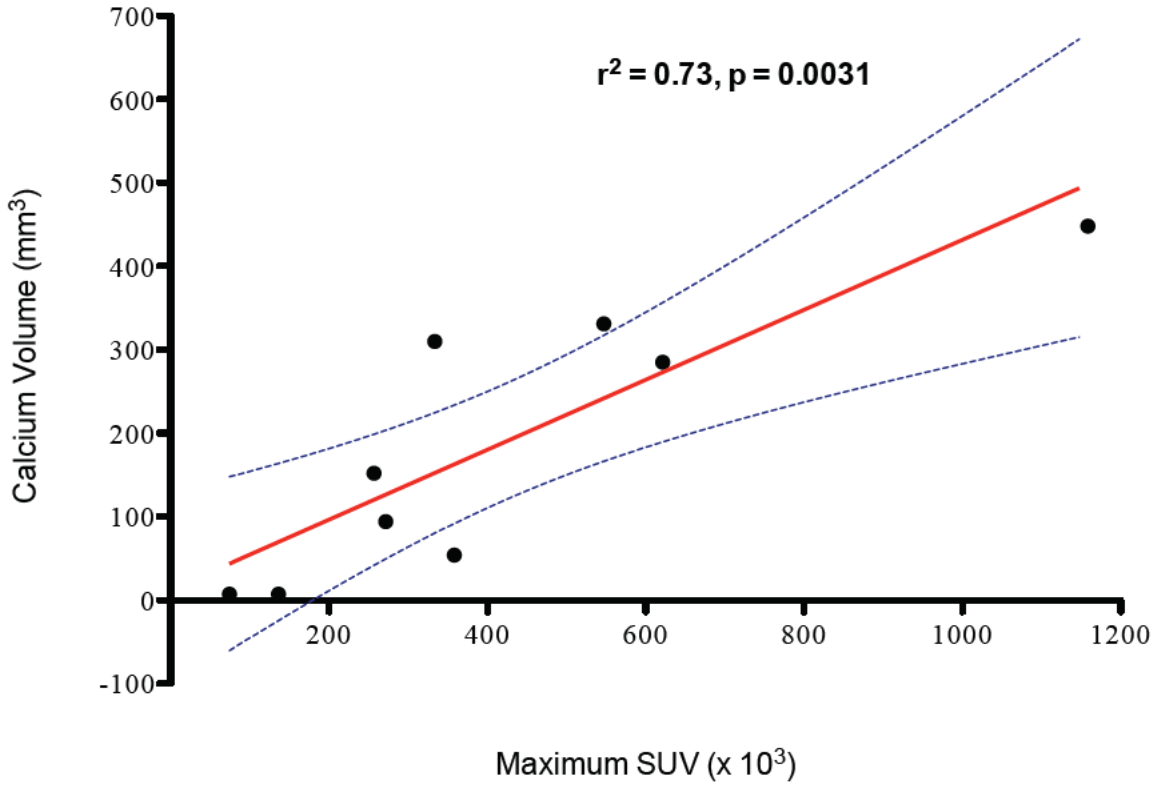

Figure 5.2. Line plot of ^{18}F-fluoride positron emission tomography activity (measured by maximum standardised uptake value [x10^3]) *versus* computed tomography valve calcium volume (mm^3).

Description of Individual Valve Findings

Valve 1 (Figure 5.3)

Description

Medtronic Mosaic stented porcine valve.

Macroscopic Assessment

Valve weight is 3.8g. A visible layer of pannus is seen over the ventricular surface of the valve ring but not encroaching on the cusps (grade 1 pannus). There is increased folding of cusp tissue, a large oval tear in the central region of cusp 3 and adjacent to this is thinned and friable cusp tissue with multiple fenestrations (type IV tear). There is calcification apparent at the base of cusp 3 and at the commissural attachments.

Computed Tomography

There is increased radio-opacity of the cusps consistent with fibrous thickening and partial folding. Calcification is seen at the base and at both commissures of cusp 3.

Histopathology

In all 3 cusps there is evidence of expansion of the central collagen-proteoglycan layer and organising thrombus on both surfaces (grade 2B thrombus). In cusp 3, there is calcification on the aortic surface near the commissure adjacent to cusp 2 (grade 3 calcification).

^{18}F-Fluoride Positron Emission Tomography

There is mildly increased ^{18}F-fluoride activity corresponding to pannus over the ventricular surface of the valve ring and stent posts. There is high tracer activity in cusp 3 at the commissure adjacent to cusp 2, co-localising to calcification noted on CT and histology. There is also a region of high uptake near the free edge in cusp 2, where calcification was not apparent and histology showed organising thrombus.

Valve 2 (Figure 5.4)

Description

Carpentier-Edwards' stented porcine valve.

Macroscopic Assessment

Valve weight is 3.7g. There is a layer of pannus over the ventricular surface of the valve ring which does not extend on to the cusps (grade 1 pannus). Cusp 1 appears thin and friable, with a tear near the commissure with cusp 3 (type II tear). There is mild stent creep with inward distortion of the stent post between cusps 1 and 3. From the aortic aspect, there is apparent calcification of cusp 3 near the commissure adjacent to cusp 1.

Computed Tomography

There is increased radio-opacity of the leaflets consistent with fibrous thickening and partial folding. Calcification is demonstrated at the base of cusp 3 and the commissure adjacent to leaflet 1.

Histopathology

In all cusps there is mild fibrous thickening and mild expansion of the central collagen-proteoglycan layer near the free edge. There is no evidence of thrombus. There is no calcification identified in cusps 1 and 2, however, in cusp 3 there is focal calcification at the basal region of the section (grade 2 calcification).

^{18}F-Fluoride Positron Emission Tomography

There is mildly increased ^{18}F-fluoride activity corresponding to pannus on the ventricular surface of the valve ring. There is extensive activity in the region of the commissure between cusps 1 and 3, correlating with the calcification noted on CT and histology.

Valve 3 (Figure 5.5)

Description

Carpentier-Edwards' stented porcine valve.

Macroscopic Assessment

Valve weight is 4.3g. There is pannus extending over the ventricular surface of the valve ring, predominantly beneath cusp 2 (grade 1 pannus). There is a small circular perforation in the body of cusp 2, a linear tear extending from the free edge of cusp 1, and a fenestrated perforation in the body of cusp 3 (type IV tear). There is mild stent creep with inward distortion of the stent posts on either side of cusp 1 and some elliptical deformation of the valve frame. A very large calcific nodule is apparent in the body of cusp 3, penetrating both surfaces.

Computed Tomography

Confirms severe calcification of cusp 3 with a large calcific nodule and further calcification around the commissural region, adjacent to cusp 1.

Histopathology

Tissue sections from cusps 1 and 2 demonstrate mild fibrous thickening and mild expansion of the central collagen-proteoglycan layer due to fluid insudation resulting in separation of collagen fibres. Cusp 3 exhibits severe nodular calcification erupting through both surfaces of the cusp, extending from the base to mid region of the leaflet (grade 4 calcification). There is no evidence of thrombus (grade 0 thrombus).

^{18}F-Fluoride Positron Emission Tomography

There is mildly increased ^{18}F-fluoride activity corresponding to pannus covering the ventricular surface of the sewing ring. There is high tracer uptake in cusp 3, co-

localising to the large calcific nodule in the body of the cusp, calcification seen at the commissure with cusp 1, and also mid leaflet at the free edge adjacent to cusp 2.

Valve 4 (Figure 5.6)

Description

Carpentier-Edwards' Perimount stented bovine pericardial valve.

Macroscopic Assessment

Valve weight is 3.6g. There is mild pannus extending over the ventricular surface of the valve ring and over the stent post between cusps 2 and 3 (grade 1 pannus). There is a small linear tear in cusp 1 at the stent post attachment adjacent to cusp 2 (type 1).

Computed Tomography

There are regions of increased radio-opacity representing fibrous thickening, most apparent in the region of the commissure between cusps 1 and 2. There is no evidence of calcification.

Histopathology

Tissue sections from all 3 cusps show fibrous thickening with fluid insudation and separation of collagen fibres. These changes are most marked in towards the basal region of cusps 1 and 2. There is no evidence of thrombus.

^{18}F-Fluoride Positron Emission Tomography

There is mildly increased ^{18}F-fluoride activity corresponding to the layer of pannus seen over the ventricular surface of the valve ring and extending over the stent post between cusps 2 and 3. There is also mild diffuse tracer activity in all 3 valve leaflets, highest in cusp 2.

Valve 5 (Figure 5.7)

Description

Carpentier Edward's stented porcine valve.

Macroscopic Assessment

Valve weight is 5.4g. There is a mild layer of pannus over the ventricular surface of the valve ring (grade 1 pannus). All cusps are severely disrupted with diffuse nodular calcification visible on both aortic and ventricular surfaces. There is a linear tear in the body of cusp 3 parallel to the sewing ring (type 2 tear) and a tear extending from the free edge of cusp 2 (type 1 tear).

Computed Tomography

This illustrates severe nodular calcification of all 3 cusps

Histopathology

Tissue sections from all 3 cusps shows full thickness intrinsic calcification extending the full length of the cusp (grade 4 calcification). There is no evidence of thrombus (grade 0).

^{18}F-Fluoride Positron Emission Tomography

There is very high ^{18}F-fluoride activity in all 3 cusps correlating with regions of calcification seen on CT.

Valve 6 (Figure 5.8)

Description

Sorin Mitroflow stented bovine pericardial valve.

Macroscopic Assessment

Valve weight is 2.0g. There is mild pannus over the inner ventricular surface of the sewing ring beneath cusp 3 (grade 1 pannus). All cusps appear thickened with reduced mobility. There is a tear in both cusps 2 and 3 extending from the commissure region (type 1 tear) where there is visible extensive calcification penetrating the aortic surface. There is a further small tear in cusp 1 at the commissure with cusp 2, also associated with macroscopic calcification.

Computed Tomography

Imaging demonstrates diffuse fibrous thickening and severe calcification, which is predominantly located at the commissures and free edge in all 3 cusps.

Histopathology

Sections show mild fibrous thickening secondary to fluid insudation. There is full thickness intrinsic calcification seen in all 3 cusps, which extends the full length of the cusps near the commissures (grade 4 calcification). There is no evidence of thrombus (grade 0).

^{18}F-Fluoride Positron Emission Tomography

There is very high tracer uptake in all 3 cusps co-localising to regions of tissue calcification, particularly at the commissures and in the body of cusps 1 and 3.

Valve 7 (Figure 5.9)

Description

Carpentier Edward's stented porcine valve.

Macroscopic Assessment

Valve weight is 4.2g. There is a layer of pannus extending over the ventricular surface of the valve ring and encroaching on cusps 1 and 3 (grade 2 pannus). Pannus also covers the outer fabric surface of the stent posts but does not affect the aortic surface of the valve cusps. There is a small tear in the free edge of cusp 1, near the commissure adjacent to cusp 2 (type 1 tear). There appears to be nodular calcification in this region of cusp 1, near the commissure with cusp 2. There is discolouration in the basal region of cusp 2, seen from both the aortic and ventricular aspect, which suggests the presence of thrombus.

Computed Tomography

CT demonstrates extensive calcification in cusp 1 and affecting the region of the commissure in both cusps 1 and 2.

Histopathology

Tissue sections show calcification of cusp 1 (seen on Movat pentachrome sections but not von Kossa), and organised thrombus on the surface of cusps 1 and 2 (grade 1A). There are regions of fibrous leaflet thickening.

^{18}F-Fluoride Positron Emission Tomography

There is increased ^{18}F-fluoride activity in all 3 cusps correlating with regions of calcification seen on CT, with the major focus of tracer uptake in cusp 1.

Valve 8 (Figure 5.10)

Description

St Jude Trifecta stented porcine pericardial valve.

Macroscopic Assessment

Valve weight is 5.0g. There is severe circumferential pannus covering the ventricular surface of the sewing ring and extending onto the ventricular surface of all 3 cusps (grade 3 pannus). All cusps appear thickened. There are small tears in cusp 1 and 3 at the commissures with cusp 2 (type 1 tear). There is extensive macroscopic calcification penetrating the aortic surface of cusps 1 and 3 (grade 4 calcification) and the mobility of cusp 1 is severely restricted.

Computed Tomography

Imaging demonstrates calcification associated with the pannus on the ventricular surface of cusp 1. There is severe calcification at all commissure regions and in the body of both cusp 1 and 3.

Histopathology

Sections show distorted leaflet architecture with full thickness intrinsic calcification erupting through both surfaces in cusp 1 and cusp 3 (grade 4 calcification). There is no evidence of thrombus (grade 0).

^{18}F-Fluoride Positron Emission Tomography

There is increased tracer activity which co-localises to the regions of leaflet calcification seen macroscopically and on CT, but also to the thick rim of pannus which is associated with calcification.

Valve 9 (Figure 5.11)

Description

Carpentier-Edwards' Perimount stented bovine pericardial valve.

Macroscopic Assessment

Valve weight is 6.0g. The valve cusps appear mildly thickened. There is severe pannus formation on the aortic surface of all 3 cusps. This extends along the base of each cusp parallel to the valve ring, and cusp 3 is retracted with restricted mobility (grade 4 pannus). There is no significant pannus formation over the ventricular surface of the valve. Cusps are intact with no sign of perforation or tear.

Computed Tomography

There is increased opacification consistent with fibrous leaflet thickening at the base of the cusps. Cusp 1 and cusp 2 are diffusely calcified, with calcification seen co-localising to the region of fibrous pannus at the base of cusp 2.

Histopathology

Tissue sections demonstrate intrinsic calcification within cusp 1 (grade 4 calcification), whilst calcium is not illustrated in the sections from cusp 2. There is no significant fibrosis or thrombus (grade 0) in evidence.

^{18}F-Fluoride Positron Emission Tomography

There is increased ^{18}F-fluoride activity in all 3 cusps spatially correlating with regions of fibrous thickening (pannus) and calcification. In cusp 3, high tracer uptake corresponds to fibrous thickening in the absence of calcification.

Valve 10 (Figure 5.12)

Description

Carpentier Edward's Perimount stented bovine pericardial valve.

Macroscopic Assessment

Valve weight is 6.0g. There is severe pannus formation on the aortic surface of the cusp 3, covering the valve sewing ring, a stent post, and extending over the cusp. There is cusp thickening and retraction with reduced mobility (grade 4 pannus). Nodules of calcification are macroscopically apparent in each cusp and there is dark red discolouration at the base of cusps 1 and 2 in suggestive of possibly thrombus.

Computed Tomography

CT demonstrates thickening of all 3 cusps, which is particularly marked in cusp 3. There is diffuse calcification of all 3 cusps.

Histopathology

Von Kossa staining reveals intrinsic calcification of all 3 cusps, penetrating through both leaflet surfaces (grade 4 calcification). There is fibrous thickening of all 3 cusps, with the most severe changes affecting cusp 3. Organised thrombus is evident on all 3 cusps (grade 1 thrombus).

^{18}F-Fluoride Positron Emission Tomography

There is high uptake of ^{18}F-fluoride in all 3 cusps, and around the periphery of the valve sewing ring where there is macroscopic evidence of pannus overgrowth.

Valve 11 (Figure 5.13)

Description

Carpentier Edward's Perimount stented bovine pericardial valve.

Macroscopic Assessment

Valve weight is 7.6g. There are large calcific nodules penetrating the aortic and ventricular surfaces of cusp 1 and cusp 2 (grade 4 calcification). There is a linear tear of the free edge of cusp 1, adjacent to cusp 2 (type 1 tear). There is some elliptical deformation of the valve frame. There is a patch of dark red discolouration on the ventricular surface at the base of cusp 3 and 1, suspicious for possible thrombus. There is minor pannus formation which is restricted to the ventricular surface of the valve sewing ring (grade 1 pannus).

Computed Tomography

CT illustrates areas of leaflet thickening and diffuse calcification of all 3 cusps, in particular with calcification around the valve commissures.

Histopathology

There is widespread intrinsic leaflet calcification of all 3 cusps, which is most severe in the tissue sections from cusp 1 where calcific deposits penetrate both surfaces. There appears to be a large papillary thrombus at the base of cusp 3 (grade 2/3 thrombus).

^{18}F-Fluoride Positron Emission Tomography

There is very high binding of ^{18}F-fluoride in all 3 cusps, particularly co-localising to regions of calcification around the commissures. There is mild uptake in the region of the thrombus identified at the base of cusp 3.

Valve 12 (Figure 5.14)

Description

Carpentier Edward's Perimount stented bovine pericardial valve.

Macroscopic Assessment

Valve weight is 3.1g. The valve cusps appear mildly thickened. Cusps are intact with no sign of perforation or tear. There is a circumferential rim of pannus around the ventricular surface of the valve ring with limited extension onto the ventricular surface of all 3 cusps. There is pannus reaching around the outer margin of the sewing ring onto the aortic surface of the base of cusp 3, again with limited extension onto the cusp but no apparent restriction of cusp mobility (grade 2 pannus). There is a patch of thickening in the body of cusp 1, however, no definite calcification is evident.

Computed Tomography

There is an isolated small fibrotic nodule in the free edge of cusp 3. There is diffuse calcification within the circumferential rim of subvalvular pannus without involving the cusps.

Histopathology

Histology shows loss of collagen architecture and fragmentation in cusp 1, cusp thickening with fibrosis and organised thrombus on the surface of leaflet 2, and fibrosis at the base of leaflet 3. There is no evidence of cusp calcification on micro-CT or histology (grade 0 calcification).

^{18}F-Fluoride Positron Emission Tomography

There is increased ^{18}F-fluoride uptake in the valve cusps around the commissural regions and at the base of cusp 3 co-localising to the region of pannus extending onto

the cusp. There is extensive ^{18}F-fluoride uptake correlating with the rim of subvalvular pannus encircling the valve ring.

Valve 13 (Figure 5.15)

Description

Sorin Mitroflow bovine pericardial valve.

Macroscopic Assessment

Valve weight is 4.9g. All 3 cusps appear grossly thickened. There are tears in cusps 2 and 3 at the commissural attachment (type 2 tear). There is a patch of dark red discolouration in the body of cups 1 suggesting possible thrombus. There is a nodular texture to the cusp surface but no macroscopically evident calcification penetrating either cusp surface. There is mild pannus formation over the outer surface of the stent posts but this does not encroach the cusps (grade 1 pannus).

Computed Tomography

All cusps are markedly thickened. There is severe diffuse calcification of cusps 1 and 3 (grade 4 calcification). There is no calcification apparent in cusp 2 but there is severe non-calcific thickening in the body of the cusp.

Histopathology

Von Kossa staining does not demonstrate tissue calcification as clearly seen on micro-CT. There is evidence of fibrosis , fluid insudation and disruption of collagen architecture resulting in severe thickening of all 3 cusps. There is organised thrombus on the aortic surface at the base of cusp 1 and 3 (grade 1A).

^{18}F-Fluoride Positron Emission Tomography

There is very high uptake of ^{18}F-fluoride in the valve cusps. The highest regions of activity correspond with aggregates of calcium in cusps 1 and 3. There is also significant ^{18}F-fluoride uptake in the body and at the base of cusp 2 in the absence of calcification.

Valve 14 (Figure 5.16)

Description

Carpentier Edward's stented porcine valve.

Macroscopic Assessment

Valve weight is 3.4g. There is a tear in the free edge of cusp 3 and an oval tear in the body of cusp 2 (type 3 tear). There is very severe pannus formation encircling the valve ring and extending onto all 3 cusps on both the aortic and ventricular surfaces, such that cusp mobility is restricted (grade 4 pannus). There is no visible calcification.

Computed Tomography

There is increased opacification consistent with fibrous leaflet thickening at the base of the cusps. There is a calcific nodule within the pannus covering the ventricular surface of cusp 1 (grade 3 calcification) and further small flecks of calcium at the base of cusp 3 and at the commissure between cusps 2 and 3.

Histopathology

Histology demonstrates regions of fibrosis with leaflet thickening in all 3 cusps. No calcification is seen in the sections sampled. There is no evidence of thrombus (grade 0).

^{18}F-Fluoride Positron Emission Tomography

There is increased ^{18}F-fluoride uptake correlating with the circumferential pattern of pannus overgrowth and with a focus of high uptake co-localising to the calcification at the base of cusp 1 noted on micro-CT.

Valve 15 (Figure 5.17)

Description

Medtronic Hancock stented porcine valve.

Macroscopic Assessment

Valve weight is 6.7g. There are linear tears along the free edge of each cusp (type 1 tears). There are calcific nodules penetrating the aortic surface of cups 1 and just beneath the surface of cusp 3. There is a thin, translucent layer of pannus covering the fabric sewing ring with mild extension onto the valve cusps. There is cusp thickening with a dark red discolouration on the ventricular surface at the base of cusp 1 suspicious for thrombus.

Computed Tomography

There is a very long calcific nodule in cusp 1 extending the length of the free edge from the commissure to the leaflet tip, adjacent to cusp 2. There are further small calcium deposits near the base of cusp 2, and extending from both free margins of cusp 3.

Histopathology

Von Kossa staining identifies intrinsic calcification of all 3 cusps, with the most severe changes in cusp 1 where calcium penetrates the surface (grade 4 calcification). There is fibrous thickening in all cusps and organised thrombus at the base of cusp 1 (grade 2).

^{18}F-Fluoride Positron Emission Tomography

There is increased ^{18}F-fluoride activity in all 3 cusps correlating with regions of calcification, and highest where a large calcific nodule is noted in cusp 1. There is also

^{18}F-fluoride uptake associated with regions of non-calcific leaflet thickening at the base of the 3 valve cusps.

FIGURE 5.3.

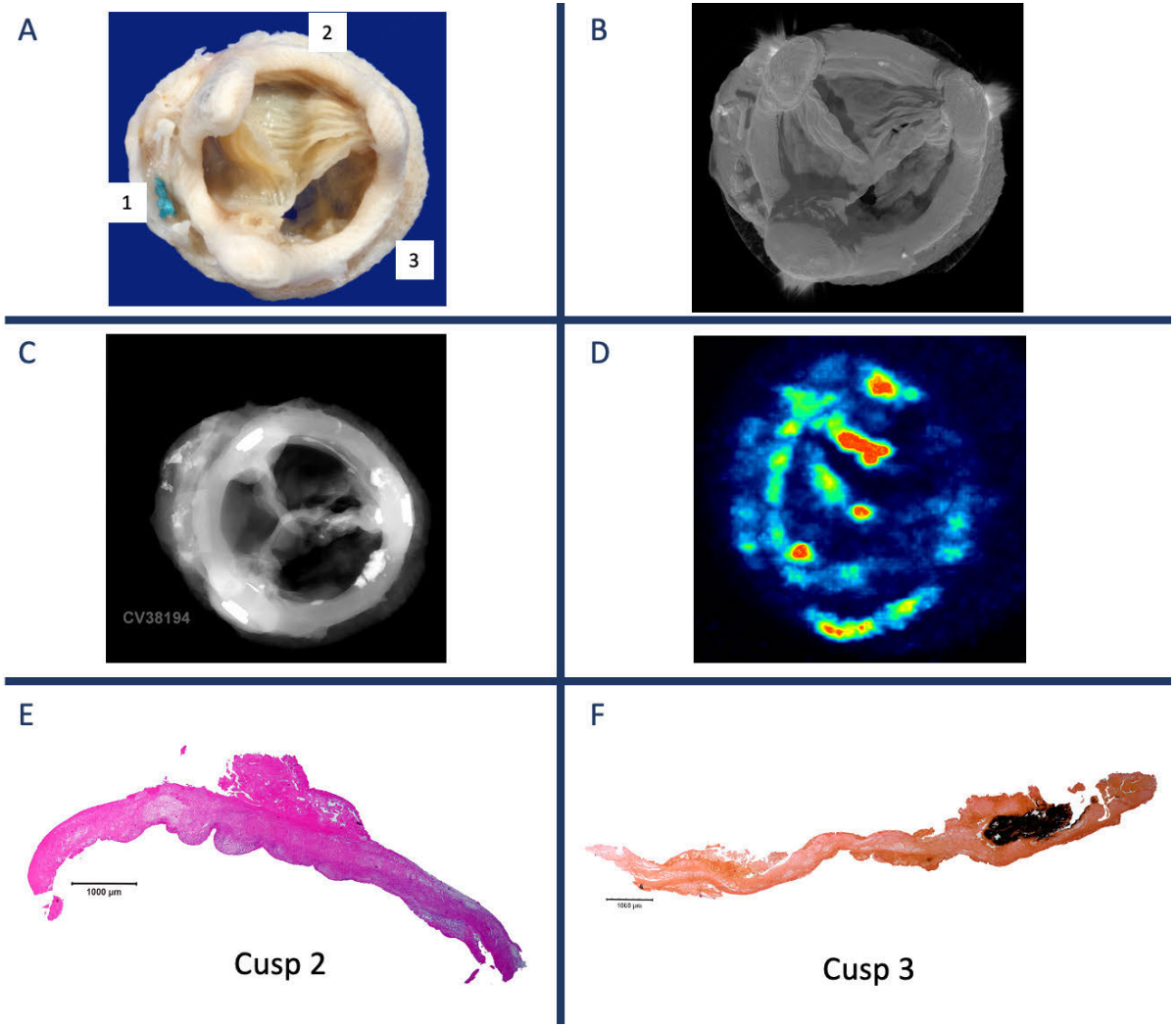

Valve 1

Macroscopic appearance of explanted bioprosthetic valve from the aortic aspect (A). Computed tomography surface-rendered *en face* image (B) and maximum intensity projection image of valve (C). ^{18}F-Fluoride positron emission tomography image of valve (D). H&E stain of section from cusp 2 showing organized thrombus (E) and von Kossa stain of section from cusp 3 showing intrinsic calcification (F).

FIGURE 5.4.

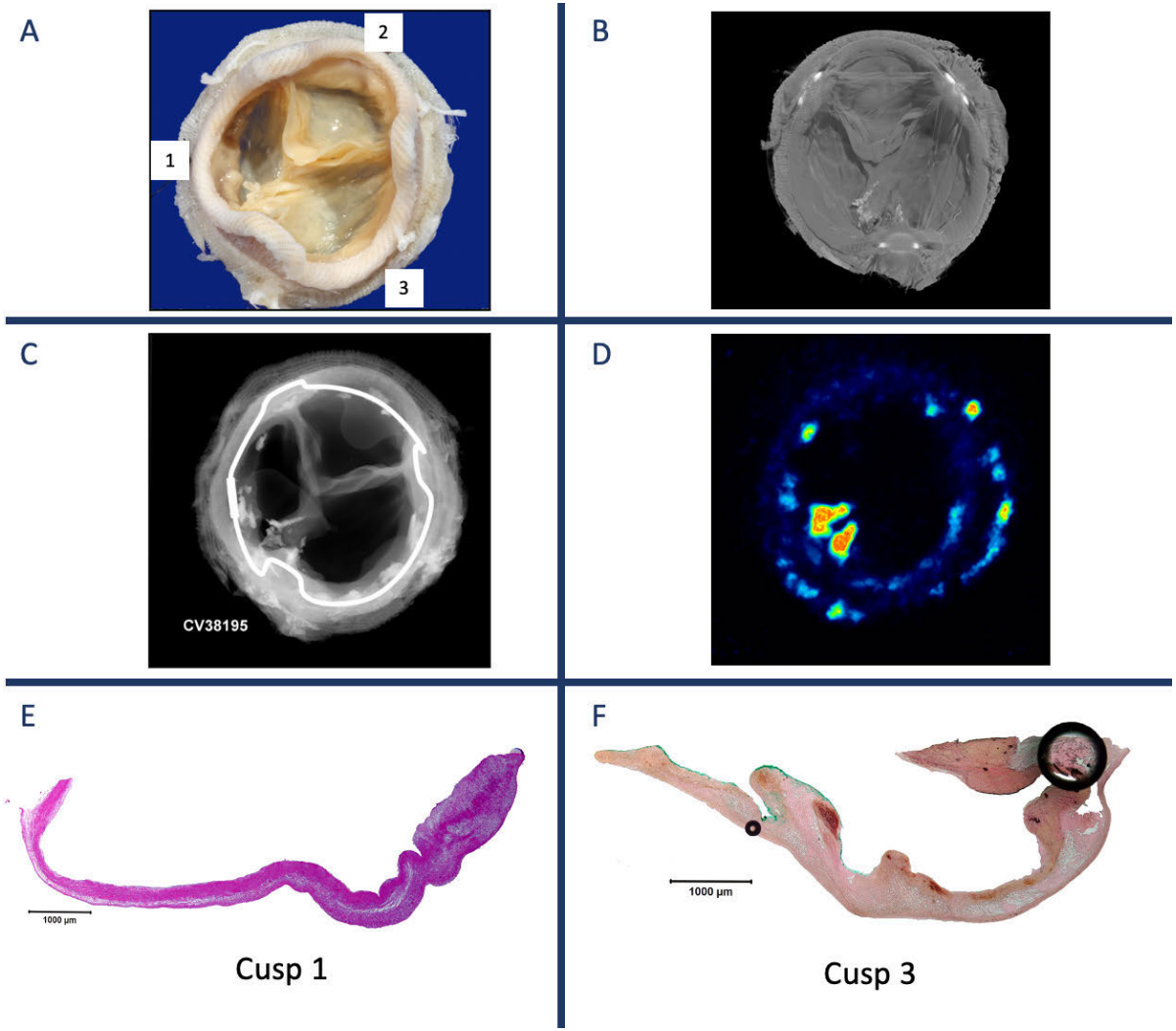

Valve 2

Macroscopic appearance of explanted bioprosthetic valve from the aortic aspect (A). Computed tomography surface-rendered *en face* image (B) and maximum intensity projection image of valve (C). ^{18}F-Fluoride positron emission tomography image of valve (D). H&E stain of section from cusp 1 showing fibrous thickening (E) and von Kossa stain of section from cusp 3 showing focal calcification (F).

FIGURE 5.5.

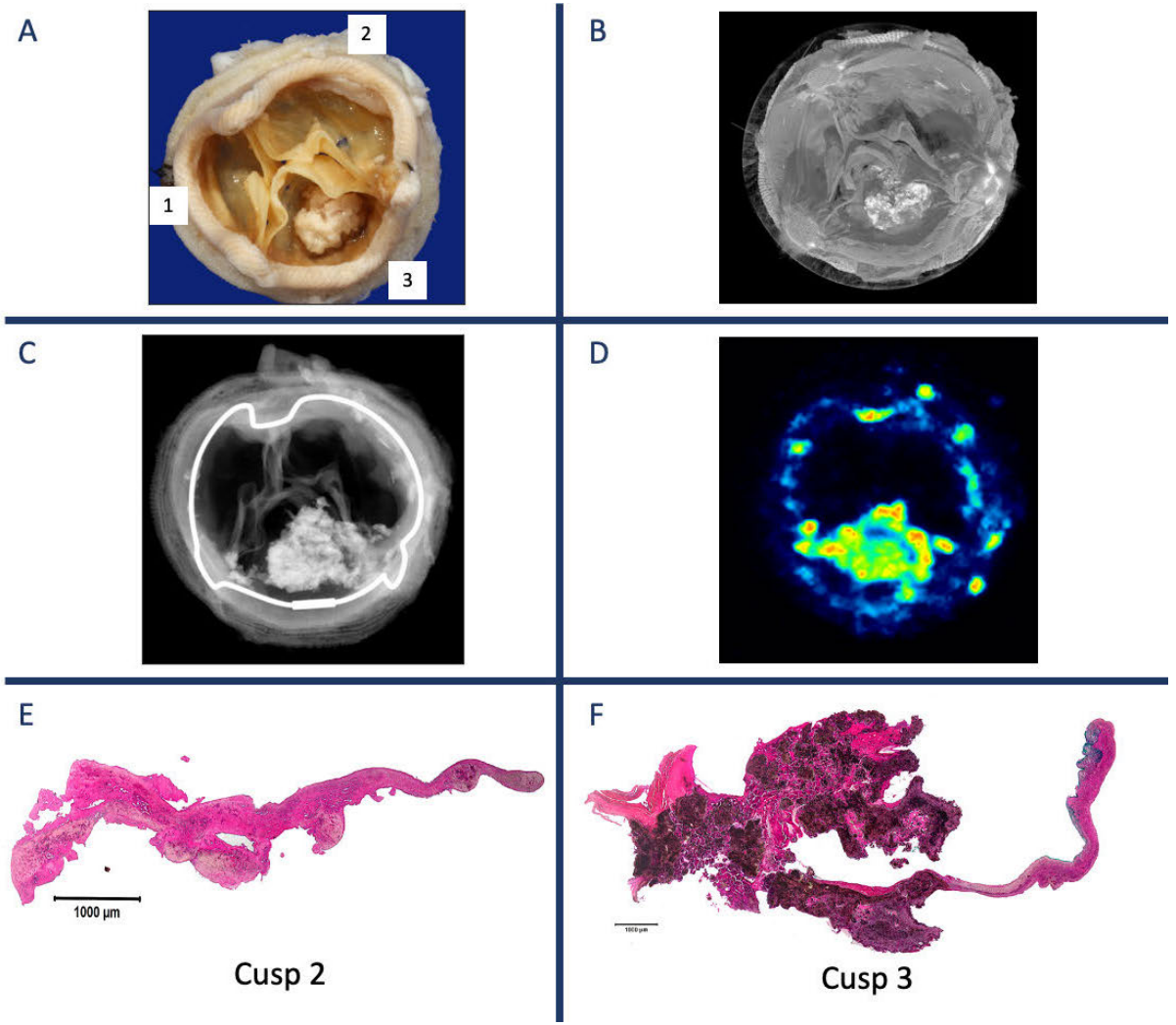

Macroscopic appearance of explanted bioprosthetic valve from the aortic aspect (A). Computed tomography surface-rendered *en face* image (B) and maximum intensity projection image of valve (C). ^{18}F-Fluoride positron emission tomography image of valve (D). H&E stain of section from cusp 2 showing fibrous thickening and structural degeneration due to fluid insudation (E), and von Kossa stain of section from cusp 3 showing intrinsic nodular calcification erupting through both surfaces (F).

FIGURE 5.6.

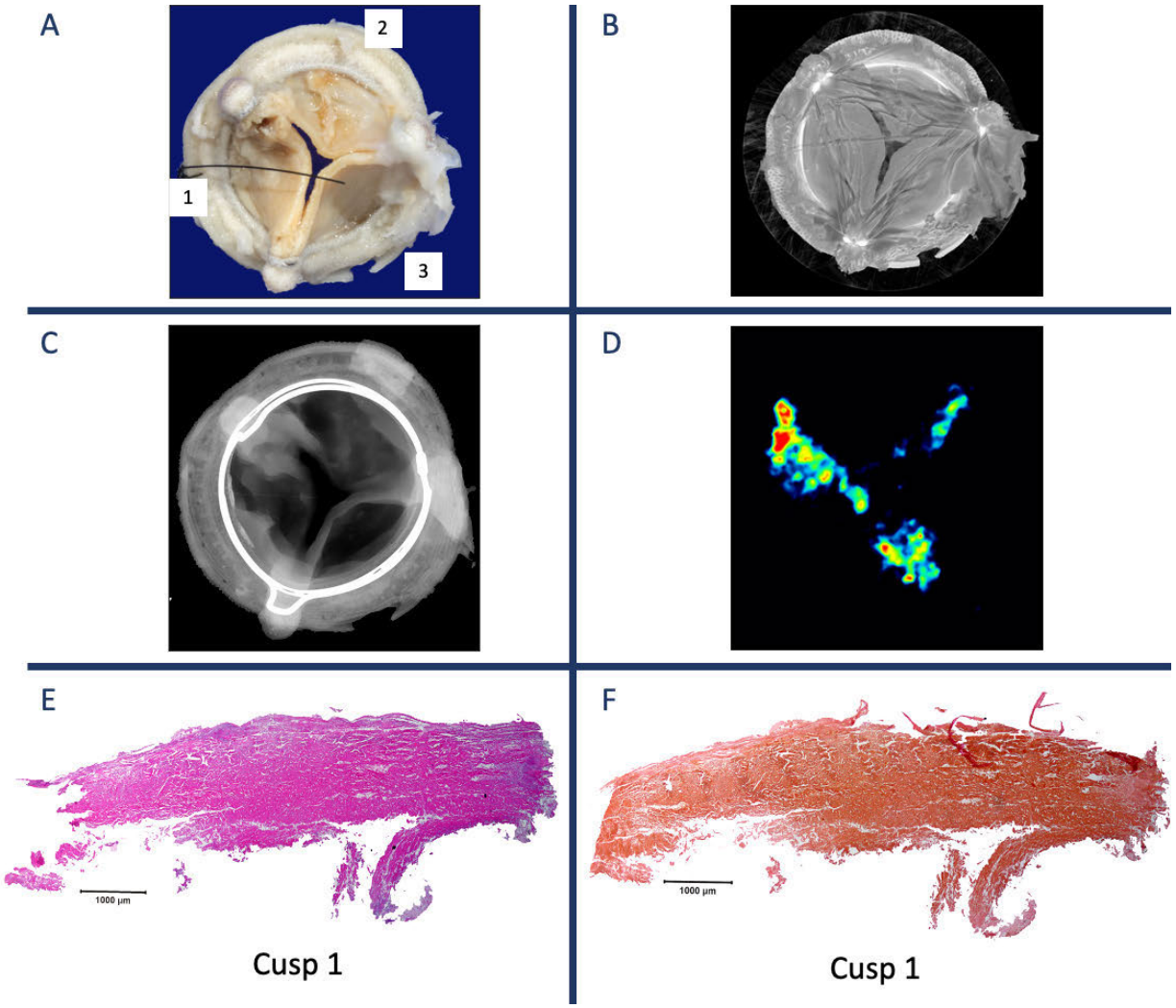

Valve 4

Macroscopic appearance of explanted bioprosthetic valve from the aortic aspect (A). Computed tomography surface-rendered *en face* image (B) and maximum intensity projection image of valve (C). ^{18}F-Fluoride positron emission tomography image of valve (D). H&E stain of section from cusp 1 showing fibrous thickening, chronic inflammation and separation of collagen fibres due to fluid insudation (E). Von Kossa stain of section from cusp 1 without evidence of calcification (F).

FIGURE 5.7.

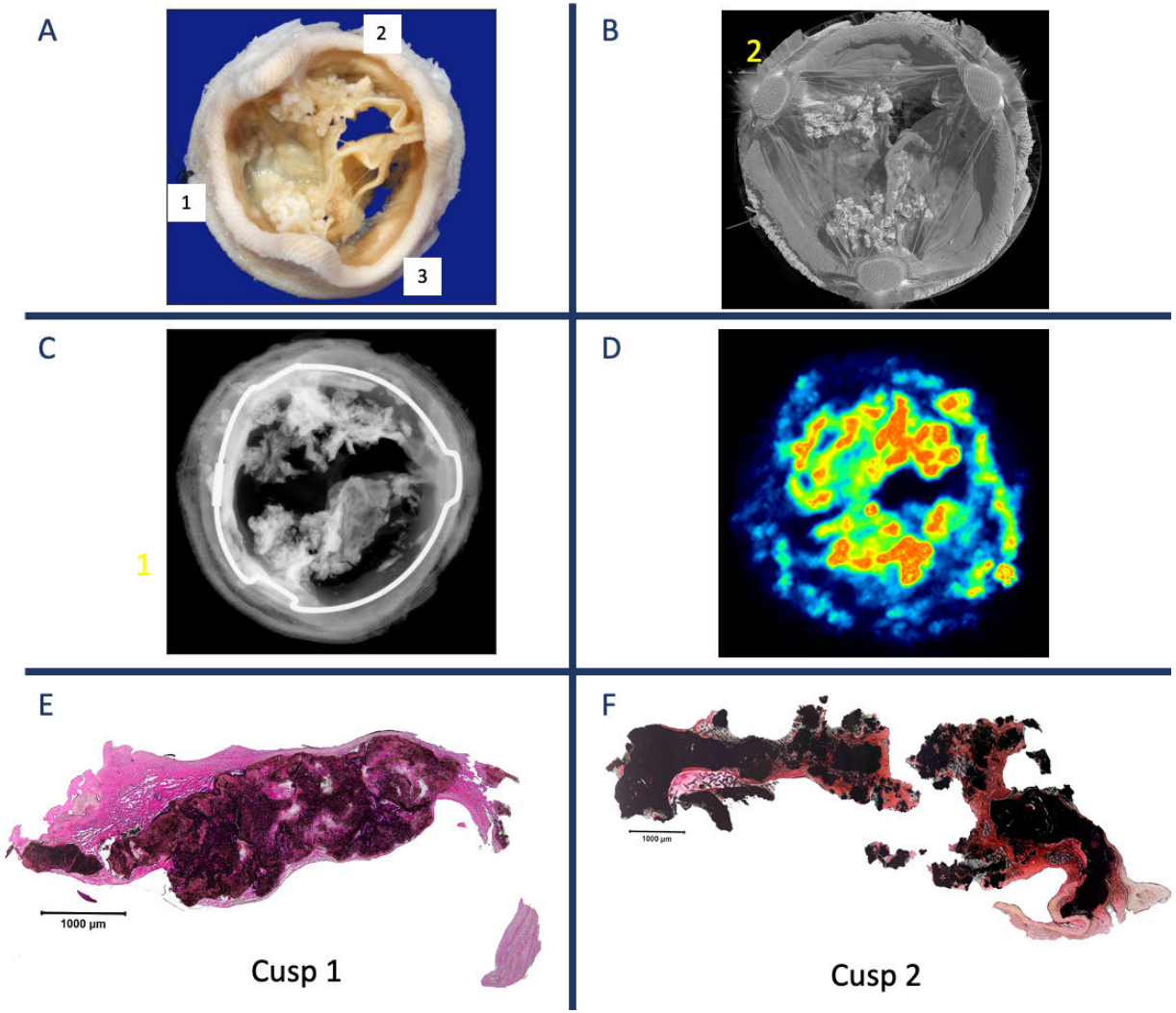

Valve 5

Macroscopic appearance of explanted bioprosthetic valve from the aortic aspect (A). Computed tomography surface-rendered *en face* image (B) and maximum intensity projection image of valve (C). ^{18}F-Fluoride positron emission tomography image of valve (D). H&E stain of section from cusp 1 (E) and von Kossa stain of section from cusp 2 both showing full thickness intrinsic calcification (F).

FIGURE 5.8.

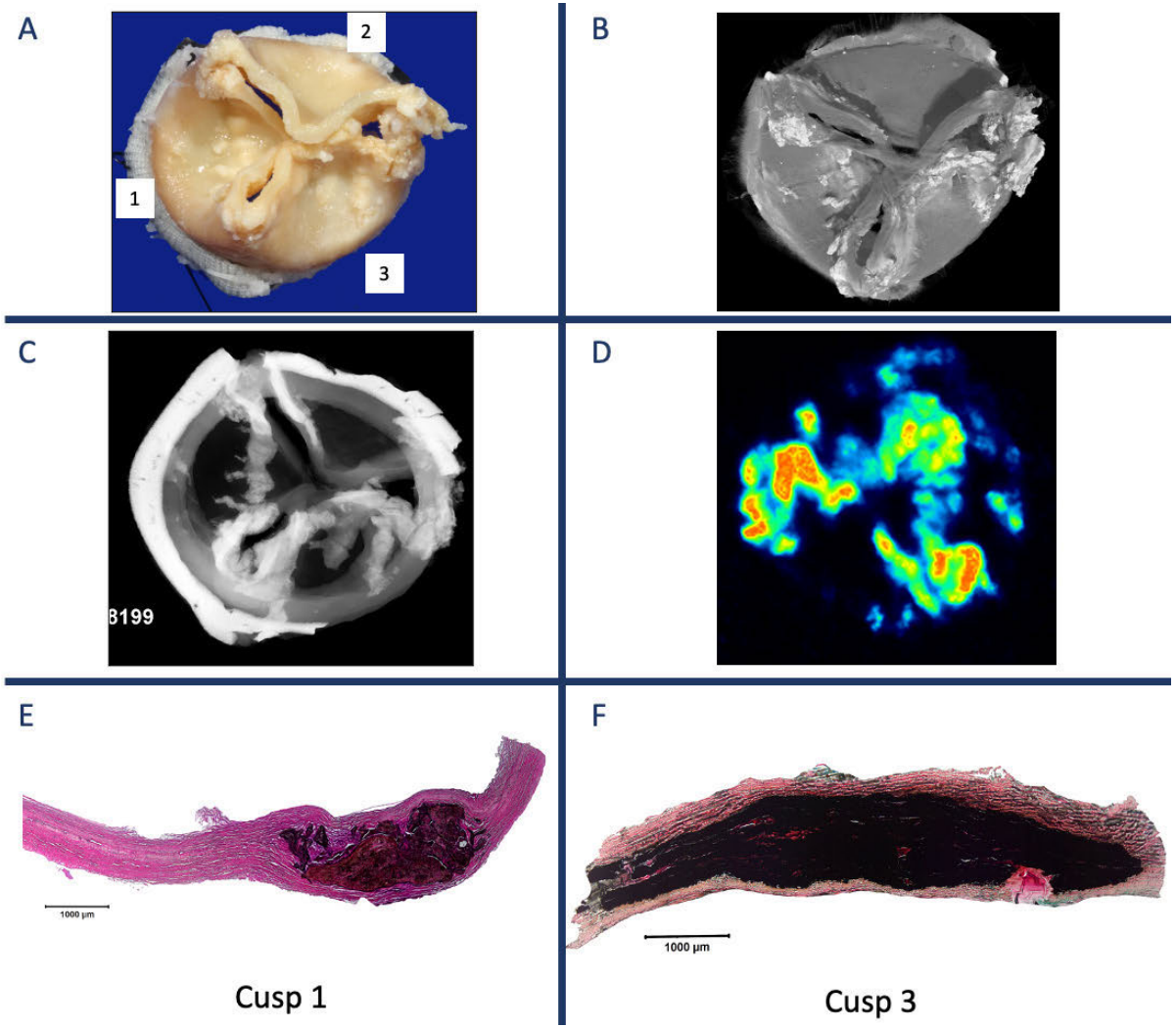

Valve 6

Macroscopic appearance of explanted bioprosthetic valve from the aortic aspect (A). Computed tomography surface-rendered *en face* image (B) and maximum intensity projection image of valve (C). ^{18}F-Fluoride positron emission tomography image of valve (D). H&E stain of section from cusp 1 (E) and von Kossa stain of section from cusp 3, both showing full thickness intrinsic calcification (F).

FIGURE 5.9.

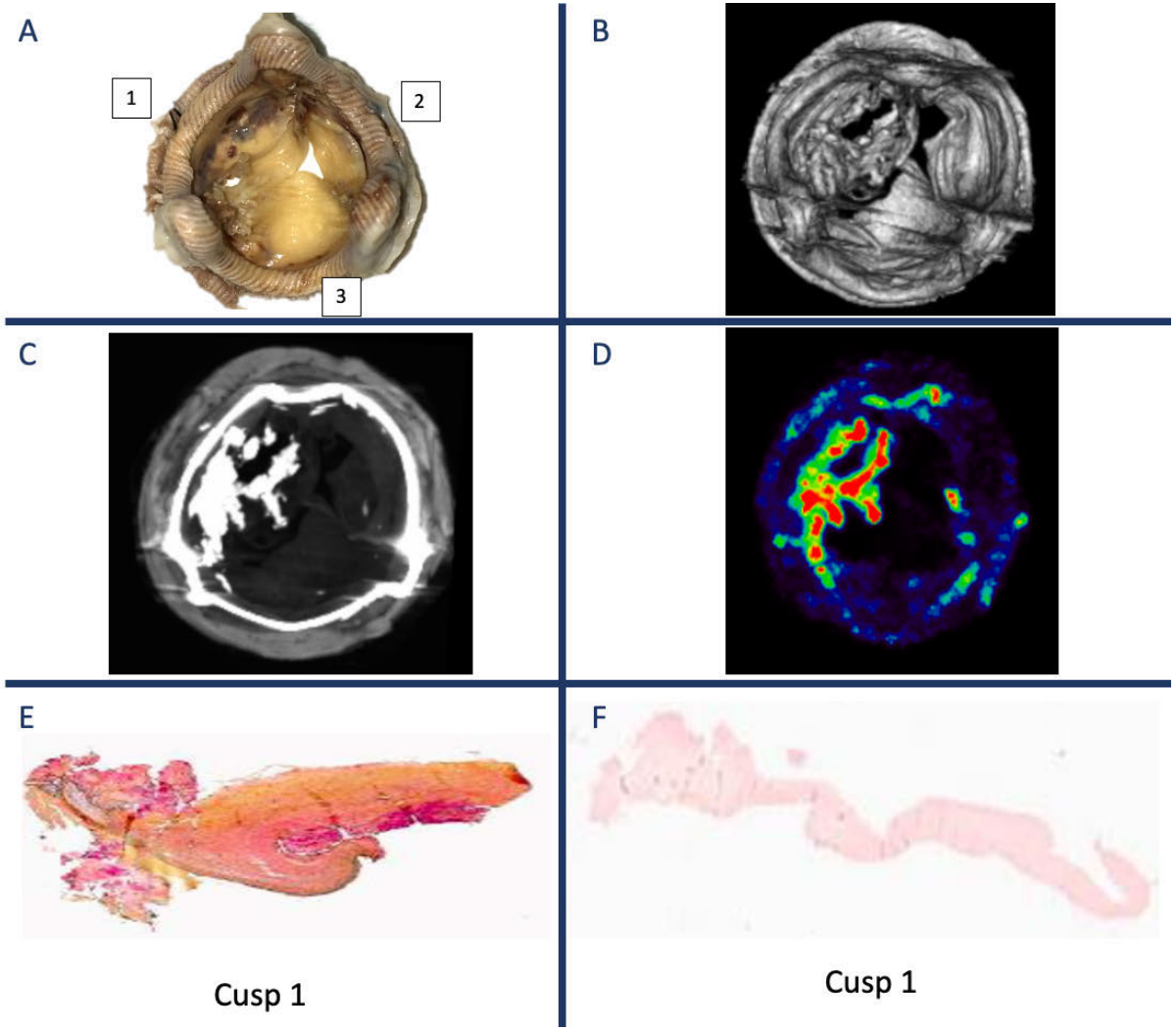

Macroscopic appearance of explanted bioprosthetic valve from the aortic aspect (A). Computed tomography surface-rendered *en face* image (B) and maximum intensity projection image of valve (C). ^{18}F-Fluoride positron emission tomography image of valve (D). Movat pentachrome stain of section from cusp 1 consistent with calcification, fibrous thickening and organised thrombus (E). Von Kossa stain does not identify calcification (F).

FIGURE 5.10.

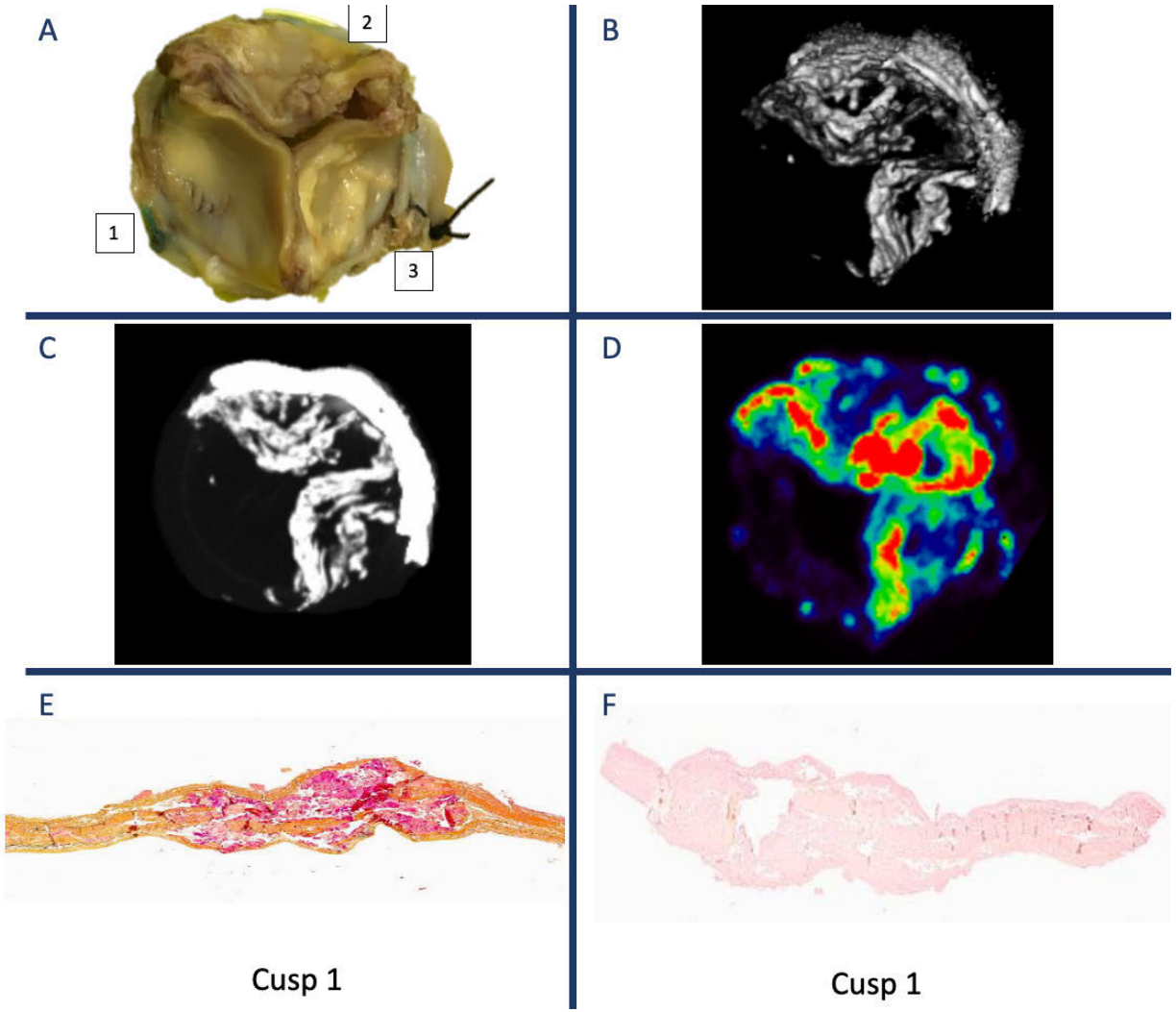

Valve 8

Macroscopic appearance of explanted bioprosthetic valve from the aortic aspect (A). Computed tomography surface-rendered *en face* image (B) and maximum intensity projection image of valve (C). ^{18}F-Fluoride positron emission tomography image of valve (D). Movat pentachrome stain of section from cusp 1 showing intrinsic calcification (E) though von Kossa stained sections do not identify calcification (F).

FIGURE 5.11.

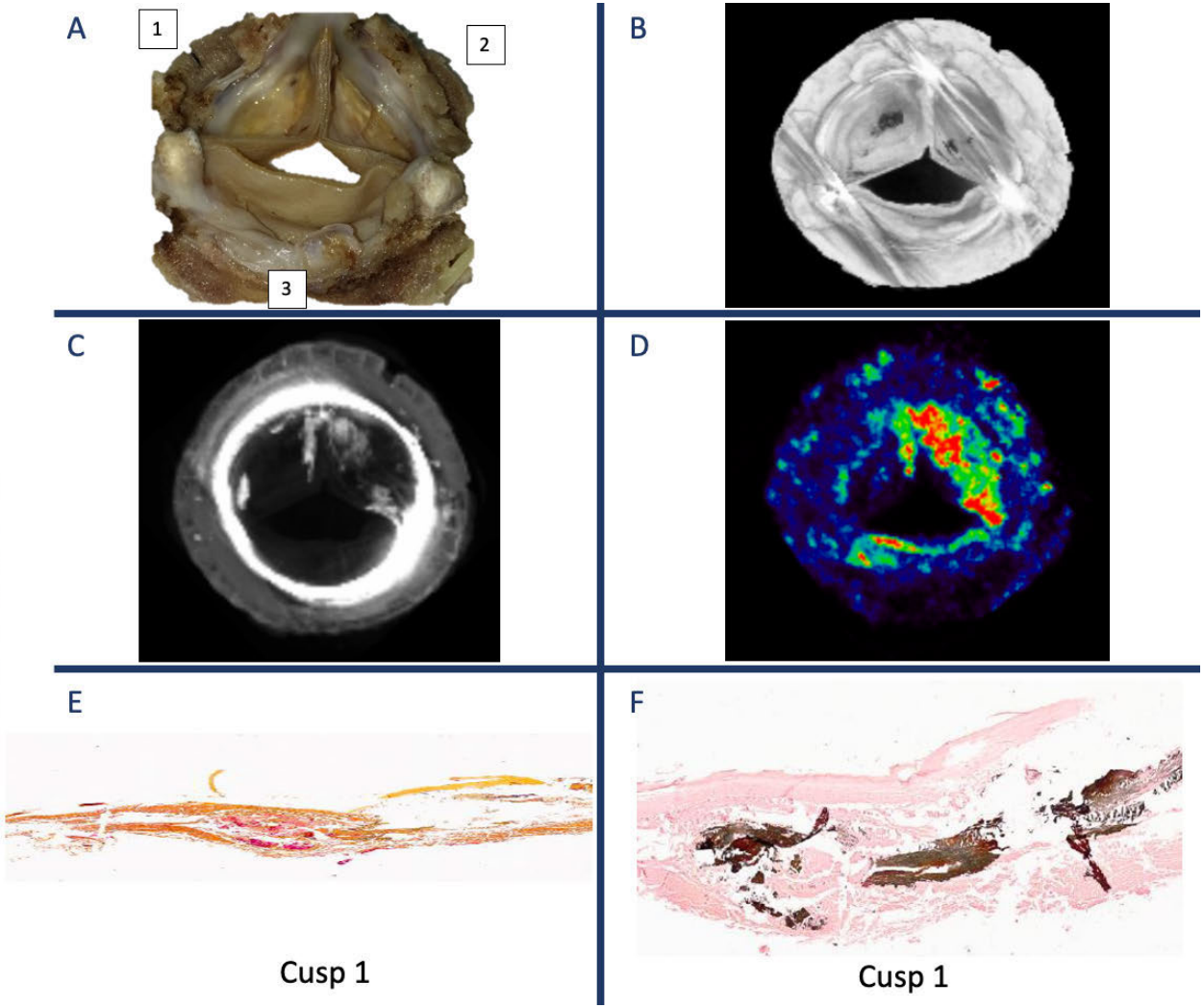

Valve 9

Macroscopic appearance of explanted bioprosthetic valve from the aortic aspect (A). Computed tomography surface-rendered *en face* image (B) and maximum intensity projection image of valve (C). ^{18}F-Fluoride positron emission tomography image of valve (D). Movat pentachrome stain (E) and von Kossa stain of sections from cusp 1 show intrinsic calcification (F).

FIGURE 5.12.

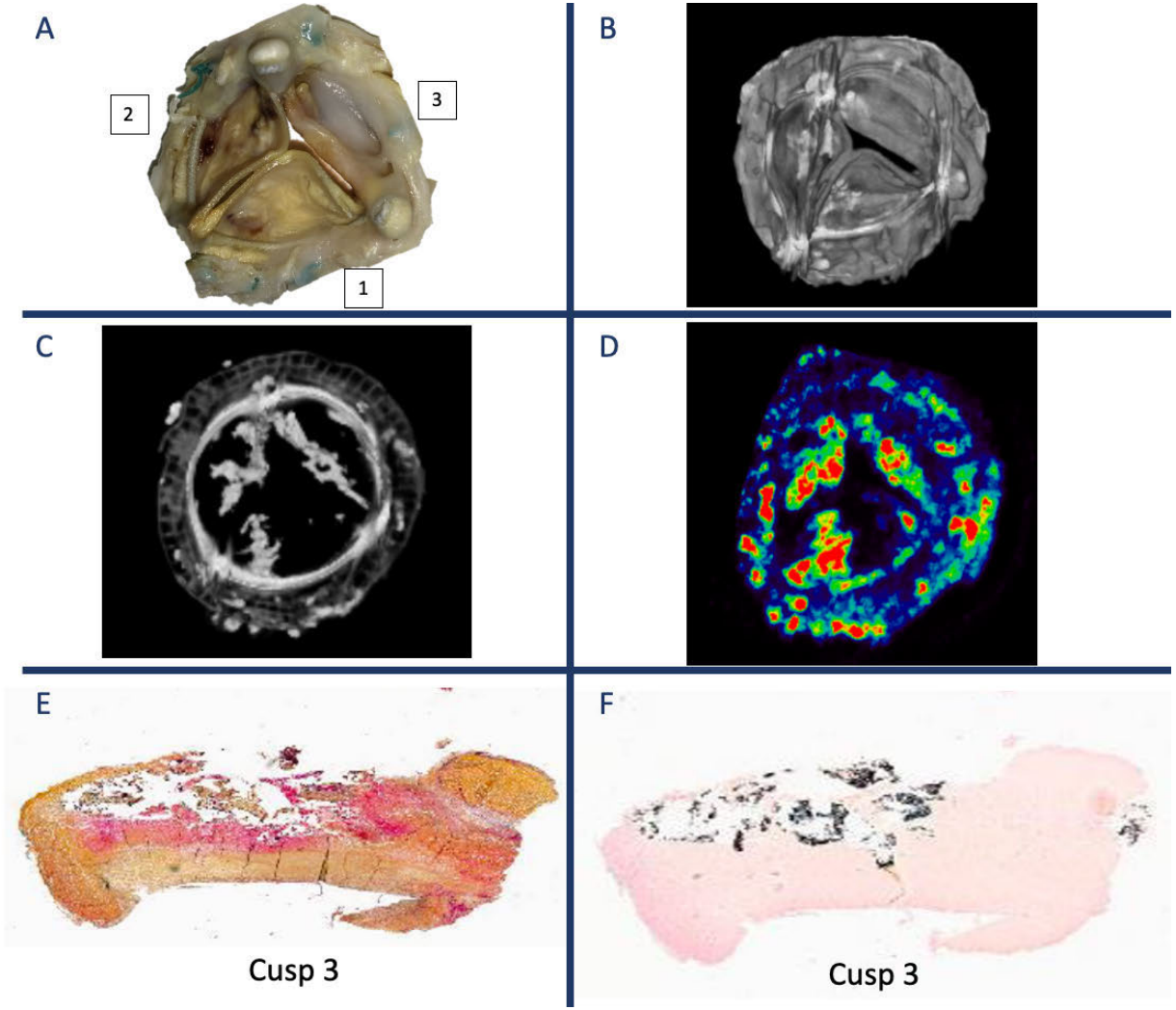

Valve 10

Macroscopic appearance of explanted bioprosthetic valve from the aortic aspect (A). Computed tomography surface-rendered *en face* image (B) and maximum intensity projection image of valve (C). ^{18}F-Fluoride positron emission tomography image of valve (D). Movat pentachrome stain of section from cusp 3 showing regions of calcification and fibrous thickening (E). Von Kossa stain of section from cusp 3 confirming the presence of intrinsic calcification, erupting through the surface (F).

FIGURE 5.13.

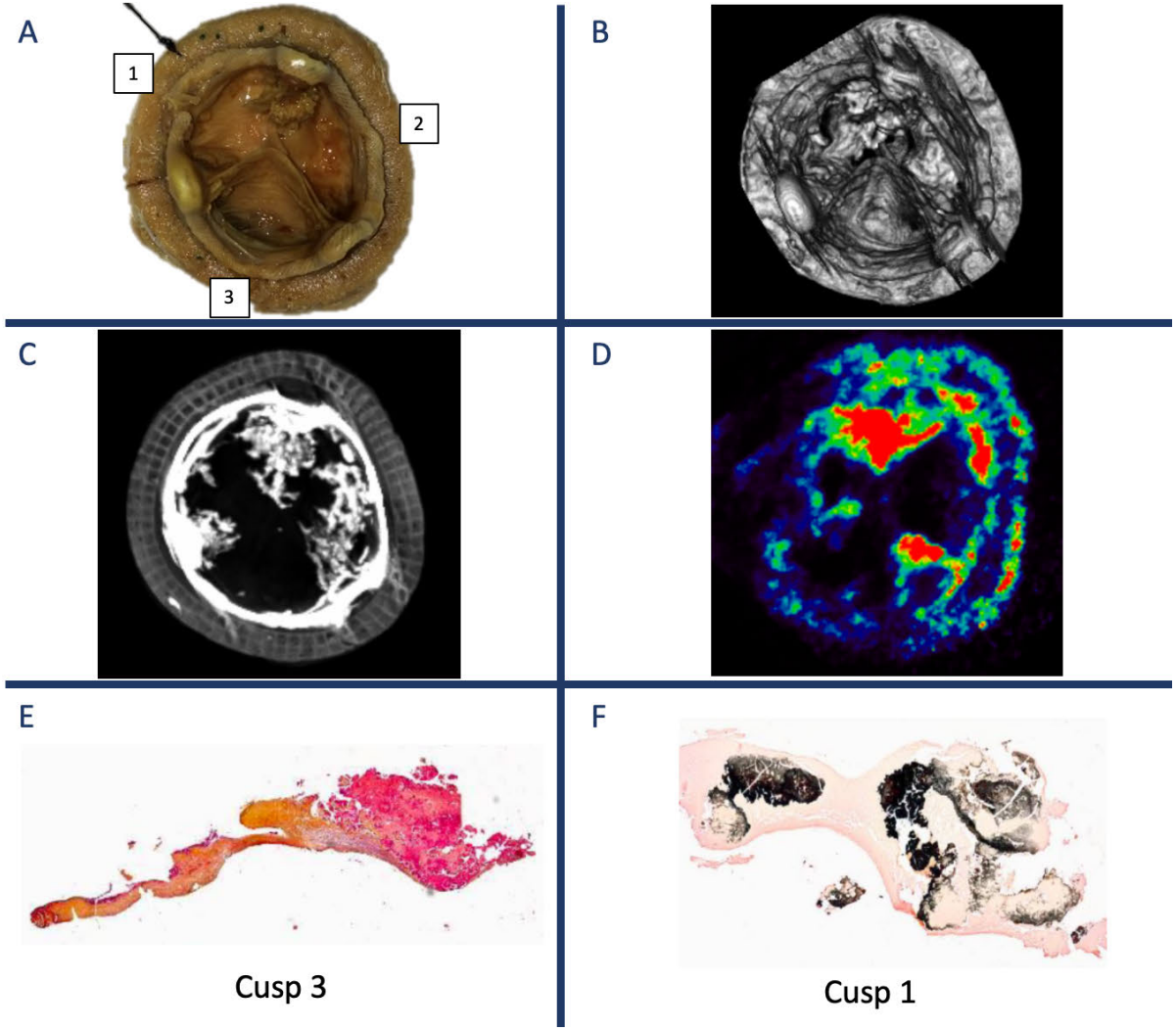

Valve 11

Macroscopic appearance of explanted bioprosthetic valve from the aortic aspect (A). Computed tomography surface-rendered *en face* image (B) and maximum intensity projection image of valve (C). ^{18}F-Fluoride positron emission tomography image of valve (D). Movat pentachrome stain of section from cusp 3 showing large papillary thrombus (E) and von Kossa stain of section from cusp 1 demonstrating diffuse intrinsic calcification (F).

FIGURE 5.14.

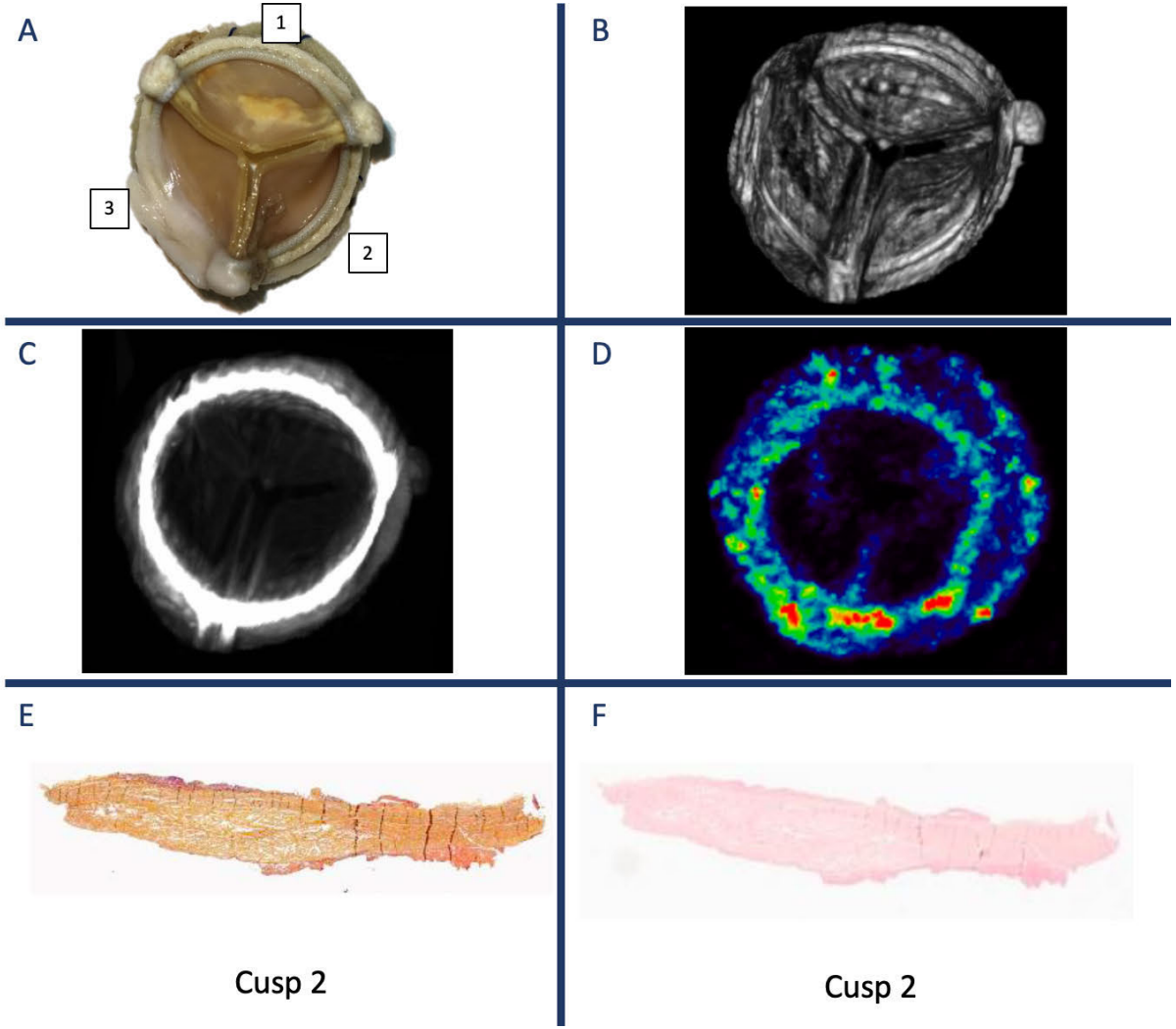

Valve 12

Macroscopic appearance of explanted bioprosthetic valve from the aortic aspect (A). Computed tomography surface-rendered *en face* image (B) and maximum intensity projection image of valve (C). ^{18}F-Fluoride positron emission tomography image of valve (D). Movat pentachrome stain of section from cusp 2 shows loss of collagen architecture, fragmentation, fluid insudation and organized thrombus on the cusp surface (E). Von Kossa stain of section from cusp 2 does not show calcification (F).

FIGURE 5.15.

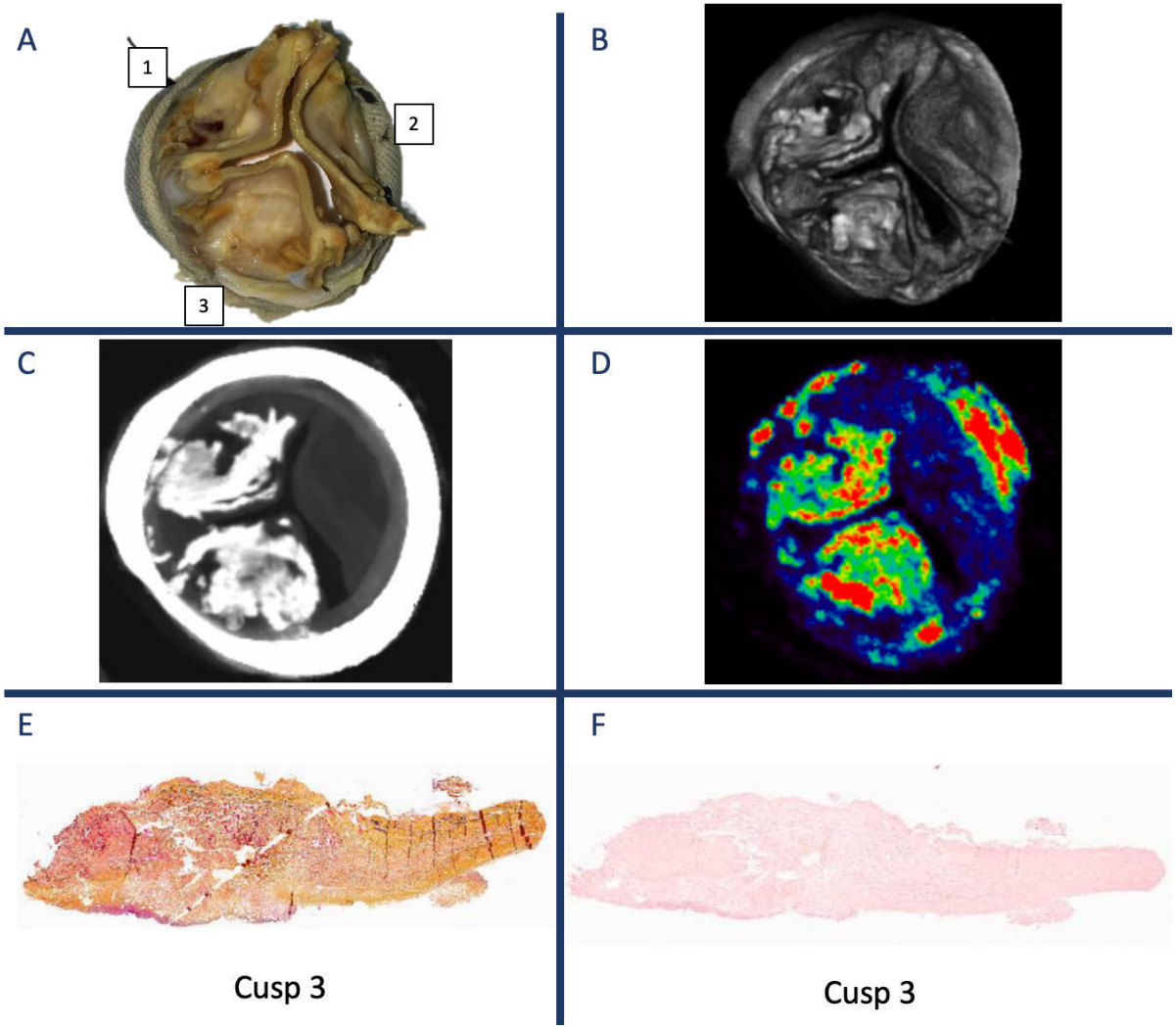

Valve 13

Macroscopic appearance of explanted bioprosthetic valve from the aortic aspect (A). Computed tomography surface-rendered *en face* image (B) and maximum intensity projection image of valve (C). ^{18}F-Fluoride positron emission tomography image of valve (D). Movat pentachrome stain of section from cusp 3 showing tissue degradation with collagen separation and fluid insudation, fibrous thickening and organized thrombus on the cusp surface (E). Von Kossa stain of section from cusp 3 does not show calcification (F).

FIGURE 5.16.

Valve 14

Macroscopic appearance of explanted bioprosthetic valve from the aortic aspect (A). Computed tomography surface-rendered *en face* image (B) and maximum intensity projection image of valve (C). ^{18}F-Fluoride positron emission tomography image of valve (D). Movat pentachrome stain of section from cusp 3 shows regions of fibrous thickening (E). There is no evidence of calcification on sections sampled for von Kossa stain from cusps 1 or 3 (F).

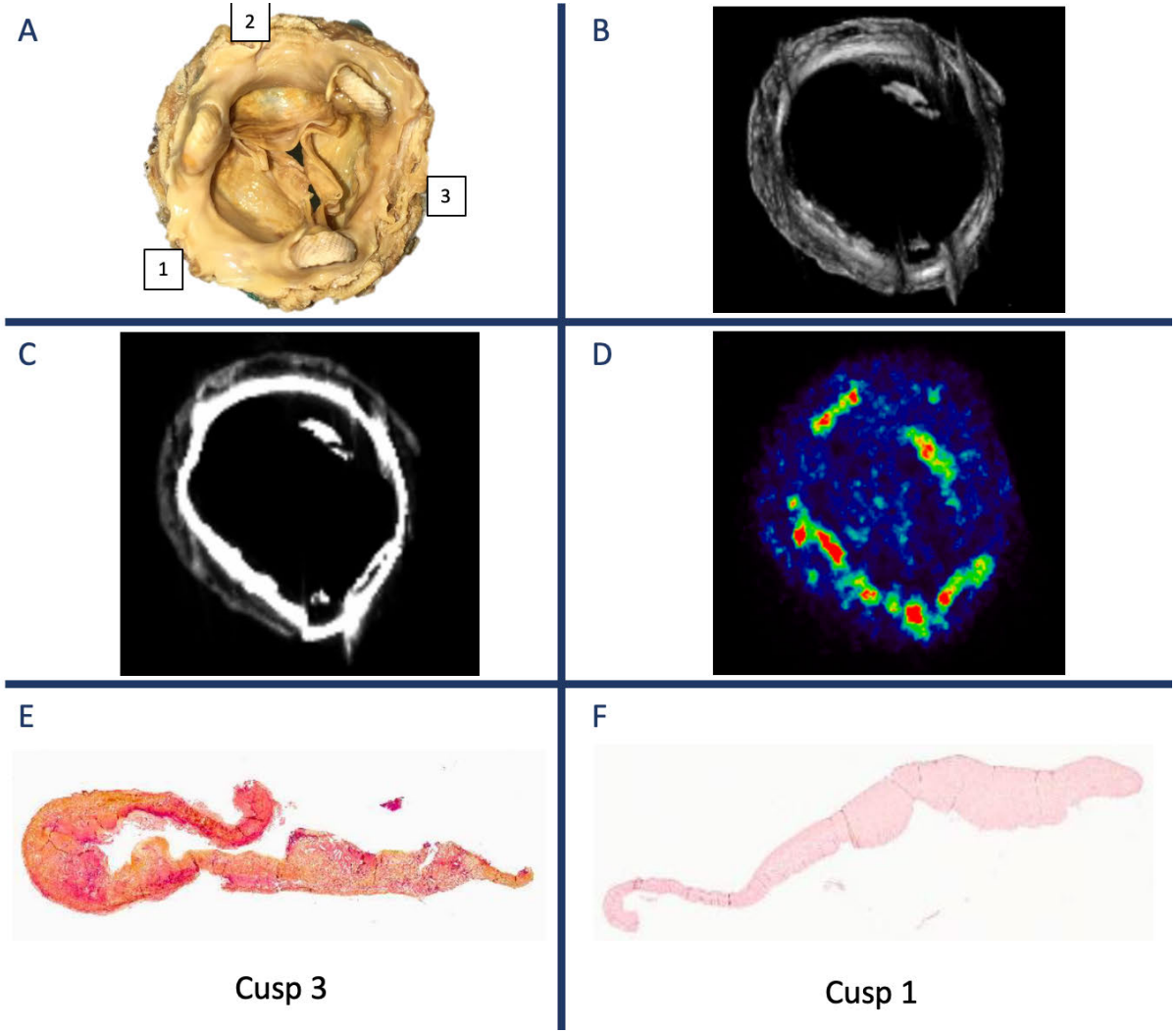

FIGURE 5.17.

Valve 15

Macroscopic appearance of explanted bioprosthetic valve from the aortic aspect (A). Computed tomography surface-rendered *en face* image (B) and maximum intensity projection image of valve (C). ^{18}F-Fluoride positron emission tomography image of valve (D). Movat pentachrome stain (E) and von Kossa stain of sections from cusp 1 demonstrate severe calcification, fibrous thickening and organized thrombus (F).

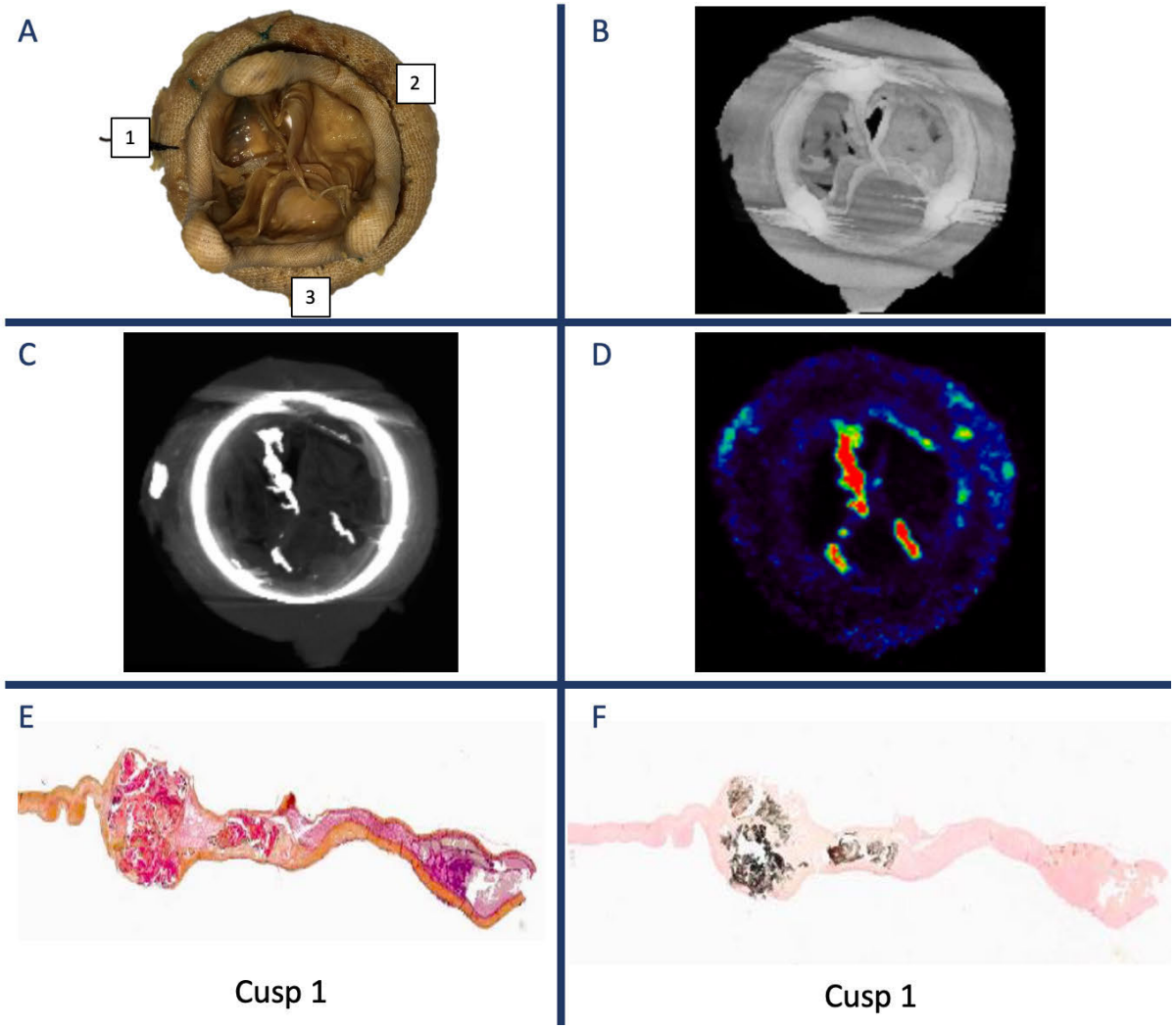

5.5 DISCUSSION

In this study we describe the features of structural valve degeneration in a series of explanted bioprosthetic heart valves by combining a detailed assessment of morphological characteristics with tissue histology, micro-computed tomography (CT) and ^{18}F-fluoride positron emission tomography (PET). We document the prevalence of leaflet calcification, fibrosis and thrombus, and use unique insights from PET/CT to help elucidate the mechanisms of bioprosthetic valve degeneration. In particular,^{18}F-fluoride PET detects nascent calcification and our findings reinforce the central role of calcification in the development of valve degeneration whilst also suggesting upstream triggers.

Explanted valves displayed clear macroscopic features of degeneration, with distortions of the valve frame, gross leaflet thickening or fragility, and cusp tears in 12 of 15 valves. Calcification was a dominant feature (in 13 of 15 valves) and micro-CT offered excellent sensitivity for the detection of calcium, superior to either direct visual inspection or tissue histology. The geographical distribution of calcium was readily appreciated by CT and showed a predilection for the leaflet commissures, which are recognised to be areas affected by high mechanical stress. This supports the important function of adverse mechanical stress in driving valve degeneration. On a microscopic level, tissue histology illustrated a particular pattern of mineralisation in bioprosthetic valves with intrinsic calcium deposition in the central regions of the cusp which propagate outwards and ultimately penetrate the surface. This observation is consistent with the theory of dystrophic calcification whereby devitalised cells and damaged

collagen and elastin structures serve as a nucleation sites for calcium phosphate within the cusp tissue.

Pannus was another prevalent feature in our series of bioprosthetic valves, with a distinctive translucent appearance which was easily recognisable on visual inspection. Pannus is a proliferation of fibrovascular tissue triggered by the host response to foreign material and typically manifests at the anastomosis of the valve sewing ring to the native annulus. In our study, pannus was universally found at least partly covering the sewing ring and encroached onto the cusps in around half of valves (7 of 15). Severe (grade 4) pannus was identified in 2 cases in which there was severe restriction or retraction of one or more cusps, and this was likely to be the major cause of valve dysfunction. In cases of pannus extending onto the valve cusps, cusp thickening was evident from micro-CT and often in a circumferential pattern around the base of the valve cusps. In several instances CT identified calcium deposition within the fibrotic tissue and histology provided corroborating evidence of an association between pannus and leaflet calcification. Our findings suggest that limited pannus growth is an essentially normal finding in bioprosthetic valve implants, and when present to a limited degree it may provide a protective covering which reduces thrombogenicity and adds tensile strength. However, more aggressive pannus overgrowth appears to provide a substrate for calcification, thereby leading to progressive structural valve degeneration, or may be a primary cause of valve failure.

Other features were less clearly discernible from macroscopic inspection and CT imaging but were detected on histological examination. These included organised

thrombus (in 6 of 15 valves) and features of tissue degradation such as loss of collagen structure, expansion of the proteoglycan layer and fluid insudation. Where present, leaflet thrombus was too limited in extent to cause haemodynamic valve dysfunction but did colocalise with regions of cusp thickening on CT and, in one instance, was associated with leaflet calcification on CT. This implies that leaflet thrombosis may more often be a subclinical event perpetuating progressive structural degeneration rather than a primary cause of valve obstruction and failure.

In our investigation of ^{18}F-fluoride as a marker of bioprosthetic valve degeneration, we first performed autoradiography and histological staining to confirm the binding of ^{18}F-fluoride to regions of calcium phosphate deposition in bioprosthetic valve tissue. We then used micro-PET/CT to examine ^{18}F-fluoride uptake in the explanted valves, demonstrating variable degrees of uptake in all of the valves. The highest ^{18}F-fluoride signal was observed to colocalise with regions of leaflet calcification and there was a positive correlation between total valve calcium volume quantified by CT and maximum ^{18}F-fluoride activity measured by PET. However, ^{18}F-fluoride activity also spatially correlated with other histological findings including fibrosis, thrombus and features of tissue degradation such as disruption of collagen architecture, even in the absence of calcium. These observations promote the theory of leaflet calcification as a final common response to bioprosthetic valve injury. In addition, it has been suggested that ^{18}F-fluoride may have the potential to bind matrix metalloproteinases which are upregulated and implicated in bioprosthesis tissue degradation (Simionescu A *et al*, 1996 b; Kato MT *et al*, J Den Res 2014).

Our study has several key strengths. First, given the scarcity and challenge of obtaining sixteen well-preserved explanted degenerated bioprosthetic valves, this represents a robust sample size from which we have been able to study a range of the most widely used stented xenograft valve models. Second, we combine high quality tissue histology performed in expert hands with the novel application of preclinical PET and CT imaging. Whilst micro-CT provides high resolution anatomical detail, ^{18}F-fluoride PET offers complementary functional information about calcification activity and therefore allows us to theorise about the mechanistic pathways leading to valve degeneration. Our multimodal imaging approach is particularly well suited to the study of bioprosthetic valves in which calcium typically aggregates in the deeper layers of cusp tissue such that degeneration is well advanced before calcification is apparent on the valve surface.

Our study also has a number of limitations. Though comparable in size to many published series, we would ideally wish to expand our sample size to strengthen the applicability of our observations. In addition, CT imaging of prosthetic valves is afflicted by artefact, principally beam hardening and photon starvation artefact, resulting from the dense materials used in manufacture of the valve frame. This in turn influences the CT attenuation correction applied to PET data, with the consequence that there may sometimes appear to be increased PET signal in regions affected by such artefact. We have optimised our scanning protocol to minimise this impact, whilst post-processing algorithms have also been described which may help correct for the issue.

In conclusion, ^{18}F-fluoride PET has been successfully used to assess calcification activity and predict disease progression in a range of cardiovascular pathology including coronary heart disease, stroke, abdominal aortic aneurysms and aortic stenosis (Joshi NV *et al*; Forsythe RF *et al*; Vesey A *et al*; Dweck *et al*). We now extend these observations to bioprosthetic valves *ex vivo* and confirm that ^{18}F-fluoride localises to regions of developing leaflet calcification on histology and high-resolution micro-PET/CT. Interestingly, a minority of bioprosthetic valves appear to degenerate without histological evidence of calcification. In these cases, there was also increased ^{18}F-fluoride activity which correlated with histological features including organised thrombus, fibrosis (pannus), gross leaflet thickening, fluid insudation and disruption of normal collagen architecture. These findings suggest that subclinical leaflet thrombosis, fibrosis and matrix degradation may all be potential upstream triggers of a calcific response. This is consistent with the theory of calcification being the final common consequence of various mechanisms of bioprosthetic valve injury and a major driver towards valve dysfunction, causing progressive cusp stiffness and obstruction as well as leaflet fragility and tears. We therefore propose that ^{18}F-fluoride PET/CT imaging may provide an informative marker of bioprosthetic valve degeneration within the clinical setting.

CHAPTER 6

DETECTION AND PREDICTION OF BIOPROSTHETIC AORTIC VALVE DEGENERATION

Cartlidge TRG, Doris MK, Sellers SL, Pawade TA, White AC, Pessotto R, Kwiecinski J, Fletcher A, Alcaide C, Lucatelli C, Densem C, Rudd JHF, van Beek EJR, Tavares A, Virmani R, Berman D, Leipsic JA, Newby DE, Dweck MR. Detection and prediction of bioprosthetic aortic valve degeneration. *J Am Coll Cardiol.* 2019;**73**:1107-1119.

6.1 ABSTRACT

Background

Bioprosthetic aortic valve degeneration is increasingly common, often unheralded and can have catastrophic consequences.

Objectives

To assess whether ^{18}F-fluoride positron emission tomography (PET) – computed tomography (CT) can detect bioprosthetic aortic valve degeneration and predict valve dysfunction.

Methods

Explanted degenerate bioprosthetic valves were examined *ex-vivo*. Patients with bioprosthetic aortic valves were recruited into two cohorts with and without prosthetic valve dysfunction and underwent *in-vivo* contrast-enhanced CT angiography, ^{18}F-fluoride PET, and serial echocardiography during 2 years of follow-up.

Results

All degenerate bioprosthetic valves displayed ^{18}F-fluoride PET uptake that co-localised with tissue degeneration on histology. In 71 patients without known bioprosthesis dysfunction, 14 had abnormal leaflet pathology on CT and 24 demonstrated ^{18}F-fluoride PET uptake (target-to-background ratio 1.55 [1.44-1.88]). Patients with increased ^{18}F-fluoride uptake exhibited more rapid deterioration in valve function compared to those without (annualised change in peak transvalvular velocity:

0.30 [0.13-0.61] *versus* 0.01 [-0.05-0.16] ms^{-1}/year, p<0.001). Indeed ^{18}F-Fluoride uptake correlated with deterioration in all the conventional echocardiographic measures of valve function assessed (e.g. change in peak velocity, r=0.72; p<0.001). Each of the 10 patients who developed new overt bioprosthesis dysfunction during follow-up had evidence of ^{18}F-fluoride uptake at baseline (target-to-background ratio 1.89 [1.46-2.59]). On multivariable analysis, ^{18}F-fluoride uptake was the only independent predictor of future bioprosthetic dysfunction.

Conclusion

^{18}F-Fluoride PET-CT identifies subclinical bioprosthetic valve degeneration, providing powerful prediction of subsequent valvular dysfunction and highlighting patients at risk of valve failure. This technique holds major promise in the diagnosis of valvular degeneration and the surveillance of patients with bioprosthetic valves.

6.2 INTRODUCTION

The implantation of bioprosthetic heart valves is increasing rapidly due to patient preference, the increasing prevalence of valve disease in an ageing population, and the emergence of transcatheter aortic valve implantation (Iung B *et al*, 2011; Nkomo VT *et al*, 2006; Brown JM *et al*, 2009; Brennan JM *et al*, 2017). In the United States, 90,000 surgical aortic valve replacements are performed annually, with over three-quarters incorporating bioprosthetic valves (Brown JM *et al*, 2009). In addition, over 80,000 transcatheter aortic valve implantation procedures have been performed since Food and Drug Administration approval in 2011 (Brennan JM *et al*, 2017). Given the finite lifespan of these valves and the rapid expansion of the population of patients requiring regular surveillance, bioprosthetic valve degeneration will become a major cause of cardiovascular morbidity and healthcare burden over the coming decades.

The pathophysiology of bioprosthetic valve degeneration is poorly understood. Whilst calcification appears to contribute to both progressive valve narrowing and leaflet tears, non-invasive methods for detecting this process have been lacking, and the triggers of valve degeneration and calcification are unknown (Pibarot P *et al*, 2009; Singhal P *et al*, 2013; Rodriguez-Gabella T *et al*, 2017). Current standard of care relies on serial echocardiography and clinical assessment aimed at detecting the valve dysfunction that occurs only towards the end stages of the degeneration process. Unfortunately, many patients present *in extremis* with unheralded valve failure due to rapid onset valvular obstruction or regurgitation, with repeat operation a high-risk undertaking. Indeed, emergency repeat aortic valve replacement surgery is associated

with a mortality of 22.6% compared to 1.4% for elective repeat surgery (Vogt PR *et al*, 2000). Detection of bioprosthetic valve degeneration is therefore highly desirable allowing at-risk patients to be identified early, offered close tailored monitoring, and optimised timing of repeat elective intervention, thereby avoiding potentially catastrophic valve failure.

^{18}F-Fluoride positron emission tomography (PET) has recently been used to image tissue calcification activity in a range of cardiovascular diseases (Dweck MR *et al*, 2012 A; Forsythe RO *et al*, 2018; Joshi NV *et al*, 2014; Vesey AT *et al*, 2017). ^{18}F-Fluoride preferentially binds to areas of developing microcalcification indicative of tissue degeneration that precede the macrocalcification detectable by computed tomography (CT) (Irkle A *et al*, 2015; Dweck MR *et al*, 2014); Jenkins WS *et al*, 2014). Given that calcification is one of the key pathological process underlying bioprosthetic valve degeneration, we hypothesised that increased ^{18}F-fluoride uptake would identify prosthetic valve degeneration and predict subsequent deterioration in bioprosthetic valve function.

6.3 METHODS

Ex-vivo Assessment of Degenerated Bioprosthetic Aortic Valves

Explanted degenerated aortic valve bioprostheses were obtained with written consent from patients undergoing repeat surgical aortic valve replacement for bioprosthetic valve failure. Valves were weighed, photographed and their macroscopic features documented. *Ex-vivo* micro-PET-CT was performed with a nano-PET-CT scanner (Mediso, Hungary) and X-ray microtomograph (Brucher, Belgium) before undergoing histological evaluation.

Clinical Study Design and Population

Patients over 40 years who had undergone previous surgical aortic valve replacement using a bioprosthetic valve were prospectively recruited into a single-centre cohort study according to defined inclusion and exclusion criteria as below (Figure 6.3). Participants were recruited if they were under routine clinical review and had (a) known evidence of bioprosthetic valve failure on echocardiography and had been referred for repeat aortic valve intervention, or (b) no known evidence of valve dysfunction or degeneration (Lancellotti P *et al*, 2016; Zoghbi WA *et al*, 2009). Written informed consent was obtained from all participants. The study (www.clinicaltrials.gov, NCT02304276) was conducted in accordance with the Declaration of Helsinki and was approved by an NHS Scotland Research Ethics Committee (14/SS/1049) and the Administration of Radioactive Substances Advisory Committee.

Study Eligibility Criteria for Patient Selection

Inclusion Criteria

Ability to give informed consent; over 40 years of age; Cohort 1: patients with a surgically implanted bioprosthetic aortic valve who are due to undergo redo-aortic valve surgery or valve-in-valve transcatheter valve implantation for bioprosthetic valve failure; Cohort 2: patients with a surgically implanted bioprosthetic aortic valve, implanted 1 month, 2 years, 5 years or 10 years prior to study recruitment and without known evidence of valve dysfunction or degeneration.

Exclusion Criteria

Inability to give informed consent; pregnancy; breastfeeding; claustrophobia; allergy to iodinated contrast; liver failure; chronic kidney disease (with estimated glomerular filtration rate <30 mL/min/1.73m^2); Paget's disease; metastatic malignancy; inability to tolerate the supine position.

Study Assessments and Data Collection

All participants underwent baseline clinical assessment including Doppler and two-dimensional echocardiography, non-contrast CT calcium scoring, contrast-enhanced CT angiography and *in-vivo* ^{18}F-fluoride PET. Participants were invited to return annually for 2 years for repeat clinical assessments and echocardiography to assess changes in bioprosthesis performance. Definitions of bioprosthetic degeneration and dysfunction vary but in this study, we used definitions from both contemporary international guideline criteria (Lancellotti P *et al*, 2016; Zoghbi WA *et al*, 2009) and a recent expert consensus statement (Dvir D *et al*, 2018). Bioprosthetic valve failure

was defined as the development of severe haemodynamic valve dysfunction combined with patient symptoms, the need for redo valve intervention or valve-related death (Capodanno D *et al*, 2017). Patients were followed up for the development of valve failure beyond the 2 year time frame using electronic patient record data.

Echocardiography

Two-dimensional and Doppler echocardiography was performed at baseline and annually for 2 years by a single experienced and British Society of Echocardiography-accredited echocardiographer using a single echocardiography scanner (Affiniti 70, Philips Healthcare) according to a standardised protocol. Aortic valve Doppler measurements were routinely assessed from the apex, suprasternal notch and right sternal edge and used to measure the peak velocity through the valve, the mean gradient and the Doppler velocity index (DVI). Mean values were taken from 3 measurements when subjects were in sinus rhythm and from 5 measurements if atrial fibrillation was present. Bioprosthetic valve regurgitation was graded as mild, moderate or severe according to guideline recommendation on the basis of visual appraisal of colour Doppler images, measurement of pressure half-time (ms) and assessment for aortic flow reversal in diastole (Lancellotti P *et al*, 2016; Zoghbi WA *et al*, 2009). In cohort 2, all 71 patients completed baseline and 1 year echocardiographic assessments, with 67 completing the 2 year visit. Measurements of relevant continuous variables were assessed as an annualised change during the follow-up period.

Defining Bioprosthetic Degeneration and Dysfunction

Prosthetic valve dysfunction was adjudicated based upon European Association of Cardiovascular Imaging/Inter-American Society of Echocardiography/Brazilian Department of Cardiovascular Imaging and American Society of Echocardiography guidelines (Lancellotti P *et al*, 2016; Zoghbi WA *et al*, 2009) using the following criteria: Doppler velocity index (DVI) <0.29 and either peak velocity >3 I or mean gradient >20 mmHg (i.e. valve dysfunction suggested by one flow-independent parameter and one flow-dependent parameter), prosthetic regurgitation of at least moderate severity or an increase in mean gradient >10 mmHg.

We also investigated an alternative definition of bioprosthetic valve degeneration and dysfunction proposed in a recent expert consensus statement: *stage 1* characterised by morphological abnormality (detected on echocardiography or computed tomography) in the absence of haemodynamic changes; *stage 2* characterised by the presence of either moderate valve obstruction, moderate regurgitation or both; stage 3 characterised by the presence of either severe valve obstruction or regurgitation (Dvir D *et al*, 2018). Central to this definition of structural valve degeneration is a deterioration in function over time, for example, new valve obstruction should be accompanied by a change in mean gradient >10mmHg associated with a decrease in Doppler velocity index and effective orifice area. Valve failure was defined as the development of severe stenosis or regurgitation resulting in the development of patient symptoms and/or the need for redo valve intervention (Brennan JM *et al*, 2017).

Positron Emission Tomography and Computed Tomography

Subjects were given 25 mg of oral metoprolol if their resting heart rate was >65 beats/min in the absence of any contraindication. A target dose of 125 MBq ^{18}F-fluoride was administered intravenously, with an effective radiation dose of 3 mSv. After 60 min, participants were imaged on a hybrid 128-detector array positron emission tomography and computed tomography (PET-CT) scanner (Biograph mCT, Siemens, Erlangen, Germany). Pharmacokinetic modelling has demonstrated that this timing provides excellent vascular tissue contrast resolution (Irkle A *et al*, 2015). A low-dose attenuation correction CT scan was performed (120 kV, 50 mAs; 5/3 mm), followed by acquisition of PET data in list mode, using a single 30-min bed position centred on the valve in 3-dimensional mode. Finally, ECG-gated aortic valve CT calcium scoring and contrast-enhanced CT angiography were performed in diastole and in held expiration.

Image Analysis

^{18}F-Fluoride PET-CT

Static PET-CT images were reconstructed with correction applied for attenuation, dead time, scatter and random coincidences, using an optimised iterative reconstruction algorithm (ultra-HD; TrueX + TOF, matrix 200, zoom 1; Gaussian filter). Analyses were performed using an OsiriX workstation (OsiriX version 8.0.3 64-bit; OsiriX Imaging Software, Geneva, Switzerland). ECG-gated contrast-enhanced CT images were reconstructed in diastole using 1-mm slices. For this purpose, ECG-gating of list mode PET data was used to reconstruct at 25% intervals of the cardiac cycle with diastolic data determined as that acquired between 50 and 75% of the R-R interval. PET and CT reconstructions were carefully co-registered in all 3 planes using the 2-D

orthogonal tool (Figure 6.1). Key points of reference were the sternum, vertebrae, blood-pool in the left ventricle (based upon the high ^{18}F-fluoride activity in the blood relative to the surrounding myocardium), the ascending aorta and the aortic arch. Fused PET and contrast-enhanced CT images were reoriented to provide *en face* images of the bioprosthetic valve with corresponding long-axis views. Images were analysed by two experienced PET/CT observers (TC, MRD). Using pre-specified criteria, CT scans were adjudicated to be abnormal if there was pannus (circumferential low-attenuation [non-calcific] material with radial thickness ≥2 mm and encroachment on the valve cusps) (Lancellotti *P et al*, 2016; Makkar RR *et al*, 2015), non-calcific leaflet thickening (focal areas of low attenuation [30-200 Hounsfield Units] cusp thickening ≥2 mm visualised in at least 2 planes) (Makkar RR *et al*, 2015; Pache G *et al*, 2016), or leaflet calcification (calcium >500 HU localised to valve cusp in at least 2 planes) (Fujita B *et al*, 2016). Leaflet calcification was further sub-divided into spotty calcification if maximum diameter <3 mm and large calcification if maximum diameter ≥3 mm (Motoyama S *et al*, 2007). PET scans were adjudicated to be abnormal if increased ^{18}F-fluoride uptake (target-to background ratio >1.3) originating in the valve cusps was observed in both *en face* and long-axis views. ^{18}F-fluoride uptake originating from the sewing ring or the aortic wall was not considered as evidence of bioprosthetic leaflet degeneration and was not quantified.

FIGURE 6.1.

Methodology for co-registration of positron emission tomography and contrast computed tomography in bioprosthetic aortic valves.

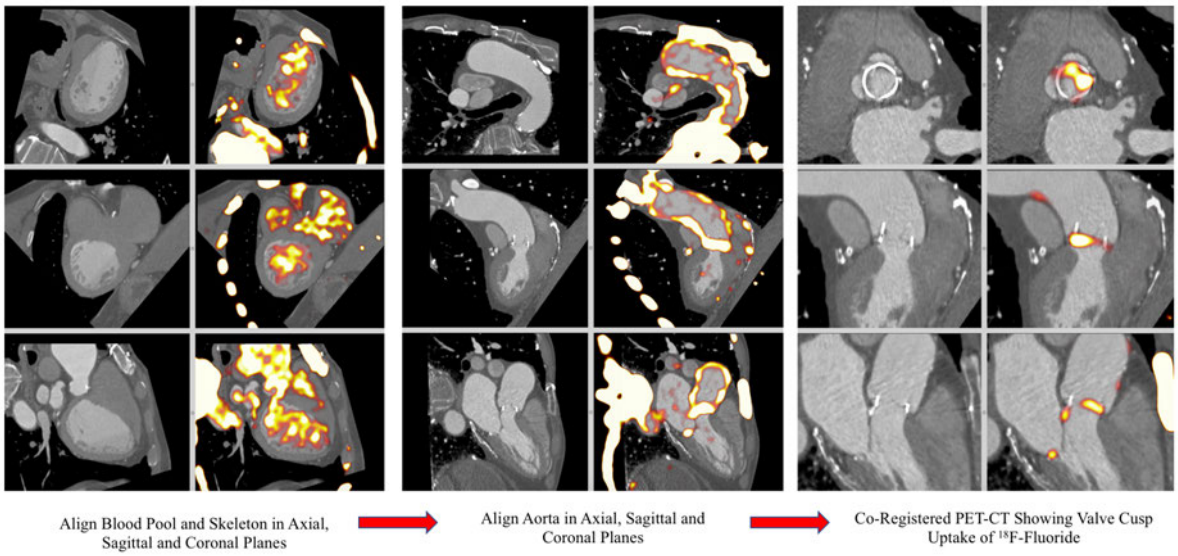

Figure 6.1. Careful alignment of the positron emission tomography (PET) activity in the cardiac blood pool with the contrast-enhanced computed tomography (CT) images is performed in 3 planes (left). This is possible because of the high ^{18}F-fluoride activity in the blood pool compared to the myocardium. Subsequently PET activity in the ascending aorta and aortic arch (center) is aligned with the CT and final refinement of co-registration is performed according to landmarks around the bioprosthetic aortic valve such as the coronary arteries and mitral valve annulus. Hybrid images are then re-orientated to provide en face images of the bioprosthetic valve with corresponding perpendicular long-axis images. Finally, the PET windowing is adjusted to the point below which blood pool activity in the aorta is visible to assess uptake in the valve leaflets.

Quantification of ^{18}F-Fluoride Uptake in Bioprosthetic Valve Leaflets

To quantify ^{18}F-fluoride uptake, a circular (area 1-cm^2) region of interest (ROI) was drawn around the area of maximal uptake originating in the valve cusps on the reorientated co-registered PET-CT images, employing a 'most diseased segment' (MDS) approach (Pawade TA *et al*, 2016). Where there was no visible uptake in the valve cusps, a 1-cm^2 circular ROI was drawn in the center of the valve. Mean and maximum standardised uptake values (SUV) were extracted from these ROIs and corrected for blood-pool activity measured in the right atrium (2-cm^2 ROIs, axial slices, at the level of the right coronary ostium) to calculate the target-to-background ratio (TBR) (Pawade TA *et al*, 2016). Mean TBR values using the MDS approach (TBR) were used as the principal comparator in the outcome analysis in keeping with data from native aortic valve ^{18}F-fluoride PET studies, although results for all PET measurements are presented (Dweck *et al*, 2014; Pawade TA *et al*, 2016). The TBR>1.3 threshold was pre-selected based upon previous vascular ^{18}F-fluoride studies and was supported by the threshold defining the upper tertile of bioprosthetic valve ^{18}F-fluoride activity observed in this study (Joshi NV *et al*, 2014).

Micro Positron Emission Tomography and Computed Tomography

Explanted bioprosthetic valves were incubated with 2 MBq ^{18}F-fluoride for 20 min and PET data were acquired over a 30-min bed time using 1:5 coincidence mode. Micro CT was then acquired (semi-circular full trajectory, maximum field of view, 720 projections, 70 kVp, exposure 300 ms and 1:1 binning) for attenuation correction and anatomical registration. PET data were reconstructed using Mediso's iterative Tera-Tomo 3D algorithm and the following settings: 4 iterations, 6 subsets, full

detector model, normal regularization, spike filter on, voxel size 0.6 mm, 400-600 keV energy window. Analysis was performed using PMOD (PMOD Technologies, Switzerland) and OsiriX (OsiriX version 8.0.3 64-bit; OsiriX Imaging Software, Geneva, Switzerland) to quantify calcium volume and ^{18}F-fluoride activity.

Histopathology

Explanted bioprosthetic valve specimens were fixed in 10% w/v buffered formalin phosphate (Fisher Chemical SF100-20) pending histological analysis. Heavily calcified samples were treated with fixative decalcifier to facilitate sectioning (Fisher Chemical, Cal-Ex II, CS511-1D). Leaflets were detached from the base of the valve frame and marked with tissue dye fixed with acetic acid to maintain orientation. Each leaflet was processed then sectioned into 2-4 mm sections and embedded in paraffin sequentially to yield 7-8 tissue cross-sections per leaflet. Paraffin sections (4 μm) were used for histology. Tissue was sectioned and stained for architecture (hematoxylin and eosin), calcium phosphate (von Kossa), thrombus and fibrosis (Movat Pentachrome).

Statistics and Data Analysis

Baseline characteristics are reported as number (percentages) for categorical variables and mean ± standard deviation or median [interquartile range] for continuous variables depending on whether variables were normally distributed. Categorical data were compared using chi-squared or Fisher's exact tests. Continuous variables were log-transformed [$\log_N(x+1)$ for positive values and $-\log_N(-x+1)$ for negative values] where not normally distributed. The point-biserial correlation coefficient was used to measure the strength and direction of the association between one dichotomous

variable and one continuous variable. One-way ANOVA was used to compare continuous data across multiple factors, with post-hoc analysis using the Bonferonni test where appropriate. The Student's *t*-test or Mann-Whitney U test were used to compare continuous outcomes between two independent groups depending on whether they were normally distributed. The Student's *t*-test or Wilcoxon signed-rank test were employed to compare paired variables. Two-tailed Pearson's correlation analysis was performed to investigate the relationship between ^{18}F-fluoride uptake and echocardiographic measures of valve function. Multivariable analysis was performed to assess the predictors of deterioration in bioprosthetic valve dysfunction (annualised change in peak velocity after 2 years). Statistical analysis was undertaken using IBM SPSS Statistics 23 and significance was taken at the two-sided 5% level ($p<0.05$).

6.4 RESULTS

Explanted Degenerate Bioprosthetic Aortic Valves

Fifteen failed explanted bioprosthetic aortic valves were obtained for *ex vivo* investigation. Micro-CT detected leaflet calcification in 13 valves, which was confirmed on histology. In contrast, all 15 valves demonstrated ^{18}F-fluoride leaflet uptake that correlated with a range of histological markers of bioprosthetic tissue degeneration. In particular, ^{18}F-fluoride activity detected both micro and macrocalcific deposits within the valve leaflets that co-localised predominantly with regions of pannus (fibrous thickening) and thrombus on histology. However, ^{18}F-fluoride uptake was additionally observed in the absence of calcification on histology at sites of leaflet thickening, fluid insudation and disrupted collagen architecture (Figure 6.2).

Clinical Cohort Study Population

Eighty participants were recruited to the clinical cohort study and underwent *in vivo* PET-CT imaging, although 2 patients were unable to complete the baseline scan (claustrophobia) and were excluded (Figure 6.3). The remaining 78 patients were 75 ±7 years old with a high prevalence of coronary artery disease and associated risk factors (Table 6.1), and a range of bioprosthetic valve models (Table 6.2 and 6.3).

Patients with Suspected Bioprosthetic Valve Failure

Seven participants were recruited to the cohort with suspected bioprosthetic valve failure. One subject proceeded to repeat surgical aortic valve replacement, 5 underwent valve-in-valve transcatheter valve implantation, and 1 subject was deemed to have

severe patient-prosthesis mismatch according to guideline criteria and therefore not considered to have valve failure (Lancellotti P *et al*, 2016; Zoghbi WA *et al*, 2009). All 6 subjects with confirmed bioprosthetic valve failure demonstrated abnormalities on both CT and ^{18}F-fluoride PET studies. CT revealed evidence of leaflet calcification in all patients (spotty calcification n=3, large calcification n=3) and less commonly non-calcific leaflet thickening (n=2), circumferential pannus (n=1) and distorted leaflet morphology (n=1). Increased ^{18}F-fluoride PET leaflet uptake was observed in the bioprosthetic valves of all these patients, and TBR values were nearly 3 times higher than in patients without known valvular dysfunction (2.91 [1.75-4.09] *versus* 1.12 [1.04-1.51], $p<0.001$). In the one patient with severe patient-prosthesis mismatch, there was no CT abnormality or ^{18}F-fluoride uptake.

FIGURE 6.2.

Ex-vivo **degenerated bioprosthetic aortic valves: macroscopic appearances, micro-computed tomography, micro-positron emission tomography and histology.**

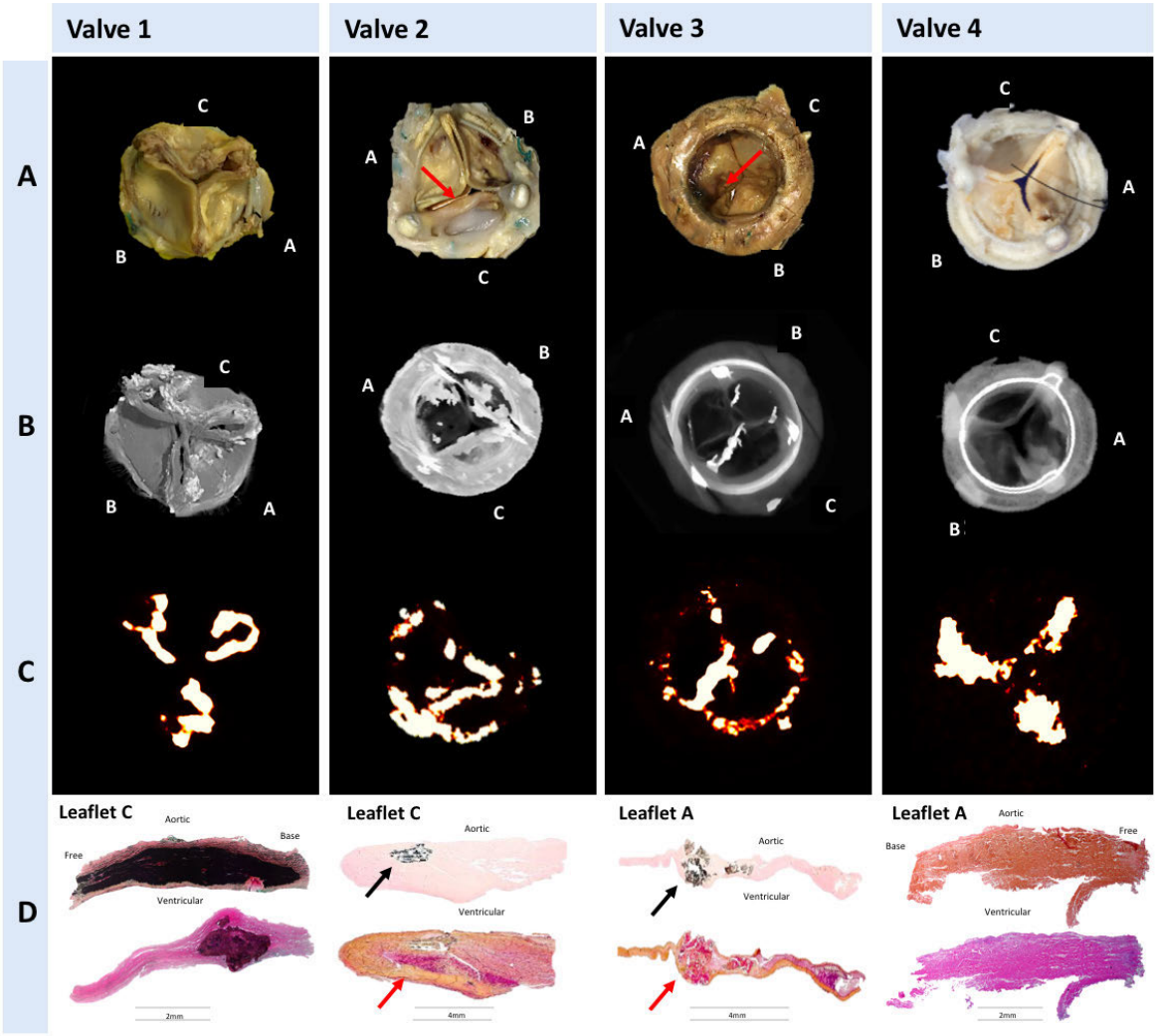

Figure 6.2. Row A. Macroscopic appearances of failed and explanted bioprosthetic valves. **Row B** Computed tomography *en face* images of the valves. **Row C** Positron emission tomography (PET) *en face* images demonstrating increased ^{18}F-fluoride uptake in all valves. **Row D.** Histology staining of sections taken from valve leaflet as indicated, with von Kossa (top row, calcium appears black), Movat Pentachrome

(bottom row valves 1 & 4) and haematoxylin & eosin (bottom row valves 2 & 3). All 4 bioprostheses demonstrate increased ^{18}F-fluoride uptake in the valve leaflets. In **Valve 1** this uptake corresponds to gross leaflet calcification observed macroscopically and on CT images with confirmation on histology (extensive black staining). In **Valve 2** increased ^{18}F-fluoride uptake is observed in association with fibrotic leaflet thickening and pannus (red arrows) with associated calcification (black arrows) observed macroscopically and on CT with confirmation on histology. In **Valve 3** increased ^{18}F-fluoride uptake is observed at the site of valve leaflet thrombus (red arrow) observed macroscopically at the base of leaflet 1, with confirmation of thrombus (red arrow) and co-localised calcification (black arrow) on histology. In **Valve 4** extensive ^{18}F-fluoride uptake is observed in the absence of calcification on CT and histology but instead in areas of leaflet thickening, marked fluid insudation and disrupted collagen architecture.

FIGURE 6.3.

CONSORT flow diagram of study recruitment, allocation, follow-up and analysis.

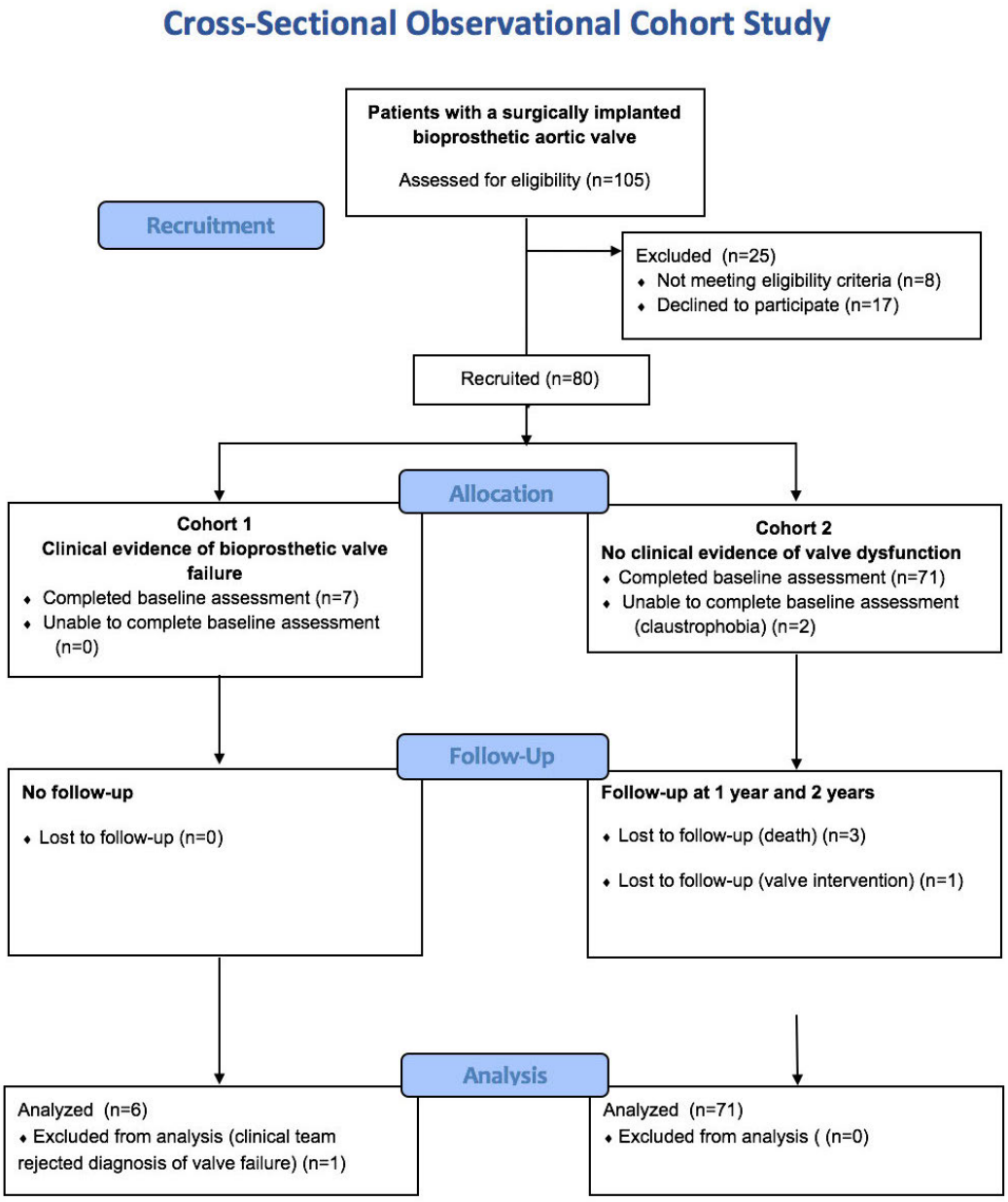

Figure 6.3. Flow diagram illustrating prospective study recruitment and allocation to pre-defined cross-sectional groups (Cohort 1: patients with suspected bioprosthetic valve failure, Cohort 2: patients under clinical review without evidence of valve

dysfunction or degeneration grouped by time from valve implantation), follow-up and analysis with 77 volunteers included in the final analysis.

TABLE 6.1.

Baseline characteristics of the clinical study population undergoing *in vivo* positron emission tomography and computed tomography imaging.

PATIENT CHARACTERISTICS						
	Patients with Valve Failure	Patients without known valve degeneration				
		ALL	1 MONTH	2 YEAR	5 YEAR	10 YEAR
CLINICAL						
Number of Subjects	6	71	9	22	20	20
Sex (% Female)	2 (33.3)	38 (46.5)	5 (55.6)	8 (36.4)	10 (50.0)	10 (50.0)
Mean Age (Years)	81.3 ± 3.2	73.9 ± 7.0	73.4 ± 9.0	73.0 ± 5.4	72.7 ± 5.1	76.4 ± 8.9
Body Mass Index (kg/m^2)	27.5 ± 4.5	26.9 ± 5.6	27.8 ± 4.7	27.7 ± 4.8	27.8 ± 5.1	24.8 ± 6.8
Systolic Blood Pressure (mmHg)	144.8 ± 18.0	153.8 ± 21.9	152.4 ± 21.2	149.8 ± 22.1	158.1 ± 15.2	154.5 ± 27.8
Diastolic Blood Pressure (mmHg)	58.0 ± 8.4	79.0 ± 11.0	82.0 ± 11.4	81.3 ± 12.0	78.6 ± 7.4	75.4 ± 12.6
Heart Rate (beats min^{-1})	72.2 ± 17.0	71.2 ± 11.8	79.8 ± 10.0	69.7 ± 11.6	73.3 ± 13.4	66.6 ± 8.9
MEDICAL HISTORY						
Hypertension	4 (66.7)	50 (70.4)	8 (88.9)	16 (72.7)	14 (70.0)	12 (60.0)
Coronary Artery Disease	4 (66.7)	29 (40.9)	5 (55.6)	7 (31.8)	6 (30.0)	11 (55.0)
Coronary Bypass Surgery	3 (50.0)	23 (32.4)	2 (22.2)	7 (31.8)	5 (25.0)	9 (45.0)
Diabetes	1 (16.7)	4 (5.6)	0 (0)	0 (0)	2 (10.0)	2 (10.0)
Hypercholesterolemia	5 (83.3)	55 (77.5)	8 (88.9)	18 (81.8)	13 (65.0)	16 (80.0)
Current Smoker	0 (0.0)	8 (11.4)	0 (0)	1 (4.6)	3 (15.0)	4 (20.0)
Ex-Smoker	3 (50.0)	29 (40.8)	4 (44.4)	10 (45.5)	7 (35.0)	8 (40.0)
MEDICATION						
Aspirin	4 (66.7)	51 (71.8)	7 (77.8)	18 (81.8)	12 (60.0)	14 (70.0)
Clopidogrel	1 (16.7)	9 (12.7)	1 (11.1)	2 (9.1)	4 (20.0)	2 (10.0)
Warfarin	2 (33.3)	4 (5.6)	0 (0.0)	1 (4.5)	3 (15.0)	0 (0.0)
Other Anticoagulant	0 (0.0)	2 (2.8)	0 (0.0)	0 (0.0)	1 (5.0)	1 (5.0)
ACEi or ARB	0 (0.0)	39 (54.9)	6 (66.7)	12 (54.5)	10 (50.0)	11 (55.0)

Beta Blocker	2 (33.3)	32 (45.1)	4 (44.4)	13 (59.1)	7 (35.0)	8 (40.0)
Statin	4 (66.7)	50 (70.4)	6 (66.7)	15 (68.2)	14 (70.0)	14 (70.0)
BIOCHEMISTRY						
Creatinine (umol/L)	102.2 ± 37.2	84.5 ± 23.4	90.3 ± 36.4	80.9 ± 17.8	89.1 ± 19.8	81.3 ± 25.4
eGFR (mL/min/1.73m^2)	48.5 ± 13.0	58 ± 7.5	53.4 ± 11.8	59.8 ± 3.2	57.1 ± 6.8	59.2 ± 8.5
ELECTROCARDIOGRAM						
Sinus rhythm	4 (66.7)	64 (91.4)	9 (100.0)	20 (95.2)	18 (90.0)	17 (85.0)
Paced Rhythm	0 (0.0)	4 (5.7)	0 (0.0)	0 (0.0)	1 (5.0)	3 (15.0)
Atrial Fibrillation	2 (33.3)	2 (2.9)	0 (0.0)	1 (4.8)	1 (5.0)	0 (0.0)
LV Hypertrophy	3 (50.0)	22 (32.4)	4 (44.4)	7 (33.3)	9 (45.0)	2 (11.1)
Strain Pattern	3 (50.0)	14 (20.6)	4 (44.4)	2 (9.5)	6 (30.0)	2 (11.1)
BASELINE ECHOCARDIOGRAPHY						
LV Systolic Dysfunction	4 (66.7)	11 (15.5)	1 (11.1)	3 (13.6)	4 (20.0)	3 (15.0)
Peak Valve Velocity (I)	3.19 [2.84-4.47]	2.73 [2.38-3.07]	2.44 [2.27-2.75]	2.68 [2.28-2.82]	2.93 [2.55-3.40]	2.85 [2.36-3.13]
Mean Valve Gradient (mmHg)	20.6 [14.03-39.50]]	15.0 [11.33-19.33]	13.00 [10.00-15.00]	13.87 [10.17-17.75]	18.5 [13.08-23.75]	17.17 [11.08-20.75]
Effective Orifice Area (cm^2)	0.52 [0.52-0.52]	1.13 [0.94-1.46]	1.33 [0.95-1.60]	1.14 [0.95-1.46]	1.03 [0.92-1.31]	1.20 [0.86-1.49]
Dimensionless Velocity Index	0.29 [0.20-0.42]	0.39 [0.33-0.44]	0.47 [0.38-0.51]	0.40 [0.36-0.43]	0.35 [0.31-0.40]	0.38 [0.31-0.46]
Prosthetic Regurgitation (≥ moderate)	5 (83.3)	2 (2.8)	0 (0.0)	0 (0.0)	0 (0.0)	2 (10.0)
Acceleration Time (ms)	*	80.3 [75.2-87.4]	87.0 [74.0-93.0]	80.0 [75.0-85.0]	79.0 [75.0-86.0]	85.0 [76.7-94.0]
Acceleration Time / LV Ejection Time	*	0.25 [0.24-0.28]	0.29 [0.25-0.31]	0.25 [0.24-0.27]	0.25 [0.23-0.27]	0.25 [0.22-0.28]
COMPUTED TOMOGRAPHY						
Abnormal Findings	6 (100.0)	14 (19.7)	0 (0.0)	3 (13.6)	4 (20.0)	7 (30.0)
Spotty Calcification	3 (50.0)	5 (7.0)	0 (0.0)	1 (4.5)	1 (5.0)	3 (15.0)
Large Calcification	3 (50.0)	0 (0.0)	0 (0.0)	0 (0.0)	0 (0.0)	0 (0.0)
Non-Calcific Leaflet Thickening	2 (33.3)	5 (7.0)	0 (0.0)	1 (4.5)	3 (15.0)	1 (5.0)
Pannus	1 (16.7)	7 (9.9)	0 (0.0)	2 (9.1)	0 (0.0)	5 (25.0)
^{18}F-FLUORIDE POSITRON EMISSION TOMOGRAPHY						
Cusp Uptake	6 (100.0)	24 (33.8)	1 (11.1)	6 (27.2)	8 (40.0)	9 (45.0)
SUV $_{MDS\ max}$	4.66 [3.16-7.57]	1.73 [1.42-2.02]	1.89 [1.42-1.99]	1.50 [1.31-1.80]	1.94 [1.39-2.26]	1.73 [1.54-2.34]

$SUV_{MDS\ mean}$	3.50 [2.64-5.90]	1.48 [1.27-1.84]	1.59 [1.29-1.82]	1.31 [1.14-1.57]	1.72 [1.21-2.05]	1.44 [1.32-2.04]
$TBR_{MDS\ max}$	3.61 [2.37-5.82]	1.31 [1.18-1.70]	1.26 [1.17-1.35]	1.26 [1.12-1.47]	1.52 [1.17-1.82]	1.47 [1.24-2.12]
$TBR_{MDS\ mean}$	2.91 [2.10-4.09]	1.12 [1.04-1.51]	1.07 [1.06-1.18]	1.11 [1.00-1.31]	1.38 [1.01-1.62]	1.15 [1.06-1.87]

Abbreviations: ACEi: angiotensin-converting enzyme inhibitor, ARB: angiotensin receptor blockade, eGFR: estimated glomerular filtration rate, LV: left ventricle, SUV: standardised uptake value, TBR: target-to-background ratio, MDS: most diseased segment.

TABLE 6.2.

The different types of bioprosthetic valve models in the clinical *in-vivo* cohorts.

MODEL OF BIOPROSTHETIC AORTIC VALVE						
	COHORT1	COHORT 2				
		TOTAL	1 MONTH	2 YEAR	5 YEAR	10 YEAR
St Jude Biocor (Porcine Stented)	0	1	0	0	0	1
Carpentier-Edwards (Porcine Stented)	1	8	0	0	3	5
Carpentier-Edwards Perimount (Pericardial Stented)	1	50	9	22	13	6
Medtronic Mosaic (Porcine Stented)	0	2	0	0	0	2
Aortech (Polymeric Stented)	0	1	0	0	0	1
Medtronic Hancock (Porcine Stented)	0	1	0	0	0	1
Vascutek Aspire (Porcine Stented)	0	3	0	0	0	3
Sorin Mitroflow (Pericardial Stented)	1	4	0	0	4	0
Edwards Prima (Porcine Stentless)	0	1	0	0	0	1
Vascutek Elan (Porcine Stentless)	1	0	0	0	0	0
St. Jude Toronto (Porcine Stentless)	1	0	0	0	0	0
Medtronic Freestyle (Porcine Stentless)	1	0	0	0	0	0

Table 6.2. The number of valves in each group (cohort 1: patients with degenerated and failing bioprosthetic valves; cohort 2: patients without previously established bioprosthetic valve degeneration) grouped according to duration of implantation.

TABLE 6.3.

Bioprosthetic valve model size in the clinical *in-vivo* cohorts

SIZE OF BIOPROSTHETIC AORTIC VALVE						
	19mm	**21mm**	**23mm**	**25mm**	**27mm**	**29mm**
St Jude Biocor (Porcine Stented)	0	0	1	0	0	0
Carpentier-Edwards (Porcine Stented)	1	0	5	2	0	1
Carpentier-Edwards Perimount (Stented Pericardial)	6	11	19	13	3	0
Medtronic Mosaic (Porcine Stented)	1	0	1	0	0	0
Aortech (Polymeric Stented)	0	0	0	0	1	0
Medtronic Hancock (Porcine Stented)	0	0	0	1	0	0
Vascutek Aspire (Porcine Stented)	0	1	1	0	1	0
Sorin Mitroflow (Pericardial Stented)	1	1	2	1	0	0
Edwards Prima Plus (Porcine Stentless)	0	1	0	0	0	0
Vascutek Elan (Porcine Stentless)	0	0	0	1	0	0
Medtronic Freestyle (Porcine Stentless)	0	0	0	1	0	0
Total	**9**	**14**	**29**	**19**	**5**	**1**

Table 6.3. The number of valves in each group (cohort 1: patients with degenerated and failing bioprosthetic valves;.cohort 2: patients without previously established bioprosthetic valve degeneration) grouped according to duration of implantation.

Patients Without Known Bioprosthetic Valve Dysfunction

In the 71 patients without known bioprosthetic valve dysfunction, surgical aortic valve replacement had been conducted 1 month (n=9), 2 years (n=22), 5 years (n=20), and >10 years (n=20) previously. The function of these different aged valves was generally within normal limits at baseline (peak velocity 2.76±0.52 ms-1, mean gradient 16.4±7.0 mmHg) (Table 6.1).

Contrast-enhanced CT images were not interpretable in 8 (11%) patients due to motion degradation and metallic blooming artefact from the valve struts. Fourteen (19%) subjects had 1 or more leaflet abnormalities on CT: spotty calcification (n=5), non-calcific leaflet thickening (n=5), and pannus (n=7) (Figure 6.4).

PET scans were interpretable in all patients. Increased ^{18}F-fluoride uptake was more common than abnormalities on CT and was seen in 24 (34%) patients (TBR 1.55 [1.44-1.88]; Figure 6.4). Similar to the ex-vivo findings increased ^{18}F-fluoride uptake co-localised with areas of spotty calcification, non-calcific leaflet thickening (suggestive of thrombus) and pannus observed on the CT, but was also observed remote from CT abnormalities (Figure 6.4).

FIGURE 6.4.

***In-vivo* ^{18}F-fluoride positron emission tomography and computed tomography imaging of patients with bioprosthetic aortic valves.**

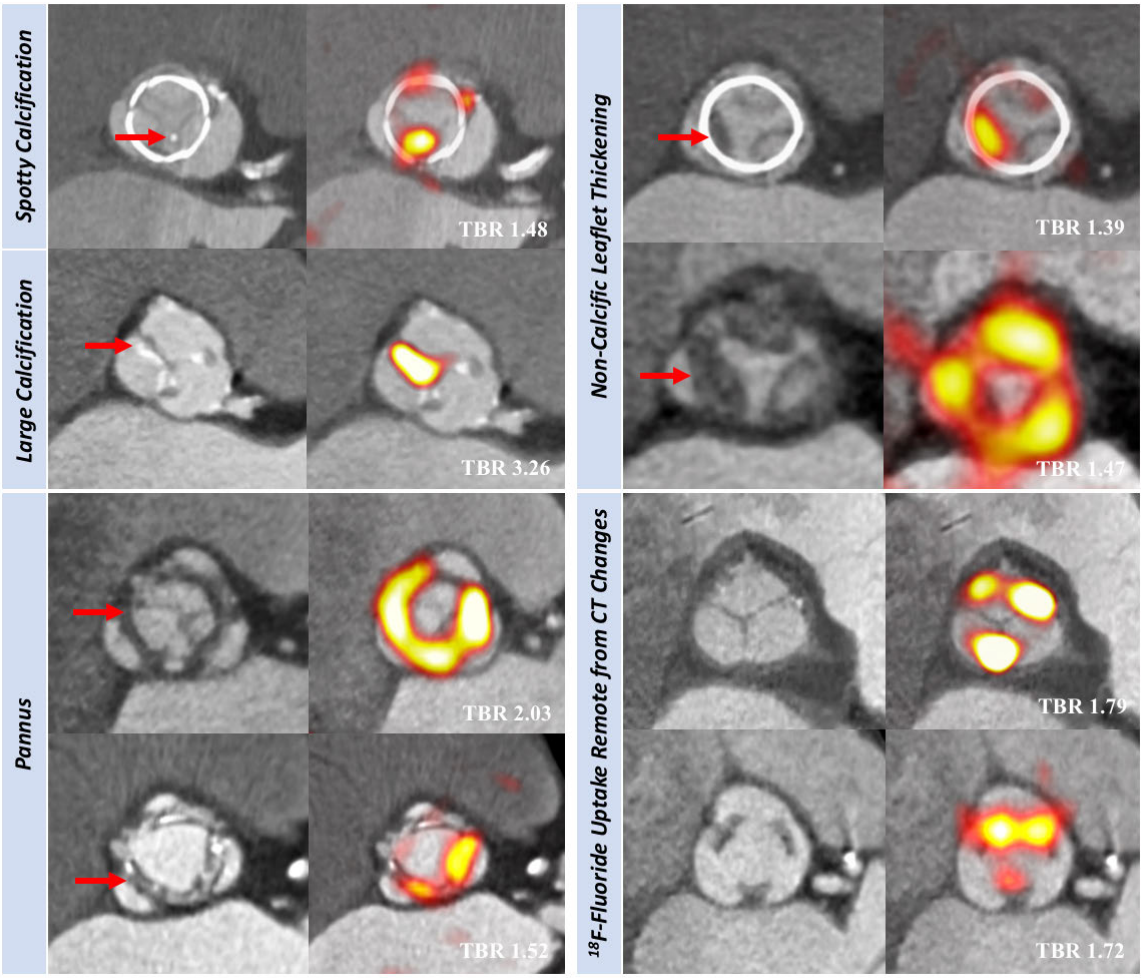

Figure 6.4. Baseline computed tomography (CT, left) and ^{18}F-fluoride positron emission tomography (PET, right) images from patients with bioprosthetic aortic valves. *En face* CT images of aortic bioprosthetic valves showing spotty calcification and large calcification (top left panel), circumferential pannus (bottom left panel) and non-calcific leaflet thickening (top right panel) (all abnormalities identified by red arrows). Hybrid *en face* PET/CT images in the same patients: increased bioprosthetic

^{18}F-fluoride activity (red/yellow areas) is observed in each patient co-localizing with the CT abnormalities. ^{18}F-fluoride activity was also commonly observed remote from leaflet changes on CT (bottom right panel). Target-to-background (TBR) values are annotated on the hybrid PET/CT images in white text.

Prediction of Bioprosthetic Valve Dysfunction

Sixty-seven of the patients without established valve degeneration at baseline underwent repeat echocardiography at 2 years and demonstrated increased peak velocities compared to baseline (2.87 [2.52-3.13] *versus* 2.73 [2.38-3.07] I, p=0.002). There was no association between hemodynamic progression and either the type or the age of the bioprosthesis (Table 6.4).

The 14 patients with abnormal CT findings appeared to demonstrate deterioration in bioprosthetic valve function after 2 years, but there was no statistical difference in disease progression compared to patients with a normal CT (change in peak velocity: 0.25 [-0.06 to 0.57] *versus* 0.10 [-0.04 to 0.31] I, p=0.232).

By contrast the 24 patients with increased ^{18}F-fluoride uptake at baseline demonstrated clear evidence of deteriorating bioprosthesis function after 2 years, whilst patients without uptake displayed no change in valve function (change in peak velocity: 0.30 [0.13 to 0.61] *versus* 0.01 [-0.05 to 0.16] I/year, p<0.001). Similarly, patients in the highest tertile of ^{18}F-fluoride uptake demonstrated greater disease progression than patients in the lower 2 tertiles (annualised change in valve peak velocity; tertile 1: 0.14 [0.05 to 0.30] *versus* tertiles 2 and 3: 0.01 [-0.02 to 0.10] I/year, p=0.006; Figure 6.5). The 4 patients with new or worsening prosthetic valve regurgitation during follow-up were amongst those in tertile 1. Moreover, bbaseline ^{18}F-fluoride uptake correlated strongly with echocardiographic measures of hemodynamic progression regardless of the method used to quantify ^{18}F-fluoride uptake (Table 6.4).

TABLE 6.4.

Factors associated with deterioration in bioprosthetic valve function (annualised change in peak velocity after 2 years): univariable analysis

UNIVARIABLE ANALYSIS OF PREDICTORS OF PROGRESSION IN PEAK VELOCITY				
	Unstandardised Coefficient (95% CI)	**Standard Error**	**Standardised Coefficient**	**Significance**
Sex	0·056 (-0·042 to 0·154)	0·049	0·138	0·256
Age	0·001 (-0·006 to 0·008)	0·004	0·039	0·752
BMI	-0·003 (-0·014 to 0·008)	0·005	-0·069	0·569
BSA	-0·096 (-0·308 to 0·115)	0·106	-0·110	0·366
Valve Age	0·003 (-0·010 to 0·016)	0·007	0·050	0·683
Valve Type	-0·011 (-0·045 to 0·024)	0·017	-0·075	0·539
Systolic BP	0·001 (-0·001 to 0·003)	0·001	0·125	0·301
Hypertension	-0·073 (-0·178 to 0·032)	0·052	-0·167	0·168
Diabetes	-0·016 (-0·207 to 0·175)	0·096	-0·020	0·867
Dyslipidaemia	-0·004 (-0·121 to 0·113)	0·059	-0·009	0·944
Smoking	0·153 (0·002 to 0·303)	0·075	0·239	**0·047***
Anticoagulation	-0·119 (-0·329 to 0·091)	0·105	-0·136	0·263
ACEi or ARB	-0·024 (-0·123 to 0·074)	0·049	-0·060	0·625
Statin	-0·028	0·054	-0·063	0·604

	(-0·135 to 0·079)			
Baseline Peak Velocity	0·001 (-0·095 to 0·098)	0·048	0·003	0·978
Abnormal CT	0·102 (-0·020 to 0·223)	0·061	0·200	0·099
Calcification on CT	0·047 (-0·129 to 0·222)	0·088	0·064	0·597
NCLT on CT	0·142 (-0·046 to 0·330)	0·094	0·179	0·137
Pannus on CT	0·068 (-0·095 to 0·231)	0·082	0·100	0·409
^{18}F-Fluoride Uptake (categorical)	0·184 (0·090 to 0·278)	0·047	0·429	**<0·001***
PET SUV $_{MDS\ mean}$	0·383 (0·253 to 0·514)	0·065	0·579	**<0·001***
PET SUV $_{MDS\ max}$	0·404 (0·280 to 0·527)	0·062	0·620	**<0·001***
PET TBR $_{MDS\ mean}$	0·499 (0·383 to 0·615)	0·058	0·720	**<0·001***
PET TBR $_{MDS\ max}$	0·466 (0·357 to 0·575)	0·055	0·718	**<0·001***

Abbreviations: ACEi: angiotensin-converting enzyme inhibitor, ARB: angiotensin receptor blockade, MDS: most diseased segment, PET: positron emission tomography, SUV: standardised uptake value, TBR: target to background ratio.

FIGURE 6.5.

Tertile analysis according to ^{18}F-fluoride PET uptake demonstrating tissue-to-background (TBR) values across the tertiles and relationship with change in valve function during follow-up.

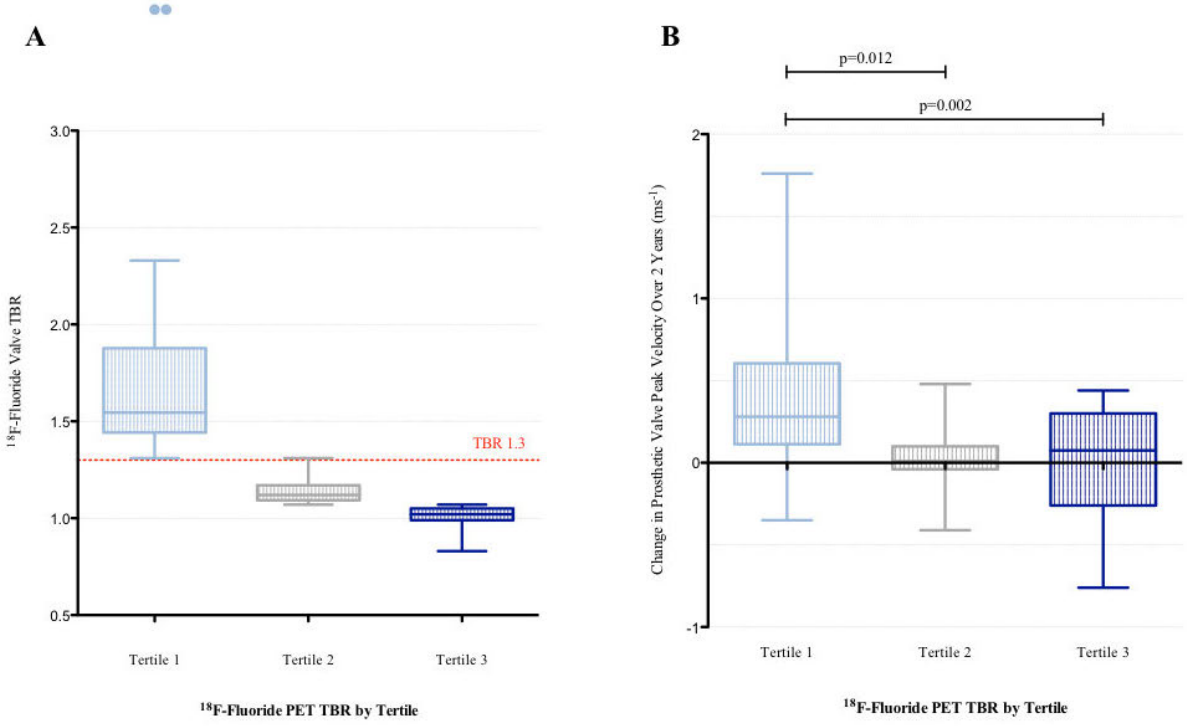

Figure 6.5. A. Box-plot illustrating the spread of ^{18}F-fluoride tissue-to-background (TBR) values when grouped into tertiles. Dashed red line represents TBR 1.3 which was the cut off for the top tertile and also the threshold for discriminating increased uptake. **B**. Box-plot demonstrating haemodynamic progression (measured by the change in peak valve velocity between baseline and 2-year follow-up) when patients were grouped by tertile according to ^{18}F-fluoride TBR values. Patients in tertile 1 (TBR >1.3) exhibited more rapid haemodynamic progression than those in the lower tertiles. The 4 patients with new or worsening prosthetic valve regurgitation during follow-up were also all amongst those in tertile 1.

Based upon international guideline criteria, 10 patients developed new bioprosthetic valve dysfunction during follow-up 2 with valve regurgitation, 6 with valve stenosis and 2 with mixed dysfunction (Lancellotti P *et al*, 2016; Zoghbi WA *et al*, 2009). Median time from valve implantation to their assessment in the study was 7.5 [5-10] years. Of these patients, 5 had an abnormal baseline CT while all 10 patients had increased ^{18}F-fluoride uptake (TBR 1.89 [1.46-2.59]) and this included the 7 patients with the highest TBR values in the cohort. Two proceeded to urgent valve re-intervention and another died of valve failure. Using the alternative criteria suggested by the recent international consensus statement (Dvir D *et al*, 2018), 16 patients met the definition of structural valve degeneration, 15 of whom demonstrated increased ^{18}F-fluoride uptake (TBR 1.54 [1.38-1.96] *versus* 1.08 [1.02-1.19], $p<0.001$). Seven patients fulfilled criteria for stage 2 or 3 structural valve degeneration, signifying the development of valve dysfunction, and they all exhibited increased baseline ^{18}F-fluoride uptake (TBR 1.89 [1.47-3.15]; Figure 6.6). Moreover ^{18}F-fluoride activity increased in a step-wise fashion across these progressive stages of structural degeneration (TBR; no degeneration: 1.08 [1.02-1.19], stage 1: 1.48 [1.34-1.64], stage 2: 1.72 [1.42-1.94], stage 3: 4.23 [3.15-5.36], post-hoc linear trend: $p<0.001$; Figure 6.6). Two patients developed overt bioprosthetic valve failure during 2-year follow-up and a further 2 patients developed valve failure on subsequent follow-up, all demonstrating high intensity ^{18}F-fluoride uptake (TBR 2.57 [1.96-3.70]) (Figure 6.7) (Capodanno D *et al*, 2017).

On univariable analysis, the only predictors of deterioration in bioprosthetic valve function (annualised change in bioprosthetic valve peak velocity) were current

smoking habit (p=0.047) and ^{18}F-fluoride PET uptake, irrespective of whether the latter was considered as a categorical or continuous variable (both p<0.001) (Table 4). On multivariable analysis incorporating age, sex, duration of valve implantation, baseline peak prosthetic valve velocity and CT findings, ^{18}F-fluoride uptake emerged as the only predictor of deterioration in bioprosthetic valve function (unstandardised coefficient 0.79 (95% CI 0.62-0.96), p<0.001; Figure 6.6 and Table 6.5).

Irrespective of the definition used, similar results were observed when the development of bioprosthetic valve dysfunction was considered as a categorical, with baseline ^{18}F-fluoride uptake emerging each time as an independent predictor on multivariable analyses (international guideline criteria: unstandardised coefficient 7.57 [standard error 2.66], p=0.004; expert consensus statement: unstandardised coefficient 6.81 [standard error 2.92], p=0.02; Table 6.6A and 6.6B) (Lancellotti P *et al*, 2016; Zoghbi WA *et al*, 2009; Dvir D *et al*, 2018). Summary of effective radiation doses shown in Table 6.7.

FIGURE 6.6.

Baseline ^{18}F-fluoride positron emission tomography uptake predicts subsequent deterioration in bioprosthetic valve function after 2 years.

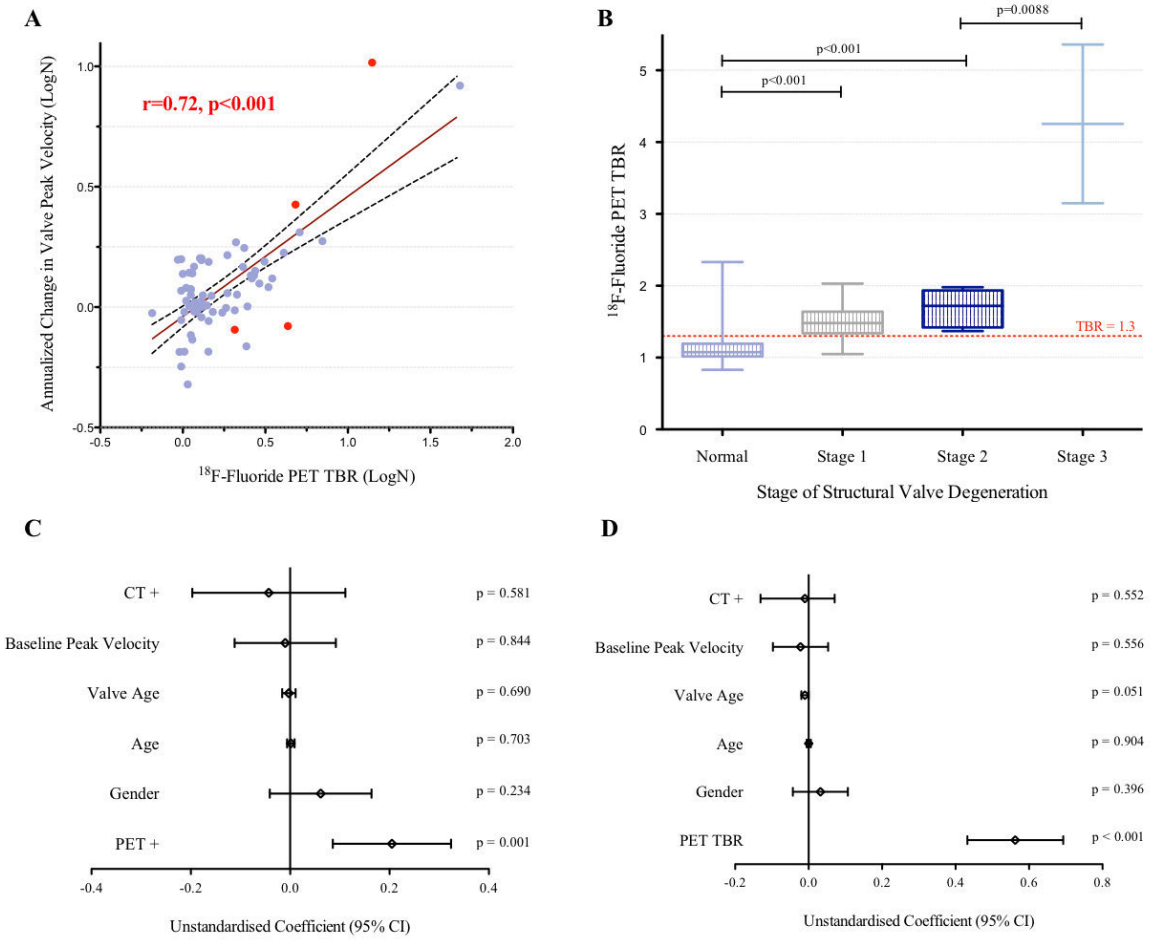

Figure 6.6. A. A strong correlation was observed between baseline ^{18}F-fluoride uptake in the bioprosthetic valves (target-to-background ratio; TBR) and subsequent progression in prosthetic valve peak velocity (log transformation applied; r=0.72, p<0.001). Red dots signify patients who developed new prosthetic valve regurgitation during follow up. **B**. ^{18}F-Fluoride uptake (perforated red line represents threshold for increased ^{18}F-fluoride uptake; TBR 1.3) in patients with different stages of structural

valve degeneration (normal: no structural or functional valve changes; stage 1 structural degeneration with morphological abnormalities but no changes in haemodynamic function; stage 2 deterioration in valve function; stage 3 rapid deterioration in valve function[19]) demonstrating incrementally higher uptake values with increasing severity of structural valve degeneration.

C & D. Forest plots of unstandardised coefficients (95% confidence intervals) from a multivariable linear regression analysis predicting change in bioprosthetic valve function (annualised change in peak velocity) during follow-up. When examining all relevant baseline characteristics, ^{18}F-Fluoride uptake was the only independent predictor of haemodynamic deterioration in valve function when used both as a dichotomous variable (PET+, TBR >1.3) I and as a continuous variable (TBR) (D).

FIGURE 6.7.

Case illustrations: baseline ^{18}F-fluoride positron emission tomography and computed tomography predict imminent failure of bioprosthetic function.

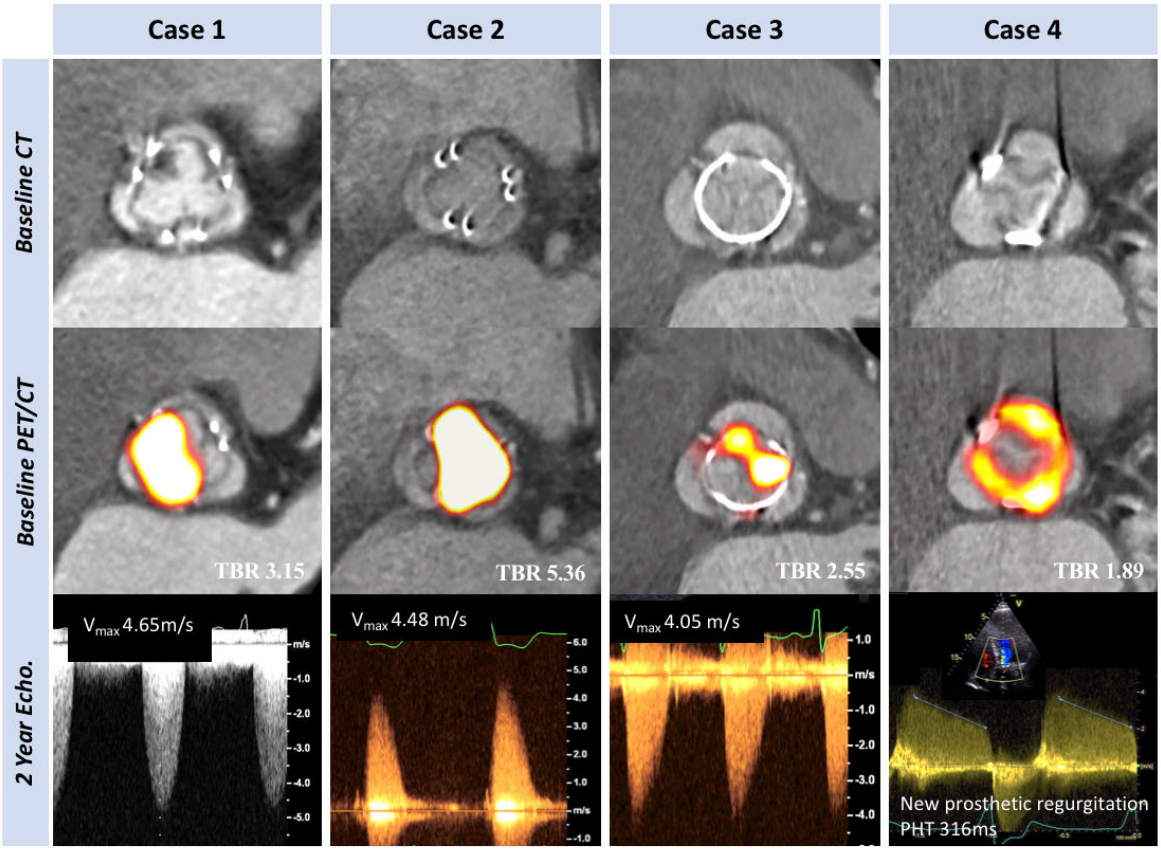

Figure 6.7. Cases 1-4 illustrate the utility of ^{18}F-fluoride positron emission tomography (PET) and computed tomography (CT) in the prediction of deteriorating valve performance. None of the patients had known bioprosthetic degeneration at baseline. *En face* contrast-enhanced CT images (**top row**) demonstrate non-calcific leaflet thickening in case 1, but no clear structural CT changes in the remaining cases. Hybrid ^{18}F-fluoride PET-CT images (**middle row**) demonstrate high intensity ^{18}F-fluoride activity in all the valves (TBR values in white italics). Doppler echocardiographic assessments of bioprosthetic valve function after follow-up

(**bottom row**). In each case new valve dysfunction has developed with progression to severe obstruction in cases 1, 2 & 3 and new moderate/severe eccentric regurgitation in case 4 (pressure half time 316 ms with holodiastolic flow reversal in aorta). Patient 1 died from valve related heart failure, patient 2 required redo-surgical valve replacement and patients 3 and 4 are undergoing work up for redo-surgery.

TABLE 6.5.

A. Factors associated with deterioration in bioprosthetic valve function (annualised change in peak velocity after 2 years): multivariable analysis using ^{18}F-fluoride PET as a continuous variable quantified by TBR.

MULTIVARIABLE LINEAR REGRESSION MODEL 1: PREDICTORS OF ANNUALISED CHANGE IN PEAK TRANSVALVULAR VELOCITY (PET AS CONTINUOUS VARIABLE)				
SUMMARY: p <0·001	**R = 0·753**	**R Square 0·567**		**Std· Error 0·142**
Variable	**Unstandardised Coefficient (95% CI)**	**Standard Error**	**Standardised Coefficient**	**Significance**
Age	0·000 (-0·005-0·006)	0·003	0·011	0·904
Sex	0·032 (-0·043-0·107)	0·038	0·079	0·396
Valve Age	-0·010 (-0·020-0·000)	0·005	-0·187	0·051
Baseline Peak Velocity	-0·022 (-0·097-0·053)	0·037	-0·055	0·556
Abnormal CT	0·030 (-0·131-0·071)	0·050	-0·059	0·552
PET TBR	0·562 (0·432-0·693)	0·065	0·801	**<0·001***

Abbreviations: CT: computed tomography, PET: positron emission tomography, TBR: target to background ratio.

B. Factors associated with deterioration in bioprosthetic valve function (annualised change in peak velocity after 2 years): multivariable analysis using ^{18}F-fluoride PET as a dichotomous variable (either normal or abnormal).

MULTIVARIABLE LINEAR REGRESSION MODEL 2: PREDICTORS OF ANNUALISED CHANGE IN PEAK TRANSVALVULAR VELOCITY (PET AS CATEGORICAL VARIABLE)				
SUMMARY: p = 0·023	**R = 0·453**	**R Square 0·205**		**Std· Error 0·192**
Variable	**Unstandardised Coefficient (95% CI)**	**Standard Error**	**Standardised Coefficient**	**Significance**
Age	0·001 (-0·006-0·009)	0·004	0·047	0·703
Sex	0·062 (-0·041-0·164)	0·051	0·15	0·234
Valve Age	-0·003 (-0·016-0·011)	0·007	-0·050	0·690
Baseline Peak Velocity	-0·010 (-0·112-0·092)	0·051	-0·025	0·844
Abnormal CT	-0·043 (-0·197-0·111)	0·077	-0·084	0·581
Abnormal PET	0·205 (0·086-0·324)	0·059	0·477	**0·001***

Abbreviations: CT: computed tomography, PET: positron emission tomography, TBR: target to background ratio.

TABLE 6.6 A.

Factors associated with the development of bioprosthetic valve dysfunction as a dichotomous variable according to expert consensus statement (Dvir D *et al*, 2018): binary logistic regression using ^{18}F-fluoride PET as a continuous variable quantified by TBR.

BINARY LOGISTIC REGRESSION: PREDICTORS OF NEW STRUCURAL VALVE DEGENERATION (PET AS CONTINUOUS VARIABLE)				
Variable	**Unstandardised Coefficient**	**Standard Error**	**Odds Ratio (95% CI)**	**Significance**
Age	0.189	0.128	1.21 (0.94-1.56)	0.140
Sex	0.956	1.574	2.60 (0.12-56.90)	0.544
Valve Age	-0.263	0.283	0.77 (0.44-1.34)	0.353
Baseline Peak Velocity	5.138	2.435	170.33 (1.44-20131.76)	**0.035***
Abnormal CT	0.663	1.551	1.94 (0.09-40.58)	0.669
PET TBR	6.814	2.924	910.52 (2.952-280843.31)	**0.020***

Abbreviations: CT: computed tomography, PET: positron emission tomography, TBR: target to background ratio.

TABLE 6.6 B.

Factors associated with the development of bioprosthetic valve dysfunction as a dichotomous variable according to echocardiography guidelines (1,2): binary logistic regression using ^{18}F-fluoride PET as a continuous variable quantified by TBR.

BINARY LOGISTIC REGRESSION: PREDICTORS OF NEW STRUCURAL VALVE DEGENERATION (PET AS CONTINUOUS VARIABLE)				
Variable	**Unstandardised Coefficient**	**Standard Error**	**Odds Ratio (95% CI)**	**Significance**
Age	-0.043	0.108	0.958 (0.775-1.183)	0.689
Sex	-0.936	1.321	0.392 (0.029-5.221)	0.479
Valve Age	-0.105	0.229	0.901 (0.575-1.411)	0.648
Baseline Peak Velocity	3.387	1.652	29.567 (1.159-754.013)	**0.040***
Abnormal CT	-0.669	1.511	0.512 (0.026-9.908)	0.658
PET TBR	7.572	2.662	1942.81 (10.53-358307.91)	**0.004***

TABLE 6.7.

Summary statistics of effective radiation dose for baseline PET-CT using up-to-date PET effective dose conversion factor 0.028 $mSv \cdot mGy^{-1}cm^{-1}$ (9)

TOTAL RADIATION DOSES						
	Number of subjects	**Mean PET effective dose (mSv)**	**Mean CT effective dose (mSv)**	**Mean total effective dose (mSv)**	**Median total effective dose (mSv)**	**Expected effective dose (mSv)**
Cohort 1	7	2.1	20.9	23.0	16.6	19.15
Cohort 2	71	2.2	13.4	15.6	13.9	19.15
All Subjects	78	2.1	14.2	16.4	14.2	19.15

Abbreviations: CT: computed tomography, PET: positron emission tomography.

6.5 DISCUSSION

In this multi-modality prospective imaging study, we have identified ^{18}F-fluoride PET-CT as the first non-invasive technique capable of detecting early bioprosthetic valve degeneration and predicting future valve dysfunction. We provide extensive validation of the technique against state-of-the-art *ex vivo* imaging and histology. This consistently demonstrated increased ^{18}F-fluoride uptake in each of the failed bioprosthetic aortic valves examined, with PET activity co-localising to areas of calcification, pannus, thrombus and disrupted tissue architecture on histology. When applied to patients in the clinical setting, ^{18}F-fluoride PET identified early valve degeneration beyond the resolution of conventional assessments and predicted the development of new valvular dysfunction and overt valve failure within the 2-year follow-up period. Indeed, ^{18}F-fluoride uptake was an independent predictor of deteriorating bioprosthetic valve performance, outperforming all other variables including valve type and age, echocardiographic and CT findings. ^{18}F-Fluoride PET-CT therefore provides a readily applicable measure of valve degeneration with the potential to transform how we monitor and treat the expanding population of patients living with bioprosthetic valves.

Our study has several major strengths. This is a comprehensive multimodal imaging study using ultrasound, CT and PET in patients with bioprosthetic aortic valves of varying implant ages. Uniquely, we have been able to correlate imaging findings with state-of-the-art *ex vivo* imaging and histological characterization of explanted valves, enabling us to validate our imaging technique and provide novel insights into the

pathogenesis of bioprosthetic valve degeneration. Moreover, our systematic prospective study design has allowed us to confirm the utility of baseline ^{18}F-fluoride PET in identifying patients at risk of developing future bioprosthetic dysfunction and overt valve failure.

A Clinical Challenge

Whilst bioprosthetic valves offer important advantages over mechanical valves, they have only limited durability (Forountan F *et al*, 2016; Bloomfield P *et al*, 1991). Indeed, bioprosthetic valve degeneration has become a major clinical issue with the growing rate of bioprosthetic valve implantation and improved long-term patient survival. Although international guidelines recommend serial echocardiography for the detection of bioprosthetic degeneration, visualization of the valve is often poor due to acoustic artefacts from the prosthesis, limiting its sensitivity (Lancellotti P *et al*, 2016; Zoghbi WA *et al*, 2009). This means that valve degeneration is frequently well advanced before clinically overt valve dysfunction is apparent. Moreover, valve obstruction often evolves rapidly, whilst the catastrophic development of valvular regurgitation due to leaflet tears is frequently unheralded and unpredictable. Novel techniques capable of detecting the earlier stages of valve degeneration and allowing personalised and better planned management strategies for patients with bioprosthetic valves are therefore highly desirable.

Insights into the Mechanism of Bioprosthetic Valve Degeneration

We and others have used ^{18}F-fluoride PET to assess cardiovascular calcification activity and tissue degeneration in a range of conditions including coronary heart

disease, stroke, abdominal aortic aneurysms and aortic stenosis (Dweck MR *et al*, 2012 A; Forsythe RO *et al*, 2018; Joshi NV *et al*, 2014; Vesey AT *et al*, 2017). We now extend these observations to bioprosthetic valves and confirm that ^{18}F-fluoride localises to regions of developing leaflet calcification on histology and high-resolution micro-PET-CT imaging. Calcification is believed to be the final common response to bioprosthetic valve injury and a major driver towards valve dysfunction, causing both progressive cusp stiffness and obstruction as well as leaflet fragility and tears. In this study, all bioprosthetic valves with established degeneration and valve failure demonstrated increased ^{18}F-fluoride uptake. Moreover, in both our *ex vivo* and *in vivo* studies, we observed a close spatial interaction of calcification with both leaflet thrombosis and pannus, suggesting these may be potential upstream triggers. In contrast, a minority of bioprosthetic valves appear to degenerate without any histological evidence of calcification. In these cases, the remarkable histological features were gross leaflet thickening, fluid insudation and disruption of normal collagen architecture. Interestingly, these valves also exhibited high levels of ^{18}F-fluoride uptake. We hypothesise that upregulation of matrix metalloproteinases may be implicated in the degradation of bioprosthetic leaflet tissue and that these proteins have the potential to bind ^{18}F-fluoride (Simionescu A *et al*, 1996 A; Kato MT *et al*, 2014). Further investigation of the mechanism of uptake is required.

Recent reports have described focal non-calcific leaflet thickening as a marker of thrombus formation (Makkar RR *et al*, 2015; Chakravarty T *et al*, 2017). Whilst these areas can cause acute valve obstruction, more commonly they do not result in any immediate hemodynamic disturbance, leading some to question their clinical

relevance. In our study, we also observed low-attenuation non-calcific leaflet thickening on CT suggestive of non-obstructive thrombus, that was associated with both increased ^{18}F-fluoride activity and delayed deterioration in valve performance over the following 2 years. Similar findings were observed in explanted valves where areas of thrombus co-localised with calcium on Von Kossa staining and exhibited increased ^{18}F-fluoride PET activity. This raises the hypothesis that bioprosthetic valve thrombosis may act as one potential trigger to valve degeneration that might be prevented with prompt detection and anticoagulation. Interestingly, recent observational data have suggested that bioprosthetic durability may be enhanced by concomitant anticoagulation therapy (Del Trigo M *et al*, 2018).

Clinical Implications

Our findings have several major implications for clinical practice. Firstly, in addition to micro and macrocalcification, ^{18}F-fluoride PET-CT can identify a range of degenerative processes including fibrosis, thrombosis and leaflet degradation with disrupted collagen architecture and fluid insudation. This has provided important insights into the pathogenesis of bioprosthetic valve failure and highlights potential targets for novel therapies aimed at improving valve durability. Secondly, ^{18}F-fluoride PET can detect and quantify the early stages of valvular degeneration and identify patients otherwise thought to have normal valves but who are in fact at high-risk of subsequent valve failure. Given the high mortality associated with emergency repeat valve replacement (Vogt PR *et al*, 2000), these patients are likely to benefit from both close tailored surveillance and early elective intervention before the onset of abrupt valve failure. Conversely patients without PET uptake, who here demonstrated very

stable valve function during follow-up, could undergo less intensive surveillance. Our data suggests that 5 years post-implantation may be an appropriate stage at which to offer a PET-CT and guide follow-up, with further studies needed. Third, ^{18}F-fluoride PET-CT appears of value in determining the presence of valvular degeneration in cases where the diagnosis and clinical management is uncertain, for example in patients with suspected patient-prosthesis mismatch. Finally, ^{18}F-fluoride PET-CT provides a readily applicable measure of valve durability that may prove useful in assessing novel prosthetic designs such as transcatheter valves before these are extended into younger and healthier patient populations.

Limitations

It was initially envisaged that serial CT calcium scoring of bioprosthetic aortic valves would also provide a marker of valve degeneration. However, in our hands we observed major artefact related to motion and the stent struts that precluded detailed analysis of CT calcium scores. Leaflet pathology was instead more successfully identified by contrast-enhanced CT, where superior anatomical detail allowed differentiation between pannus ingrowth, thrombosis or calcification, although a minority of scans still could not be accurately adjudicated. Alongside the robust information provided by ^{18}F-fluoride PET this is an important advantage of the hybrid PET/CT technique.

Although our study population is relatively large compared to other cardiovascular PET studies, external validation in a larger study population with longer follow-up would be welcome. Future studies may wish to investigate ^{18}F-fluoride activity in

novel bioprostheses, in particular aortic and mitral transcatheter valves, as well as assessing whether the bioprosthetic ^{18}F-fluoride signal is modifiable with adjuvant therapies, such as anticoagulation in patients with associated thrombus or drugs that modify calcium metabolism (e.g. bisphosphonates, denosumab).

Conclusions

In conclusion, ^{18}F-fluoride PET-CT detects early bioprosthetic valve degeneration, providing powerful prediction of subsequent deterioration in valve performance and highlighting patients at imminent risk of valve failure. This novel imaging approach has the potential to transform our understanding of bioprosthetic valve failure and the way in which we monitor and treat patients with bioprosthetic valves.

CHAPTER 7

CONCLUSIONS AND FUTURE DIRECTIONS

7.1 SUMMARY OF FINDINGS

Prior to manifesting at an advanced stage, valvular heart disease has often been asymptomatic and undetected over a prolonged period. The early pathophysiological processes are not well understood and, accordingly, we lack effective therapies to reduce or reverse disease progression until surgery or transcatheter intervention is indicated for symptomatic severe valve disease. The chronicity of degenerative valve disease, with slow subclinical progression over many years, poses a significant challenge for the detection and understanding of early disease (when treatment targets may be most readily modified), and for ascertaining the short and longterm treatment effects of medical therapies. Clinical trials of novel therapies therefore require large numbers of patients subject to prolonged follow-up at considerable expense.

CT and PET respectively offer high resolution anatomical detail and real-time quantification of biological processes *in vivo*. There has consequently been growing interest in these modalities for the assessment of cardiovascular disease. In this thesis, we investigate novel approaches to cardiac CT and PET to illuminate our understanding of disease mechanisms and improve diagnostic accuracy in both native aortic valve stenosis and bioprosthetic valve degeneration. We also propose hybrid ^{18}F-fluoride PET/CT as a method of assessing disease activity in both of these conditions, that may provide an early marker of therapeutic response in future studies.

Our comprehensive multimodality imaging approach combined echocardiography, cardiac CT and PET, and results were validated with *ex vivo* imaging and

histopathology. From our investigations, we conclude that contrast-enhanced CT angiography can be used to quantify non-calcific leaflet thickening as a surrogate of fibrosis in aortic stenosis, that fibrosis is an important pathological feature, and that the combined fibrocalcific burden holds promise as a tool to improve diagnostic accuracy (chapter 3). Furthermore, we demonstrate that ^{18}F-fluoride PET/CT is an accurate and reproducible technique for the quantification and localisation of calcification activity in aortic stenosis (chapter 4). Finally, we use *ex vivo* ^{18}F-fluoride PET/CT and histology to elucidate the importance of calcification as a common final pathway in bioprosthetic valve degeneration (chapter 5), then show that ^{18}F-fluoride PET/CT can be used in patients with bioprosthetic aortic valves to detect early valve degeneration, predict the development of valve dysfunction and identify those at risk of early valve failure (chapter 6).

7.2 CT angiography detects calcification and fibrosis of the aortic valve and provide insights into the contribution of fibrosis and calcification in the pathogenesis of aortic stenosis.

International guidelines recommend non-contrast CT calcium scoring of the aortic valve (CT-AVC) as an additional method of assessing aortic stenosis severity when echocardiographic measurements are discordant (Baumgartner H *et al*, 2015). However, CT-AVC offers limited detail about valve morphology and the anatomical distribution of calcium in the valve and surrounding structures. Moreover, it demonstrates only moderate associations with hemodynamic severity by echocardiography and women consistently demonstrate lower calcium burden for a given degree of valvular stenosis. CT-AVC is unable to account for valve fibrosis, an important contributor to valve stenosis, and may therefore misclassify disease severity, particularly in young women and those with bicuspid aortic valves (Shen M *et al*, 2016; Simard L *et al*, 2016).

In this thesis, we developed a novel approach to CT angiography that allows assessment of both valve calcification and non-calcific leaflet thickening (a surrogate for valve fibrosis) in patients with aortic stenosis. In total, 143 volunteers with varying degrees of aortic stenosis underwent echocardiography, CT-AVC and CT angiography as part of a randomised controlled trial. CT angiography was able to quantify valve non-calcific and calcific leaflet volumes with excellent inter-observer reproducibility, and we demonstrated that non-calcific leaflet volumes in the aortic stenosis cohort were more than double those in a sex-matched control group. Our innovative technique

provided unique insights into the pathophysiology of aortic stenosis, with fibrosis appearing to predominate in women and patients with mild stenosis, whilst calcification dominated in men and those with severe stenosis. Moreover, we proposed a novel anatomical measure of aortic stenosis severity, the fibro-calcific burden, that incorporated both fibrotic and calcific valve thickening. This summary measure demonstrated excellent agreement with echocardiographic assessments of hemodynamic disease severity and *ex vivo* valve weight that were superior to CT-AVC alone. We were able to reproduce similar findings in an independent external cohort and were also able to validate imaging markers of valve fibrosis with tissue histology from explanted valves.

By way of limitations, the technique was relatively time consuming and became less accurate at the upper and lower extremes of blood pool contrast attenuation. Furthermore, the limited proportion of women (~20%) in the study population necessitates that further investigation be performed in a larger cohort.

In conclusion, CT angiography allowed robust and reproducible quantification of both valve leaflet fibrosis and calcification in patients with aortic stenosis. Our observations indicate that the factors driving aortic stenosis progression both evolve with time and are different in men and women. Moreover, the fibro-calcific burden provides a novel assessment of aortic stenosis severity potentially offering closer agreement with echocardiographic assessments than CT-AVC. Further work is now required to validate the fibro-calcific burden, and to establish both diagnostic thresholds for severity and its prognostic value. CT angiography is already widely performed in many

centres and may, in future, provide a valuable tool to confirm aortic stenosis severity in patients with discordant echocardiographic measurements or low-flow states.

7.3 ^{18}F-Fluoride PET/CT can be established as an accurate and reproducible technique to assess disease activity in aortic stenosis.

In this thesis, we continued our investigation of non-invasive imaging methods in the assessment of native aortic valve stenosis. ^{18}F-Fluoride binds preferentially to regions of newly developing microcalcification, and ^{18}F-fluoride PET/CT has been shown to measure disease activity and predict progression in aortic stenosis (Jenkins WSA *et al*, 2015). Here we studied the acquisition and analysis of ^{18}F-fluoride PET/CT.

A total of 15 volunteers with varying degrees of aortic stenosis underwent CT aortic valve calcium scoring, CT angiography and ^{18}F-fluoride PET on two separate occasions, no more than 3 months apart. Prior investigations of PET/CT had been performed using non-contrast CT and PET without ECG gating. We first improved the spatial localisation of tracer uptake by using contrast-enhanced CT imaging and ECG-gated PET data, such that activity could be localised to regions within individual leaflets. This demonstrated that calcification activity is most commonly observed at sites of high mechanical stress, for example, at the valve commissures and regions of leaflet coaptation.

Second, we improved the scan-rescan reproducibility of aortic valve ^{18}F-fluoride PET/CT, achieving excellent agreement statistics for measurement of the $TBR_{MDSmean}$. This was accomplished by sampling and correcting for background blood pool activity in the right atrium, rather than the brachiocephalic vein as had been done in previous investigations, where measurements were less susceptible to error from partial

voluming effect and inaccuracies in PET/CT co-registration. Another improvement was achieved by using the most diseased segment (MDS) approach: measuring activity in the two adjacent slices with the highest uptake, rather than quantifying uptake in the whole valve. The key advantage of this was to remove the challenge of determining the boundaries of the valve. The resulting improved reproducibility (<±10%) makes ^{18}F-fluoride a potentially attractive biomarker of efficacy in future clinical trials, requiring relatively few patients to demonstrate reductions in valvular calcification activity. Inter-observer reproducibility was also excellent using the modified approach.

In conclusion, we optimised ^{18}F-fluoride PET/CT imaging of the aortic valve to offer accurate spatial resolution, excellent scan-rescan and inter-observer reproducibility. ^{18}F-Fluoride PET/CT holds promise as a method to better understand calcification activity in aortic stenosis and as a surrogate endpoint to assess efficacy of novel therapies for aortic stenosis.

7.4 Assessment of degenerated bioprosthetic valves with micro-^{18}F-fluoride PET/CT and correlating histology will provide novel insight about the mechanisms of bioprosthetic valve degeneration.

Degeneration of bioprosthetic valves is an increasingly relevant clinical problem as a result of the increasing incidence of aortic stenosis in our ageing population, expansion in the availability of transcatheter valve implantation, and the increased life expectancy of people with prosthetic valves. Despite advances in valve production, bioprosthetic valves have limited durability and calcification is one of the dominant features of valve failure. Nonetheless, the pathogenesis of bioprosthetic valve degeneration is complex and incompletely understood.

In this thesis, we investigated the pathogenesis of bioprosthetic valve degeneration in a series of 16 explanted degenerated bioprosthetic valves. We documented morphological findings, performed micro-^{18}F-fluoride PET/CT and tissue histology.

Calcification was a central feature of degenerated valves (found in 88%) and was best appreciated by CT. The spatial distribution of calcium showed a predilection for leaflet commissures and free margins, regions recognised to be affected by high mechanical stress. Histology revealed a pattern of intrinsic calcium deposition in the deep layers of the cusp, propagating outwards and ultimately penetrating the surface. Pannus was another prevalent feature, universally present over the sewing ring and extending onto the valve cusps in 47%. Severe pannus was likely to be the cause of valve failure in 2 cases. CT and histology identified calcium within regions of pannus, suggesting that

pannus overgrowth may be a substrate for calcification. Other features detected on histology included organised thrombus (in 40%) and markers of tissue degradation such as loss of collagen structure, fluid insudation and expansion of the proteoglycan layer.

We validated ^{18}F-fluoride as a marker of calcium phosphate deposition in bioprosthetic valve tissue by correlating autoradiography and histological staining. We then used ^{18}F-fluoride PET/CT to demonstrate significant ^{18}F-fluoride binding in all the explanted valves. The highest ^{18}F-fluoride signal colocalised with regions of calcification and there was a positive correlation between calcium volume quantified by CT and ^{18}F-fluoride activity measured by PET. ^{18}F-Fluoride signal also correlated with histological evidence of fibrosis, thrombus and features of tissue degradation such as disruption of collagen architecture.

In conclusion, we confirmed that calcification is a central finding in degenerated bioprosthetic valves, whilst fibrosis (pannus), thrombus and degradation of structural components are other common features. We discovered that ^{18}F-fluoride localises to regions of calcification on histology but also to a lesser extent these other features of degeneration, suggesting these may be upstream triggers. This substantiates the theory of leaflet calcification as the final common response to various mechanisms of bioprosthetic valve injury.

7.5 ^{18}F-Fluoride PET/CT can be applied to the assessment of bioprosthetic aortic valves to detect and predict structural valve degeneration.

Although international guidelines recommend serial echocardiography for the detection of bioprosthetic degeneration,(16,17) visualisation of the valve is often poor due to acoustic artefacts from the prosthesis, limiting its sensitivity. This means that valve degeneration is frequently well advanced before it is clinically apparent. Moreover, valve obstruction often evolves rapidly, whilst valvular regurgitation due to leaflet tears is frequently unheralded and catastrophic. Novel techniques capable of detecting the earlier stages of valve degeneration are therefore highly desirable.

Having established the utility of pre-clinical ^{18}F-fluoride PET/CT in the investigation of bioprosthetic valve degeneration *ex vivo,* we went on to perform the first prospective observational cohort study of ^{18}F-fluoride PET/CT in patients with bioprosthetic aortic valves. A total of 80 volunteers were recruited into two cohorts, with and without prosthetic valve dysfunction, and underwent contrast-enhanced CT angiography, ^{18}F-fluoride PET, and serial echocardiography during 2 years of follow-up.

In patients with echocardiographic evidence of severe prosthetic valve dysfunction, all exhibited abnormalities on CT (e.g. calcification, hypoattenuation leaflet thickening) and very high uptake of ^{18}F-fluoride. In patients without echocardiographic evidence of prosthetic valve dysfunction, 20% had abnormal leaflet pathology on CT and 34% had increased ^{18}F-fluoride PET uptake. Patients with increased ^{18}F-fluoride uptake

demonstrated more rapid deterioration in valve function compared to those without. Indeed ^{18}F-fluoride uptake correlated with deterioration in all echocardiographic measures of valve function. Each of the 10 patients who developed new bioprosthesis dysfunction during follow-up had evidence of increased ^{18}F-fluoride uptake at baseline. On multivariable analysis, ^{18}F-fluoride uptake was the only independent predictor of future bioprosthetic dysfunction.

In other important findings, we investigated aortic valve calcium scoring as a method with which to monitor disease progression in bioprosthetic valve degeneration. However, we observed significant artefact related to motion and the dense materials present in prosthetic valves which precluded reliable analysis. Alternatively, a very small minority of contrast-enhanced CT scans were of suboptimal quality such that they could not be accurately adjudicated and, in combination with reliable data from ^{18}F-fluoride PET, this was an advantage of hybrid PET/CT.

In conclusion, ^{18}F-Fluoride PET-CT identified subclinical bioprosthetic valve degeneration beyond the capability of conventional assessments, provided powerful prediction of subsequent valve dysfunction and highlighted patients at risk of imminent valve failure. Although further investigation is required, this novel imaging approach has the potential to transform our understanding of bioprosthetic valve failure and the way in which we monitor and treat patients with bioprosthetic valves.

7.6 FUTURE DIRECTIONS

The work in this thesis presents a number of opportunities for further investigations to reinforce and develop the role of cardiac PET/CT in the assessment of native and bioprosthetic valve disease.

A combined assessment of fibrosis and calcification may offer incremental diagnostic benefit over established imaging modalities in aortic stenosis. However, further work is now required to validate the fibro-calcific burden in a larger patient population, to establish its prognostic value and to provide robust thresholds that can be used in clinical practice to identify patients with severe and non-severe aortic stenosis. In addition, the image analysis method used in our study is time consuming and fragmented across several different software tools. Work is therefore underway to refine the image analysis with a bespoke integrated software solution that can facilitate more rapid processing whilst maintaining accuracy and reproducibility. This will accelerate potential uptake in the clinical setting.

The study population that contributed the data used in chapters 3 and 4 was part of a randomised controlled trial of anti-calcific therapies, alendronate and denosumab, in the treatment of aortic stenosis (SALTIRE 2, NCT02132026) that is due to report in the near future. On the basis of our investigations in chapter 4 establishing the accuracy and reproducibility of aortic valve ^{18}F-fluoride PET/CT, ^{18}F-fluoride uptake has been incorporated as a surrogate endpoint of therapeutic effectiveness in this trial. This will help to clarify, for the first time, whether ^{18}F-fluoride is modifiable with drug therapy.

In chapter 4, it was noted that ECG-gating of PET data had a detrimental effect on the reproducibility of maximum measures of ^{18}F-fluoride uptake. The future development of advanced image processing that corrects for both cardiac and respiratory motion without discarding PET data may improve the reproducibility of maximum uptake measurements, which may then be more sensitive to change than mean measurements and better able to detect the effects of disease modifying therapies.

Projects are underway to expand the investigation of PET/CT in bioprosthetic valve disease, as described in chapters 5 and 6. This work includes a planned extension of the cohort study undertaken in chapter 6 which will allow comparison of imaging findings and clinical outcomes in patients who have received transcatheter aortic valve replacement with patients who have received surgically implanted bioprosthetic valves. Although the population in our clinical cohort study in chapter 6 is relatively large compared to other cardiovascular PET studies, external validation in a larger study population with longer follow-up would also be welcome. Thereafter, it would be interesting to explore whether the ^{8}F-fluoride signal in bioprosthetic valves is modifiable with developments in valve technology designed to reduce potential for calcification, or with the use of anti-calcific or anticoagulant therapies. Finally, our observations on the prevalence and possible causative role of subclinical leaflet thrombosis in bioprosthetic valve degeneration have prompted the recent commencement of an observational study of novel thrombus PET tracer ^{18}F-GP1, which binds to glycoprotein IIb/IIIa receptors on activated platelets, in patients with bioprosthetic aortic valves (NCT04073875). In the longer term, we hope this may

evolve into a tool for improved detection of valve thrombosis and for evaluating the impact of emergent treatment strategies.

7.7 PERSPECTIVE

The investigations described in this thesis support the exciting future role of non-invasive cardiovascular imaging, with potential to illuminate our understanding of disease processes and to improve the care we deliver to patients. In the setting of valvular heart disease, clinicians are almost entirely reliant upon non-invasive methods of assessment. The novel imaging techniques we describe might add significantly to current practice by combining anatomical and functional information to promote more individually tailored approaches to clinical care. In particular, functional molecular imaging offers great promise as an early indicator of disease-modifying intervention and there is abundant potential for development of new PET tracers. Here we have established a robust methodology with which ^{18}F-fluoride PET/CT can now be employed as a biomarker of aortic stenosis in large clinical trials and demonstrated a role in the assessment of bioprosthetic valves, to which it is perhaps uniquely well suited. Further work is now required to ensure that these advances ultimately translate into benefit to patients.

BIBLIOGRAPHY

- Achenbach S, Delgado V, Hausleiter J, *et al.* SCCT expert consensus document on computed tomography imaging before transcatheter aortic valve implantation (TAVI)/transcatheter aortic valve replacement (TAVR). J Cardiovasc CT 2012;6:366-380.
- Aggarwal S.R, Clavel M.-A, Messika-Zeitoun D, *et al*. Sex differences in aortic valve calcification measured by multidetector computed tomography in aortic stenosis. Circ Cardiovasc Imaging. 2013;6:40–47.
- Aikawa E, Nahrendorf M, Sosnovik D, *et al*. Multimodality molecular imaging identifies proteolytic and osteogenic activities in early aortic valve disease. Circulation 2007;115:377-86.
- Alavi SH, Groves EM, Kheradvar A. The effects of transcatheter valve crimping on pericardial leaflets. Ann Thorac Surg. 2014 Apr;97(4):1260-6.
- Allard MF, Thompson CR, Baldelli RJ, McNab JS, Babul SA, Betts JM, McManus BM, Jamieson WR, Ling H, Miyagishima RT. Commissural region dehiscence from the stent post of Carpentier-Edwards bioprosthetic cardiac valves. Cardiovasc Pathol. 1995 Jul-Sep;4(3):155-62.
- Arabkhani B, Bekkers JA, Andrinopoulou ER, *et al*. Allografts in aortic position: Insights from a 27-year, single-centre prospective study. J of Thoracic and Cardiovasc Surg. 2016:152(6).
- Arsalan M, Walther T. Durability of prostheses for transcatheter aortic valve implantation. Nat Rev Cardiol. 2016 Jun;13(6):360-7.

- Baumgartner H, Falk V, Bax JJ, *et al*; ESC Scientific Document Group. 2017 ESC/EACTS Guidelines for the management of valvular heart disease. Eur Heart J 2017;38:2739–2791.
- Blackman DJ, Saraf S, MacCarthy PA, Myat A, Anderson SG, Malkin CJ, Cunnington MS, Somers K, Brennan P, Manoharan G, Parker J, Aldalati O, Brecker SJ, Dowling C, Hoole SP, Dorman S, Mullen M, Kennon S, Jerrum M, Chandrala P, Roberts DH, Tay J, Doshi SN, Ludman PF, Fairbairn TA, Crowe J, Levy RD, Banning AP, Ruparelia N, Spence MS, Hildick-Smith D. Long-Term Durability of Transcatheter Aortic Valve Prostheses. J Am Coll Cardiol. 2019 Feb 12;73(5):537-545.
- Bloch O, Golde P, Dohmen PM, *et al*. Immune response in patients receiving a bioprosthetic heart valve: lack of response with decellularized valves. Tissue Eng Part A. 2011; 17:2399–2405.
- Bloomfield P, Wheatley DJ, Prescott RJ, *et al*. Twelve year comparison of a Bjork-Shiley mechanical heart valve with porcine bioprostheses. N Engl J Med 1991;324:573–9.
- Bohbot Y, Kowalski C, Rusinaru D, *et al*. Impact of mean transaortic pressure gradient on long-term outcome in patients with severe aortic stenosis and preserved left ventricular ejection fraction. J Am Heart Assoc. 2017;6.
- Böer U, Buettner FFR, Schridde A, *et al*. Antibody formation towards porcine tissue in patients implanted with crosslinked heart valves is directed to antigenic tissue proteins and αGal epitopes and is reduced in healthy vegetarian subjects. Xenotransplantation. 2017; 24:e12288.

- Bossé Y, Miqdad A, Fournier D, *et al*. Refining molecular pathways leading to calcific aortic valve stenosis by studying gene expression profile of normal and calcified stenotic human aortic valves. Circ Cardiovasc Genet. 2009;2:489–498.
- Bourguignon T, Bouquiaux-Stablo AL, Loardi C, Mirza A, Candolfi P, Marchand M, Aupart MR. Very late outcomes for mitral valve replacement with the Carpentier-Edwards pericardial bioprosthesis: 25-year follow-up of 450 implantations. J Thorac Cardiovasc Surg. 2014 Nov;148(5):2004-2011.
- Brennan JM, Thomas L, Cohen D, *et al*. Transcatheter versus surgical aortic valve replacement: propensity-matched comparison. J Am Coll Cardiol 2017;70:439-450.
- Brown JM, O'Brien SM, Wu C, *et al*. Isolated aortic valve replacement in North America comprising 108,687 patients in 10 years: changes in risks, valve types, and outcomes in the Society of Thoracic Surgeons National Database. J Thorac Cardiov Sur 2009;137:82-90.
- Bucay N, Sarosi I, Dunstan CR, Morony S, Tarpley J, Capparelli C, Scully S, Tan HL, Xu W, Lacey DL, Boyle WJ, Simonet WS. Osteoprotegerin-deficient mice develop early onset osteoporosis and arterial calcification. Genes Dev. 1998 May 1;12(9):1260-8.
- Bushra R, Steeds R, Brewerton H, *et al*. A Guideline Protocol for the Assessment of Aortic Stenosis, Including Recommendations for Echocardiography in Relation to Transcatheter Aortic Valve Implantation. J British Soc Echo (ECHO) 2012;9-18.

- Butany J, Vanlerberghe K, Silver MD. Morphologic findings and causes of failure in 24 explanted Ionescu-Shiley low-profile pericardial heart valves. Human Pathol 1992;23:1224-33.
- Butany J, Leask R. The failure modes of biological prosthetic heart valves. J Long Term Eff Med Implants. 2001;11(3-4):115-35.
- Butany J, Nair V, Leong SW, Soor GS, Feindel C. Carpentier-Edwards Perimount valves – morphological findings in surgical explants. J Card Surg 2007;22:7-12.
- Capodanno D, Petronio AS, Prendergast B, *et al*. Standardized definitions of structural deterioration and valve failure in assessing long-term durability of transcatheter and surgical aortic bioprosthetic valves: a consensus statement from the European Association of Percutaneous Cardiovascular Interventions (EAPCI). Endorsed by the European Society of Cardiology (ESC) and the European Association for Cardio-Thoracic Surgery (EACTS). Eur Heart J 2017;38:3382-3390.
- Capoulade R, Chan KL, Yeang C, *et al*. Oxidized Phospholipids, Lipoprotein(a), and Progression of Calcific Aortic Valve Stenosis. JACC 2015;66(11):1236-1246.
- Carpentier A, Lemaigre G, Robert L, *et a*l. Biological factors affecting long-term results of valvular heterografts. J Thorac Cardiovasc Surg. 1969;58:467-483.
- Chakravarty T, Sondergaard L, Friedman J, *et al*. Subclinical leaflet thrombosis in surgical and transcatheter bioprosthetic aortic valves: an observational study. Lancet 2017;389:2383–2392.

- Chen J, Fan J, Wang S, *et al*. Secreted Klotho attenuates inflammation-associated aortic valve fibrosis in senescence-accelerated mice P1. Hypertension. 2018;71:877-885.
- Chen J, Lin Y & Sun Z. Deficiency in the anti-aging gene Klotho promotes aortic valve fibrosis through AMPKalpha-mediated activation of RUNX2. Aging Cell. 2016;15: 853-860.
- Chen W & Dilsizian V. PET assessment of vascular inflammation and atherosclerotic plaques: SUV or TBR? J Nuclear Med : official publication, Society of Nuclear Medicine 2015;56:503-4.
- Chen JH, Chen WL, Sider KL, Yip CY, Simmons CA. β-catenin mediates mechanically regulated, transforming growth factor-β1-induced myofibroblast differentiation of aortic valve interstitial cells. Arterioscler Thromb Vasc Biol. 2011 Mar;31(3):590-7.
- Chenot F, Montant P, Goffinet C, Pasquet A, Vancraeynest D, Coche E, Vanoverschelde JL, Gerber BL. Evaluation of anatomic valve opening and leaflet morphology in aortic valve bioprosthesis by using multidetector CT: comparison with transthoracic echocardiography. Radiology. 2010 May;255(2):377-85.
- Clavel MA, Messika-Zeitoun D, Pibarot P, *et al*. The complex nature of discordant severe calcified aortic valve disease grading: new insights from combined Doppler echocardiographic and computed tomographic study. J Am Coll Cardiol 2013;62:2329–2338.
- Clavel MA, Pibarot P, Messika-Zeitoun D, *et al*. Impact of aortic valve calcification, as measured by MDCT, on survival in patients with aortic

stenosis: results of an international registry study. J Am Coll Cardiol. 2014;64(12):1202-13.

- Coffey S, Cairns BJ & Lung B. The modern epidemiology of heart valve disease. Heart. 2016;102:75-85.
- Córdoba-Soriano JG, Puri R, Amat-Santos I, Ribeiro HB, Abdul-Jawad Altisent O, del Trigo M, Paradis JM, Dumont E, Urena M, Rodés-Cabau J. Valve thrombosis following transcatheter aortic valve implantation: a systematic review. Rev Esp Cardiol (Engl Ed). 2015 Mar;68(3):198-204
- Côté N, Pibarot P, Clavel MA. Incidence, risk factors, clinical impact, and management of bioprosthesis structural valve degeneration. Curr Opin Cardiol. 2017 Mar;32(2):123-129.
- Côté N, El Husseini D, Pépin A, Guauque-Olarte S, Ducharme V, Bouchard-Cannon P, Audet A, Fournier D, Gaudreault N, Derbali H, McKee MD, Simard C, Després JP, Pibarot P, Bossé Y, Mathieu P. ATP acts as a survival signal and prevents the mineralization of aortic valve. J Mol Cell Cardiol. 2012 May;52(5):1191-202.
- David TE, Armstrong S, Maganti M. Hancock II bioprosthesis for aortic valve replacement: the gold standard of bioprosthetic valves durability? Ann Thorac Surg. 2010 Sep;90(3):775-81.
- Dalgliesh AJ, Parvizi M, Noble C, *et al*. Effect of cyclic deformation on xenogeneic heart valve biomaterials. PloS One. 2019; 14:e0214656.
- d'Arcy JL, Coffey S, Loudon MA, Kennedy A, Pearson-Stuttard J, Birks J, Frangou E, Farmer AJ, Mant D, Wilson J, Myerson SG, Prendergast BD. Large-scale community echocardiographic screening reveals a major burden

of undiagnosed valvular heart disease in older people: the OxVALVE Population Cohort Study. Eur Heart J 2016; Dec 14;37(47):3515-3522.

- Daubert MA, Weissman NJ, Hahn RT, *et al*. Long-Term Valve Performance of TAVR and SAVR: A Report From the PARTNER I Trial [published online ahead of print, 2016 Dec 8]. *JACC Cardiovasc Imaging*. 2016;S1936-878X(16)30895-6.
- Deck JD, Thubrikar MJ, Schneider PJ, *et al*. Structure, stress, and tissue repair in aortic valve leaflets. Cardiovasc Res 1988;22:7-16.
- Del Trigo M, Muñoz-García AJ, Latib A, *et al*. Impact of anticoagulation therapy on valve hemodynamic deterioration following transcatheter aortic valve replacement. Heart Published Online: 13 February 2018. Doi:10.1136/heartjnl-2017-312514.
- Didier R, Eltchaninoff H, Donzeau-Gouge P, Chevreul K, Fajadet J, Leprince P, Leguerrier A, Lièvre M, Prat A, Teiger E, Lefevre T, Tchetché D, Carrié D, Himbert D, Albat B, Cribier A, Sudre A, Blanchard D, Rioufol G, Collet F, Houel R, Dos Santos P, Meneveau N, Ghostine S, Manigold T, Guyon P, Cuisset T, Le Breton H, Delepine S, Favereau X, Souteyrand G, Ohlmann P, Doisy V, Lognoné T, Gommeaux A, Claudel JP, Bourlon F, Bertrand B, Iung B, Gilard M. Five-Year Clinical Outcome and Valve Durability After Transcatheter Aortic Valve Replacement in High-Risk Patients. Circulation. 2018 Dec 4;138(23):2597-2607.
- Dweck MR, Boon NA & Newby DE. Calcific aortic stenosis: a disease of the valve and the myocardium. J Am Coll Cardiol 2012 a;60:1854-63.

- Dweck MR, Jenkins WS, Vesey AT, *et al*. 18F-sodium fluoride uptake is a marker of active calcification and disease progression in patients with aortic stenosis. Circ Cardiovasc Imag 2014;7:371-8.
- Dweck MR, Jones C, Joshi NV, *et al*. Assessment of valvular calcification and inflammation by positron emission tomography in patients with aortic stenosis. Circulation 2012 b;125:76-86.
- Dweck MR, Williams MC, Moss AJ, *et al*. Computed tomography and cardiac magnetic resonance in ischaemic heart disease. J Am Coll Cardiol 2016:68:2201-2216.
- Dvir D, Webb J, Brecker S, Bleiziffer S, Hildick-Smith D, Colombo A, Descoutures F, Hengstenberg C, Moat NE, Bekeredjian R, Napodano M, Testa L, Lefevre T, Guetta V, Nissen H, Hernández JM, Roy D, Teles RC, Segev A, Dumonteil N, Fiorina C, Gotzmann M, Tchetche D, Abdel-Wahab M, De Marco F, Baumbach A, Laborde JC, Kornowski R. Transcatheter aortic valve replacement for degenerative bioprosthetic surgical valves: results from the global valve-in-valve registry. Circulation. 2012 Nov 6;126(19):2335-44.
- Dvir D, Bourguignon T, Otto CM, *et al*. Standardized definition of structural valve degeneration for surgical and transcatheter bioprosthetic valves. Circulation 2018;137:388-399.
- Egbe AC, Pislaru SV, Pellikka PA, Poterucha JT, Schaff HV, Maleszewski JJ, Connolly HM. Bioprosthetic Valve Thrombosis Versus Structural Failure: Clinical and Echocardiographic Predictors. J Am Coll Cardiol. 2015 Dec 1;66(21):2285-2294

- Fayad ZA, Mani V, Woodward M, *et al*. Safety and efficacy of dalcetrapib on atherosclerotic disease using novel non-invasive multimodality imaging (dal-PLAQUE): a randomised clinical trial. Lancet (London, England 2011;378:1547-59.
- Fiedler AG, Tolis G Jr. Surgical treatment of valvular heart disease: overview of mechanical and tissue prostheses, advantages, disadvantages, and implications for clinical use. Curr Treat Options Cardiovasc Med. 2018;20:7.
- Flameng W, Herregods MC, Vercalsteren M, Herijgers P, Bogaerts K, Meuris B. Prosthesis-patient mismatch predicts structural valve degeneration in bioprosthetic heart valves. Circulation. 2010 May 18;121(19):2123-9.
- Foroutan F, Guyatt GH, O'Brien K, *et al*. Prognosis after surgical replacement with a bioprosthetic aortic valve in patients with severe symptomatic aortic stenosis: systematic review of observational studies. BMJ 2016;354:i5065.
- Forsythe RO, Dweck MR, McBride OMB, *et al*. 18F-Sodium fluoride uptake in abdominal aortic aneurysms: the SoFIA3 study. J Am Coll Cardiol 2018;71:513-523.
- Freeman RV, Otto CM. Spectrum of calcific aortic valve disease: pathogenesis, disease progression, and treatment strategies. Circulation. 2005 Jun 21;111(24):3316-26.
- Fujita B, Kutting M, Seiffert M, *et al*. Calcium distribution patterns of the aortic valve as a risk factor for the need of permanent pacemaker implantation after transcatheter aortic valve implantation. Eur Heart J Cardiovasc Imaging 2016;17:1385-1393.

- Garg V, Muth AN, Ransom JF, Schluterman MK, Barnes R, King IN, Grossfeld PD, Srivastava D. Mutations in NOTCH1 cause aortic valve disease. Nature. 2005 Sep 8;437(7056):270-4.
- Gates KV, Xing Q & Griffiths LG. Immunoproteomic identification of noncarbohydrate antigens eliciting graft-specific adaptive immune responses in patients with bovine pericardial bioprosthetic heart valves. Proteomics Clin Appl. 2019; 13:e1800129.
- Gurvitch R, Webb JG, Yuan R, *et al*. Aortic Annulus Diameter Determination by Multidetector Computed Tomography : Reproducibility, Applicability, and Implications for Transcatheter Aortic Valve Implantation, JACC-Cardiovasc Inte 2011;4 :1235-1245.
- Helske S, Syvaranta S, Kupari M, *et al*. Possible role for mast cell-derived cathepsin G in the adverse remodelling of stenotic aortic valves. Eur Heart J. 2006;27:1495–1504.
- Hinton RB, Lincoln J, Deutsch GH, *et al*. Extracellular matrix remodelling and organization in developing and diseased aortic valves. Circ Res 2006; 98:1431–1438.
- Hinz B. Formation and function of the myofibroblast during tissue repair. J Invest Dermatol. 2007;127:526–537.
- Holen J, Aaslid R, Landmark K, *et al*. Determination of pressure gradient in mitral stenosis with a non-invasive ultrasound Doppler technique. Acta Med Scand. 1976;199:455-460.

- Installé J, Nzeusseu A, Bol A, *et al*. (18)F-fluoride PET for monitoring therapeutic response in Paget's disease of bone. J Nucl Med. 2005;46:1650–1658.
- Irkle A, Vesey AT, Lewis DY, *et al*. Identifying active vascular microcalcification by (18)F-sodium fluoride positron emission tomography. Nat Commun 2015;6:7495.
- Isihara T, Ferrans VJ, Boyce SW, Jones M, Roberts WC. Structure and classification of cuspal tears and perforations in porcine bioprosthetic cardiac valves implanted in patients. Am J Cardiol 1981;48:665-78.
- Iung B & Vahanian A. Epidemiology of valvular heart disease in the adult. Nat Rev Cardiol 2011;8(3):162–72.
- Jaffer IH, Fredenburgh JC, Hirsh J, Weitz JI. Medical device-induced thrombosis: what causes it and how can we prevent it? J Thromb Haemost. 2015 Jun;13 Suppl 1:S72-81.
- Jamieson WR, Munro AI, Miyagishima RT, Allen P, Burr LH, Tyers GF. Carpentier-Edwards standard porcine bioprosthesis: clinical performance to seventeen years. Ann Thorac Surg. 1995 Oct;60(4):999-1006.
- Jenkins WS, Vesey AT, Shah AS, *et al*. Valvular (18)F-Fluoride and (18)F-Fluorodeoxyglucose Uptake Predicts Disease Progression and Clinical Outcome in Patients With Aortic Stenosis. J Am Coll Cardiol. 2015;8;66(10):1200-1.
- Jenkins WSA, Shah AS, Pringle MAH, *et al*. 18F-NaF is a predictor of progression and outcome in Aortic Valve Disease. J Am Coll Cardiol 2014;63(12_S): doi:101016/S0735-1097(14)60995-5 2014.

- Jian B, Narula N, Li QY, *et al*. Progression of aortic valve stenosis: TGF-beta1 is present in calcified aortic valve cusps and promotes aortic valve interstitial cell calcification via apoptosis. Ann Thorac Surg. 2003;75:457–465.
- Johnston DR, Soltesz EG, Vakil N, Rajeswaran J, Roselli EE, Sabik JF 3rd, Smedira NG, Svensson LG, Lytle BW, Blackstone EH. Long-term durability of bioprosthetic aortic valves: implications from 12,569 implants. Ann Thorac Surg. 2015 Apr;99(4):1239-47.
- Joshi NV, Vesey AT, Williams MC, *et al*. 18F-Fluoride positron emission tomography for identification of ruptured and high-risk coronary atherosclerotic plaques: a prospective clinical trial. Lancet 2014;383:705-713.
- Kaden JJ, Bickelhaupt S, Grobholz R, Haase KK, Sarikoç A, Kiliç R, Brueckmann M, Lang S, Zahn I, Vahl C, Hagl S, Dempfle CE, Borggrefe M. Receptor activator of nuclear factor kappaB ligand and osteoprotegerin regulate aortic valve calcification. J Mol Cell Cardiol. 2004 Jan;36(1):57-66.
- Kapadia SR, Leon MB, Makkar RR, *et al*. 5-year outcomes of transcatheter aortic valve replacement compared with standard treatment for patients with inoperable aortic stenosis (PARTNER 1): a randomised controlled trial. *Lancet*. 2015;385(9986):2485-2491.
- Kato MT, Bolanho A, Zarella BL, *et al*. Sodium fluoride inhibits MMP-2 and MMP-9. J Den Res 2014;93:74-77.
- Konakci KZ, Bohle B, Blumer R, Hoetzenecker W, Roth G, Moser B, Boltz-Nitulescu G, Gorlitzer M, Klepetko W, Wolner E, Ankersmit HJ. Alpha-Gal on bioprostheses: xenograft immune response in cardiac surgery. Eur J Clin Invest. 2005 Jan;35(1):17-23.

- Kong WK, Regeer MV, Ng AC, *et al*. Sex Differences in Phenotypes of Bicuspid Aortic Valve and Aortopathy: Insights From a Large Multicenter, International Registry. Circ Cardiovasc Imaging. 2017;10:e005155.
- Kopanidis A, Pantos I, Alexopoulos N, Theodorakakos A, Efstathopoulos E, Katritsis D. Aortic Flow Patterns After Simulated Implantation of Transcatheter Aortic Valves. Hellenic J Cardiol. 2015 Sep-Oct;56(5):418-28
- Lancellotti P, Pibarot P, Chambers J, *et al*. Recommendations for the imaging assessment of prosthetic heart valves: a report from the European Association of Cardiovascular Imaging endorsed by the Chinese Society of Echocardiography, the Inter-American Society of Echocardiography, and the Brazilian Department of Cardiovascular Imaging. *Eur Heart J-Card Img* 2016;17(6):589-590.
- Levy RJ, Schoen FJ, Howard SL. Mechanism of calcification of porcine bioprosthetic aortic valve cusps: role of T-lymphocytes. Am J Cardiol. 1983 Sep 1;52(5):629-31.
- Lila N, McGregor CG, Carpentier S, Rancic J, Byrne GW, Carpentier A. Gal knockout pig pericardium: new source of material for heart valve bioprostheses. J Heart Lung Transplant. 2010 May;29(5):538-43.
- Lim HG, Choi SY, Yoon EJ, Kim SH, Kim YJ. In vivo efficacy of alpha-galactosidase as possible promise for prolonged durability of bioprosthetic heart valve using alpha1,3-galactosyltransferase knockout mouse. Tissue Eng Part A. 2013 Nov;19(21-22):2339-48.
- Lindman BR, Clavel MA, Methieu P, *et al*. Calcific Aortic Stenosis. Nat Rev Dis Primers. 2016;2:16006.

- Litmanovich DE, Ghersin E, Burke DA, *et al*. Imaging in Transcatheter Aortic Valve Replacement (TAVR): role of the radiologist. Insights into imaging 2014;5:123-45.
- Lovekamp JJ, Simionescu DT, Mercuri JJ, *et al*. Stability and function of glycosaminoglycans in porcine bioprosthetic heart valves. Biomaterials. 2006; 27:1507–1518.
- Mack MJ, Leon MB, Smith CR, *et al*. for the PARTNER 1 Trial Investigators. 5-year outcomes of transcatheter aortic valve replacement or surgical aortic valve replacement for high surgical risk patients with aortic stenosis (PARTNER 1): a randomised controlled trial. Lancet. 2015;385:2477–2484.
- Mahjoub H, Mathieu P, Sénéchal M, *et al*. ApoB/ApoA-I ratio is associated with increased risk of bioprosthetic valve degeneration. *J Am Coll Cardiol*. 2013;61(7):752-761.
- Makkar RR, Fontana G, Jilaihawi H, *et al*. Possible subclinical leaflet thrombosis in bioprosthetic aortic valves. N Engl J Med 2015;373:2015-2024.
- Manji RA, Zhu LF, Nijjar NK, *et al*. Glutaraldehyde-fixed bioprosthetic heart valve conduits calcify and fail from xenograft rejection. Circulation. 2006; 114:318–327.
- Messika-Zeitoun D, Aubry MC, Detaint D, *et al*. Evaluation and clinical implications of aortic valve calcification measured by electron-beam computed tomography. Circulation. 2004;110:356-362.
- Milano A, Guglielmi C, De Carlo M, Di Gregorio O, Borzoni G, Verunelli F, Bortolotti U. Valve-related complications in elderly patients with biological

and mechanical aortic valves. Ann Thorac Surg. 1998 Dec;66(6 Suppl):S82-7.

- Minners J, Allgeier M, Gohlke-Baerwolf C, *et al*. Inconsistent grading of aortic valve stenosis by current guidelines: haemodynamic studies in patients with apparently normal left ventricular function. Heart 2010;96:1463-1468.
- Motoyama S, Kondo T, Sarai M, *et al*. Multislice computed tomographic characteristics of coronary lesions in acute coronary syndromes. J Am Coll Cardiol 2007;50:319-326.
- Puri R, Auffret V, Rodés-Cabau J. Bioprosthetic Valve Thrombosis. J Am Coll Cardiol. 2017 May 2;69(17):2193-2211. doi: 10.1016/j.jacc.2017.02.051. Erratum in: J Am Coll Cardiol. 2017 Jul 4;70(1):121.
- Nair V, Law KB, Li AY, *et al*. Characterizing the inflammatory reaction in explanted Medtronic Freestyle stentless porcine aortic bioprosthesis over a 6-year period. Cardiovasc Pathol. 2012; 21:158–168.
- Natorska J, Marek G, Sadowski J, *et al*. Presence of B cells within aortic valves in patients with aortic stenosis: Relation to severity of the disease. J Cardiol. 2016;67:80–85.
- New SE & Aikawa E. Molecular imaging insights into early inflammatory stages of arterial and aortic valve calcification. Circ Res. 2011;108:1381-1391.
- New SE, Goettsch C, Aikawa M, *et al*. Macrophage-derived matrix vesicles: an alternative novel mechanism for microcalcification in atherosclerotic plaques. Circ Res. 2013; 113:72–77.
- Nigam V, Srivastava D. Notch1 represses osteogenic pathways in aortic valve cells. J Mol Cell Cardiol. 2009 Dec;47(6):828-34.

- Nkomo VT, Gardin JM, Skelton TN, *et al*. Burden of valvular heart diseases: a population-based study. Lancet 2006;368:1005-11.
- Nsaibia MJ, Mahmut A, Mahjoub H, *et al*. Association between plasma lipoprotein levels and bioprosthetic valve structural degeneration. Heart. 2016; 102:1915–1921.
- Nuvoli S, Fiore V, Babudieri S, Galassi S, Bagella P, Solinas P, Spanu A, Madeddu G. The additional role of 18F-FDG PET/CT in prosthetic valve endocarditis. Eur Rev Med Pharmacol Sci. 2018 Mar;22(6):1744-1751.
- Osnabrugge RL, Mylotte D, Head SJ, *et al*. Aortic stenosis in the elderly: disease prevalence and number of candidates for transcatheter aortic valve replacement: a meta-analysis and modelling study. J Am Coll Cardiol. 2013;62:1002-12.
- Otto CM, Burwash IG, Legget ME, *et al*. Prospective study of asymptomatic valvular aortic stenosis: clinic, echocardiographic, and exercise predictors of outcome. Circulation. 1997;95:2262-2270.
- Otto C, Kuusisto J, Reichenbach DD, *et al*. Characterization of the Early Lesion of Degenerative Valvular Aortic Stenosis. Histological and Immunohistochemical Studies. Circulation. 1994;90(2):844-853.
- Otto CM, Nishimura RA, Bonow RO, Carabello BA, Erwin JP 3rd, Gentile F, Jneid H, Krieger EV, Mack M, McLeod C, O'Gara PT, Rigolin VH, Sundt TM 3rd, Thompson A, Toly C. 2020 ACC/AHA Guideline for the Management of Patients With Valvular Heart Disease: Executive Summary: A Report of the American College of Cardiology/American Heart Association Joint

Committee on Clinical Practice Guidelines. Circulation. 2021 Feb 2;143(5):e35-e71.

- Pache G, Schoechlin S, Blanke P, *et al*. Early hypo-attenuated leaflet thickening in balloon-expandable transcatheter aortic heart valves. Eur Heart J 2016;37:2263–2271.
- Pachulski RT & Chan KL. Progression of aortic valve dysfunction in 51 adult patients with congenital bicuspid aortic valve: assessment and follow up by Doppler echocardiography. Br heart J. 1993;69:237-240.
- Pawade TA, Cartlidge TR, Jenkins WS, *et al*. Optimization and reproducibility of aortic valve 18F-fluoride positron emission tomography in patients with aortic stenosis. Circ-Cardiovasc Imag 2016;9:e005131.
- Pawade TA, Newby DE & Dweck MR. Calcification in Aortic Stenosis: The Skeleton Key. J Am Coll Cardiol. 2015 Aug 4;66(5):561-77.
- Pawade T, Sheth T, Guzzetti E, *et al*. Why and How to Measure Aortic Valve Calcification in Patients With Aortic Stenosis. JACC Cardiovasc Imaging. 2019 Sep;12(9):1835-1848.
- Pawade TA, Clavel MA, Tribouilloy C, *et al*. Computed Tomography Aortic Valve Calcium Scoring in Patients With Aortic Stenosis. Circ Cardiovasc Imag 2018;11(3)e007146.
- Pibarot P & Dumesnil JG. Prosthetic Heart Valves: Selection of the Optimal Prosthesis and Long-Term Management. Circulation 2009;119:1034-1048.
- Pibarot P, Weissman NJ, Stewart WJ, Hahn RT, Lindman BR, McAndrew T, Kodali SK, Mack MJ, Thourani VH, Miller DC, Svensson LG, Herrmann HC, Smith CR, Rodés-Cabau J, Webb J, Lim S, Xu K, Hueter I, Douglas PS, Leon

MB. Incidence and sequelae of prosthesis-patient mismatch in transcatheter versus surgical valve replacement in high-risk patients with severe aortic stenosis: a PARTNER trial cohort--a analysis. J Am Coll Cardiol. 2014 Sep 30;64(13):1323-34.

- Rashid HN, Brown AJ, McCormick LM, Amiruddin AS, Be KK, Cameron JD, Nasis A, Gooley RP. Subclinical Leaflet Thrombosis in Transcatheter Aortic Valve Replacement Detected by Multidetector Computed Tomography - A Review of Current Evidence. Circ J. 2018 Jun 25;82(7):1735-1742.
- Reul GJ Jr, Cooley DA, Duncan JM, Frazier OH, Hallman GL, Livesay JJ, Ott DA, Walker WE. Valve failure with the Ionescu-Shiley bovine pericardial bioprosthesis: analysis of 2680 patients. J Vasc Surg. 1985 Jan;2(1):192-204.
- Rodriguez-Gabella T, Pierre Voisine P, Puri R, *et al*. Aortic bioprosthetic valve durability: incidence, mechanisms, predictors, and management of surgical and transcatheter valve degeneration. J Am Coll Cardiol 2017;70:1013-1028.
- Rossebo AB, Pedersen TR, Boman K, *et al*. Intensive lipid lowering with simvastatin and ezetimibe in aortic stenosis. The New England journal of medicine 2008;359:1343-56.
- Rubeaux M, Joshi N, Dweck MR, *et al*. Motion correction of 18F-sodium fluoride PET for imaging coronary atherosclerotic plaques. Journal Of Nuclear Medicine: Official Publication, Society Of Nuclear Medicine 2015.
- Sacks MS. A review on the biomechanical effects of fatigue on the porcine bioprosthetic heart valve. J Long Term Eff Med Implants. 2017; 27:181–197.

- Sakaue T, Nakaoka H, Shikata F, *et al*. Biochemical and histological evidence of deteriorated bioprosthetic valve leaflets: the accumulation of fibrinogen and plasminogen. Biol Open. 2018; 7:bio034009.
- Schoen FJ. Evolving Concepts of cardiac valve dynamics: the continuum of development, functional structure, pathobiology, and tissue engineering. Circulation. 2008;118:1864-1880.
- Schoen FJ, Levy RJ. Founder's Award, 25th Annual Meeting of the Society for Biomaterials, perspectives. Providence, RI, April 28-May 2, 1999. Tissue heart valves: current challenges and future research perspectives. J Biomed Mater Res. 1999 Dec 15;47(4):439-65.
- Schoen FJ, Levy RJ. Calcification of tissue heart valve substitutes: progress toward understanding and prevention. Ann Thorac Surg. 2005 Mar;79(3):1072-80.
- Schoen FJ, Fernandez J, Gonzalez-Lavin L, Cernaianu A. Causes of failure and pathologic findings in surgically removed Ionescu-Shiley standard bovine pericardial heart valve bioprostheses: emphasis on progressive structural deterioration. Circulation 1987;76:618-27.
- Sénage T, Le Tourneau T, Foucher Y, Pattier S, Cueff C, Michel M, Serfaty JM, Mugniot A, Périgaud C, Carton HF, Al Habash O, Baron O, Roussel JC. Early structural valve deterioration of Mitroflow aortic bioprosthesis: mode, incidence, and impact on outcome in a large cohort of patients. Circulation. 2014 Dec 2;130(23):2012-20.

- Shen M, Tastet L, Capoulade R, *et al*. Effect of age and aortic valve anatomy on calcification and haemodynamic severity of aortic stenosis. Heart 2016;103:32-39.
- Shetty R, Pibarot P, Audet A, *et al*. Lipid-mediated inflammation and degeneration of bioprosthetic heart valves. Eur J Clin Invest. 2009; 39:471–480.
- Siddiqui RF, Abraham JR, Butany J. Bioprosthetic heart valves: modes of failure. Histopathology. 2009 Aug;55(2):135-44.
- Simard L, Cote N, Dagenais F, *et al*. Sex-related discordance between aortic valve calcification and haemodynamic severity of aortic stenosis. Circ Research 2016:120:681-691.
- Simionescu A, Simionescu DT & Deac RF. Matrix metalloproteinases in the pathology of natural and bioprosthetic cardiac valves. Cardiovasc Pathol. 1996 a; 5:323–332.
- Simionescu A, Simionescu DT & Deac RF. Biochemical pathways of tissue degeneration in bioprosthetic cardiac valves. The role of matrix metalloproteinases. ASAIO J 1996 b;42:561-7.
- Simionescu DT. Prevention of calcification in bioprosthetic heart valves: challenges and perspectives. Expert Opin Biol Ther. 2004; 4:1971–1985.
- Singhal P, Luk A & Butany J. Bioprosthetic Heart Valves: Impact of implantation on biomaterials. ISRN Biomaterials 2013;2013:728791.
- Srivatsa SS, Harrity PJ, Maercklein PB, Kleppe L, Veinot J, Edwards WD, Johnson CM, Fitzpatrick LA. Increased cellular expression of matrix proteins that regulate mineralization is associated with calcification of native human and

porcine xenograft bioprosthetic heart valves. J Clin Invest. 1997 Mar 1;99(5):996-1009.

- Steiner I, Krbal L, Rozkos T, *et al*. Calcific aortic valve stenosis: Immunohistochemical analysis of inflammatory infiltrate. Pathol Res Pract. 2012;208:231–234.
- Stewart BF, Siscovick D, Lind BK, *et al*. Clinical factors associated with calcific aortic valve disease. Cardiovascular Health Study. J Am Coll Cardiol. 1997;29:630-634.
- Stritzke J, Linsel-Nitschke P, Markus MR, *et al.* Association between degenerative aortic valve disease and long-term exposure to cardiovascular risk factors: results of the longitudinal population-based KORA/MONICA survery. Eur Heart J. 2009;30:2044-2053.
- Sucosky P, Balachandran K, Elhammali A, *et al*. Altered shear stress stimulates upregulation of endothelial VCAM-1 and ICAM-1 in a BMP-4- and TGF-beta1-dependent pathway. Arterioscler Thromb Vasc Biol. 2009;29:254–260.
- Syväranta S, Helske S, Laine M, *et al*. Vascular endothelial growth factor-secreting mast cells and myofibroblasts: a novel self-perpetuating angiogenic pathway in aortic valve stenosis. Arterioscler Thromb Vasc Biol. 2010;30:1220–1227.
- Tastet L, Enriquez-Sarano M, Capoulade R, *et al*. Impact of aortic valve calcification and sex on haemodynamic progression and clinical outcomes in AS. J Am Coll Cardiol. 2017;69:2096-2098.
- Tawakol A, Migrino RQ, Bashian GG, *et al*. In vivo 18F-fluorodeoxyglucose positron emission tomography imaging provides a noninvasive measure of

carotid plaque inflammation in patients. Journal of the American College of Cardiology 2006;48:1818-24.

- Taylor PM, Allen SP & Yacoub MH. Phenotypic and functional characterization of interstitial cells from human heart valves, pericardium and skin. J Heart Valve Dis. 2000;9:150–158.)
- Teshima H, Hayashida N, Yano H, *et al.* Obstruction of St Jude Medical valves in the aortic position: histology and immunohistochemistry of pannus. J Thorac Cardiovasc Surg. 2003; 126:401–407.
- Thanassoulis G, Massaro JM, Cury R, *et al*. Associations of long-term and early adult atherosclerosis with aortic and mitral valve calcium. J Am Coll Cardiol. 2010;55:2491-2498.
- Thanassoulis G, Campbell CY, Owens DS, *et al*. Genetic Associations with Valvular Calcification and Aortic Stenosis. N Eng J Med 2013; 368:503-512.
- Thyregod HGH, Ihlemann N, Jørgensen TH, Nissen H, Kjeldsen BJ, Petursson P, Chang Y, Franzen OW, Engstrøm T, Clemmensen P, Hansen PB, Andersen LW, Steinbrüchel DA, Olsen PS, Søndergaard L. Five-Year Clinical and Echocardiographic Outcomes from the Nordic Aortic Valve Intervention (NOTION) Randomized Clinical Trial in Lower Surgical Risk Patients. Circulation. 2019 Feb 1.
- Tsimikas S., Willeit P, Willeit J, *et al*. Oxidation-specific biomarkers, prospective 15-year cardiovascular and stroke outcomes, and net reclassification of cardiovascular events. J Am Coll Cardiol 2012;60:2218–2229.

- Vesely I. The evolution of bioprosthetic heart valve design and its impact on durability. Cardiovasc Pathol. 2003 Sep-Oct;12(5):277-86.
- Vesey AT, Jenkins WSA, Irkle A, *et al*. ^{18}F-Fluoride and ^{18}F-fluorodeoxyglucose positron emission tomography after transient ischemic attack or minor ischemic stroke: case–control study. Circ-Cardiovasc Imag 2017;10:e004976.
- Vogt PR, Brunner-LaRocca HP, Sidler P, *et al*. Reoperative Surgery for Degenerated Aortic Bioprostheses: Predictors for Emergency Surgery and Reoperative Mortality. Eur J Cardio-Thorac 2000;17:134-139.
- Wheatley DJ, Fisher J, Reece IJ, *et al*. Primary tissue failure in pericardial heart valves. J Thorac Cardiovasc Surg. 1987 Sep;94(3):367-74. PMID: 3626599.
- Winchester R, Wiesendanger M, O'Brien W, *et al.* Circulating activated and effector memory T cells are associated with calcification and clonal expansions in bicuspid and tricuspid valves of calcific aortic stenosis. J Immunol. 2011;187:1006–1014.
- Wu HD, Maurer MS, Friedman RA, *et al*. The lymphocytic infiltration in calcific aortic stenosis predominantly consists of clonally expanded T cells. J Immunol. 2007;178:5329–5339.
- Yang X, Fullerton DA, Su X, *et al*. Pro-osteogenic phenotype of human aortic valve interstitial cells is associated with higher levels of Toll-like receptors 2 and 4 and enhanced expression of bone morphogenetic protein 2. J Am Coll Cardiol. 2009 a;53:491–500.
- Yang X, Meng X, Su X, *et al*. Bone morphogenic protein 2 induces Runx2 and osteopontin expression in human aortic valve interstitial cells: role of Smad1

and extracellular signal-regulated kinase 1/2. J Thorac Cardiovasc Surg. 2009 b;138:1008–1015.

- Yetkin E & Waltenberger J, Molecular and cellular mechanisms of aortic stenosis, Int J Cardiol 2009;135:4–13
- Zheng KH, Tsimikas S, Pawade T, *et al*. Lipoprotein (a) and Oxidised Phospholipids Promote Valve Calcification in Patients with Aortic Stenosis. JACC 2019;73:2150-2162.
- Zoghbi WA, Chambers JB, Dumesnil JG, *et al*. Recommendations for Evaluation of Prosthetic Valves With Echocardiography and Doppler Ultrasound. *J Am Soc Echocardiog* 2009;22(9):975–1014.

APPENDIX

Patient information sheets

- 18F-FAABULOUS Study, Cohort 1 308
- 18F-FAABULOUS Study, Cohorts 2 and 3 314

Patient consent forms

- 18F-FAABULOUS Study, Cohort 1 320
- 18F-FAABULOUS Study, Cohorts 2 and 3 322

ARSAC licences 324

Ethical Board Approval 326

Volunteer Information Sheet

Cohort 1

THE 18F-FAABULOUS STUDY

18F-FLUORIDE ASSESSMENT OF AORTIC BIOPROSTHESES DURABILITY AND OUTCOMES

You are being invited to take part in a research study. Before you decide whether or not to participate, it is important that you understand why the research is being done and what it will involve. Please read the following information carefully and discuss it with others if you wish.

If there is anything that is not clear or if there are questions you would like to ask then please contact us for further information. Alternatively, you can also contact Dr Cruden, who is not directly involved in this study but who can give you independent advice. He can be contacted via the Royal Infirmary of Edinburgh switchboard on 0131 536 1000 by asking for his secretary.

What is the purpose of the study?
Narrowing of the main outlet valve of the heart (aortic stenosis) is the most common form of heart valve disease in the western world and replacing this valve is the most frequently performed heart valve operation. The majority of replacement valves are made from animal tissue with the benefit that, unlike metal valves, they do not require blood-thinning treatment afterwards. Recently, procedures have developed to replace the aortic valve using a key-hole technique, thereby avoiding the need for open heart surgery. However, whilst we know that traditional surgical tissue valves last on average between 10 and 15 years we do not know how long the new key-hole valves will endure.

The main purpose of this study is therefore to use a special type of scan called “PET-CT” to investigate what happens to these tissue valves (both surgical and key-hole). This scan can measure the activity of “*calcification”* which causes hardening and chalkiness of the valve and is the main way in which such valves fail. We believe that these scans will predict how long the different types of replacement valve are likely to last and potentially to predict when, and in whom, they will need replaced.

Why have I been invited?
You have been invited to take part in this research because you previously had a tissue heart valve replacement and are being considered for a repeat valve replacement operation.

Do I have to take part?
No. It is entirely up to you to decide whether or not to take part. If you do decide to take part, you are still free to withdraw at any time without having to give a reason. A decision not to take part or to withdraw at a later stage will not affect the standard of care you receive or your legal rights.

What will happen to me if I take part?
You have been provided with this information sheet and will be given at least 24 hours to read it over before being contacted by a member of the research team. They will give you an opportunity to ask any questions that you might have and ask if you wish to participate in the study. If you agree to take part, we will arrange a date close to your operation for you to attend the Clinical Research Facility at the Royal Infirmary of Edinburgh.

At this visit, we will again discuss the study to ensure that you understand eveything and will ask for your written consent. As part of a general assessment, we will ask about your symptoms, undertake a full examination of your heart, record an electrical tracing of your heart and take some blood tests (~60ml = 4 tablespoons of blood will be taken). This volume of blood will allow for a range of immediate tests to be performed and also provide samples for storage which will be valuable in future research studies.

We will then arrange for you to have a PET-CT scan of the heart, to take place during the same visit wherever possible. The PET-CT scan provides detailed images of the heart and will require injection of a special tracer about 60 minutes before the scan via a plastic tube (cannula) in one of your veins. This special tracer called radiolabelled 18F-fluoride is radioactive and highlights areas of active calcium formation in the heart. It has been used in humans for 40 years with no major harmful effects. Prior to the scan you may also require a medicine called metoprolol or verapamil in order to slow your heart rate. Slowing your heart rate will improve the quality of images obtained and minimise the dose of radiation which is required for the scan. This will be prescribed by an experienced doctor after considering your personal medical history and any possible interactions with medications which you already take. This medication may need to be taken as a tablet for several days prior to the scan and as an injection through the cannula at the time of the scan. During the PET-CT there will be a further injection of an iodine-based contrast “dye” via the cannula in your arm in order to obtain more detailed information from the images.

The process of taking consent is likely to take 30 minutes, the clinical assessment will take 30 minutes and the PET-CT will take 90 minutes, starting with injection of the tracer 60 minutes prior to the scan. We therefore estimate that your initial visit to hospital will take around 2 hours 30 mins.

The second stage of your involvement in the study will be at the time of your operation. The surgeon will remove your existing replacement heart valve before implanting a new replacement valve. The existing heart valve is normally thrown away but we will keep it and perform detailed analysis on it. This will not affect your operation in any way.

What happens to the blood and tissue samples that are taken?
Some blood and tissue samples will be taken for immediate tests and other samples will be retained in an anonymised fashion to be frozen and stored so that further tests may be performed in the future. We will store these samples for a maximum of 10 years after which time they will be destroyed in accordance with standard NHS Lothian procedure.

What are the possible benefits of taking part?

You will be contributing to our understanding of the disease process that affects aortic valve replacements. The information that we gather will help us to evaluate which valve replacement options are most effective and particularly to compare the durability of new techniques with traditional approaches. This study is the first of its kind to use such imaging technology and, depending on the results obtained, this technology may become a valuable tool for identifying patients at risk of needing further treatment and for testing new treatments.

What are the possible disadvantages and risks of taking part?

A PET-CT scan is a routine medical procedure and is itself associated with very few side effects. The most important side effects are exposure to ionising radiation and potential reaction to the contrast dye. We have a well-developed protocol for PET-CT imaging that minimises radiation exposure and have clear procedures for managing contrast reactions.

The exact amount of radiation used during this type of scan varies but is approximately 7 times the amount that you would normally receive in a year from natural background sources of radiation. The lifetime risk of developing a cancer from the extra radiation in this scan is small: 1 in 1200. To put this number in context, in the average population 1 in 4 people develop cancer during their lifetime. Therefore your risk would increase from 300 in 1200 to 301 in 1200. If you are female and there is a possibility that you are pregnant then we will ask to perform a pregnancy test. Radiation can cause damage to babies in the womb so we need to ensure that no scans are performed on pregnant women.

There is a low risk of harmful effects on the kidneys or developing an allergic reaction from the contrast dye used in the PET-CT scan. The risk from contrast exposure in this study will be minimised by excluding patients who have significant kidney disease or a history of allergic reactions to contrast dye. If you feel unwell after the scan or have any concerns then you should contact a member of the research team on the number provided or contact 999 in the unlikely event of an emergency.

The use of medication to slow the heart rate of patients prior to a PET-CT scan is a well established procedure which improves the quality of images and minimises the dose of radiation required. Such medication will only be prescribed if it is required and by an experienced doctor after reviewing your medical history and current list of medication. The medications which may be used are called metoprolol and verapamil. Metoprolol belongs to a family of drugs called ‘beta-blockers’ and potential side effects include cold hands/feet, fatigue, erectile dysfunction, a reduction in your blood pressure and making you feel breathless. These effects are all reversible upon stopping the medication. We would avoid giving metoprolol to anybody with a history of asthma, airway spasm, a slow heart rate or acute symptoms of heart failure. Verapamil belongs to a family of drugs called ‘calcium channel-blockers’ with potential side effects including constipation, nausea, headache, ankle swelling and a reduction in blood pressure. Similarly, these effects are all reversible upon stoping the medication and we would avoid giving verapamil to anybody with a history of a slow heart rate or acute symptoms of heart failure. You may be asked to take one of these medications for a number of days prior to your scan, in which case you will be provided with clearly labelled medication and instructions on how and when it should be taken. More commonly, metoprolol or verapamil is given to patients immediately prior to the scan as an injection via a plastic tube in one of the veins and this will be under the direct supervision of an experienced doctor. If you have any questions about the

medication or concerns about side effects then please contact a member of the research team.

Finally, participating in the study will require that you devote some time to consultations and scans. We will endeavour to make these as time-efficient and convenient for you as possible. We are also happy to reimburse reasonable travel expenses incurred whilst travelling to study visits - please ask a member of the research team about this.

What if something abnormal is found in my scans or other tests?
As part of this study we will obtain images of your chest, focusing on your heart. After your scan, a specialist will examine these pictures (this will not be done on the day of your study). There is a small possibility that we will identify unexpected or unrelated changes in the heart or other chest organs. You should be aware that because our pictures are taken for a specific research purpose, not all abnormalities that might be detected by other CT or PET scans are necessarily seen. On rare occasions, we might find an abnormality that is significant and which should be investigated further. Similarly, we will be performing blood tests that may identify unexpected abnormalities that could require additional follow-up or treatment. If we find such a significant abnormality from the scan or blood tests then we will inform you and contact your GP in order to organise appropriate ongoing care.

Although a significant abnormality is unlikely, you should be aware that if such an abnormality is detected then this may have consequences for your treatment. In addition, important incidental findings may have implications for your existing and future insurance policies (such as increased insurance premiums or difficulty arranging cover) and we would strongly advise that you consult your insurance provider in such an event.

What happens if I lose the capacity to make decisions?
If you should lose the capacity to make decisions, we would retain and make use of identifiable information and tissue which had already been collected but there would be no further participation in the study.

Will my taking part in this study be kept confidential?
All information that is collected about you during the course of the research will be kept strictly confidential and there are laws which safeguard your privacy at every stage. Your participation in the study will be recorded in your medical notes. Any information about you that leaves the NHS or University will have your name and address removed so that you cannot be recognised from it.

Will my GP be informed?
As long as you agree, we will let your GP know about your participation in the study. If any incidental findings are picked up during our tests then these will be reported to your GP to consider further tests or review as appropriate.

What will happen to the results of the research study?
Once we have completed the study and analysed the results, we will submit a paper for publication in one of the scientific journals. The results may also be presented at scientific meetings but you will not be identifiable in any published or presented results. For patients

who are interested, we will notify you of any publications arising from this research and provide you with periodic updates in a newsletter via post or email.

Who is organising the study?
The study is being organised through the University of Edinburgh in collaboration with Papworth Hospital, Cambridge and Bichat University Hospital, Paris. The British Heart Foundation is funding the research. Your doctors will not be paid for including you in this study.

Who has reviewed the study?
An NHS Research Ethics Committee has reviewed and approved the study.

Contact for further information
If you have any questions about the study then please contact Dr Tim Cartlidge via telephone on 07732973884 or e-mail at timothy.cartlidge@nhs.net or Dr Marc Dweck (Chief Investigator) at marc.dweck@ed.ac.uk.

If you would like to discuss this study with an independent party then please contact Dr Cruden, Consultant Cardiologist, who is not directly involved with the study and can offer independent advice. Please contact him via his secretary through the Royal Infirmary switchboard on 0131 536 1000.

If you wish to make a complaint about the study please contact NHS Lothian.
NHS Lothian Complaints Team
2nd Floor, Waverley Gate
2-4 Waterloo Place
Edinburgh, EH1 3EG
Tel: 0131 465 5708
complaints.team@nhslothian.scot.nhs.uk.

Thank you for taking the time to read this information sheet

PATIENT JOURNEY THROUGH STUDY

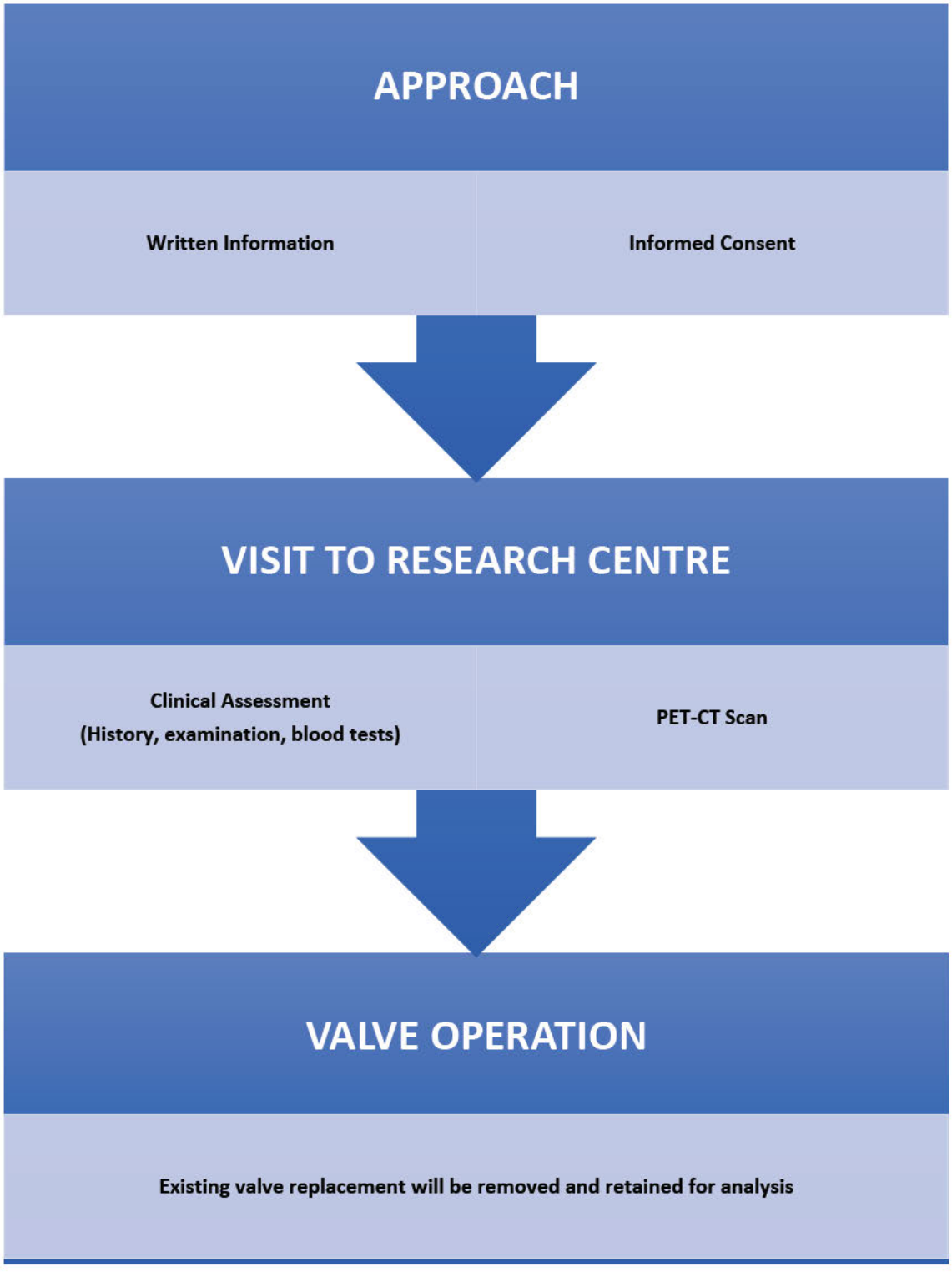

Volunteer Information Sheet

Cohorts 2 and 3

THE 18F-FAABULOUS STUDY

18F-FLUORIDE ASSESSMENT OF AORTIC BIOPROSTHESES DURABILITY AND OUTCOMES

You are being invited to take part in a research study. Before you decide whether or not to participate, it is important that you understand why the research is being done and what it will involve. Please read the following information carefully and discuss it with others if you wish.

If there is anything that is not clear or if there are questions you would like to ask then please contact us for further information. Alternatively, you can also contact Dr Cruden, who is not directly involved in this study but who can give you independent advice. He can be contacted via the Royal Infirmary of Edinburgh switchboard on 0131 536 1000 by asking for his secretary.

What is the purpose of the study?
Narrowing of the main outlet valve of the heart (aortic stenosis) is the most common form of heart valve disease in the western world and replacing this valve is the most frequently performed heart valve operation. The majority of replacement valves are made from animal tissue with the benefit that, unlike metal valves, they do not require blood-thinning treatment afterwards. Recently, procedures have developed to replace the aortic valve using a key-hole technique, thereby avoiding the need for open heart surgery. However, whilst we know that traditional surgical tissue valves last on average between 10 and 15 years we do not know how long the new key-hole valves will endure.

The main purpose of this study is therefore to use a special type of scan called “PET-CT” to investigate what happens to these tissue valves (both surgical and key-hole). This scan can measure the activity of “*calcification”* which causes hardening and chalkiness of the valve and is the main way in which such valves fail. We believe that these scans will predict how long the different types of replacement valve are likely to last and potentially to predict when, and in whom, they will need replaced.

Why have I been invited?
You have been invited to take part in this research because you have a tissue heart valve replacement.

Do I have to take part?
No. It is entirely up to you to decide whether or not to take part. If you do decide to take part, you are still free to withdraw at any time without having to give a reason. A decision not to take part or to withdraw at a later stage will not affect the standard of care that you receive or your legal rights.

What will happen to me if I take part?
You have been provided with this information sheet and will be given at least 24 hours to read it over before being contacted by a member of the research team. We will give you an opportunity to ask any questions that you might have and ask if you wish to participate in the study. If you agree to take part, we will arrange a date for you to attend the Clinical Research Facility at the Royal Infirmary of Edinburgh.

At this visit, we will again discuss the study to ensure that you understand eveything and will ask for your written consent. As part of a general assessment, we will ask about your symptoms, undertake a full examination of your heart, record an electrical tracing of your heart (ECG) and take some blood tests (~60ml = 4 tablespoons of blood will be taken). This volume of blood will allow for a range of immediate tests to be performed and provide samples for storage which will be valuable in future research studies. We will also arrange an ultrasound scan of the heart called an echocardiogram.

We will then organise for you to have a PET-CT scan of the heart, to take place during the same visit wherever possible. The PET-CT scan provides detailed images of the heart and will require injection of a special tracer about 60 minutes before the scan via a plastic tube (cannula) in one of your veins. This special tracer called radiolabelled 18F-fluoride is radioactive and highlights areas of active calcium formation in the heart. It has been used in humans for 40 years with no major harmful effects. Prior to the scan you may also require a medicine called metoprolol or verapamil in order to slow your heart rate. Slowing your heart rate will improve the quality of images obtained and minimise the dose of radiation which is required for the scan. This will be prescribed by an experienced doctor after considering your personal medical history and any possible interactions with medications which you already take. This medication may need to be taken as a tablet for several days prior to the scan and as an injection through the cannula at the time of the scan. During the PET-CT there will be a further injection of an iodine-based contrast “dye” via the cannula in your arm in order to obtain more detailed information from the images.

The process of taking consent, the clinical assessment and echocardiogram is likely to take 90 minutes in total and the PET-CT will take a further 90 minutes, starting from injection of the tracer 60 minutes prior to the scan. We therefore estimate that your initial visit to hospital will take around 3 hours in total.

After the initial study visit, we will then ask you to return to the Royal Infirmary of Edinburgh for follow-up at 1 year and 2 years. This will again involve asking about your symptoms, undertaking an examination of your heart, recording an ECG, performing an echocardiogram and taking further blood samples. These visits will take around 90 minutes each. The 2 year follow-up visit will be combined with a repeat CT scan to acquire pictures of your replacement heart valve for comparison with the baseline images. The CT scan will take around 30 minutes and will again involve injection of an iodine-based contrast “dye” via a cannula in your arm.

Thereafter, follow-up will be conducted via a brief telephone consultation annually at 3, 4 and 5 years. As part of the study, if you encounter any health complications relating to your replacement heart valve then your hospital team will share this information with the research team.

What happens to the blood samples that are taken?

Some blood is taken for immediate tests. Any samples obtained from you will be retained in an anonymised fashion and will then be frozen and stored so that further tests may be performed in the future. We will store these samples for a maximum of 10 years after which time they will be destroyed in accordance with standard NHS Lothian procedure.

What are the possible disadvantages and risks of taking part?

PET-CT scans are routine medical procedures and are associated with very few side effects. The most important side effects are exposure to ionising radiation and potential reaction to the contrast dye. We have a well-developed protocol for PET-CT imaging that minimises radiation exposure and have clear procedures for managing contrast reactions.

The exact amount of radiation used during this type of scan varies but is approximately 9 times the amount that you would normally receive in a year from natural background sources of radiation. The lifetime risk of developing a cancer from the extra radiation in this scan is 1 in 625. To put this number in context, in the average population 1 in 4 people develop cancer during their lifetime. Therefore your risk would increase from 250 in 1000 to 252 in 1000. If you are female and there is a possibility that you are pregnant then we will ask to perform a pregnancy test. Radiation can cause damage to babies in the womb so we need to ensure that no scans are performed on pregnant women.

There is a low risk of harmful effects on the kidneys or developing an allergic reaction from the contrast dye used in the PET-CT scan. The risk from contrast exposure in this study will be minimised by excluding patients who have significant kidney disease or a history of allergic reactions to contrast dye. If you feel unwell after the scan or have any concerns then you should contact a member of the research team on the number provided or contact 999 in the unlikely event of an emergency.

The use of medication to slow the heart rate of patients prior to a PET-CT scan is a well-established procedure which improves the quality of images and minimises the dose of radiation required. Such medication will only be prescribed if it is required and by an experienced doctor after reviewing your medical history and current list of medication. The medications which may be used are called metoprolol and verapamil. Metoprolol belongs to a family of drugs called ‘beta-blockers’ and potential side effects include cold hands/feet, fatigue, erectile dysfunction, a reduction in your blood pressure and making you feel breathless. These effects are all reversible upon stopping the medication. We would avoid giving metoprolol to anybody with a history of asthma, airway spasm, a slow heart rate or acute symptoms of heart failure. Verapamil belongs to a family of drugs called ‘calcium channel-blockers’ with potential side effects including constipation, nausea, headache, ankle swelling and a reduction in blood pressure. Similarly, these effects are all reversible upon stoping the medication and we would avoid giving verapamil to anybody with a history of a slow heart rate or acute symptoms of heart failure. You may be asked to take one of these medications for a number of days prior to your scan, in which case you will be provided with clearly labelled medication and instructions on how and when it should be taken. More commonly, metoprolol or verapamil is given to patients immediately prior to the scan as an injection via a plastic tube in one of the veins and this will be under the direct supervision of an experienced doctor. If you have any questions about the medication or concerns about side effects then please contact a member of the research team.

Finally, participating in the study will require that you devote some time to consultations and scans. We will endeavour to make these as time-efficient and convenient for you as possible. We are also happy to reimburse reasonable travel expenses incurred whilst travelling to study visits - please ask a member of the research team about this.

What if something abnormal is found in my scans or other tests?
As part of this study we will obtain images of your chest, focusing on your heart. After your scan, a specialist will examine these pictures (this will not be done on the day of your study). There is a small possibility that we will identify unexpected or unrelated changes in the heart or other chest organs. You should be aware that because our pictures are taken for a specific research purpose, not all abnormalities that might be detected by other CT or PET scans are necessarily seen. On rare occasions, we might find an abnormality that is significant and which should be investigated further. Similarly, we will be performing blood tests that may identify unexpected abnormalities that could require additional follow-up or treatment. If we find such a significant abnormality from the scan or blood tests then we will inform you and contact your GP in order to organise appropriate ongoing care.

Although a significant abnormality is unlikely, you should be aware that if such an abnormality is detected then this may have consequences for your treatment. In addition, important incidental findings may have implications for your existing and future insurance policies (such as increased insurance premiums or difficulty arranging cover) and we would strongly advise that you consult your insurance provider in such an event.

What happens if I lose the capacity to make decisions?
If you should lose the capacity to make decisions, we would retain and make use of identifiable information and tissue which had already been collected but there would be no further participation in the study.

Will my taking part in this study be kept confidential?
All information that is collected about you during the course of the research will be kept strictly confidential and there are laws which safeguard your privacy at every stage. Your participation in the study will be recorded in your medical notes. Any information about you that leaves the NHS or University will have your name and address removed so that you cannot be recognised from it.

Will my GP be informed?
As long as you agree, we will let your GP know about your participation in the study. If any incidental findings are picked up during our tests then these will be reported to your GP to consider further tests or review as appropriate.

What will happen to the results of the research study?
Once we have completed the study and analysed the results, we will submit a paper for publication in one of the scientific journals. The results may also be presented at scientific meetings but you will not be identifiable in any published or presented results. For those patients who are interested, we will notify you of any publications arising from this research and provide you with periodic updates in a newsletter via post or email.

Who is organising the study?

The study is being organised through the University of Edinburgh in collaboration with Papworth Hospital, Cambridge and Bichat University Hospital, Paris. The British Heart Foundation is funding the research. Your doctors will not be paid for including you in this study.

Who has reviewed the study?

An NHS Research Ethics Committee has reviewed and approved the study.

Contact for further information

If you have any questions about the study then please contact Dr Tim Cartlidge via telephone on 07732973884 or e-mail at timothy.cartlidge@nhs.net or Dr Marc Dweck (Chief Investigator) at marc.dweck@ed.ac.uk.

If you would like to discuss this study with an independent party then please contact Dr Cruden, Consultant Cardiologist, who is not directly involved with the study and can offer independent advice. Please contact him via his secretary through the Royal Infirmary switchboard on 0131 536 1000.

If you wish to make a complaint about the study please contact NHS Lothian.
NHS Lothian Complaints Team
2nd Floor, Waverley Gate
2-4 Waterloo Place
Edinburgh, EH1 3EG
Tel: 0131 465 5708
complaints.team@nhslothian.scot.nhs.uk.

Thank you for taking the time to read this information sheet

PATIENT JOURNEY THROUGH STUDY

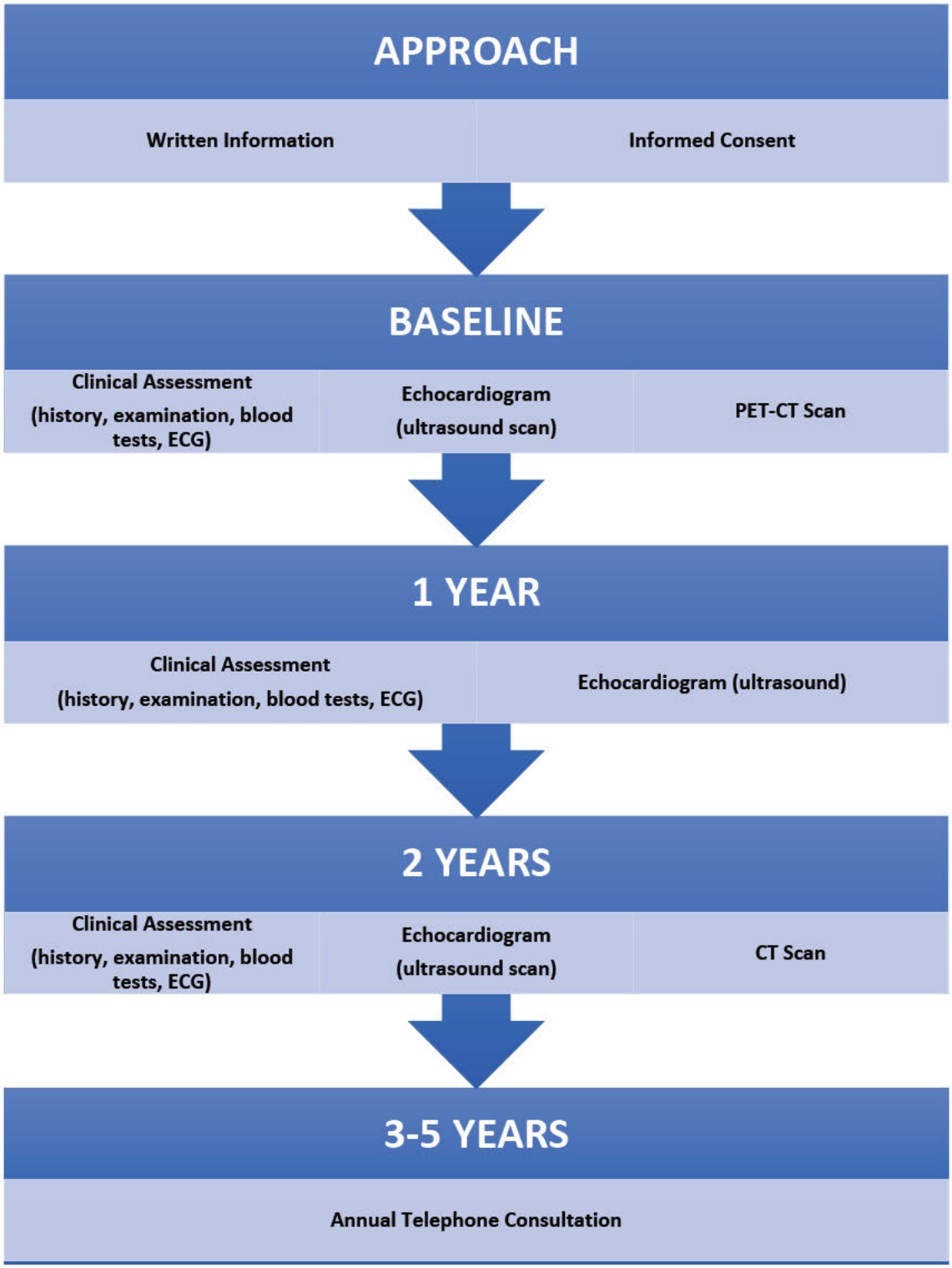

Patient Name:

Patient DoB:

Patient Identification Number for this trial:

CONSENT FORM

THE 18F-FAABULOUS STUDY

18F-FLUORIDE ASSESSMENT OF AORTIC BIOPROSTHESES DURABILITY AND OUTCOMES

Cohort 1

Name of Researchers: Dr Marc R. Dweck and Professor David E. Newby

Please initial all boxes

1. I confirm that I have read and understand the information sheet dated 15/09/14 (Cohort 1) for the above study. I have had the opportunity to consider the information, ask questions and have had these answered satisfactorily. ☐
2. I agree to participate, understand that my participation is voluntary and that I am free to withdraw at any time without giving any reason, without my medical care or legal rights being affected. ☐
3. I understand that this will not influence the medical treatment that is planned for me in any way. ☐
4. I understand that the PET CT scan performed will be associated with exposure to a dose of radiation. ☐
5. I understand that the PET CT scan will require the administration of contrast agent and a radioactive tracer. ☐
6. I understand that any information related to my case will be stored in an ☐

anonymised manner.

7. I understand that anonymised blood samples and heart valve tissue will be stored (under NHS Lothian's Tissue Governance Standards) for analysis as part of this study. ☐

8. I understand that anonymised blood samples and heart valve tissue will be stored (under NHS Lothian's Tissue Governance Standards) for potential use in future research studies which will be subject to further ethical approval. ☐

9. I understand that relevant sections of my medical notes and data collected during the study may be looked at by individuals from the regulatory authorities and from the Sponsors (NHS Lothian and The University of Edinburgh) where it is relevant to my taking part in this research. I give permission for those individuals to have access to my records. ☐

10. I agree to my GP being informed of my participation in the study, and that he or she will be informed of any incidental findings of clinical significance arising from my participation in the study. ☐

11. I agree to the further use of identifiable data/tissue in the event of a loss of capacity. ☐

_____	_____	_____
Name of Participant	Date	Signature

_____	_____	_____
Name of Person taking consent	Date	Signature

Patient Name:

Patient DoB:

Patient Identification Number for this trial:

CONSENT FORM

THE 18F-FAABULOUS STUDY

18F-FLUORIDE ASSESSMENT OF AORTIC BIOPROSTHESES DURABILITY AND OUTCOMES

Cohorts 2 and 3

Name of Researchers: Dr Marc R. Dweck and Professor David E. Newby

Please initial all boxes

12. I confirm that I have read and understand the information sheet dated 01/12/14 (Cohorts 2 and 3) for the above study. I have had the opportunity to consider the information, ask questions and have had these answered satisfactorily. ☐
13. I agree to participate, understand that my participation is voluntary and that I am free to withdraw at any time without giving any reason, without my medical care or legal rights being affected. ☐
14. I understand that this will not influence the medical treatment that is planned for me in any way. ☐
15. I understand that the PET CT and CT scans performed will be associated with exposure to a dose of radiation. ☐
16. I understand that the PET CT scan will require the administration of a contrast agent and a radioactive tracer. ☐
17. I understand that any information related to my case will be stored in an ☐

anonymised manner.

18. I understand that anonymised blood samples will be stored (under NHS Lothian's Tissue Governance Standards) for analysis as part of this study. ☐

19. I understand that anonymised blood samples will be stored (under NHS Lothian's Tissue Governance Standards) for potential use in future research studies which will be subject to further ethical approval. ☐

20. I understand that relevant sections of my medical notes and data collected during the study may be looked at by individuals from the regulatory authorities and from the Sponsors (NHS Lothian and The University of Edinburgh) where it is relevant to my taking part in this research. I give permission for those individuals to have access to my records. ☐

21. I agree to my GP being informed of my participation in the study, and that he or she will be informed of any incidental findings of clinical significance arising from my participation in the study. ☐

22. I agree to the further use of identifiable data/tissue in the event of a loss of capacity. ☐

_____	_____	_____
Name of Participant	Date	Signature

_____	_____	_____
Name of Person taking consent	Date	Signature

CERTIFICATE

FOR THE

ADMINISTRATION OF RADIOACTIVE MEDICINAL PRODUCTS

Certificate Reference Number RPC 577 / 3258 / 32128

It is hereby certified for the purposes of the Medicines (Administration of Radioactive Substances) Regulations 1978, amended by the Medicines (Administration of Radioactive Substances) Amendment Regulations 1995, that

Prof Edwin Jacques Rudolph van BEEK
Royal Infirmary of Edinburgh
51 Little France Crescent
Edinburgh
EH16 4SA

may administer until ***22-Sep-2019*** *the radioactive medicinal products specified in the Schedule to this certificate for the purpose(s) there specified.*

For The Secretary of State for Health

Health Protection
Toxicology and Radiation
Department of Health

Prof Edwin Jacques Rudolph van BEEK
Royal Infirmary of Edinburgh
51 Little France Crescent
Edinburgh
EH16 4SA

Date of Certificate 23-September-2014

Schedule to Research Certificate Number RPC 577 / 3258 / 32128

Research Project

18F-Fluoride Assessment of Aortic Bioprostheses Durability and Outcome

Serial	Nuclide	Chemical Form
9a31	18F	NaF

End of Certificate Schedule

Lothian NHS Board

South East Scotland Research Ethics Committee 01

Waverley Gate
2-4 Waterloo Place
Edinburgh
EH1 3EG
Telephone 0131 536 9000
Fax 0131 465 5789

www.nhslothian.scot.nhs.uk

Date 24 September 2014
Your Ref
Our Ref

Enquiries to: Sandra Wyllie
Extension: 35473
Direct Line: 0131 465 5473
Email:

Dr Marc Dweck
BHF Centre for Cardiovascular Science
Queen's Medical Research Institute
47 Little France Crescent
Edinburgh
EH16 4TJ

Dear Dr Dweck

Study title: **18F-Fluoride Assessment of Aortic Bioprostheses Durability and Outcomes**
REC reference: **14/SS/1049**
IRAS project ID: **147780**

Thank you for your letter of 19 September 2014, responding to the Committee's request for further information on the above research and submitting revised documentation.

The further information has been considered on behalf of the Committee by the Chair.

We plan to publish your research summary wording for the above study on the HRA website, together with your contact details. Publication will be no earlier than three months from the date of this opinion letter. Should you wish to provide a substitute contact point, require further information, or wish to make a request to postpone publication, please contact the REC Manager, Mrs Sandra Wyllie, sandra.wyllie@nhslothian.scot.nhs.uk.

Confirmation of ethical opinion

On behalf of the Committee, I am pleased to confirm a favourable ethical opinion for the above research on the basis described in the application form, protocol and supporting documentation as revised, subject to the conditions specified below.

Conditions of the favourable opinion

The favourable opinion is subject to the following conditions being met prior to the start of the study.

Management permission or approval must be obtained from each host organisation prior to the start of the study at the site concerned.

Management permission ("R&D approval") should be sought from all NHS organisations involved in the study in accordance with NHS research governance arrangements.